Ensemble density functional approach to electronic excitations : exact theory and approximations using quantum embedding

Filip Cernatic

UNIVERSITÉ DE STRASBOURG

ÉCOLE DOCTORALE DES SCIENCES CHIMIQUES

Institut de Chimie UMR 7177

THÈSE présentée par :

Filip CERNATIC

soutenue le : **22 septembre 2023**

pour obtenir le grade de : **Docteur de l'Université de Strasbourg**

Discipline/ Spécialité : Chimie / Chimie Théorique

Ensemble density functional approach to electronic excitations: Exact theory and approximations using quantum embedding.

THÈSE dirigée par :

M. Emmanuel FROMAGER	Professeur, Université de Strasbourg, France
M. Vincent ROBERT	Professeur, Université de Strasbourg, France

RAPPORTRICES :

Mme. Neepa MAITRA	Professeure, Rutgers University, United States of America
Mme. Pina ROMANIELLO	Chargée de Recherche, Université Paul Sabatier, Toulouse

---

EXAMINATEURS :

M. Julien TOULOUSE	Maître de conférences, Sorbonne Université, France
Mme. Lucia REINING	Directrice de recherche, École polytechnique, France

---

INVITÉ :

M. Saad YALOUZ	Chargé de Recherche, Université de Strasbourg, France

"The highest activity a human being can attain is learning for understanding, because to understand is to be free."

Baruch Spinoza

Acknowledgements

Overcome with a feeling of special kind of poignancy, I realize that the three years of being a PhD student have passed by quite rapidly. This work is the culmination of a life chapter that I will hold in very high regard and cherish every memory of it. It was also one of the most challenging periods of my life in many aspects, but challenge is what forces an individual to grow and acquire new abilities to continue on the path to greater understanding of the world and themselves. However, such a path can hardly be treaded alone, and there are many people to whom I am indebted a great deal for helping me reach my destination.

First of all, I would like to express sincere gratitude to my supervisors Emmanuel Fromager and Vincent Robert for entrusting me with this big project. The perfect balance of scientific rigour and curiosity for your subjects of interest, as well as the wealth of knowledge and experience you have provided me, will become inalienable companions of my future scientific endeavours. Your encouragement to believe in myself and keep going forward during the hardest of times is also something I will never forget. I am indeed very lucky to have had you as my supervisors, and I hope our paths will cross again in the future.

I am also very indebted to Saad Yalouz, for his share of invaluable knowledge, and for having built all the necessary computational tools, without which I would be unable to test my ideas, sharpen my skills in coding, and sometimes even find interesting discoveries in my scientific work.

In addition, my acknowledgements go to all the members of the jury. I would like to thank Neepa Maitra and Pina Romaniello, for reviewing my manuscript, and accepting to judge my work, and Julien Toulouse and Lucia Reining, for accepting to read and judge my thesis work.

A big thanks goes to my young colleagues Pablo, Oussama, Sajanthan and Lucie, with whom I have shared the PhD experience. Your friendship has been invaluable and has enriched my experience in the lab and outside, during all the moments we have shared together. I would like to thank Paola for helping me with all the administrative tasks, and Sylvie for technical assistance with computers. I must also not forget to show appreciation to other members of Laboratoire de Chimie

Quantique: Chantal, Christophe, Etienne and Roberto, who I have got to know more closely during these three years.

Finally, it goes without saying that nothing of this could have been achieved without continuous encouragement from my mother Anica and my brother Jurij. And I also acknowledge my former mentor and good friend Črtomir Podlipnik, as well as my other friends from Slovenia. I am thankful to you all for being on my side through thick and thin, and supporting my passion about science.

Table of Contents

Papers

I. Cernatic, F.; Senjean, B.; Robert, V.; Fromager, E. "Ensemble Density Functional Theory of Neutral and Charged Excitations." *Topics in Current Chemistry (Z)* **380**, 4 (2022).

II. Cernatic, F.; Loos, P.-F.; Senjean, B. and Fromager, E. "Exact ensemble density functional theory of neutral electronic excitations revisited: An extended N-centered approach to exchange-correlation derivative discontinuities", in preparation (2023).

III. Cernatic, F.; Yalouz, S. "Quantum embedding strategy for multiple electronic states", in preparation (2023).

IV. Cernatic, F.; Lasorne, B.; Fromager, E. "Perspectives in ensemble DFT of electronic excited states", invited "Perspective" paper, to be submitted to JCP (2023).

V. Cernatic, F.; Yalouz, S.; and Fromager, E. "Self-consistent local potential functional embedding theory of many-electron ensembles", in preparation (2023).

Acronyms

The following is a list of acronyms most commonly used throughout this thesis.

Acronyms	Meaning
kRDM	k-electron Reduced Density Matrix (for $k \geq 1$)
BSE	Bethe-Salpeter Equation
CASCI	Complete Active Space Configuration Interaction
CASPT2	Complete Active Space Perturbation Theory
CASSCF	Complete Active Space Self-Consistent Field
CI	Configuration Interaction
CC	Coupled Cluster
DFA	Density-Functional Approximation
DFT	Density-Functional Theory
DMET	Density Matrix Embedding Theory
eDFT	Ensemble Density-Functional Theory
FCI	Full Configuration Interaction
HF	Hartree-Fock
Ht-DMFET	Householder-transformed Density Matrix Functional Embedding Theory
KS-DFT	Kohn-Sham Density Functional Theory
LDA	Local Density Approximation
LPFET	Local Potential Functional Embedding Theory
MCSCF	Multi-Configurational Self-Consistent Field
MO	Molecular Orbital
MP2	Møller-Plesset second-order
PPLB	Perdew-Parr-Levy-Balduz
NEVPT2	n-Electron Valence State Perturbation Theory
SCF	Self-Consistent Field
SVD	Singular Value Decomposition
TD-DFT	Time-Dependent Density-Functional Theory
TGOK	Theophilou-Gross-Oliveira-Kohn
UEG	Uniform Electron Gas
WFT	Wavefunction Theory

Résumé en français

Introduction

Dans cette thèse, nous visons à pousser plus loin le développement théorique du formalisme de la fonctionnelle de la densité d'ensemble pour décrire les excitations électroniques. Pour le reste de la discussion, nous supposons que nous avons affaire à un système électronique isolé. L'état de ce système ayant l'énergie la plus basse est appelé état fondamental, tandis que les états ayant des énergies plus élevées sont appelés états excités. Comprendre comment le système réagit à l'excitation est d'un grand intérêt dans de nombreuses branches de la science qui utilisent la théorie quantique, telles que la photochimie et la spectroscopie, mais aussi pour la conception de nouveaux matériaux. Comme nous le verrons bientôt, la description des états fondamentaux électroniques est déjà une tâche difficile, puisque nous devons résoudre le problème de l'interaction de plusieurs électrons de la nature quantique. Dans la plupart des cas, il faut développer des approximations astucieuses de la solution exacte qui réduisent les coûts de calcul, sans trop compromettre la précision des résultats. On peut raisonnablement s'attendre à ce que le traitement des états excités soit encore plus difficile.

De nos jours, les excitations électroniques sont le plus souvent traitées par des méthodes de réponse, telles que la *théorie de la fonctionelle de la densité dépendante du temps* (time-dependent density-functional theory - TD-DFT) [1, 2] et les méthodes basées sur les fonctions de Green de nombreux corps (methods, based on many-body Green's functions) [3, 4, 5, 6, 7, 8, 9], qui sont très bien connues dans la physique de la matière condensée. La méthode TD-DFT à réponse linéaire avec l'équation de Casida [10] s'est avérée très efficace dans le traitement des excitations neutres dans les molécules et les matériaux. Certaines limitations de la TD-DFT à réponse linéaire sont la description à référence unique, qui est insuffisante pour les

situations de (quasi-)dégénérescence, telles que les intersections coniques [2] et les croisements évités dans les molécules, et avec l'approximation adiabatique couramment utilisée, l'absence d'excitations multiples. En outre, la résolution de l'équation de Casida entraîne un coût de calcul modéré, ce qui rend la méthode plus coûteuse que la méthode DFT standard de Kohn-Sham [11]. Le formalisme de la fonction de Green a permis de décrire avec succès les excitations chargées, mais aussi neutres, avec la méthode GW [3, 4, 5, 6], et l'équation *Bethe-Salpeter* (BSE) [7, 8], respectivement. Ces méthodes ont également un coût de calcul modéré (dans leurs implémentations les plus simples) et ne sont pas couramment utilisées en chimie quantique, bien qu'elles aient récemment fait l'objet d'un intérêt croissant [12]. Les méthodes couramment utilisées en chimie quantique sont les méthodes basées sur la fonction d'onde multiconfigurationnelle, telles que la méthode *champ autocohérent complet de l'espace actif* (complete active space self-consistent field - CASSCF) [13], ou la méthode *state-averaged CASSCF* (SA-CASSCF) [14], qui sont utilisées pour décrire les états de basse énergie dans les molécules. Bien que très précises, ces méthodes nécessitent beaucoup d'expérience de la part de l'utilisateur et sont trop coûteuses pour être applicables à de grandes molécules. Pour faire face aux coûts de calcul, les méthodes d'*embedding quantique* (quantum embedding - QE), qui utilisent des combinaisons de différentes approches, ont suscité l'intérêt au cours des dernières décennies. Un exemple de ces méthodes, qui est également utilisé dans cette thèse, est la *théorie d'embedding de la matrice de densité* (density matrix embedding theory - DMET) [15, 16, 17].

Les développements réalisés dans cette thèse portent sur la construction de méthodes de calcul "d'ensemble" pour accéder à la structure électronique de plusieurs états quantiques à la fois. Un premier grand axe porte sur l'extension de la *théorie de la fonctionnelle de la densité* (DFT), initialement focalisée sur l'état fondamental, aux ensembles d'états électroniques (fondamental + excités) donnant ainsi naissance au concept de *DFT d'ensemble* (ensemble density-functional theory - eDFT), qui a suscité un intérêt croissant au cours des dernières décennies en tant que méthode alternative peu coûteuse pour le traitement des excitations électroniques. Les aspects formels et pratiques du DFT d'ensemble sont discutés en détail et différentes approches pour le développement d'approximations de la

fonctionnelle de la densité pour l'énergie d'échange-corrélation d'ensemble sont introduits. Ces approches sont illustrées par des calculs numériques réalisés sur le dimère asymétrique de Hubbard. De plus, un nouveau formalisme DFT d'ensembles "N-centrés" étendu est proposé, qui combine les excitations neutres et chargées en un seul ensemble, mettant ainsi en lumière le concept de dérivée discontinue pour les excitations neutres. Un second grand axe de cette thèse porte sur des calculs quantiques de type fonction d'onde. Dans ce travail, nous proposons une stratégie "d'embedding quantique" pour décrire plusieurs états électroniques à la fois, au moyen du partitionnement de la matrice densité à un electron basée sur l'utilisation de transformations de Householder [18, 19]. L'efficacité et les limites de cette nouvelle approche sont illustrées par des simulations numériques sur des Hamiltonien de Hubbard et des molécules de petite tailles.

Chapitre 1: Différentes variantes de la théorie de la structure électronique de l'état fondamental

La description des états électroniques stationnaires est l'une des principales tâches de la théorie de la structure électronique. À cet égard, divers systèmes physiques sont pris en considération. En chimie quantique, les atomes, les molécules et les arrangements moléculaires sont étudiés. En physique de la matière condensée, les matériaux en vrac sont généralement modélisés comme des systèmes étendus. Dans tous les cas, l'objectif fondamental de la théorie de la structure électronique est le même: résoudre l'équation de Schrödinger à plusieurs électrons. Il s'agit toutefois d'une tâche très exigeante, et c'est pour cette raison qu'une pléthore de méthodologies différentes ont été développées, en grande partie guidées par le compromis entre la précision et l'efficacité des calculs. Nous commençons notre discussion sur les différentes méthodes par celles basées sur la *théorie de la fonction d'onde* (wave-function theory - WFT).

Théorie de la fonction d'onde

Dans la théorie quantique, tout ce que nous pouvons savoir sur un système physique est donné par son état quantique, $|\Psi\rangle$, qui, comme nous le montrerons dans les sous-sections suivantes, est un objet assez complexe. Lorsque nous étudions des phénomènes statiques tels que les géométries d'équilibre en chimie quantique, $|\Psi\rangle$

est obtenu comme solution (état propre) de l'équation de Schrödinger indépendante du temps,

$$\hat{H}\,|\Psi\rangle = E\,|\Psi\rangle\,, \tag{1}$$

où $\hat{H}$ est l'opérateur Hamiltonien, qui décrit les énergies cinétiques et les interactions des particules constituant le système, et E est le niveau d'énergie du système dans l'état propre $|\Psi\rangle$. Il s'agit d'un problème de valeurs propres qui est d'une grande importance dans la théorie de la structure électronique. Différents Hamiltoniens sont utilisés en fonction du système considéré et de la complexité des phénomènes étudiés. Dans la théorie de la fonction d'onde indépendante du temps *ab initio*, combiné avec l'approximation de Born-Oppenheimer [20], nous sommes intéressés à l'Hamiltonien électronique $\hat{H}_{\mathrm{e}}$, qui, dans la représentation de position, se lit comme suit,

$$\begin{aligned}\hat{H}_{\mathrm{e}} &= \hat{T}_{\mathrm{e}} + \hat{W}_{\mathrm{ee}} + \hat{V}_{\mathrm{ne}} \\ &\equiv -\frac{1}{2}\sum_{i=1}^{N}\nabla_i^2 + \sum_{i=1}^{N}\sum_{j>i}^{N}\frac{1}{|\mathbf{r}_i-\mathbf{r}_j|} - \sum_{i=1}^{N}\sum_{A=1}^{M}\frac{Z_A}{|\mathbf{r}_i-\mathbf{R}_A|}.\end{aligned} \tag{2}$$

L'équation de Schrödinger indépendante du temps de l'Hamiltonien électronique se lit comme suit,

$$\hat{H}_{\mathrm{e}}(\{\mathbf{R}_A\})\,|\Psi_{\mathrm{e}}(\{\mathbf{R}_A\})\rangle = E_{\mathrm{e}}(\{\mathbf{R}_A\})\,|\Psi_{\mathrm{e}}(\{\mathbf{R}_A\})\rangle\,, \tag{3}$$

où la fonction d'onde électronique $\Psi_{\mathrm{e}}(\{\mathbf{r}_i\},|\,\{\mathbf{R}_A\})$ dépend des coordonnées des électrons $\{\mathbf{r}_i\}$, ainsi que des coordonnées nucléaires $\{\mathbf{R}_A\}$ de manière paramétrique. Pour faciliter la résolution de l'équation de Schrödinger ci-dessus, il est important de connaître au moins quelques propriétés mathématiques que la fonction d'onde d'un système physique réaliste doit remplir. En général, la fonction d'onde Ψ doit inclure des informations sur tous les électrons du système. Chaque électron possède quatre degrés de liberté, comprenant trois coordonnées spatiales $\mathbf{r} = (x, y, z) \in \mathbb{R}^3$ et une coordonnée de spin $\sigma \in \{\uparrow, \downarrow\}$ où $\uparrow$ et $\downarrow$ représentent les valeurs propres ($+1/2$ et $-1/2$, respectivement) de l'opérateur de projection de spin $\hat{S}_z$. En outre, la fonction d'onde doit être intégrable au carré si elle doit représenter un état quantique lié,

$$\int d\mathbf{x}_1 \int d\mathbf{x}_2 \,\ldots\, \int d\mathbf{x}_N |\Psi(\mathbf{x}_1, \mathbf{x}_2, \ldots, \mathbf{x}_N)|^2 \;=\; 1, \tag{4}$$

où l'intégration sur une seule coordonnée spin-espace $\mathbf{x}$ est formellement représentée comme une composition de l'intégration sur trois coordonnées spatiales et de la sommation sur la seule variable spin,

$$\int d\mathbf{x} \equiv \int d\mathbf{r} \sum_{\sigma\in\{\uparrow,\downarrow\}} . \tag{5}$$

La fonction d'onde doit également être antisymétrique par rapport à la permutation des coordonnées de spin de deux électrons quelconques,

$$\forall i,j \quad \Psi(...,\mathbf{x}_i,....,\mathbf{x}_j,...) = -\Psi(...,\mathbf{x}_j,....,\mathbf{x}_i,...), \tag{6}$$

de sorte que la probabilité de trouver deux électrons de même spin au même endroit s'évanouit, $|\Psi(...,\mathbf{x}_i,....,\mathbf{x}_j = \mathbf{x}_i,...)|^2 = 0$. C'est ce que l'on appelle le principe d'exclusion de Pauli [21]. Cette dernière condition peut être réalisée en prenant un produit antisymétrique d'un ensemble de spin-orbitales, *i.e.* fonctions à un seul électron $\{\phi_k(\mathbf{x})\}_{k=1}^N$, qui est connu comme le déterminant de Slater,

$$\Phi(\mathbf{x}_1,\mathbf{x}_2,\ldots,\mathbf{x}_N) := \frac{1}{\sqrt{N!}}\begin{vmatrix} \phi_1(\mathbf{x}_1) & \phi_2(\mathbf{x}_1) & \ldots & \phi_N(\mathbf{x}_1) \\ \phi_1(\mathbf{x}_2) & \phi_2(\mathbf{x}_2) & \ldots & \phi_N(\mathbf{x}_2) \\ \vdots & \vdots & \ddots & \vdots \\ \phi_1(\mathbf{x}_N) & \phi_2(\mathbf{x}_N) & \ldots & \phi_N(\mathbf{x}_N) \end{vmatrix}, \tag{7}$$

Le déterminant de Slater est un ingrédient nécessaire de la méthode *Hartree-Fock* (HF) [22, 23], qui est la base bien connue des méthodes plus avancées en chimie quantique.

Analysons maintenant les méthodes standard de la théorie de la structure électronique des états fondamentaux, en commençant par la méthode HF. Dans la version restreinte à enveloppe fermée de la méthode HF (restricted closed-shell Hartree-Fock), la fonction d'onde totale du système est approximée par un seul déterminant de Slater Φ, construit à partir d'un ensemble d'orbitales moléculaires (molecular orbital - MO) $\{\varphi_i(\mathbf{r})\}_{i=1}^{N/2}$. L'objectif est de trouver les meilleures MO possibles qui minimisent la valeur d'espérance suivante de l'Hamiltonien électronique, $\langle\Phi|\hat{H}_\mathrm{e}|\Phi\rangle$, qui se lit comme suit,

$$\langle\Phi|\hat{H}_\mathrm{e}|\Phi\rangle = 2\sum_{i=1}^{N/2}\langle\varphi_i|\hat{h}|\varphi_i\rangle + \sum_{i=1}^{N/2}\sum_{j=1}^{N/2}\Big[2\langle\varphi_i\varphi_j|\varphi_i\varphi_j\rangle - \langle\varphi_i\varphi_j|\varphi_j\varphi_i\rangle\Big], \tag{8}$$

où $\hat{h} = -(1/2)\nabla^2_{\mathbf{r}} + v_{\rm ne}(\mathbf{r})$ est la partie à un électron de l'Hamiltonien électronique, qui comprend l'énergie cinétique électronique et l'attraction électron-nucléaire, et

$$\langle \varphi_i \varphi_j | \varphi_k \varphi_l \rangle := \int\int d\mathbf{r}_1 d\mathbf{r}_2 \frac{\varphi_i^*(\mathbf{r}_1)\, \varphi_j^*(\mathbf{r}_2)\, \varphi_k(\mathbf{r}_1)\, \varphi_l(\mathbf{r}_2)}{|\mathbf{r}_1 - \mathbf{r}_2|}. \tag{9}$$

Les orbitales qui minimisent Eq. (8) obéissent à l'ensemble des équations intégro-différentielles couplées, connues sous le nom d'équations de Hartree-Fock,

$$\hat{F}[\{\varphi_j\}]\varphi_i(\mathbf{r}) = \varepsilon_i \varphi_i(\mathbf{r}), \tag{10}$$

où $\hat{F}$ est l'opérateur de Fock dépendant de l'orbitale,

$$\hat{F} = \hat{h}_{\rm core} + \sum_{j=1}^{N/2} \left(2\hat{\mathcal{J}}_j - \hat{\mathcal{K}}_j \right). \tag{11}$$

Le premier terme du côté droit de l'équation ci-dessus,

$$\hat{h}_{\rm core} = -\frac{1}{2}\nabla^2_{\mathbf{r}} - \sum_{A=1}^{M} \frac{Z_A}{|\mathbf{r} - \mathbf{R}_A|}, \tag{12}$$

est la somme de l'énergie cinétique d'un électron et de l'attraction électron-nucléaire, et le second terme est constitué du potentiel de Coulomb (local) et du potentiel d'échange (non local), respectivement,

$$\hat{\mathcal{J}}_j \varphi_i(\mathbf{r}) = \left(\int d\mathbf{r}' \frac{\varphi_j^*(\mathbf{r}')\varphi_j(\mathbf{r}')}{|\mathbf{r} - \mathbf{r}'|} \right) \times \varphi_i(\mathbf{r}), \tag{13}$$

$$\hat{\mathcal{K}}_j \varphi_i(\mathbf{r}) = \left(\int d\mathbf{r}' \frac{\varphi_j^*(\mathbf{r}')\varphi_i(\mathbf{r}')}{|\mathbf{r} - \mathbf{r}'|} \right) \times \varphi_j(\mathbf{r}). \tag{14}$$

Comme les équations HF dépendent des vecteurs propres, elles doivent être résolues de manière autocohérente. L'approche commune consistant à développer les orbitales moléculaires dans une base d'orbitales atomiques a été proposée indépendamment par Roothaan [24] et Hall [25].

L'énergie HF, que nous obtenons en insérant les solutions des Eqs. (10) dans l'Eq. (8), est l'énergie la plus basse que l'on puisse obtenir en utilisant un seul déterminant de Slater. L'énergie exacte de l'état fondamental dans l'approximation de Born-Oppenheimer est toujours inférieure. L'énergie de corrélation, un terme inventé par Löwdin [26], est la différence entre les deux énergies,

$$E_{\rm c} = E - E_{\rm HF} < 0. \tag{15}$$

La théorie Hartee-Fock elle-même contient déjà une certaine corrélation. Celle-ci est due à l'intégrale d'échange, qui diminue l'énergie totale pour chaque paire d'électrons de même spin. Cet effet est également appelé corrélation de Fermi, ce qui signifie que deux électrons de même spin ne peuvent pas occuper le même point dans l'espace (équivalemment, la même MO). Cependant, dans les systèmes réalistes, il existe des effets de corrélation que la méthode HF ne prend pas en compte. Dans la littérature, ils sont communément regroupés dans la corrélation dynamique et la corrélation statique. La corrélation dynamique peut être prise en compte en approximant la véritable fonction d'onde comme une combinaison linéaire de déterminants de Slater générés par des excitations de la fonction d'onde occupés (dans le déterminant HF de l'état fondamental) vers les MO virtuels (inoccupés), à condition qu'un seul déterminant de Slater soit une bonne approximation de départ. Dans certains cas, il existe un autre effet appelé corrélation forte ou statique, qui survient lorsque différents déterminants de Slater sont strictement ou quasi dégénérés, et qu'ils doivent tous être pris en compte. Par conséquent, dans les cas où la corrélation statique est importante, la fonction d'onde de référence doit être multidéterminante.

Les corrélations dynamique et statique sont décrites à l'aide des méthodes dites post-HF. La méthode de l'interaction de configuration (configuration interaction - CI) est l'une des méthodes les plus simples pour récupérer la corrélation dynamique. Dans la méthode CI, la fonction d'onde de l'état fondamental est écrite comme la combinaison linéaire suivante,

$$|\Psi_{\mathrm{CI}}\rangle = |\Phi_{\mathrm{HF}}\rangle + \sum_i \sum_a C_i^a \, |\Phi_i^a\rangle + \sum_{i>j} \sum_{a>b} C_{ij}^{ab} \, \left|\Phi_{ij}^{ab}\right\rangle + \ldots, \tag{16}$$

où $|\Phi_i^a\rangle$ est obtenu en excitant un électron de l'orbitale occupée (dans $|\Phi_{\mathrm{HF}}\rangle$) i vers l'orbitale de spin inoccupée a, et ainsi de suite. Les coefficients CI, $\mathbf{C} = \{C_I\}_I$ sont obtenus par minimisation variationnelle de la valeur espérée $\langle\Psi_{\mathrm{CI}}(\mathbf{C})|\hat{H}_{\mathrm{e}}|\Psi_{\mathrm{CI}}(\mathbf{C})\rangle$ tout en maintenant les orbitales HF fixes. Si nous prenons en considération toutes les excitations possibles pour un ensemble de bases atomiques donné, nous obtenons la méthode dite *interaction de configuration complète* (full configuration interaction - FCI), qui est exacte pour un ensemble de base de orbitales donné. Malheureusement, l'échelle de la FCI est exponentielle, ce qui rend cette méthode inutile pour la plupart des applications. En fait, l'échelle exponentielle de nombreuses méthodes

très précises basées sur la fonction d'onde est l'une des principales raisons pour lesquelles d'autres méthodes ont été développées, telles que la *théorie de la fonctionelle de la densité* (density-functional theory - DFT) et la théorie de l'embedding quantique. En ce qui concerne la méthode CI pratique, nous pouvons tronquer l'expansion FCI aux excitations simples (configuration interaction singles - CIS), aux excitations doubles (configuration interaction with singles and doubles - CISD), et ainsi de suite. Chaque classe supplémentaire d'excitations donne une méthode plus précise.

Outre la méthode CI, les deux autres méthodes couramment utilisées sont la théorie des perturbations *Møller-Plesset* du second ordre (MP2), et la *méthode du cluster couplé* (coupled cluster - CC). Ces méthodes ne sont pas variationnelles, ce qui signifie que l'énergie approximative peut être inférieure à l'énergie réelle de l'état fondamental. Cependant, elles sont *size-consistent*, ce qui signifie que pour un système composé de sous-unités séparées à l'infini, l'énergie est additivement séparable et la fonction d'onde est multiplicativement séparable.

Les méthodes CI, MP2 et CC sont des méthodes post-HF basées sur le déterminant HF comme référence, qui conviennent pour décrire la corrélation dynamique. Dans les cas où la corrélation statique est importante, comme par exemple dans les molécules étirées, aux intersections coniques, ou aux géométries d'équilibre de certaines molécules comme l'ozone (voir Ref. [27] et les références qui y figurent), la référence HF n'est pas qualitativement correcte, parce que plusieurs orbitales HF (occupées et virtuelles) peuvent devenir dégénérées, ou presque dégénérées. Dans de tels cas, il devient nécessaire de réoptimiser les orbitales dans l'expansion CI, dans la méthode dite *champ autocohérent multiconfigurationnel* (multiconfigurational self-consistent field - MCSCF). En pratique, la première étape de la MCSCF est l'identification des configurations électroniques dominantes dans la fonction d'onde, qui sont généralement obtenues en considérant toutes les excitations possibles dans un sous-espace orbital. Dans le langage de la MCSCF, un tel sous-espace est appelé *espace orbital actif*. Ensuite, la fonction d'onde d'essai est développée comme une combinaison linéaire de déterminants de Slater ou de *fonctions d'état de configuration* (CSF) comme suit [28],

$$|\Psi(\boldsymbol{\kappa}, \mathbf{C})\rangle = e^{-\hat{\boldsymbol{\kappa}}} \sum_I C_I \, |\Phi_I\rangle \,, \tag{17}$$

où le terme exponentiel (avec paramètres $\boldsymbol{\kappa} = \{\kappa_{ij}\}_{i>j}$ fait tourner les orbitales HF (occupées et virtuelles), et le sommand I s'étend sur les configurations, générées à partir de l'espace orbital actif et du nombre d'électrons (dits actifs) distribués dans cet espace. Plusieurs méthodes multiconfigurationnelles ont été proposées, qui diffèrent par la manière dont les orbitales sont réoptimisées et dont l'espace actif est divisé. Dans la méthode *champ autocohérent de l'espace actif complet* (complete active space self-consistent field - CASSCF) [13], toutes les orbitales (doublement occupées, actives et virtuelles) sont réoptimisées et l'expansion FCI dans l'espace actif est effectuée. L'espace actif peut également être divisé en plusieurs sous-espaces avec des restrictions sur les excitations électroniques, ce qui est la pratique standard dans la méthode *champ autocohérent dans l'espace actif restreint* (restricted active space self-consistent field - RASSCF) [29, 30, 31]. Une approche encore moins coûteuse consiste à sauter complètement l'optimisation orbitale et à effectuer l'expansion FCI dans l'espace actif, composé des orbitales HF. Cela correspond à la méthode *interaction de configuration de l'espace actif complet* (complete active space configuration interaction - CASCI). Afin de récupérer la corrélation dynamique, les méthodes de théorie des perturbations multiréférences telles que la méthode *théorie des perturbations du second ordre de l'espace actif complet* (complete active space second-order perturbation theory - CASPT2) [32] et *théorie des perturbations du second ordre de l'état de valence N-électron* (N-electron valence state second-order perturbation theory - NEVPT2) [33, 34, 35], sont couramment appliquées en plus d'une méthode multiconfigurationnelle, ainsi que d'autres méthodes non basées sur la théorie des perturbations, telles que le *interaction de configuration multiréférence* (multireference configuration interaction - MRCI) [36, 37, 38], et la méthode *methode du cluster couplé multiréférence* (multireference coupled cluster - MRCC) [39, 40, 41, 42, 43].

Théorie de la fonctionnelle de la densité

La théorie de la fonctionnelle de la densité (DFT) est la méthode de mécanique quantique la plus utilisée en chimie quantique et en physique du solide. La variable de base de la DFT est la densité électronique, qui est obtenue en intégrant dans la fonction d'onde (précisément, dans son module carré) tous les degrés de liberté de $N-1$ électrons et tous les degrés de liberté de spin de N électrons, ce qui ne laisse qu'une fonction de 3 coordonnées spatiales - une variable énormément simplifiée par

rapport à la fonction d'onde,

$$n(\mathbf{r}) = N \sum_{\sigma=\uparrow,\downarrow} \int d\mathbf{x}_2 \int d\mathbf{x}_3 \cdots \int d\mathbf{x}_N \Psi^*(\mathbf{r},\sigma,\mathbf{x}_2,\ldots,\mathbf{x}_N)\Psi(\mathbf{r},\sigma,\mathbf{x}_2,\ldots,\mathbf{x}_N). \quad (18)$$

Par construction, il s'intègre au nombre d'électrons N.

Les racines de la DFT remontent au début du 20ème siècle avec l'introduction du modèle dit *Thomas-Fermi* (TF) [44, 45]. À cet égard, la première fonctionnelle de densité dérivée est celle de l'énergie cinétique des électrons libres,

$$T_{\mathrm{TF}}[n] = C_{\mathrm{TF}} \int d\mathbf{r}\, n(\mathbf{r})^{5/3}, \quad (19)$$

où $C_{\mathrm{TF}} = 3(3\pi^2)^{2/3}/10$ est la constante de Thomas-Fermi en unités atomiques. Toutefois, les fondements rigoureux de la théorie de la fonctionnelle de la densité ont été consolidés en 1964 [46], lorsque Hohenberg et Kohn ont présenté deux théorèmes établissant l'unicité de l'énergie de l'état fondamental en tant que fonctionnelle de la densité de l'état fondamental. Le premier théorème de Hohenberg-Kohn établit que la correspondance entre le potentiel externe v_{ext} et la densité de l'état fondamental $n_0 = n_{\Psi_0[v_{\mathrm{ext}}]}$ est bijective, de sorte que l'état fondamental, ainsi que le potentiel externe, sont des fonctionnelles de la densité de l'état fondamental: $|\Psi_0\rangle = |\Psi[v_{\mathrm{ext}}]\rangle = |\Psi[n_0]\rangle$ et $v_{\mathrm{ext}}(\mathbf{r}) = v_{\mathrm{ext}}[n_0](\mathbf{r})$. Cela implique que le principe variationnel peut être reformulé comme une minimisation sur les densités. À cette fin, la fonctionnelle de la densité universelle de Hohenberg-Kohn a été introduite [46],

$$F_{\mathrm{HK}}[n] := \langle \Psi[n]|\hat{T} + \hat{W}_{\mathrm{ee}}|\Psi[n]\rangle, \quad (20)$$

qui est universelle dans le sens où elle est indépendante du potentiel externe v_{ext}. Ensuite, dans le second théorème de Hohenberg-Kohn, on montre que l'énergie de l'état fondamental pour un v_{ext} donné, est atteinte à la densité de l'état fondamental $n_0 = n_{\Psi_0[v_{\mathrm{ext}}]}$ par minimisation sur les densités d'électrons comme suit,

$$E_0[v_{\mathrm{ext}}] = E_0[n_0] = \min_n \left\{ F_{\mathrm{HK}}[n] + \int d\mathbf{r}\, v_{\mathrm{ext}}(\mathbf{r}) n(\mathbf{r}) \right\}. \quad (21)$$

Le problème du principe du minimum ci-dessus est qu'il n'est défini que pour les densités qui proviennent de la résolution du problème des valeurs propres d'un Hamiltonien avec v_{ext}. Il s'agit des densités dites *v-représentables*, dont l'ensemble n'est pas connu explicitement. Levy [47, 48], et plus tard Lieb [49], qui ont redéfini la

fonctionnelle de densité universelle $F_{\mathrm{HK}}[n]$ dans une minimisation contrainte sur toutes les fonctions d'onde Ψ qui produisent une densité désirée n, ont trouvé une solution,

$$F_{\mathrm{LL}}[n] := \min_{\Psi \to n} \langle \Psi | \hat{T} + \hat{W}_{\mathrm{ee}} | \Psi \rangle = \langle \Psi[n] | \hat{T} + \hat{W}_{\mathrm{ee}} | \Psi[n] \rangle. \tag{22}$$

Cette définition est communément appelée la formulation de recherche sous contrainte de Levy-Lieb, qui autorise toutes les densités N-représentables, c'est-à-dire celles qui sont obtenues à partir d'un état antisymétrique à N électrons. Par conséquent, le principe variationnel pour l'énergie électronique peut être décomposé en une procédure de minimisation en deux étapes,

$$\begin{aligned} E_0[v_{\mathrm{ext}}] &= \min_{\Psi} \left\{ \langle \Psi | \hat{T} + \hat{W}_{\mathrm{ee}} + \hat{V}_{\mathrm{ext}} | \Psi \rangle \right\} \\ &= \min_{n} \left\{ \min_{\Psi \to n} \langle \Psi | \hat{T} + \hat{W}_{\mathrm{ee}} | \Psi \rangle + \int d\mathbf{r}\, v_{\mathrm{ext}}(\mathbf{r}) n(\mathbf{r}) \right\} \\ &= \min_{n} \left\{ F_{\mathrm{LL}}[n] + \int d\mathbf{r}\, v_{\mathrm{ext}}(\mathbf{r}) n(\mathbf{r}) \right\}. \end{aligned} \tag{23}$$

Contrairement à $F_{\mathrm{HK}}[n]$, $F_{\mathrm{LL}}[n]$ résout le problème de la v-représentabilité. Il existe une définition encore plus générale de la fonctionnelle universelle, qui a été fournie par Lieb [49]. La fonctionnelle de Lieb repose sur les fondements mathématiques rigoureux de l'analyse convexe. En se basant sur la propriété que l'énergie de l'état fondamental $E_0[v]$ est concave sur l'ensemble de tous les potentiels possibles v, Lieb a montré que $F_{\mathrm{L}}[n]$ est la transformée de Legendre-Fenchel de $E_0[v]$,

$$F_{\mathrm{L}}[n] \equiv \sup_{v} \left\{ E_0[v] - \int d\mathbf{r}\, v(\mathbf{r}) n(\mathbf{r}) \right\}. \tag{24}$$

Cette construction est également appelée *la maximisation de Lieb* (Lieb maximization). $F_{\mathrm{L}}[n]$ est une enveloppe convexe de $F_{\mathrm{LL}}[n]$ avec la propriété $F_{\mathrm{L}}[n] \leq F_{\mathrm{LL}}[n]$.

La fonctionnelle universelle $F[n]$ introduite précédemment dans ses différentes formulations, détient, en principe, toute l'information de tout système d'intérêt, grâce aux théorèmes de Hohenberg-Kohn. Cependant, son utilisation pratique est plutôt limitée, car elle implique la connaissance de systèmes à plusieurs corps en interaction. Face à ce problème, Kohn et Sham ont proposé en 1965 une solution astucieuse. Dans la théorie de la fonctionnelle de la densité de Kohn-Sham (KS-DFT), la fonctionnelle de la densité universelle est divisée en deux contributions comme suit,

$$F[n] = T_{\mathrm{s}}[n] + E_{\mathrm{Hxc}}[n], \tag{25}$$

où le premier terme, $T_{\mathrm{s}}[n]$, est la fonctionnelle (de la densité) d'énergie cinétique sans interaction. Il peut être obtenu à partir de $F[n]$ (avec n'importe quel formalisme), en mettant à zéro l'opérateur d'énergie d'interaction $\hat{W}_{\mathrm{ee}}$. Dans le formalisme de Levy-Lieb, elle s'écrit comme suit,

$$T_{\mathrm{s}}[n] = \min_{\Psi \to n} \langle \Psi | \hat{T} | \Psi \rangle = \langle \Psi[n] | \hat{T} | \Psi[n] \rangle. \tag{26}$$

Le terme restant dans l'Eq. (25), $E_{\mathrm{Hxc}}[n]$, est appelé la fonctionnelle *Hartree-échange-corrélation* (Hxc), qui encode tous les effets de nombreux électrons au-delà du niveau de calcul du champ moyen, tels que l'énergie cinétique et la répulsion de Coulomb des électrons. En insérant la décomposition KS de la fonctionnelle universelle dans Eq. (21), il est possible de montrer que la densité électronique minimisante peut être obtenue à partir d'un déterminant de Slater unique $|\Phi_{\mathrm{KS}}\rangle$, dont les orbitales sont des solutions des équations KS,

$$\left(-\frac{\nabla_{\mathbf{r}}^2}{2} + v_{\mathrm{ext}}(\mathbf{r}) + v_{\mathrm{Hxc}}[n_{\Phi_{\mathrm{KS}}}] \right) \varphi_i(\mathbf{r}) = \varepsilon_i \varphi_i(\mathbf{r}), \tag{27}$$

où

$$v_{\mathrm{Hxc}}[n_{\Phi_{\mathrm{KS}}}] = \left. \frac{\delta E_{\mathrm{Hxc}}[n]}{\delta n(\mathbf{r})} \right|_{n=n_{\Phi_{\mathrm{KS}}}} \tag{28}$$

est le potentiel de Hartree-échange-corrélation (Hxc). La densité électronique à l'état fondamental est, en principe, exactement reproduite par les orbitales KS comme suit,

$$n_{\Phi_{\mathrm{KS}}}(\mathbf{r}) = 2 \sum_{i=1}^{N/2} |\varphi_i(\mathbf{r})|^2 = n_{\Psi_0}(\mathbf{r}). \tag{29}$$

En pratique, une fois qu'un *approximation fonctionnelle de la densité* (density-functional approximation - DFA) particulier de la fonctionnelle d'énergie Hxc est choisi, les équations KS sont résolues de manière autocohérente, avec la même procédure que celle décrite pour les équations de Roothaan-Hall dans la théorie HF.

Théories de l'embedding quantique

Les méthodes de fonction d'onde de la chimie quantique que nous avons mentionnées jusqu'à présent sont très développées et très précises pour fournir des détails sur la structure électronique, mais elles sont généralement coûteuses. L'échelle exponentielle du nombre de configurations avec la taille du système limite l'applicabilité des

méthodes de fonction d'onde très précises (telles que FCI et CCSD(T)) aux petites molécules [28]. D'autre part, la *théorie de la fonctionnelle de la densité de Kohn-Sham* (Kohn-Sham density-functional theory - KS-DFT) est couramment utilisée pour étudier des molécules et des matériaux de tailles et de complexités différentes. Cependant, elle ne parvient pas à décrire la forte corrélation électronique, qui joue un rôle important dans de nombreux systèmes intéressant les physiciens et les chimistes. À cet égard, l'une des solutions est *l'embedding quantique* (quantum embedding - QE), dont l'idée est de diviser le système étudié en fragments plus petits. Chaque fragment est ensuite couplé au reste du système par l'intermédiaire d'un petit nombre de degrés de liberté représentatifs, généralement appelés le "bain quantique", et résolu à l'aide d'une méthode précise de "haut niveau". La partie restante est traitée à un "bas niveau", généralement au niveau du champ moyen. En tant qu'étape d'affinage, un critère de cohérence peut être imposé pour faire correspondre une certaine quantité (la fonction d'onde, la fonction de Green, la 1RDM ou la densité électronique) de la description de haut niveau à celle du champ moyen. De cette façon, le coût de calcul du traitement du système complet avec une méthode de haut niveau est considérablement réduit. Plusieurs techniques d'embedding ont été proposées en fonction de la quantité choisie et de la représentation des degrés de liberté utilisés dans le partitionnement. En chimie quantique, *frozen-density embedding* (FDE) [50, 51] et la théorie de la fonctionelle de la densité du sous-système [52, 53] (subsystem density-functional theory) sont des exemples de méthodes d'embedding qui utilisent le partitionnement de l'espace réel et la densité électronique de la DFT comme variable de base. L'embedding de la WFT dans la DFT a également été proposée [54, 55, 56, 57, 58], dans laquelle une méthode basée sur la WFT est (souvent) utilisée pour traiter les parties chimiquement pertinentes du système complet, et l'environnement est traité avec la DFT. La *Théorie de champ moyen dynamique* (dynamical mean-field theory - DMFT) [59, 60, 61, 62, 63, 64, 65, 66, 67] et la plus récente *théorie de l'embedding de la matrice de densité* (density-matrix embedding theory - DMET) [15, 16, 17, 68], qui ont été initialement appliquées à la physique de la matière condensée, fonctionnent avec une base orbitale locale. Ils utilisent la fonction de Green à un électron et la *matrice de densité réduite à un électron* (one-electron reduced density matrix theory - 1RDM), respectivement, comme variables

de base. Dans ce qui suit, la DMET, qui est pertinente par rapport à l'un des projets de ce doctorat, est présentée brièvement.

La théorie de l'embedding de la matrice de densité (DMET) a été introduite par Knizia et Chan en 2012, proposée comme une alternative statique (indépendante de la fréquence) à la DMFT pour décrire les systèmes de réseaux avec de fortes corrélations locales. L'approche générale de la DMET peut être décomposée en deux étapes:

1. Diviser le système à corps multiples complet en fragments locaux qui ne se chevauchent pas dans la base orbitale localisée et, pour chaque fragment, trouver les degrés de liberté effectifs *bain quantique* de l'environnement. L'espace fragment+bain à corps multiples forme le *cluster d'embedding* de taille réduite par rapport au système complet.

2. Résoudre une équation de Schrödinger effective du cluster précédemment obtenu. Utiliser la solution de l'état fondamental de cluster pour obtenir des contributions locales approximatives à l'énergie de l'état fondamental et à d'autres propriétés du système complet.

Dans les applications pratiques de DMET, les deux étapes impliquent inévitablement des approximations. Plus de détails sur la théorie exacte dans DMET, et la mise en œuvre de la stratégie d'embedding d'une seule impureté sont donnés dans le texte principal de cette thèse (Section 1.3, rédigée en anglais).

Chapitre 2: Systèmes modèles et Hamiltoniens modèles

Les Hamiltoniens modèles décrivent des versions simplifiées de systèmes "réels", ne contenant que les caractéristiques essentielles à la description du problème qui nous intéresse. Contrairement aux Hamiltoniens *ab initio* tels que l'Hamiltonien électronique dans Eq. (2), les Hamiltoniens modèles contiennent une poignée de paramètres réglables en tant qu'approximations des opérateurs cinétique, potentiel et de répulsion des électrons. Parfois, même des modèles très simples offrent des aperçus théoriques surprenants sur les propriétés des molécules et des matériaux. Deux des modèles utilisés dans cette thèse sont le modèle de Hubbard unidimensionnel [69, 70, 71, 72] et le dimère asymétrique de Hubbard. Pour ce dernier,

l'Hamiltonien est écrit dans la seconde quantification comme suit,

$$\hat{H}_{\text{Hdim}} \equiv -t \sum_{\sigma\in\{\uparrow,\downarrow\}} (\hat{c}^{\dagger}_{0\sigma}\hat{c}_{1\sigma} + \hat{c}^{\dagger}_{1\sigma}\hat{c}_{0\sigma}) + U\sum_{i=0}^{1}\hat{n}_{i\uparrow}\hat{n}_{i\downarrow} + \frac{\Delta v}{2}(\hat{n}_1 - \hat{n}_0), \tag{30}$$

où $\hat{c}^{\dagger}_{i\sigma}$ et $\hat{c}_{i\sigma}$ sont les opérateurs de création et d'annihilation pour le site i, $\hat{n}_{i\sigma} = \hat{c}^{\dagger}_{i\sigma}\hat{c}_{i\sigma}$, $\hat{n}_i = \hat{n}_{i\sigma} + \hat{n}_{i\sigma}$, t est le paramètre d'énergie cinétique, U est la répulsion électronique locale du site, et $(\Delta v \neq 0)$ est la différence de potentiel entre le site 1 et le site 0. Ces dernières années, le dimère de Hubbard a été le modèle de choix pour étudier les caractéristiques et les limites de la DFT et de la TD-DFT, ainsi que pour étudier de nouveaux concepts [73, 74, 75, 76, 77, 78].

Chapitre 3: Approches temporelles des excitations électroniques

Dans ce chapitre, nous nous intéressons aux méthodes dépendantes du temps pour étudier les états excités. Le deux de ces méthodes couramment utilisées pour les excitations électroniques sont la *théorie de la fonctionnelle de la densité dépendante du temps* (time-dependent density-functional theory - TD-DFT) qui est aujourd'hui la méthode de choix pour le calcul des excitations neutres dans les molécules et les solides [2, 79, 80], et la théorie des fonctions de Green (à plusieurs corps), qui est bien connue en physique. Les deux approches standard de la fonction de Green pour les excitations chargées et neutres sont respectivement la méthode GW et la méthode de l'équation de Bethe-Salpeter. Dans ce résumé, nous ne faisons qu'un bref survol des principaux aspects de la TD-DFT.

Théorie de la fonctionnelle de la densité

La TD-DFT, semblable à la DFT pour les états fondamentaux, repose sur une base rigoureuse connue sous le nom de théorème de Runge-Gross (RG) [1] qui établit les observables comme des fonctionnelles de la densité dépendant du temps. La plupart des applications pratiques de TD-DFT utilisées aujourd'hui sont mises en œuvre dans le régime de réponse linéaire (LR-TD-DFT). L'équation de travail de la LR-TD-DFT est l'équation de Casida [10, 2], qui est une équation aux valeurs propres généralisée qui se lit comme suit dans l'espace du produit occupé-virtuel

(ia, jb) des orbitales KS,

$$\begin{bmatrix} \mathbf{A}(\omega) & \mathbf{B}(\omega) \\ \mathbf{B}^*(\omega) & \mathbf{A}^*(\omega) \end{bmatrix} \begin{bmatrix} \mathbf{X}(\omega) \\ \mathbf{Y}(\omega) \end{bmatrix} = \omega \begin{bmatrix} -1 & 0 \\ 0 & 1 \end{bmatrix} \begin{bmatrix} \mathbf{X}(\omega) \\ \mathbf{Y}(\omega) \end{bmatrix}, \tag{31}$$

où les éléments des matrices $\mathbf{A}$ et $\mathbf{B}$ se lisent,

$$\begin{aligned} \mathbf{A}_{ia,jb}(\omega) &= \delta_{ij}\delta_{ab}(\varepsilon_a - \varepsilon_i) + \langle \varphi_i\varphi_b | f_{\text{Hxc}}(\omega) | \varphi_a\varphi_j \rangle, \\ \mathbf{B}_{ia,jb}(\omega) &= \langle \varphi_i\varphi_j | f_{\text{Hxc}}(\omega) | \varphi_a\varphi_b \rangle. \end{aligned} \tag{32}$$

où $f_{\text{Hxc}}(\omega)$ est le kernel de Hartree-échange-corrélation (Hxc). La taille de la matrice de l'équation de Casida est $(2 \times N_{occ} \times N_{virt})^2$. La présence de virtuels entraîne des coûts de calcul supplémentaires par rapport aux calculs KS-DFT de l'état fondamental. En outre, en raison de la dépendance en fréquence du noyau Hxc, il y a plus de solutions que la taille de la matrice ne le permet. Cependant, dans la plupart des applications pratiques, l'*approximation adiabatique* (adiabatic approximation - AA) est utilisée, dans laquelle la fonctionnelle de densité Hxc à l'état fondamental est utilisée à la place du kernel Hxc, qui est indépendant de la fréquence, c'est-à-dire $f_{\text{Hxc}}^{\text{AA}} = f_{\text{Hxc}}(\omega = 0)$. L'inconvénient majeur de l'AA est que les excitations multiples sont totalement absentes du spectre prédit. En outre, la LR-TD-DFT présente d'autres difficultés, telles que la modélisation des excitations de transfert de charge [81, 82, 83], et des intersections coniques [84, 85]. En ce qui concerne ces problèmes, la TGOK-DFT est proposée dans ce travail comme une méthode alternative pour décrire les excitations neutres, qui a la capacité de traiter des états multiples de manière équilibrée, avec les mêmes orbitales (contrairement à la LR-TD-DFT, qui est basée sur les orbitales KS-DFT de l'état fondamental).

Chapitre 4: Approches indépendantes du temps pour les excitations électroniques neutres

Les approches indépendantes du temps pour décrire les états excités sont surtout utilisées en chimie quantique. Une méthode très couramment utilisée est le *state-averaged CASSCF* (SA-CASSCF) [14], dans lequel l'énergie moyenne d'un ensemble de fonctions d'onde d'une symétrie spatiale et de spin donnée est optimisée, en utilisant le même ensemble d'orbitales. On obtient ainsi des états fondamentaux orthonormés et des états excités de basse énergie, ce qui est pratique pour traiter les (quasi-)dégénérescences. Cette méthode est adaptée à la description d'un

petit nombre d'états dans les molécules, par exemple à proximité d'intersections coniques ou de croisements évités, où une optimisation équilibrée des orbitales pour les états fondamentaux et excités est préférable (plutôt que d'utiliser des orbitales optimisées pour l'état fondamental). Au cours des dernières décennies, *la théorie de la fonctionnelle de la densité d'ensemble* (ensemble density-functional theory - eDFT) basée sur le principe variationnel *Theophilou-Gross-Oliveira-Kohn* (TGOK) [86, 87, 88, 89, 90] a été proposée comme une alternative peu coûteuse à d'autres méthodes bien établies pour décrire les états excités.

Théorie de la fonctionnelle de la densité d'ensemble des excitations neutres (TGOK-DFT)

La TGOK-DFT a été formulée à la fin des années 1980 par Gross, Oliveira et Kohn [88, 89, 90] et est une généralisation de l'équiensemble DFT de Theophilou [86, 87]. Contrairement à la KS-DFT, qui est une théorie de l'état fondamental, la TGOK-DFT peut décrire à la fois l'état fondamental et l'état excité (neutre). Dans ce contexte, la densité d'ensemble est utilisée comme variable de base (à la place de la densité de l'état fondamental). La base de la TGOK-DFT est le principe variationnel suivant (appelé TGOK) qui, pour des poids ordonnés $\mathtt{w}_I \geq \mathtt{w}_{I+1} \geq 0$, avec $I \geq 0$, se lit comme suit,

$$E^{\mathbf{w}} = \sum_I \mathtt{w}_I E_I \leq \sum_I \mathtt{w}_I \left\langle \tilde{\Psi}_I \middle| \hat{H} \middle| \tilde{\Psi}_I \right\rangle, \tag{33}$$

où $\left\{\tilde{\Psi}_I\right\}$ est un ensemble de fonctions d'onde d'essai orthonormées de N-électron, $\mathbf{w} = (\mathtt{w}_1, \mathtt{w}_2, \ldots)$ représente la collection de poids d'ensemble qui sont attribués aux états excités, et $E_I \equiv E_I^N$ sont les énergies de l'état fondamental ($I = 0$) et des états excités à N électrons ($I > 0$) $\left|\Psi_I^N\right\rangle$. Notez que la limite inférieure $E^{\mathbf{w}}$, qui est l'énergie exacte de l'ensemble, n'est pas une observable. Il s'agit simplement d'une quantité auxiliaire (artificielle) à partir de laquelle les propriétés d'intérêt, telles que l'énergie d'excitation, peuvent être extraites, comme suit,

$$\frac{\partial E^{\mathbf{w}}}{\partial \mathtt{w}_I} = E_I - E_0. \tag{34}$$

Dans la formulation DFT des ensembles TGOK, l'énergie de l'ensemble est obtenue

comme suit [89],

$$E^{\mathbf{w}} = \min_{n \to N} \left\{ F^{\mathbf{w}}[n] + \int \mathrm{d}\mathbf{r}\, v_{\mathrm{ext}}(\mathbf{r}) n(\mathbf{r}) \right\}, \tag{35}$$

où la minimisation est restreinte aux densités d'électrons de N, *i.e.*, $\int d\mathbf{r}\, n(\mathbf{r}) = N$, et la fonctionnelle de la densité universelle TGOK

$$F^{\mathbf{w}}[n] := \sum_I \mathtt{w}_I \left\langle \Psi_I^{\mathbf{w}}[n] | \hat{T} + \hat{W}_{\mathrm{ee}} | \Psi_I^{\mathbf{w}}[n] \right\rangle, \tag{36}$$

qui est évaluée à partir des fonctions propres de la fonctionnelle de la densité $\{\Psi_I^{\mathbf{w}}[n]\}$ qui remplissent la contrainte de la densité $\sum_I \mathtt{w}_I n_{\Psi_I^{\mathbf{w}}[n]}(\mathbf{r}) = n(\mathbf{r})$, est l'analogue pour les ensembles TGOK de la fonctionnelle universelle de Hohenberg–Kohn (voir Eq. (20)). Dans la formulation KS standard de TGOK-DFT [89], la fonctionnelle TGOK est divisée en fonctionelle cinétique sans interaction et le fonctionelle de Hartree-xc (Hxc), par analogie avec la KS-DFT classique:

$$F^{\mathbf{w}}[n] = T_{\mathrm{s}}^{\mathbf{w}}[n] + E_{\mathrm{Hxc}}^{\mathbf{w}}[n]. \tag{37}$$

De même que pour la KS-DFT, il est possible de dériver un ensemble d'équations TGOK-DFT autocohérentes,

$$\left(-\frac{\nabla_{\mathbf{r}}^2}{2} + v_{\mathrm{ext}}(\mathbf{r}) + v_{\mathrm{Hxc}}^{\mathbf{w}}[n^{\mathbf{w}}](\mathbf{r}) \right) \varphi_p^{\mathbf{w}}(\mathbf{r}) = \varepsilon_p^{\mathbf{w}} \varphi_p^{\mathbf{w}}(\mathbf{r}), \tag{38}$$

où

$$v_{\mathrm{Hxc}}^{\mathbf{w}}[n](\mathbf{r}) = \frac{\delta E_{\mathrm{Hxc}}^{\mathbf{w}}[n]}{\delta n(\mathbf{r})} \tag{39}$$

est le potentiel de la fonctionnelle de la densité Hxc de l'ensemble. Dans la théorie exacte, les orbitales KS de l'ensemble reproduisent la densité exacte de l'ensemble,

$$n^{\mathbf{w}}(\mathbf{r}) = \sum_I \mathtt{w}_I n_{\Psi_I}(\mathbf{r}). \tag{40}$$

Chapitre 5: Théorie de la fonctionnelle de la densité d'ensemble des excitations chargées

L'ensemble *N-centré* (N-centered ensemble) [91] peut être considéré comme la version "grand canonique" des ensembles TGOK à l'état fondamental. Il est

construit à partir des états fondamentaux de M-électrons où les trois valeurs possibles de $M \in \{N-1, N, N+1\}$ sont centrées sur N, (d'où le nom "N-centré".) L'énergie d'ensemble N-centré exacte est définie comme suit [91],

$$E_0^{\boldsymbol{\xi}} = \xi_- E_0^{N-1} + \xi_+ E_0^{N+1} + \left(1 - \xi_- \frac{N-1}{N} - \xi_+ \frac{N+1}{N}\right) E_0^N, \tag{41}$$

où les deux poids d'ensemble N-centré ξ_- et ξ_+, qui décrivent l'enlèvement/addition d'un électron du/au système N-électron respectivement, sont rassemblés dans

$$\boldsymbol{\xi} \equiv (\xi_-, \xi_+)\,. \tag{42}$$

A partir de l'énergie d'ensemble N-centré, nous pouvons extraire la gap fondamentale comme suit,

$$\frac{\partial E_0^{\boldsymbol{\xi}}}{\partial \xi_-} + \frac{\partial E_0^{\boldsymbol{\xi}}}{\partial \xi_+} = E_0^{N-1} + E_0^{N+1} - 2E_0^N = E_{\text{gap}}^{\text{fund}}. \tag{43}$$

Nous pouvons également extraire les énergies individuelles cationiques, anioniques et neutres, respectivement, comme suit,

$$E_0^{N-1} = \frac{N-1}{N}\left(E_0^{\boldsymbol{\xi}} - \xi_+ \frac{\partial E_0^{\boldsymbol{\xi}}}{\partial \xi_+} + \left(\frac{N}{N-1} - \xi_-\right)\frac{\partial E_0^{\boldsymbol{\xi}}}{\partial \xi_-}\right), \tag{44}$$

$$E_0^{N+1} = \frac{N+1}{N}\left(E_0^{\boldsymbol{\xi}} - \xi_- \frac{\partial E_0^{\boldsymbol{\xi}}}{\partial \xi_-} + \left(\frac{N}{N+1} - \xi_+\right)\frac{\partial E_0^{\boldsymbol{\xi}}}{\partial \xi_+}\right), \tag{45}$$

and

$$E_0^N = E_0^{\boldsymbol{\xi}} - \xi_- \frac{\partial E_0^{\boldsymbol{\xi}}}{\partial \xi_-} - \xi_+ \frac{\partial E_0^{\boldsymbol{\xi}}}{\partial \xi_+}. \tag{46}$$

À partir des équations (44)–(46), nous pouvons obtenir des théorèmes exacts sur le potentiel d'ionisation $I_0^N = E_0^{N-1} - E_0^N$ et l'affinité $A_0^N = E_0^N - E_0^{N+1}$ des électrons. Cela se fait dans le formalisme DFT des ensembles N-centrés, qui peut être dérivé en complète analogie avec TGOK-DFT.

Chapitre 6: Énergies d'échange et de corrélation dans la DFT d'ensemble

Le présent chapitre se concentre sur la fonctionelle Hxc de l'ensemble, qui est traitée comme une somme des fonctions d'échange et de corrélation de Hartree de l'ensemble,

$$E_{\text{Hxc}}^{\mathbf{w}}[n] \;\; = E_{\text{Hx}}^{\mathbf{w}}[n] + E_{\text{c}}^{\mathbf{w}}[n]. \tag{47}$$

Le contenu de ce chapitre, y compris les résultats numériques, s'inspire principalement des sections 4 et 5 du chapitre du livre intitulé "Ensemble density functional theory of neutral and charged excitations" (voir Ref. [92]). Dans ce résumé, seuls les aspects de l'énergie de corrélation d'ensemble, $E_{\rm c}^{\mathbf{w}}[n]$, et les résultats numériques correspondants sur le dimère asymétrique de Hubbard sont discutés. Par commodité, nous continuons à nous concentrer sur les ensembles TGOK, mais la discussion s'applique à d'autres types d'ensembles comme, par exemple, les ensembles N-centrés [91] ou les ensembles thermiques [93, 94, 95, 78].

À notre connaissance, très peu de travaux ont abordé la construction de DFAs de corrélation d'ensemble dépendant du poids à partir des premiers principes. Nous nous concentrons ci-après sur l'application de deux DFA courants qui reposent sur le recyclage des fonctions de densité de l'état fondamental pour la description de l'énergie de corrélation d'ensemble. Nous étudions également le point subtil récemment discuté dans la corrélation d'ensemble, à savoir la présence de *corrélations induites par l'état* (state-driven - SD correlations) et de *corrélations induites par la densité* (density-driven - DD correlations) [96, 97], et examinons une possibilité des décompositions SD/DD. Les deux DFA de l'état fondamental pour les énergies de corrélation et le concept de décomposition SD/DD sont étudiés dans le modèle du dimère de asymétrique de Hubbard. Dans ce système modèle simple, les énergies de corrélation exactes (deux électrons et singulets) du bi-ensemble de corrélation fonctionnelle de densité $E_{\rm c}^{\mathbf{w}}(n)$ peuvent être évaluées par maximisation de Lieb [98, 76] à partir des expressions analytiques suivantes pour les énergies d'interaction [78, 99, 100] :

$$E_I(\Delta v) = \frac{2U}{3} + \frac{2r}{3}\cos\left(\theta + \frac{2\pi}{3}(I+1)\right), \;\; I = 0, 1, \tag{48}$$

où

$$r = \sqrt{3(4t^2 + \Delta v^2) + U^2} \tag{49}$$

et

$$\theta = \frac{1}{3}\arccos\left[\frac{9U(\Delta v^2 \, - \, 2t^2) \, - \, U^3}{r^3}\right]. \tag{50}$$

Les densités exactes de l'état fondamental et de l'état excité sont alors obtenues à partir du théorème de Hellmann–Feynman comme suit,

$$n_{\Psi_I} \; = \; 1 \; - \; \frac{\partial E_I(\Delta v)}{\partial \Delta v}, \tag{51}$$

et l'équation polynomiale cubique que les énergies remplissent (voir l'Appendix de la Ref. [98]). Par convention, n_{Ψ_I} est la densité (l'occupation) sur le site 0 du dimère de Hubbard (voir Eq. (30)). La densité bi-ensemble résultante se lit comme $n^{\mathtt{w}} = (1-\mathtt{w})n_{\Psi_0} + \mathtt{w}\, n_{\Psi_1}$. Dans ce modèle, l'énergie de corrélation exacte du bi-ensemble DD se lit explicitement comme suit,

$$\begin{aligned} E_{\rm c}^{\mathtt{w},\rm DD}(n^{\mathtt{w}}) = &-\mathtt{w}(n^{\mathtt{w}}-1)(n_{\Psi_1}-1) \\ &\times\left[\frac{2t}{\sqrt{(1-\mathtt{w})^2-(1-n^{\mathtt{w}})^2}} + \frac{U(1+\mathtt{w})}{(1-\mathtt{w})^2}\right]. \end{aligned} \tag{52}$$

Par conséquent, l'énergie de corrélation SD est calculée comme $E_{\rm c}^{\mathtt{w},\rm SD}(n^{\mathtt{w}}) = E_{\rm c}^{\mathtt{w}}(n^{\mathtt{w}}) - E_{\rm c}^{\mathtt{w},\rm DD}(n^{\mathtt{w}})$. Les deux DFA que nous testons sont les suivants: Une description de l'énergie de corrélation d'ensemble utilisant la fonctionelle d'état fondamental (indépendante du poids) (GS-ec) [101, 98],

$$E_{\rm c}^{\mathtt{w}}(n^{\mathtt{w}}) \overset{\rm GS-ec}{\approx} E_{\rm c}(n^{\mathtt{w}}), \tag{53}$$

où $E_{\rm c}(n) = E_{\rm c}^{\mathtt{w}=0}(n)$, et l'approximation GS-ic suivante, qui évalue l'énergie de corrélation à l'état fondamental pour chaque état KS individuel de l'ensemble $\Phi_I^{\mathtt{w}}$,

$$\begin{aligned} E_{\rm c}^{\mathtt{w}}(n^{\mathtt{w}}) &\overset{\rm GS-ic}{\approx} (1-\mathtt{w})E_{\rm c}(n_{\Phi_0^{\mathtt{w}}}) + \mathtt{w}E_{\rm c}(n_{\Phi_1^{\mathtt{w}}}) \\ &= (1-\mathtt{w})E_{\rm c}(n_{\Phi_0^{\mathtt{w}}}) + \mathtt{w}E_{\rm c}(n=1). \end{aligned} \tag{54}$$

Dans la suite, le potentiel local sera fixé. Il est alors analogue au potentiel externe des calculs *ab initio*, d'où la notation $\Delta v = \Delta v_{\rm ext}$.

La Figure 1 montre la dépendance en poids de l'énergie de corrélation d'ensemble (et ses composantes SD et DD), ainsi que les deux DFAs testés (Gs-ec et Gs-ic), du dimère de Hubbard pour différents régimes d'asymétrie et de corrélation. Une caractéristique particulière peut être observée: lorsque le modèle passe d'un régime symétrique à un régime asymétrique et est fortement corrélé $\Delta v_{\rm ext} \ll U$, ou pour des régimes d'asymétrie et de corrélation comparables avec $\Delta v_{\rm ext} \approx U$, les corrélations DD deviennent importantes et négatives, tandis que les corrélations SD évoluent dans la direction opposée, en particulier dans le cas de l'équiensemble ($\mathtt{w} = 1/2$), parfois utilisé dans les calculs. La valeur élevée des corrélations SD et DD par rapport à l'énergie de corrélation de l'ensemble n'est clairement pas favorable au développement des approximations de la fonctionnelle de la densité. En outre, ce

projet a mis en évidence la difficulté de trouver un point de départ théoriquement rigoureux et utile pour le développement d'approximations pour la corrélation dans la eDFT. Bien que les corrélations DD doivent clairement être prises en compte, le recyclage des approximations des fonctionnelles densité de l'état fondamental pourrait être une direction à envisager. Cela est soutenu par l'observation de la Figure 1, selon laquelle dans le cas asymétrique $\Delta v_{\text{ext}} = U$, les approximations standard GS-ic et GS-ec donnent des énergies de corrélation d'ensemble qui sont du même ordre de grandeur que les énergies de corrélation exactes, contrairement aux énergies de corrélation SD et DD.

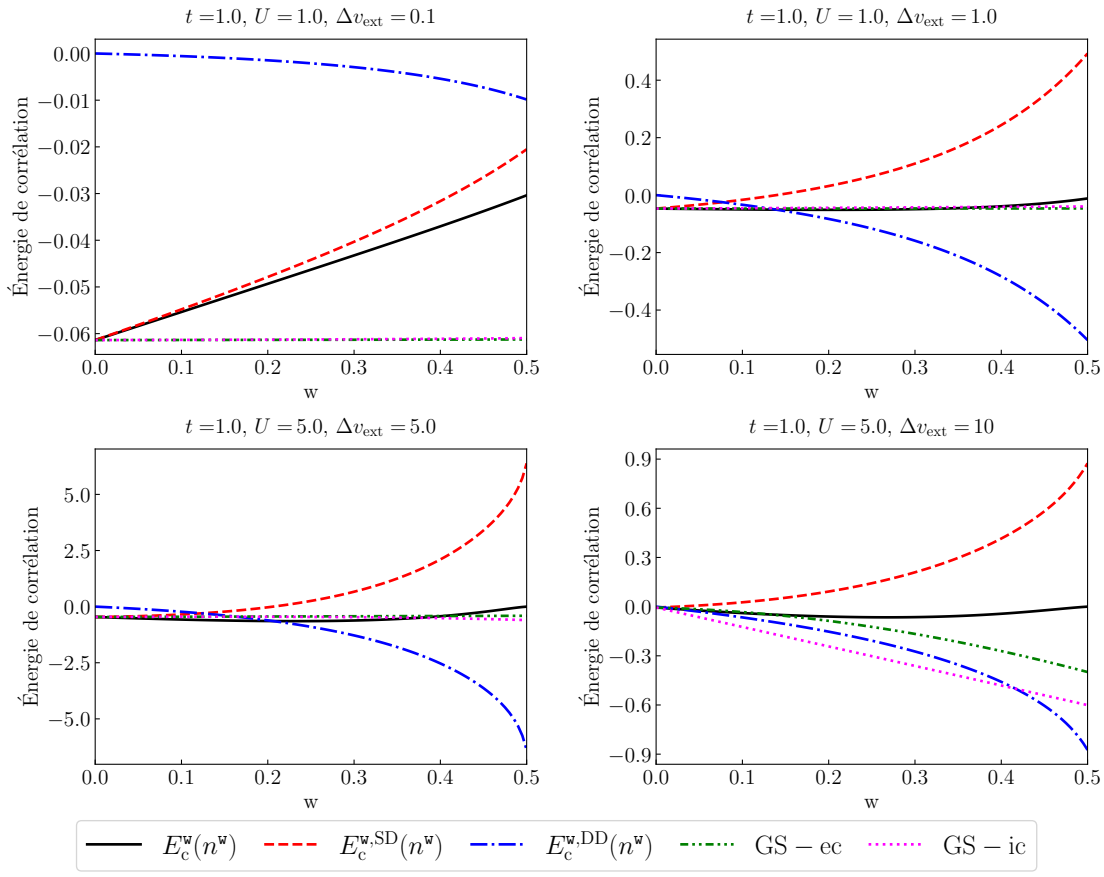

Figure 1: Décomposition SD/DD exacte de l'énergie de corrélation de l'ensemble en fonction du poids du bi-ensemble $\mathtt{w}$ dans différents régimes d'asymétrie et de corrélation. Une comparaison est faite avec les énergies de corrélation d'ensemble approximatives GS-ec et GS-ic, à des fins d'analyse. Voir le texte pour plus de détails.

Chapitre 7: Dérivées discontinues dans la DFT d'ensemble pour les excitations électroniques neutres : Une perspective des ensembles N-centrés

Dans ce chapitre, nous exploitons la ressemblance entre la DFT d'ensemble N-centré [91] et la TGOK-DFT [86, 87, 88, 89, 90] afin de fournir une description en principe exacte de la densité fonctionnelle d'ensemble des états excités ionisés. Le formalisme d'ensemble qui en résulte, où les états excités neutres sont incorporés dans un ensemble N-centré régulier, sera appelé *formalisme d'ensemble N-centré étendu* (extended N-centered ensemble formalism). Nous proposons de combiner les ensembles TGOK et les ensembles N-centrés de la manière suivante,

$$\begin{aligned}\hat{\Gamma}^{\boldsymbol{\xi}} \overset{\text{TGOK}+Nc}{=} &\left(1 - \sum_{\nu>0} \frac{N_\nu}{N} \xi_\nu\right) |\Psi_0\rangle\langle\Psi_0| \\ &+ \sum_{\nu>0} \xi_\nu \, |\Psi_\nu\rangle\langle\Psi_\nu| \,,\end{aligned} \tag{55}$$

où $\Psi_0 \equiv \Psi_0^N$ est l'état fondamental de référence à N électrons auquel tous les processus d'excitation possibles (neutres et chargés, y compris les excitations à électrons multiples) peuvent s'appliquer. Par construction, la densité de l'ensemble N-centré étendu ci-dessus s'intègre toujours au nombre d'électrons N, comme en TGOK-DFT. Le fait que le nombre net d'électrons dans l'ensemble ne varie pas avec les poids de l'ensemble, contrairement à la DFT pour les nombres fractionnaires d'électrons (PPLB) [102], est absolument central dans la description des discontinuités de la dérivée xc en tant que comme des dérivées de poids d'ensemble [103, 92]. Grâce à ce formalisme, il est possible d'obtenir une quantification exacte des énergies orbitales KS. Pour le démontrer, nous appliquons le formalisme général à un type particulier d'ensemble N-centré étendu, composé d'états d'électrons N fondamentaux et excités (avec des poids ξ_ν^N) et l'état fondamental à $(N-1)$ électrons (avec poids $\xi_- := \xi_0^{N-1}$), *i.e.*,

$$\boldsymbol{\xi} \equiv \left(\left\{\xi_\nu^N\right\}_{\nu>0}, \xi_-\right). \tag{56}$$

Les potentiels d'ionisation exacts à l'état fondamental et à l'état excité sont les suivants (sans perte de généralité, nous nous concentrons sur les excitations d'un

seul électron),

$$
\begin{aligned}
I_\nu^N \underset{\nu\geq 0}{=} -\varepsilon_{N+\nu}^{\boldsymbol{\xi}} - \frac{1}{N}\left(E_{\mathrm{Hxc}}^{\boldsymbol{\xi}}[n^{\boldsymbol{\xi}}] - \int d\mathbf{r}\, v_{\mathrm{Hxc}}^{\boldsymbol{\xi}}(\mathbf{r}) n^{\boldsymbol{\xi}}(\mathbf{r})\right) \\
+ \left(1+\frac{\xi_-}{N}\right)\left.\frac{\partial E_{\mathrm{Hxc}}^{\boldsymbol{\xi}}[n]}{\partial \xi_-}\right|_{n=n^{\boldsymbol{\xi}}} \\
+ \sum_{\lambda>0}\left(\frac{\xi_\lambda^N}{N} - \delta_{\lambda\nu}\right)\left.\frac{\partial E_{\mathrm{Hxc}}^{\boldsymbol{\xi}}[n]}{\partial \xi_\lambda^N}\right|_{n=n^{\boldsymbol{\xi}}}.
\end{aligned}
\tag{57}
$$

Si nous choisissons dans l'équation ci-dessus de faire l'identification suivante $I_\nu^N = -\varepsilon_{N+\nu}^{\boldsymbol{\xi}}$, (exactification du théorème de Koopmans), le potentiel Hxc de l'ensemble N-centré étendu, $v_{\mathrm{Hxc}}^{\boldsymbol{\xi}}$, sera *uniquement* défini pour toutes les valeurs des poids de l'ensemble $\boldsymbol{\xi}$. Une conséquence essentielle de l'imposition d'une telle contrainte sur le potentiel Hxc de l'ensemble est l'apparition de la discontinuité de la dérivée pour les excitations neutres - une caractéristique qui a été mise en évidence à l'origine par Levy [104]. Il se lit comme suit,

$$
\begin{aligned}
&\int \frac{d\mathbf{r}}{N}\left(v_{\mathrm{Hxc}}^{\boldsymbol{\xi}_\nu^N\to\mathbf{0}^+}(\mathbf{r}) - v_{\mathrm{Hxc}}^{\boldsymbol{\xi}_\nu^N=\mathbf{0}}(\mathbf{r})\right) n_{\Psi_0^N}(\mathbf{r}) \\
&= \left.\frac{\partial E_{\mathrm{Hxc}}^{\boldsymbol{\xi}_\nu^N}[n_{\Psi_0^N}]}{\partial \xi_\nu^N}\right|_{\boldsymbol{\xi}_\nu^N=0},
\end{aligned}
\tag{58}
$$

où

$$
\boldsymbol{\xi}_\nu^N \underset{notation}{\equiv} \left(\boldsymbol{\xi}_\nu^N, 0, 0, \ldots, 0, \xi_- \to 0^+\right). \tag{59}
$$

Cette procédure d'ajustement alternative et explicite du potentiel Hxc ne repose pas sur le comportement asymptotique de la densité [104, 103, 92], ce qui signifie qu'elle n'est pas seulement applicable aux systèmes moléculaires *ab initio*, mais qu'elle devrait également être transférable à des modèles d'un réseau de taille finie ou à des systèmes étendus, par exemple. Nous montrons dans la Figure 2 ci-dessous que dans ce formalisme, la discontinuité de la dérivée est également observée dans le dimère asymétrique de Hubbard.

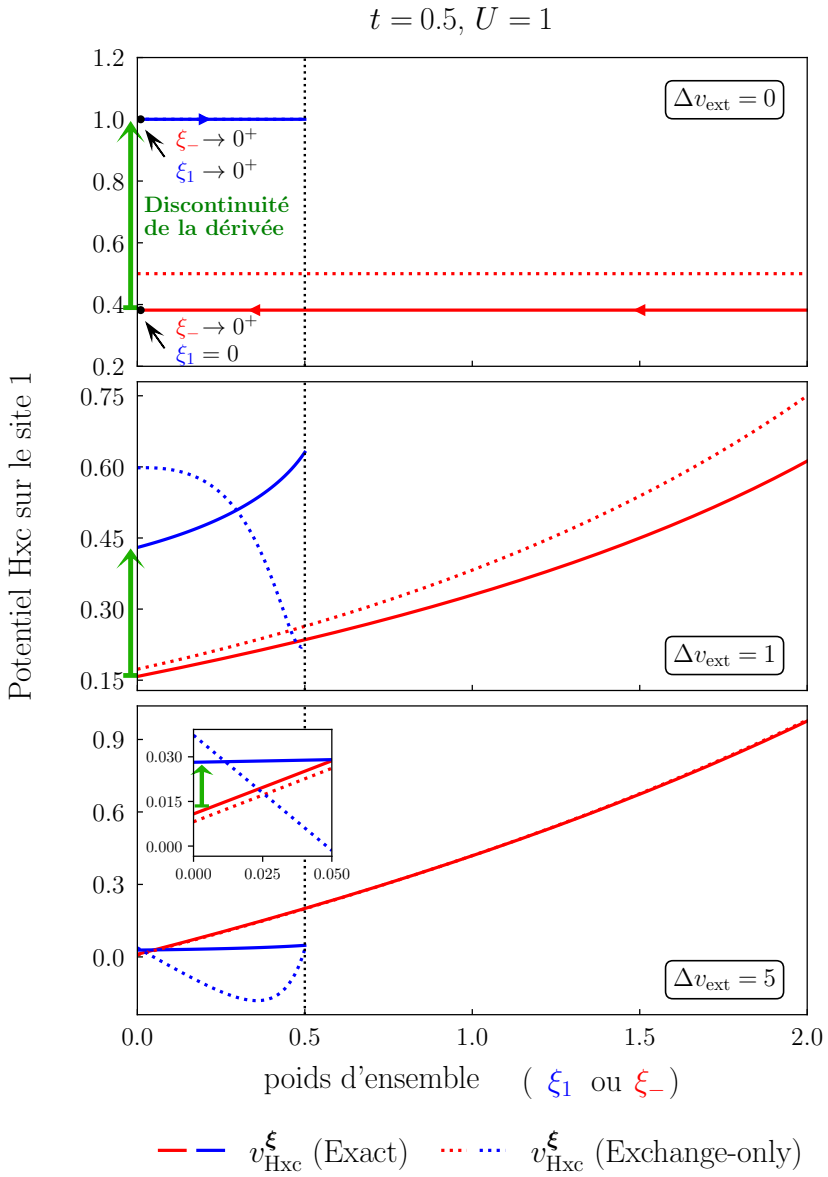

Figure 2: Variation du potentiel Hxc exact de l'ensemble N-centré étendu, et de son approximation exchange-only (qui consiste à utiliser $E^{\boldsymbol{\xi}}_{\text{Hx}}(n)$ à la place de la fonctionnelle Hxc complète dans Eq. (57)), avec les poids d'ensemble dans le dimère de Hubbard avec différentes asymétries. Pour chaque cas, la discontinuité de la dérivée est mise en évidence par la flèche verte aux valeurs limites des poids d'ensemble. La ligne noire verticale (en pointillés) à $\xi_1 = 1/2$ indique la position de l'equiensemble TGOK.

Chapitre 8: Stratégie d'embedding quantique pour les ensembles d'états électroniques

Dans ce chapitre, nous présentons une stratégie d'embedding pour décrire les excitations neutres des molécules, où l'objectif n'est pas de calculer le spectre entier mais un petit nombre d'excitations de basse énergie. Pour cette raison, nous adoptons le formalisme des ensembles TGOK, qui permet un traitement systématique et équilibré de tous les états individuels pour les excitations d'intérêt. Par analogie avec la théorie de l'embedding de la matrice de densité (density matrix embedding theory - DMET) [15, 16] et la Householder transformed density matrix functional embedding theory (Ht-DMFET) [105], il s'avère que nous pouvons concevoir un cluster d'embedding adapté à plusieurs états, en utilisant des transformations de Householder successives sur l'ensemble TGOK de champ moyen.

Nous nous intéressons à la description de l'excitation singulet la plus basse pour un système. Comme point de départ, nous choisissons une description du champ moyen (ou sans interaction) du système complet, où l'idée est de trouver une base appropriée de spin-orbitales qui offre un cluster d'embedding pour l'ensemble TGOK d'états fondamentaux et états excités singuliers,

$$\hat{\Gamma}^{\xi} = (1-\xi)\left|\Phi_0\right\rangle\!\left\langle\Phi_0\right| + \xi\left|{}^1\Phi_h^l\right\rangle\!\left\langle{}^1\Phi_h^l\right|, \tag{60}$$

où $0 \leq \xi \leq 1/2$ tel que le principe variationnel de TGOK est respecté, $|\Phi_0\rangle$ est le déterminant de Slater de l'état fondamental du champ moyen (HF ou KS), et $|{}^1\Phi_h^l\rangle$ est la configuration de l'état excité du champ moyen avec l'excitation simple HOMO $\rightarrow$LUMO basée sur $|\Phi_0\rangle$. Il est possible de montrer qu'en appliquant des transformations de Householder successives [18, 19] sur la 1RDM de l'ensemble (voir Eq. (60)), $\gamma^{\xi}_{ij\sigma} = \mathrm{Tr}\left[\hat{\Gamma}^{\xi}\hat{c}^{\dagger}_{i\sigma}\hat{c}_{j\sigma}\right] = (1-\xi)\gamma^{\Phi_0}_{ij\sigma} + \xi\gamma^{{}^1\Phi_h^l}_{ij\sigma}$ dans la base spin-orbitale locale, nous obtenons une base spin-orbitale dans laquelle la 1RDM de l'ensemble est transformée en une structure bloc-diagonale, un bloc étant le cluster avec une impureté et trois spin-orbitales de bain, et un autre étant l'environnement de ce cluster. Ce résultat est représenté schématiquement dans la Figure 3, qui le compare à l'embedding d'un seul état du DMET standard (et du Ht-DMFET).

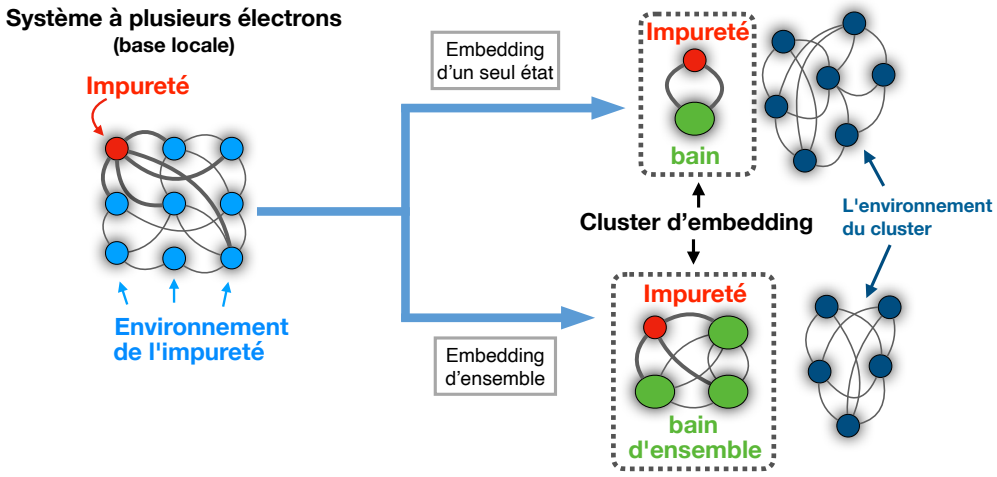

Figure 3: Comparaison des clusters d'embedding pour les états uniques et les ensembles à deux états.

L'apparition du cluster d'embedding pour les ensembles a été exploitée dans la conception d'une stratégie d'embedding à deux états pour décrire l'état fondamental et le premier état excité (singulet). L'essence de notre stratégie est que les approximations locales pour ces deux états individuels sont obtenues à partir de l'Hamiltonien d'embedding suivant,

$$\hat{\mathcal{H}}^{\text{ens}-\text{emb.}} = \hat{\mathcal{Q}}\hat{H}\hat{\mathcal{Q}} - \mu_1\hat{n}_1, \tag{61}$$

où l'opérateur de projection $\hat{\mathcal{Q}}$ s'étend sur l'espace de Fock de l'impureté + trois spin-orbitales de bain d'ensemble (voir Figure 3), et μ_1 est le potentiel chimique sur l'impureté (précisément, site 1), qui est ajustée pour optimiser le nombre d'électrons selon la fonction de coût suivante,

$$\text{CF}(\{\mu_i\}) = \sum_{I=0,1}\left(\sum_{i=1}^{L}\langle\Psi_I^{\mathcal{C}_i}(\mu_i)|\hat{n}_i|\Psi_I^{\mathcal{C}_i}(\mu_i)\rangle - N\right)^2, \tag{62}$$

où les potentiels chimiques $\{\mu_i\}_{1\leq i\leq L}$ sont optimisés pour chaque site dans les calculs d'embedding séparés. Ensuite, les fonctions d'onde du cluster d'embedding $\{\Psi_I^{\mathcal{C}_i}\}$ sont utilisées pour construire les approximations des énergies globales, selon l'approche appelée *partitionnement démocratique* (democratic partitioning) [17].

Cette stratégie a été appliquée à trois systèmes simples, l'un étant un système *ab initio*, et les deux autres des systèmes modèles. Nous montrons dans ce résumé les résultats du système *ab initio* de dimères d'hydrogène (utilisé à l'origine par Tran *et al.* [106]). La Figure 4 montre les résultats exacts (FCI) et d'embedding pour l'état fondamental et le premier état excité (singulet) du système de dimères d'hydrogène le long de la courbe de dissociation des dimères. Les résultats FCI ont été obtenus avec le logiciel python QuantNBody [107]. Les résultats de l'embedding montrent un très bon accord avec les résultats FCI pour toutes les valeurs de la distance intermoléculaire considérées. D'une manière similaire que pour l'embedding *single-shot* de DMET [17], nous avons également effectué des calculs d'embedding avec ajustement du potentiel chimique sur chaque atome d'hydrogène, afin d'obtenir le nombre (globalement) correct d'électrons dans l'état fondamental et l'état excité. Il s'avère que la correction du potentiel chimique a un effet négligeable sur les résultats, probablement parce que le système est homoatomique.

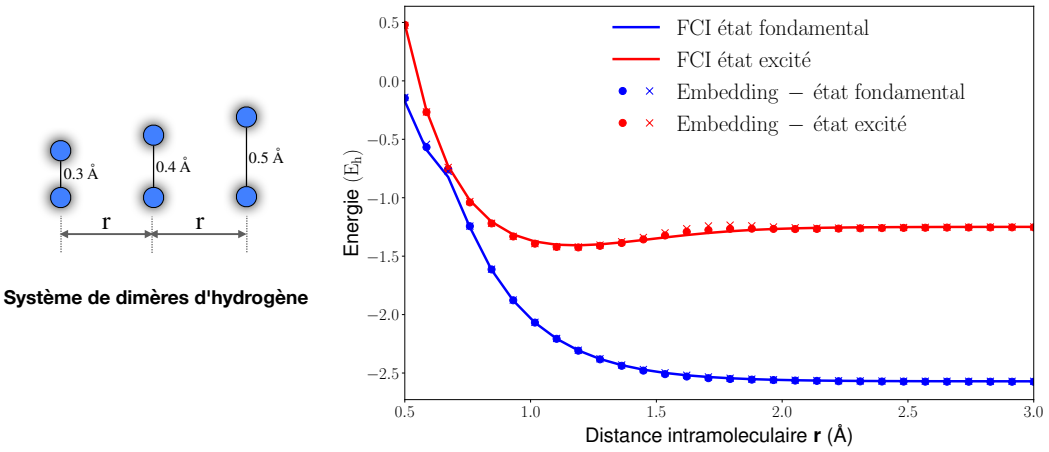

Figure 4: À gauche: représentation une schématique du système *ab initio* de dimères d'hydrogène de Tran *et al.* [106]. À droite: les courbes de dissociation de l'état fondamental et du premier état excité singulet de FCI (lignes bleues et rouges, respectivement), et résultats de l'embedding correspondants (marqueurs bleus et rouges, respectivement) pour le même modèle. Les résultats de l'embedding sont représentés avec et sans ajustement du potentiel chimique (marqueurs en points (•) et en croix (×), respectivement).

Conclusions de la thèse

Dans ce manuscrit, nous avons discuté en détail des excitations électroniques et présenté différentes méthodes standard utilisées pour décrire les excitations neutres et chargées. Le travail central de cette thèse a été la continuation du développement de formalisme d'ensemble indépendant du temps, qui est une alternative à d'autres formalismes bien établis en chimie quantique et en physique de la matière condensée. Nous avons discuté de divers aspects formels et pratiques particuliers à la théorie de la fonctionelle de la densité d'ensemble (ensemble density-functional theory - eDFT), et nous avons fait de nouveaux développements théoriques. Bien que la DFT d'ensemble présente un grand potentiel dans la description de divers types d'excitations et qu'elle soit capable de surmonter certaines limitations d'autres approches plus standard, telles que les méthodes de réponse linéaire, il reste encore de nombreux défis à relever avant que le formalisme d'ensemble n'engendre des méthodes pratiques largement utilisées.

Introduction

The world that surrounds us, consists of many different objects, which have well-defined structure with volume and boundaries. At least that is how we perceive them by our senses. They also possess continuously varying amounts of energy (e.g. kinetic and potential energy). This is not the case for objects at a small enough size scale, such as the order of ångstrom (equal to 10^{-10} m), with which we are concerned in this thesis. At such scales, classical physics breaks down, and quantum effects take precedence. The latter are theoretically described by quantum mechanics, which emerged in the early decades of the 20th century. Among many other strange things occurring in the quantum world, we find that small systems, such as molecules, can only have discrete values of energy, so-called energy levels. For each energy level there is an associated stationary state, which may be stable with time or not. Assuming we are dealing with an isolated system, the state of that system with the lowest energy is called the ground state, while those with higher energies are called excited states. Exciting the system into a higher-energy state requires input of the right amount of energy from an outside source, such as heat and electromagnetic radiation. Understanding how the system reacts upon excitation is of great interest in many branches of science that make use of quantum theory, such as photochemistry and spectroscopy, but also for designing new materials.

In this thesis we aim at pushing further the theoretical development of the ensemble density functional formalism for describing electronic excitations. As we will discuss shortly, describing electronic ground states is already a difficult task, since we have to solve the interacting many-electron problem. For most practical purposes, one has to develop clever approximations to the exact solution that reduce computational costs, without compromising too much the accuracy of results. We should reasonably expect that dealing with excited states will be even more challenging.

Nowadays, electronic excitations are most commonly tackled with response methods, such as the *time-dependent density-functional theory* (TD-DFT) [1, 2] and methods, based on many-body Green's functions [3, 4, 5, 6, 7, 8, 9], which are very well-known in condensed-matter physics. The linear-response TD-DFT method with the Casida equation [10] has proven to be very successful in the treatment of neutral excitations in molecules and materials. Some limitations of linear-response TD-DFT are the single-reference description, which is insufficient for situations with (near-)degeneracies, such as conical intersections between the ground state and the excited states [2] in molecules, and with its commonly used adiabatic approximation, the lack of double and higher excitations. Furthermore, solving the Casida equation entails a moderate computational cost, which makes the method more expensive than the regular Kohn-Sham DFT [11]. The Green's function formalism has been successful in describing charged, but also neutral excitations with the GW method [3, 4, 5, 6], and the *Bethe-Salpeter equation* (BSE) [7, 8], respectively. These methods are also of moderate computational cost (in their simplest implementations), are not routinely used in quantum chemistry, although recently they have attracted increasing interest in this respect [12]. The commonly used methods in quantum chemistry are the multiconfigurational wavefunction-based methods, such as the *complete active space self-consistent field* (CASSCF) method [13], or its *state-averaged* version (SA-CASSCF) [14], which are used for describing low-lying states in molecules. Although very accurate, these methods require a lot of user experience, and are too expensive to be applicable to large molecules. As a way of dealing with computational costs of obtaining accurate descriptions of many-electron wavefunctions, *quantum embedding* (QE) methods, which use combinations of different approaches, have been attracting interest in recent decades. An example of the latter, which is also used in this thesis, is *density matrix embedding theory* (DMET) [15, 16, 17].

In the present thesis, we turn our attention to the formalism of *ensemble density functional theory* (eDFT), which has been gaining increasing interest over last decades as a low-cost alternative method for treatment of electronic excitations. The first eDFT developed was the *Theophilou-Gross-Oliveira-Kohn* DFT (TGOK-DFT) [86, 87, 88, 90, 89] for neutral excitations. Its extension to charged excitations is the N-centered eDFT [91] by Senjean and Fromager, which is also an alternative

approach to the traditional *Perdew-Parr-Levy-Balduz* (PPLB) DFT for charged excitations [102]. The appealing feature of eDFT methods is that the computational cost is essentially the same as that of KS-DFT for ground states. However, the challenging aspect is now designing density-functional approximations (DFAs) for ensemble exchange-correlation (xc) functionals, which depend both on electron density and ensemble weights of the excitations of interest. We will discuss various formal and practical aspects of ensemble DFT, and development of approximations, throughout Chapters 4 to 8.

This thesis is organized as follows. In Chapter 1, we review the basics of the electronic structure problem, and all the standard methods that are nowadays used in electronic structure theory for ground states, and briefly review quantum embedding methods, which are gaining increasing interest in recent years. We begin in Section 1.1 with reviewing the standard wavefunction methods in quantum chemistry, such as the *Hartree-Fock* (HF) method, and the *configuration interaction* (CI) method, as well as multiconfigurational methods. Then, in Section 1.2, we switch to *density-functional theory* (DFT), where we discuss exact DFT, the Kohn-Sham approach (KS-DFT), and mention the most commonly used *density-functional approximations* (DFAs). The chapter concludes with Section 1.3, where we provide a summary of some quantum embedding methods used in chemistry and condensed-matter physics, and discuss density-matrix embedding theory (DMET) in more detail. The latter is a key ingredient in one of the projects of this thesis, which is presented in Chapter 8.

In Chapter 2, we briefly discuss about model systems, and introduce the two models that are used throughout this PhD thesis, i.e. the one-dimensional Hubbard model [69, 70, 71, 72], and the asymmetric Hubbard dimer [73, 74, 75, 76, 77, 78].

In Chapter 3, we turn our attention to excited states. This chapter is reserved for time-dependent methods for describing electronic excitations. In Section 3.1, we review linear response TD-DFT, deriving key equations, and discussing the features and challenges of this method in its common implementation with the so-called Casida equation. Following that, in Section 3.2, we introduce the theory of many-body Green's functions, and review the GW method for charged excitations, and the Bethe-Salpeter equation method for neutral excitations.

Chapter 4 is reserved for time-independent methods for describing neutral excitations. In Section 4.1, we provide a summary of the wavefunction-based and DFT-based time-independent methods with applications in quantum chemistry. In Section 4.2, we introduce the formal aspects of TGOK ensemble density functional theory (TGOK-DFT) for neutral excitations, and derive key equations for extracting the neutral excitation energies in the context of ensemble formalism and its density-functionalization.

In Chapter 5, the N-centered ensemble DFT is presented, which is a generalization of TGOK-DFT to charged excitations. We discuss extensively about the ionization potential and affinity theorems, and the fundamental gap problem, all of which pose a challenge in DFT. In light of the topic of this chapter, we also introduce the traditional Perdew-Parr-Levy-Balduz (PPLB) DFT approach for charged excitations, where describing the fundamental gap entails the knowledge of derivative discontinuity of the *exchange-correlation* (xc) density functional in PPLB. Then, in Section 5.3, we relate the derivative discontinuity to the ensemble weight derivative of the xc functional for N-centered ensembles, and in Section 5.4, we present a way to suppress the derivative discontinuity within the context of N-centered eDFT.

In Chapter 6, we return to discussing the TGOK-DFT, this time from a practical point of view. The goal of this chapter is to present different approaches for designing DFAs for the ensemble *Hartree-exchange-correlation* (Hxc) functional. Section 6.1 briefly presents the approximations for the ensemble *Hartree-exchange* (Hx) functional, and points out advantages and disadvantages of each approach. Section 6.2 discusses various approaches for approximating the ensemble correlation functional, including recycling the ground-state DFAs [108], and designing weight-dependent *local density approximations* (LDAs) based on the *uniform electron gas* (UEG) model [109, 110]. Density-driven correlations are also discussed [96, 97], and an exact decomposition of the ensemble correlation energy into *state-driven* (SD) and *density-driven* (DD) correlations originally introduced by Fromager [97] is presented. Results of two different ground-state DFAs and the exact SD/DD decomposition are shown for the Hubbard dimer for various asymmetry and correlation regimes.

In Chapter 7, we present the extended N-centered ensembles, which combine the

TGOK and the N-centered ensembles into a single, unified formalism for describing both neutral and charged excitations. It is shown that in the perspective of N-centered ensembles, we can exactify the KS orbital energies for a neutral excitation of interest. We also show that such an exactification is conditioned by the appearance of the derivative discontinuity for neutral excitations, an observation that was first derived by Levy [104], but is now made more general for any system, including finite and infinite lattice systems. Proof-of-concept results are shown for the Hubbard dimer in various asymmetry regimes.

In Chapter 8, which is the last chapter of this thesis, we present an embedding strategy for multiple states, which combines the formalism of TGOK ensembles and the bath construction technique of the *Householder-transformed density-matrix functional embedding theory* (Ht-DMFET) [105, 111]. We show that, by means of successive Householder transformations on the ensemble *one-electron reduced density matrix* (1RDM), we can construct an embedding cluster for ensembles of ground and excited states of mean-field (or non-interacting) systems. This result is exploited for computing approximations to true ground and excited states inside the correlated embedding cluster. The strategy is applied on three simple toy systems, with promising results, but also new challenges. We finish the chapter by pointing out different possibilities for improvement of the present strategy, and also the prospect of turning the present embedding into a self-consistent approach for designing DFAs for TGOK ensembles.

Finally, this thesis closes with conclusions and perspectives.

Chapter 1

Different flavors of ground-state electronic structure theory

The description of stationary electronic states is one of the main tasks of electronic structure theory. In this respect, various physical systems are considered. In quantum chemistry, atoms, molecules, and molecular arrangements are studied, while in condensed matter physics, materials in their bulk are usually modelled as extended systems. Depending on the problem at hand, one may require the knowledge of one or many electronic states of a given system. For example, studying chemical reactions and prediction of reaction rates requires knowledge of the ground-state energy along a certain reaction coordinate [112]. Determining the feasibility of a certain photochemical reaction, or studying interactions with matter and light requires knowledge of several, including excited states, and possibly the whole molecular spectrum. In any case, the fundamental underlying objective of electronic structure is the same: Solve the many-electron Schrödinger equation.

This, however, is a very demanding task, and for this reason, a plethora of different methodologies have been developed, largely guided by the tradeoff between accuracy and computational efficiency. Essentially, most of them can be placed into two big groups - methods of *wavefunction theory* (WFT), and methods based on reduced quantity theories. The former (WFT) deals with the many-electron wavefunction, which is the central object of Schrödinger formulation of quantum mechanics. For a comprehensive book on WFT-based methods in

electronic structure theory, see Ref. [28] and references therein. The latter group focuses on quantities that are mathematically simpler than the wavefunction, and comprises several formalisms, including but not limited to, *density-functional theory* (DFT) [46, 11], *one-electron reduced density matrix functional theory* (1RDMFT) [113], and the theory of (many-body) Green's functions (for more on Green's functions, see Ref. [65]). In last decades, novel formalisms have emerged, such as quantum embedding [114], which make use of both WFT and reduced quantity theories and, as such, are better placed in a separate category.

This chapter serves as a review for a subset of these methods for the description of electronic ground states. The emphasis is put on methods that are relevant for the introduction of novel methods for excited states put forth in later chapters. We first focus on wavefunction theory in Section 1.1. Our discussion begins in Subsection 1.1.1 with the introduction of the *ab initio* many-electron problem within the Born-Oppenheimer approximation, In Subsection 1.1.2, we review the standard WFT-based methods, starting with the *Hartree-Fock* (HF) theory. Built on the HF foundation are the so-called *post-Hartree-Fock* (post-HF) methods, which can be grouped under variational and nonvariational methods. The former contains the family of *configuration interaction* (CI) methods, the most accurate of which is the *full configuration interaction* (FCI) method. The latter group contains the many-body perturbation theory and the coupled-cluster method, for example. After WFT-based methods, and a brief introduction to reduced quantity theories, *Kohn-Sham density-functional theory* (KS-DFT) is introduced in Section 1.2. The chapter concludes with *quantum embedding* (QE) theories in Section 1.3, with particular focus on *density matrix embedding theory* (DMET), which is used as a basis for developing the ensemble embedding approach for excited states in the last chapter of this thesis.

1.1 Wavefunction theory

1.1.1 Basic concepts in Wavefunction theory

1.1.1.1 *Ab initio* theory and electronic Hamiltonian

In quantum theory, everything we can ever know about a physical system is given by its quantum state, $|\Psi\rangle$, which, as will be shown in the following subsections, is quite a complex object. The evolution of the system's quantum state in time is governed by the time-dependent Schrödinger equation [115], which in atomic units reads as,

$$\hat{H}\,|\Psi(t)\rangle = i\frac{\partial\,|\Psi(t)\rangle}{\partial t}, \tag{1.1}$$

where $\hat{H}$ is the Hamiltonian operator, which describes kinetic energies and interactions of particles constituting the system. If $\hat{H}$ is time-independent, which is usually the case when we are studying static properties such as equilibrium geometries in quantum chemistry, the wavefunction can be factorized into a time-independent component, operated on by a unitary time-evolution operator, $|\Psi(t)\rangle = e^{-i\hat{H}(t-t_0)/\hbar}\,|\Psi(t_0)\rangle$, where $|\Psi(t_0)\rangle$ is an initial state. If the latter happens to be an eigenvector of $\hat{H}$, it is called a stationary state $|\Psi(t_0)\rangle = |\Psi\rangle$, which is described by the time-independent Schrödinger equation,

$$\hat{H}\,|\Psi\rangle = E\,|\Psi\rangle\,, \tag{1.2}$$

where E is energy level of the system in the eigenstate $|\Psi\rangle$. This is an eigenvalue problem which is of paramount importance in electronic structure theory. Depending on the system of interest, and complexity of phenomena we are studying, different Hamiltonians are employed. In time-independent *ab initio* wavefunction theory, the starting point is the molecular Hamiltonian. For M nuclei and N electrons, its position representation, in atomic units, is given as,

$$\begin{aligned}\hat{H} &= \hat{T}_{\mathrm{N}} + \hat{V}_{\mathrm{NN}} + \hat{T}_{\mathrm{e}} + \hat{W}_{\mathrm{ee}} + \hat{V}_{\mathrm{ne}} \\ &\equiv -\frac{1}{2}\sum_{A=1}^{M}\frac{\nabla_A^2}{M_A} + \sum_{A=1}^{M}\sum_{B>A}^{M}\frac{Z_A Z_B}{|\mathbf{R}_A - \mathbf{R}_B|} \\ &\quad -\frac{1}{2}\sum_{i=1}^{N}\nabla_i^2 + \sum_{i=1}^{N}\sum_{j>i}^{N}\frac{1}{|\mathbf{r}_i - \mathbf{r}_j|} - \sum_{i=1}^{N}\sum_{A=1}^{M}\frac{Z_A}{|\mathbf{r}_i - \mathbf{R}_A|}.\end{aligned} \tag{1.3}$$

The first two terms on the right-hand side of the above equation are purely nuclear kinetic energy, and Coulomb repulsion, respectively. The next two terms are

analogous quantities for electrons, while the last term is the Coulomb attraction between electrons and nuclei. The exact solution to this Hamiltonian (also called the nonadiabatic solution) takes into account the quantum mechanical nature of both electrons and nuclei. Its wavefunction Ψ can be formally expanded in a complete product of two basis function sets, one for electrons, $\{\Psi_k(\{\mathbf{r}_i\})\}_{k\geq 0}$, and one for nuclei, $\{\chi_l(\{\mathbf{R}_A\})\}_{l\geq 0}$ [116],

$$\Psi(\{\mathbf{r}_i\}\,,\,\{\mathbf{R}_A\}) = \sum_{kl} C_{kl}\Psi_k(\{\mathbf{r}_i\})\;\chi_l(\{\mathbf{R}_A\}). \tag{1.4}$$

An equivalently exact description is the Born-Huang expansion [117], in which the wavefunction is expanded as a single summation over electronic functions dependent on nuclear geometry $\{\Psi_k(\{\mathbf{r}_i\}\,|\,\{\mathbf{R}_A\})\}_{k\geq 0}$, and purely nuclear functions,

$$\Psi(\{\mathbf{r}_i\}\,,\,\{\mathbf{R}_A\}) = \sum_{k} \Psi_k(\{\mathbf{r}_i\}\,|\,\{\mathbf{R}_A\})\;\chi_k(\{\mathbf{R}_A\}). \tag{1.4 \textit{bis}}$$

In practice, it is impossible to obtain the exact solution to the problem of motions of electrons and nuclei in the complete electronic and nuclear basis. Finite-size expansions of the sort in Eq. (1.4 *bis*) are employed in general nonadiabatic theory, which is out of the scope of this thesis. However, in most electronic structure problems of quantum chemistry, we can make reasonable assumptions to approximate our problem. In particular, due to the relative heaviness of the nuclei of most elements compared to the one of the electron ($m_\mathrm{e}/M_\mathrm{N} \ll 1$), we can assume that the nuclear motions are much slower, and electrons will instantaneously adapt to any infinitesimal change in nuclear positions (adiabatic theorem). This leads to the so-called Born-Oppenheimer approximation [20], in which the nuclear and electronic motion is treated in a separate manner (strongly coupled though), according to which the wavefunction is approximated as a single product[1],

$$\Psi\left(\{\mathbf{r}_i\}\,,\,\{\mathbf{R}_A\}\right) \approx \Psi_\mathrm{e}(\{\mathbf{r}_i\}\,|\,\{\mathbf{R}_A\})\;\chi(\{\mathbf{R}_A\}). \tag{1.5}$$

The detailed account of various steps leading to the approximate form in Eq. (1.5) is somewhat involved, but the main point is that nuclear dependence is now treated

[1]The single product form in Eq. (1.5) is made formally exact in the exact factorization approach [118, 119, 120]. This is inspired by probability theory [121]: given two sets of random variables, A and B, their joint probability distribution can be written as a product $p(A,B) = p(A\,|\,B)p(B)$, where $p(A\,|\,B)$ is conditional probability for A given B, and $p(B)$ is marginal probability for B.

parametrically. In other words, for each molecular geometry, we solve the following N-electron Schrödinger equation,

$$\hat{H}_{\mathrm{e}}(\{\mathbf{R}_A\})\,|\Psi_{\mathrm{e}}(\{\mathbf{R}_A\})\rangle = E_{\mathrm{e}}(\{\mathbf{R}_A\})\,|\Psi_{\mathrm{e}}(\{\mathbf{R}_A\})\rangle\,, \tag{1.6}$$

where $\hat{H}_{\mathrm{e}}$ is the electronic Hamiltonian,

$$\begin{aligned}\hat{H}_{\mathrm{e}} &= \hat{T}_{\mathrm{e}} + \hat{W}_{\mathrm{ee}} + \hat{V}_{\mathrm{ne}} \\ &\equiv -\frac{1}{2}\sum_{i=1}^{N}\nabla_i^2 + \sum_{i=1}^{N}\sum_{j>i}^{N}\frac{1}{|\mathbf{r}_i - \mathbf{r}_j|} - \sum_{i=1}^{N}\sum_{A=1}^{M}\frac{Z_A}{|\mathbf{r}_i - \mathbf{R}_A|}.\end{aligned} \tag{1.7}$$

Solving the above electronic eigenvalue problem yields ground and excited electronic states for a given molecular configuration. After obtaining the ground-state electronic energy, we can reintroduce the operators from Eq. (1.3) acting on nuclei, which gives the Hamiltonian for the nuclear motions in the field of electrons,

$$\hat{H}_{\mathrm{n}} \equiv \frac{1}{2}\sum_{A=1}^{M}\frac{\nabla_A^2}{M_A} + \sum_{A=1}^{M}\sum_{B>A}^{M}\frac{Z_A Z_B}{|\mathbf{R}_A - \mathbf{R}_B|} + E_{\mathrm{e}}(\{\mathbf{R}_A\}). \tag{1.8}$$

The sum of last two terms on the right-hand side of above equation is known as the potential energy surface (PES) - a useful theoretical concept in searching for stable molecular geometries or studying chemical reactions. Scanning over all possible nuclear arrangements and solving the above equation gives information on nuclear motion. If PESs for individual electronic states are well-separated, *i.e.* $E_{\mathrm{e}0}(\{\mathbf{R}_A\}) \ll E_{\mathrm{e}1}(\{\mathbf{R}_A\}) \ll \ldots$ then the Born-Oppenheimer approximation is reasonable. However, under certain situations, such as conical intersections, this approximation breaks down, and more involved nonadiabatic theory is necessary. In any case, regardless of the level of theory used for the description of nuclear motions, we have to obtain the electronic wavefunction, which, as we shall see shortly, is a rather complicated object.

1.1.1.2 Structure of the wavefunction

Let us now focus on the electronic Schrödinger equation in the Born-Oppenheimer approximation (Eq. (1.6)). To facilitate solving this equation, it is important to know at least some mathematical properties that the many-electron wavefunction Ψ of a realistic physical system should fulfill. Firstly, the wavefunction has to include the information on all the electrons in the system. Each electron has four degrees

of freedom, comprising of three spatial $\mathbf{r} = (x, y, z) \in \mathbb{R}^3$ and one spin coordinate $\sigma \in \{\uparrow, \downarrow\}$ where $\uparrow$ and $\downarrow$ represent the eigenvalues ($+1/2$ and $-1/2$, respectively) of the spin-projection operator $\hat{S}_z$. In addition, the wavefunction has to be square-integrable if it were to represent a bound quantum state.

$$\int d\mathbf{x}_1 \int d\mathbf{x}_2 \ \ldots \int d\mathbf{x}_N |\Psi(\mathbf{x}_1, \mathbf{x}_2, \ldots, \mathbf{x}_N)|^2 \ = \ 1, \tag{1.9}$$

where the integration over a single spin-space coordinate $\mathbf{x}$ is formally represented as a composition of integration over three spatial coordinates and summation over the single spin variable,

$$\int d\mathbf{x} \equiv \int d\mathbf{r} \sum_{\sigma \in \{\uparrow, \downarrow\}} . \tag{1.10}$$

The space of square-integrable wavefunctions is denoted as $L^2(\mathbb{R}^{3N} \times \{\uparrow, \downarrow\}^N)$[2]. Many functions with vastly different mathematical properties belong to this space. Fortunately, one fundamental physical principle, called the Pauli exclusion principle [21], allows us to nail down a constraint that the electronic wavefunction has to follow. In particular, it should be antisymmetric with respect to permutation of spin-space coordinates of any two electrons,

$$\forall i, j \quad \Psi(..., \mathbf{x}_i, ..., \mathbf{x}_j, ...) = -\Psi(..., \mathbf{x}_j, ..., \mathbf{x}_i, ...), \tag{1.12}$$

so that the probability of finding two electrons of the same spin in the same spot vanishes, $|\Psi(..., \mathbf{x}_i, ..., \mathbf{x}_j = \mathbf{x}_i, ...)|^2 = 0$. This can be realized in the following way. Consider a set of spin-orbitals, *i.e.* single-electron functions $\{\phi_k(\mathbf{x})\}_{k=1}^{\infty}$, which is assumed to be complete for the single-particle Hilbert space $L^2(\mathbb{R}^3 \times \{\uparrow, \downarrow\})$. Each spin-orbital is a product of spatial and spin function, $\phi_i(\mathbf{x}) \equiv \varphi_{i,\sigma_i}(\mathbf{x}) = \varphi_i(\mathbf{r}) \times \delta_{\sigma_i \sigma}$. In chemistry, the spatial function is usually (but not necessarily) called *molecular orbital* (MO). Then, the total N-electron wavefunction can be expanded in the space of determinants of products of spin-orbitals, which are known as Slater determinants [122]. Concretely, for a subset consisting of N spin-orbitals, $\{\phi_k(\mathbf{x})\}_{k=1}^{N}$, we

[2] In general, $L^p(\mathbb{R}^{3q} \times \{\uparrow, \downarrow\}^q)$ is a set of functions for which the following norm is finite,

$$\|f\|_q := \left(\int d\mathbf{x}_1 \int d\mathbf{x}_2 \ \ldots \int d\mathbf{x}_q |f(\mathbf{x}_1, \mathbf{x}_2, \ldots, \mathbf{x}_q)|^p \right)^{1/p} < \infty, \tag{1.11}$$

where the integration over $\{\mathbf{x}_i\}_{1 \leq i \leq q}$ is given by Eq. (1.10).

first write a product approximation to the many-electron wavefunction,

$$\Psi(\mathbf{x}_1, \mathbf{x}_2, \ldots, \mathbf{x}_N) \approx \phi_1(\mathbf{x}_1)\, \phi_2(\mathbf{x}_2) \ldots \phi_N(\mathbf{x}_N), \tag{1.13}$$

which is called Hartee product [123]. Evidently, the Hartree product does not fulfill the constraint in Eq. (1.12), although it was used as approximate wavefunction in the so-called Hartree method [124]. Then, the Slater determinant is obtained by considering all possible permutations of Hartree products from the set $\{\phi_k(\mathbf{x})\}_{k=1}^{N}$,

$$\Phi(\mathbf{x}_1, \mathbf{x}_2, \ldots, \mathbf{x}_N) := \frac{1}{\sqrt{N!}} \begin{vmatrix} \phi_1(\mathbf{x}_1) & \phi_2(\mathbf{x}_1) & \ldots & \phi_N(\mathbf{x}_1) \\ \phi_1(\mathbf{x}_2) & \phi_2(\mathbf{x}_2) & \ldots & \phi_N(\mathbf{x}_2) \\ \vdots & \vdots & \ddots & \vdots \\ \phi_1(\mathbf{x}_N) & \phi_2(\mathbf{x}_N) & \ldots & \phi_N(\mathbf{x}_N) \end{vmatrix}, \tag{1.14}$$

where $1/\sqrt{N!}$ is the normalization factor. Replacing the Hartree product with the Slater determinant is key to the well-known Hartree-Fock (HF) method [22, 23], which is an improvement over the Hartree method.

In general, any N-electron wavefunction can be expanded in the basis of Slater determinants of all possible combinations of spin-orbitals. However, this approach becomes inconvenient rather quickly with increasing number of electrons. Fortunately, the second quantization formalism introduces a convenient abstraction in the form of creation/annihilation operators, which takes the burden of imposing antisymmetry on the wavefunction. It can be shown (see Appendix A) that a Slater determinant is built by a string of fermionic creation operators acting on the abstract vacuum state (no electrons), as follows. For example, the previous Slater determinant can be written as,

$$|\Phi\rangle = \hat{c}_1^\dagger \hat{c}_2^\dagger \ldots \hat{c}_N^\dagger |\text{vac}\rangle, \tag{1.15}$$

where $\hat{c}_i^\dagger \equiv \hat{c}_{i\sigma_i}^\dagger$ creates an electron in the i-th spin-orbital. Then, the exact wavefunction can be written as a linear combination of all possible Slater determinants as follows,

$$|\Psi\rangle = \sum_{i<j<\ldots<l} C_{ij\ldots l} \hat{c}_i^\dagger \hat{c}_j^\dagger \ldots \hat{c}_l^\dagger |\text{vac}\rangle, \tag{1.16}$$

where $C_{ij\ldots l}$ are the expansion coefficients, which are the sought-after quantities of many wavefunction-based methods in quantum chemistry. Essentially, all of the

standard quantum chemical methods (including post-HF, multiconfigurational and multireference methods) deal with finding the optimal expansion coefficients, taking the accuracy and computational speed into account such that the best possible tradeoff is achieved for a given problem at hand. This is what will be discussed in the remainder of this chapter.

1.1.2 Standard methods in electronic structure theory for ground states

1.1.2.1 Variational and nonvariational methods

The exact ground-state solution to the many-electron problem is generally out of reach for most realistic systems, and devising approximate methods becomes a necessity. There exist two classes of approximate methods, namely variational and nonvariational, arising from two equivalent mathematical formulations of the time-independent electronic structure problem. In the variational formulation, we have for any Hamiltonian $\hat{H}$, and any normalized quantum state $|\tilde{\Psi}\rangle$, the following inequality,

$$E_0 \leq \langle\tilde{\Psi}|\hat{H}|\tilde{\Psi}\rangle, \tag{1.17}$$

where E_0 is the ground-state energy of the system, described by $\hat{H}$. This can be written as a minimization,

$$E_0 = \min_{\tilde{\Psi}} \left\{ \langle\tilde{\Psi}|\hat{H}|\tilde{\Psi}\rangle \right\}, \tag{1.18}$$

which is known as the Rayleigh-Ritz variational principle. This is the basis of variational wavefunction methods in quantum chemistry (Hartree-Fock, configuration interaction, and multiconfigurational methods). All of these methods employ a parameter-dependent trial state $|\Psi(\boldsymbol{\alpha})\rangle$, where the optimal set of parameters $\boldsymbol{\alpha_0}$ satisfies the following stationarity condition,

$$\frac{\partial}{\partial\boldsymbol{\alpha}} \frac{\langle\Psi(\boldsymbol{\alpha})|\hat{H}|\Psi(\boldsymbol{\alpha})\rangle}{\langle\Psi(\boldsymbol{\alpha})|\Psi(\boldsymbol{\alpha})\rangle}\bigg|_{\boldsymbol{\alpha}=\boldsymbol{\alpha_0}} = 0. \tag{1.19}$$

The other class of approximate methods does not rely on the variational principle, but rather on parametrizing the eigenvalue equation directly,

$$\left[\hat{H}\left|\Psi(\boldsymbol{\alpha})\right\rangle - E(\boldsymbol{\alpha})\left|\Psi(\boldsymbol{\alpha})\right\rangle\right]_{\boldsymbol{\alpha}=\boldsymbol{\alpha_0}} = 0, \tag{1.20}$$

and projecting onto appropriate many-electron subspaces to find the optimal parameters $\boldsymbol{\alpha_0}$. Methods based on the *many-body perturbation theory* (MBPT), and the *coupled-cluster* (CC) method, belong to this class.

What follows is a review of the two variational methods which are relevant for this thesis work, *i.e.* the HF and configuration interaction, followed by the reviews of non-variational and multiconfigurational methods.

1.1.2.2 The Hartree-Fock method

The *Hartee-Fock* (HF) method is often the starting point for development of other more advanced methods in quantum chemistry. In the restricted closed-shell version of the HF method[3], which will be discussed here, the total system's wavefunction is approximated by a single Slater determinant Φ, constructed from a set of molecular orbitals[4] (MOs) $\{\varphi_i(\mathbf{r})\}_{i=1}^{N/2}$. The goal is to find the best possible MOs that minimize the following expectation value of the electronic Hamiltonian, $\langle\Phi|\hat{H}_\mathrm{e}|\Phi\rangle$. According to the Slater-Condon rules [122, 125], this expectation value, which is also known as the Hartree-Fock energy, is written as,

$$\langle\Phi|\hat{H}_\mathrm{e}|\Phi\rangle = 2\sum_{i=1}^{N/2}\langle\varphi_i|\hat{h}|\varphi_i\rangle + \sum_{i=1}^{N/2}\sum_{j=1}^{N/2}\Big[2\langle\varphi_i\varphi_j|\varphi_i\varphi_j\rangle - \langle\varphi_i\varphi_j|\varphi_j\varphi_i\rangle\Big], \tag{1.21}$$

where $\hat{h} = -(1/2)\nabla^2_{\mathbf{r}} + v_\mathrm{ne}(\mathbf{r})$ is the one-electron part of the electronic Hamiltonian, which comprises electronic kinetic energy, and electron-nuclear attraction. In the second term on the right-hand side of Eq. (1.21), the two integrals are the Coulomb

[3]In restricted HF, we place two electrons in each MO, one with spin up, and one with spin down. In second quantization, this means $\hat{c}^\dagger_{2i-1}\left|vac\right\rangle = \hat{c}^\dagger_{i\uparrow}\left|vac\right\rangle = \left|\varphi_i\right\rangle\otimes\left|\uparrow\right\rangle$ and $\hat{c}^\dagger_{2i}\left|vac\right\rangle = \hat{c}^\dagger_{i\downarrow}\left|vac\right\rangle = \left|\varphi_i\right\rangle\otimes\left|\downarrow\right\rangle$ for $i = 1, 2, \ldots, N/2$. In unrestricted HF, different spin electrons are placed in different (not necessarily orthonormal) MOs, $\hat{c}^\dagger_{2i-1}\left|vac\right\rangle = \left|\varphi_{i\uparrow}\right\rangle\otimes\left|\uparrow\right\rangle$ and $\hat{c}^\dagger_{2i}\left|vac\right\rangle = \left|\varphi_{i\downarrow}\right\rangle\otimes\left|\downarrow\right\rangle$ for $i = 1, 2, \ldots, N/2$. Orthonormality of spin-orbitals is then assured by the spin part.

[4]Throughout the rest of this section, unless specified oherwise, we work with molecular obitals, or more generally, spatial orbitals, and assume spin degrees of freedom have been integrated out in all expectation values.

and exchange integral, respectively written in physicists' notation[5],

$$J_{ij} \equiv \langle \varphi_i \varphi_j | \varphi_i \varphi_j \rangle := \int\int d\mathbf{r}_1 d\mathbf{r}_2 \frac{\varphi_i^*(\mathbf{r}_1)\,\varphi_j^*(\mathbf{r}_2)\,\varphi_i(\mathbf{r}_1)\,\varphi_j(\mathbf{r}_2)}{|\mathbf{r}_1 - \mathbf{r}_2|}, \tag{1.23}$$

$$K_{ij} \equiv \langle \varphi_i \varphi_j | \varphi_j \varphi_i \rangle := \int\int d\mathbf{r}_1 d\mathbf{r}_2 \frac{\varphi_i^*(\mathbf{r}_1)\,\varphi_j^*(\mathbf{r}_2)\,\varphi_j(\mathbf{r}_1)\,\varphi_i(\mathbf{r}_2)}{|\mathbf{r}_1 - \mathbf{r}_2|}. \tag{1.24}$$

The minimization condition can be stated by the following Lagrangian,

$$\mathcal{L}[\{\varphi_i\}, \{\varepsilon_{ij}\}] = \langle \Phi[\{\varphi_i\}] | \hat{H}_\mathrm{e} | \Phi[\{\varphi_i\}] \rangle - \sum_{i=1}^{N/2} \sum_{j>i}^{N/2} \varepsilon_{ij} \left(\langle \varphi_i | \varphi_j \rangle - \delta_{ij} \right), \tag{1.25}$$

such that

$$\frac{\delta L}{\delta \varphi_i^*(\mathbf{r})} = 0, \quad \frac{\partial L}{\partial \varepsilon_{ij}} = 0, \tag{1.26}$$

where ε_{ij} are Lagrange multipliers that ensure orthonormality of molecular orbitals. This technique is presented in more detail in Ref. [126]. Another way of obtaining the optimized MOs is by means of orbital rotation, where the Slater determinant is parametrized in the second quantization as follows,

$$|\Phi(\boldsymbol{\kappa})\rangle = e^{-\hat{\kappa}} |\Phi\rangle, \tag{1.27}$$

where $|\Phi\rangle$ is a trial determinant, and $\hat{\kappa}$ is the singlet rotation quantum operator,

$$\hat{\kappa} = \sum_{i>j} \sum_{\sigma} \kappa_{ij} \left(\hat{c}_{i\sigma}^\dagger \hat{c}_{j\sigma} - \hat{c}_{j\sigma}^\dagger \hat{c}_{i\sigma} \right) \tag{1.28}$$

endowed with orbital rotation parameters $\boldsymbol{\kappa} \equiv \{\kappa_{ij}\}_{i>j}$. Then, the Hartree-Fock energy is parametrized with $\boldsymbol{\kappa}$ as

$$E_\mathrm{HF}(\boldsymbol{\kappa}) = \langle \Phi(\boldsymbol{\kappa}) | \hat{H}_\mathrm{e} | \Phi(\boldsymbol{\kappa}) \rangle, \tag{1.29}$$

such that the minimum is obtained by the following stationarity condition

$$\left. \frac{\partial E_\mathrm{HF}(\boldsymbol{\kappa})}{\partial \kappa_{ij}} \right|_{\boldsymbol{\kappa}=\boldsymbol{\kappa}_0} = 0. \tag{1.30}$$

[5]This is to be distinguished from another commonly used chemists' notation,

$$(\varphi_i \varphi_j | \varphi_k \varphi_l) := \int\int d\mathbf{r}_1 d\mathbf{r}_2 \frac{\varphi_i^*(\mathbf{r}_1)\,\varphi_j(\mathbf{r}_1)\,\varphi_k^*(\mathbf{r}_2)\,\varphi_l(\mathbf{r}_2)}{|\mathbf{r}_1 - \mathbf{r}_2|}, \tag{1.22}$$

which is related to the physicists' notation by, $(\varphi_i \varphi_j | \varphi_k \varphi_l) = \langle \varphi_i \varphi_k | \varphi_j \varphi_l \rangle$. In this thesis, we use the latter (physicists').

Complete derivation of the optimization within this approach is presented in Ref. [28]. Either way, *i.e.* via Lagrangian or orbital rotation formulation, minimization of respective function(al) yields the set of coupled integro-differential equations for the MOs, known as the Hartree-Fock equations,

$$\hat{F}[\{\varphi_j\}]\varphi_i(\mathbf{r}) = \varepsilon_i\varphi_i(\mathbf{r}), \tag{1.31}$$

where $\hat{F}$ is the orbital-dependent Fock operator,

$$\hat{F} = \hat{h}_{\text{core}} + \sum_{j=1}^{N/2}\left(2\hat{\mathcal{J}}_j - \hat{\mathcal{K}}_j\right). \tag{1.32}$$

The first term on the right-hand side of above equation,

$$\hat{h}_{\text{core}} = -\frac{1}{2}\nabla_{\mathbf{r}}^2 - \sum_{A=1}^{M}\frac{Z_A}{|\mathbf{r}-\mathbf{R}_A|}, \tag{1.33}$$

is the sum of one-electron kinetic energy and electron-nuclear attraction, and the second term consists of the (local) Coulomb, and (non-local) exchange potential, respectively,

$$\hat{\mathcal{J}}_j\varphi_i(\mathbf{r}) = \left(\int d\mathbf{r}'\frac{\varphi_j^*(\mathbf{r}')\varphi_j(\mathbf{r}')}{|\mathbf{r}-\mathbf{r}'|}\right)\times\varphi_i(\mathbf{r}), \tag{1.34}$$

$$\hat{\mathcal{K}}_j\varphi_i(\mathbf{r}) = \left(\int d\mathbf{r}'\frac{\varphi_j^*(\mathbf{r}')\varphi_i(\mathbf{r}')}{|\mathbf{r}-\mathbf{r}'|}\right)\times\varphi_j(\mathbf{r}). \tag{1.35}$$

Finally, the problem remains of how to approach the solution to the Hartree-Fock equations. Since the HF equations are eigenvector-dependent, they must be solved self-consistently. Roothaan [24] and Hall [25] independently proposed that molecular orbitals are obtained as linear combinations of atomic orbitals $\chi_\mu(\mathbf{r})$, centered on nuclei. In this respect, each MO can be written as,

$$\varphi_i(\mathbf{r}) = \sum_{\mu=1}^{K} C_{\mu i}\chi_\mu(\mathbf{r}), \tag{1.36}$$

where K is the dimension of the atomic orbital basis set. The goal becomes to find the optimal coefficients $C_{\mu i}$. Evidently, we have to deal with a finite amount of $K \geq N/2$ atomic orbitals, which imposes incompleteness error to the HF method. The problem of which orbitals to use for a given system deserves a separate discussion, but briefly, for quantum chemical computations, many basis sets have been

developed, which include functions of various shapes, such as Slater-type, Gaussian-type, and polarization functions.

Let us now derive the Roothaan-Hall equations. By inserting Eq. (1.36) into Eq. (1.31), we first obtain an approximation (because of finite basis set) to the Hartree-Fock equations,

$$\hat{F}\sum_{\mu=1}^{K} C_{\mu i}\chi_{\mu}(\mathbf{r}) \approx \varepsilon_i \sum_{\mu=1}^{K} C_{\mu i}\chi_{\mu}(\mathbf{r}). \tag{1.37}$$

Multiplying on the left by $\chi_{\nu}^{*}(\mathbf{r})$ and integrating, we obtain

$$\sum_{\mu=1}^{K}\left(\int d\mathbf{r}\chi_{\nu}^{*}(\mathbf{r})\hat{F}\chi_{\mu}(\mathbf{r})\right)C_{\mu i} = \varepsilon_i \sum_{\mu=1}^{K}\left(\int d\mathbf{r}\chi_{\nu}^{*}(\mathbf{r})\chi_{\mu}(\mathbf{r})\right)C_{\mu i}. \tag{1.38}$$

If we define the Fock matrix, and the atomic orbital overlap matrix, respectively, as,

$$F_{\mu\nu} := \int d\mathbf{r}\chi_{\mu}^{*}(\mathbf{r})\hat{F}\chi_{\nu}(\mathbf{r}), \tag{1.39}$$

$$S_{\mu\nu} := \int d\mathbf{r}\chi_{\mu}^{*}(\mathbf{r})\chi_{\nu}(\mathbf{r}), \tag{1.40}$$

then Eq. (1.38) can be compacted as,

$$\sum_{\mu=1}^{K} F_{\nu\mu}C_{\mu i} = \varepsilon_i \sum_{\mu=1}^{K} S_{\nu\mu}C_{\mu i}. \tag{1.41}$$

The Fock matrix depends on its solutions, *i.e.* the molecular orbitals, or equivalently, on atomic orbital expansion coefficients, $C_{\mu i}$ (see Eq. (1.36)). The final form of the so-called Roothaan-Hall equations can be written as,

$$\mathbf{F}(\mathbf{C})\mathbf{C} = \mathbf{S}\mathbf{C}\boldsymbol{\varepsilon}. \tag{1.42}$$

The iterative *self-consistent field* (SCF) procedure for solving this equation can be summarized as follows,

1. For a given physical system (*e.g.* molecule) start with a basis set and obtain an initial guess for the MO coefficients ($\mathbf{C}_0$) - matrix. There are many possibilities, one approach would be to obtain MO coefficients from a Hückel Hamiltonian, for example.

2. Evaluate the Fock matrix: $\mathbf{F}(\mathbf{C}_n)$. Crucially, only the MOs with lowest $N/2$ orbital energies at a given iteration step are considered occupied and contribute to the Coulomb and Exchange integrals. This is known as the Aufbau principle.

3. Solve the generalized eigenvalue problem (equation above) to obtain a guess for new $\mathbf{C}_{n+1}$ matrix.

4. If, according to some measure (*e.g.* Frobenius norm), the difference between MO coefficient matrices is small enough, *i.e.* $\|\mathbf{C}_{n+1} - \mathbf{C}_n\|_{\text{Frob.}} <$ tolerance, terminate the iteration, otherwise return to the step 2 with new guess $\mathbf{C}_{n+1}$, and continue until step 4 is satisfied.

The computational bottleneck of the above SCF procedure is step 2, which includes evaluation of two-electron Coulomb and exchange integrals (Eqs. (1.23) and (1.24), respectively). This makes the HF method scale as $\mathcal{O}(K^4)$ with the basis set size K if all two-electron integrals are calculated. In practice, this is often not necessary, and efficient implementations have been developed to reduce the quartic scaling [112]. Solving Eq. (1.42) with the above SCF procedure yields the so-called *canonical* orbitals, which are used to obtain the HF energy,

$$E_{\text{HF}} = 2\sum_{i=1}^{N/2} h_{ii} + \sum_{i=1}^{N/2}\sum_{j=1}^{N/2} (2J_{ij} - K_{ij})\,. \tag{1.43}$$

As the basis set approaches completeness ($K \to \infty$), the Hartree-Fock limit is reached, which is the lowest possible energy one can obtain using a single Slater determinant. The exact ground-state energy within the Born-Oppenheimer approximation is always lower. Correlation energy, a term coined by Löwdin [26], is the difference between the two energies,

$$E_{\text{c}} = E - E_{\text{HF}} < 0. \tag{1.44}$$

The term "correlation energy" defined this way is a tad misleading. If we consider as "electron correlation" any energetic contribution that arises from the description of electronic structure beyond the completely independent electron picture of the Hartree product (see Eq. (1.13)) then even the Hartee-Fock theory itself does describe some correlation. The latter is due to the exchange integral (see Eq. (1.24))

terms, which are a consequence of the Slater determinant approximation that properly antisymmetrizes the Hartree product. The exchange integral lowers the total energy for each pair of electrons of the same spin. This effect is also called Fermi correlation, which signifies that two electrons of the same spin cannot occupy the same point in space (equivalently, the same MO). For opposite-spin electrons, there is no additional term beside Coulomb integral which is present as an average approximation of Coulomb repulsion for all electrons. In realistic systems, however, there are correlation effects that HF method misses. In the literature, they are commonly grouped under dynamical correlation and static correlation. In HF theory, each electron can be seen as interacting with a mean-field cloud of the other electrons spread over the molecule. However, the probability of finding any given electron at some point in space, regardless of spin, depends on instantaneous positions of other electrons due to Coulomb repulsion. This effect is called dynamical correlation. If a single Slater determinant is a good starting point (in other words, it recovers the vast majority of the total energy of molecule), then the dynamical correlation can be accounted for by approximating the true wavefunction as a linear combination of Slater determinants generated through excitations from the occupied (in the ground-state HF determinant) MOs to the virtual (unoccupied) MOs like in the *configuration interaction* (CI) method or in *n-th order Møller–Plesset perturbation theory* (MPn). In some cases, however, there is another effect called strong or static correlation, which arises when different Slater determinants are strictly or quasi degenerate. In molecular systems, this happens in specific situations, such as bond breaking, and potential energy surface crossings. Strong correlation requires a multideterminantal reference wavefunction, and consequently, more involved reference computational methods such as the *complete active space configuration interaction* (CASCI) and *complete active space self-consistent field* (CASSCF) methods.

1.1.2.3 Configuration interaction

The single Slater determinant approximation in the HF method can be straightforwardly improved upon without any further molecular orbital optimization. Assuming that all MOs which are obtained by solving the Hartee-Fock equations, occupied

and unoccupied (virtual), are a reasonable[6] basis for the single-electron Hilbert space, then the set of Slater determinants obtained from all possible distributions of the N electrons among all (occupied and virtual) HF MOs, is a reasonable basis for expanding the true system's wavefunction. In fact, these Slater determinants can be obtained simply by "exciting" electrons from the HF occupied orbitals to virtual orbitals. If we label occupied HF spin-orbitals as i, j and virtual ones as a, b, then,

$$|\Phi_{\mathrm{HF}}\rangle = \prod_{i=1}^{N} \hat{c}_i^\dagger \, |vac\rangle \, . \tag{1.45}$$

From $|\Phi_{\mathrm{HF}}\rangle$, we obtain singly, doubly, etc. excited determinants as,

$$|\Phi_i^a\rangle = \hat{c}_a^\dagger \hat{c}_i \, |\Phi_{\mathrm{HF}}\rangle \, , \tag{1.46}$$

$$\left|\Phi_{ij}^{ab}\right\rangle = \hat{c}_a^\dagger \hat{c}_b^\dagger \hat{c}_i \hat{c}_j \, |\Phi_{\mathrm{HF}}\rangle \, , \tag{1.47}$$

which are then used for expanding the wavefunction. This leads to the *configuration interaction* (CI) method. The so-called CI expansion reads as,

$$|\Psi_{\mathrm{CI}}\rangle = |\Phi_{\mathrm{HF}}\rangle + \sum_i \sum_a C_i^a \, |\Phi_i^a\rangle + \sum_{i>j} \sum_{a>b} C_{ij}^{ab} \left|\Phi_{ij}^{ab}\right\rangle + \ldots \tag{1.48}$$

which can also be written more abstractly as,

$$|\Psi_{\mathrm{FCI}}\rangle = |\Phi_{\mathrm{HF}}\rangle + \sum_S C_S \, |\Phi_S\rangle + \sum_D C_D \, |\Phi_D\rangle + \ldots \, , \tag{1.49}$$

to emphasize that different terms contain single, double, and multiple excitations in order. The CI coefficients $\mathbf{C} = \{C_I\}_I$ can be obtained from the variational principle (Eq. (1.19)),

$$\frac{\partial E_{\mathrm{CI}}(\mathbf{C})}{\partial \mathbf{C}} = \frac{\partial}{\partial \mathbf{C}} \frac{\langle \Psi_{\mathrm{CI}}(\mathbf{C}) | \hat{H}_{\mathrm{e}} | \Psi_{\mathrm{CI}}(\mathbf{C}) \rangle}{\langle \Psi_{\mathrm{CI}}(\mathbf{C}) | \Psi_{\mathrm{CI}}(\mathbf{C}) \rangle} = 0, \tag{1.50}$$

[6]The exact many-electron wavefunction should fulfill two additional constraints, namely the *nuclear cusp* and *Coulomb cusp* condition. In practice, the MOs used to construct Slater determinants almost never fulfill the *nuclear cusp* condition, except if expanded in STO basis sets, and cannot reproduce the *Coulomb cusp* for any basis set at all. The latter condition is imposed in *explicitly correlated methods*, which introduce the electron repulsion $r_{12} = |\mathbf{r}_1 - \mathbf{r}_2|^{-1}$ in the many-electron wavefunction. These methods, although well-known, are not standard in quantum chemistry [28].

which leads to the following eigenvalue problem,

$$\mathbf{HC} = \mathcal{E}\mathbf{C}, \tag{1.51}$$

with $\mathbf{H}$ is the CI matrix, given by,

$$H_{IJ} = \langle \Phi_I | \hat{H}_\mathrm{e} | \Phi_J \rangle. \tag{1.52}$$

If we take into consideration all possible excitations for a given basis set, then we obtain the so-called *full configuration interaction* (FCI) method (so-called *exact diagonalization* in physics). Let us estimate the size of the FCI matrix. For a basis set of K atomic orbitals and N electrons, there are $\binom{2K}{N}$ possible Slater determinants, considering that we can put at most 2 electrons in each spatial orbital. Considering the minimal basis set scenario, $K = N$, we can, using Stirling's formula, estimate the scaling of the FCI matrix size with the number of electrons in the system,

$$N_\mathrm{determinants} = \binom{2N}{N} = \frac{(2N)!}{(N!)^2} \approx \frac{1}{\sqrt{\pi N}} e^{2N \ln 2}. \tag{1.53}$$

As we see, the scaling is exponential, which makes the FCI method useless for most applications. In fact, exponential scaling in most highly accurate wavefunction-based methods is one of the main reasons for developing other methods, such as *density-functional theory* (DFT), and quantum embedding theory, both of which will be discussed later in this chapter (Sections 1.2 and 1.3, respectively). Nevertheless, since FCI provides exact diagonalization of the electronic Hamiltonian in a given finite basis set, it is still used for benchmarking calculations on small molecules, and in embedding theory for diagonalizing Hamiltonians in embedding clusters. If we want to make the method more practical, we have to resort to approximations that make the diagonalization of the CI matrix affordable. Fortunately, the situation is not so dire. Firstly, we can realize that the CI matrix is rather sparse, for at least three reasons.

1. Due to the Brillouin theorem, single excitations are not coupled to the Hartree-Fock determinant, *i.e.* the matrix elements of HF and all singly excited determinants are zero,

$$\langle \Phi_\mathrm{HF} | \hat{H}_\mathrm{e} | \Phi_S \rangle \overset{\text{Brillouin th.}}{=} 0. \tag{1.54}$$

2. Due to Slater-Condon rules [122, 125], all CI matrix elements which couple two Slater determinants that differ by more than two excitations (*e.g.* HF-Triples, Singles-Quadruples etc.) are also automatically zero. Hence the CI matrix can be generally expressed as,

$$\begin{array}{c} \\ \langle\Phi_{\mathrm{HF}}| \\ \langle\Phi_S| \\ \langle\Phi_D| \\ \langle\Phi_T| \\ \vdots \end{array} \begin{array}{c} \begin{array}{ccccc} |\Phi_{\mathrm{HF}}\rangle & |\Phi_S\rangle & |\Phi_D\rangle & |\Phi_T\rangle & \dots \end{array} \\ \begin{bmatrix} E_{\mathrm{HF}} & 0 & \langle\Phi_{\mathrm{HF}}|\hat{H}_{\mathrm{e}}|\Phi_D\rangle & 0 & \dots \\ 0 & \langle\Phi_S|\hat{H}_{\mathrm{e}}|\Phi_S\rangle & \langle\Phi_S|\hat{H}_{\mathrm{e}}|\Phi_D\rangle & \langle\Phi_S|\hat{H}_{\mathrm{e}}|\Phi_T\rangle & \dots \\ \langle\Phi_D|\hat{H}_{\mathrm{e}}|\Phi_{\mathrm{HF}}\rangle & \langle\Phi_D|\hat{H}_{\mathrm{e}}|\Phi_S\rangle & \langle\Phi_D|\hat{H}_{\mathrm{e}}|\Phi_D\rangle & \langle\Phi_D|\hat{H}_{\mathrm{e}}|\Phi_T\rangle & \dots \\ 0 & \langle\Phi_T|\hat{H}_{\mathrm{e}}|\Phi_S\rangle & \langle\Phi_T|\hat{H}_{\mathrm{e}}|\Phi_D\rangle & \langle\Phi_T|\hat{H}_{\mathrm{e}}|\Phi_T\rangle & \dots \\ \vdots & \vdots & \vdots & \vdots & \ddots \end{bmatrix} \end{array} \quad (1.55)$$

3. In cases of molecular symmetry, determinants that belong to different irreducible representations of the symmetry group are also uncoupled, yielding zero matrix elements.

All these facts lead to substantial sparsification of the CI matrix. Secondly, not all excitations are equally important in terms of magnitude of CI coefficients. For example, we can truncate the FCI expansion to single excitations - which gives the *configuration interaction with singles* (CIS) method, to double excitations, giving the *configuration interaction with singles and doubles* (CISD) method, and so on. Each class of excitations yields a more accurate method. Due to the Brillouin theorem, CIS affords no improvement in energies over the HF result. However, singly excited determinants are associated to orbital relaxation, which is important for calculating molecular properties, [112]. The first actual improvement in ground state energy may be achieved by the *configuration interaction doubles* (CID) method. Next in order of accuracy is CISD, which couples single and double excitations, and already reasonably well describes dynamical correlation. It is also not too costly, scaling as $\mathcal{O}(K^6)$ with basis set size K, which makes it useful for a large variety of systems. By comparison, CISD with triples (CISDT), and CISD with triples and quadruples (CISDTQ) scale as $\mathcal{O}(K^8)$ and $\mathcal{O}(K^{10})$, respectively, which is already too expensive for anything but small molecules and small basis sets [112].

Truncated CI methods can also be used for describing excited states and excitation energies, which are approximated from higher eigenvalues of the CI matrix. In this respect, CIS gives cheap estimates to excitation energies which are very similar to

linear response *time-dependent Hartree-Fock (TDHF)* (see section 3.2.2). However, going beyond CIS is required in order to obtain more accurate exctations and correct ordering of excited states (for example, see Figure 4.15 in Ref. [112]).

There is one important energetic property called *size-consistency*, which might be wrongly reproduced by truncated versions of the CI method. Suppose we have a bipartite molecule characterized by $A \cup B$, where A and B are sets of molecular orbitals spanning the two subsystems, separated by some distance R. A computational method is said to be *size-consistent*, if the approximate energy of molecule is additive for infinite separation,

$$\lim_{R\to\infty} E^{\text{Approx.}}(A \cup B, R) = E^{\text{Approx.}}(A) + E^{\text{Approx.}}(B). \tag{1.56}$$

This requires the total wavefunction to be multiplicatively separable,

$$\lim_{R\to\infty} \left|\Psi^{\text{Approx.}}(A \cup B, R)\right\rangle = \left|\Psi^{\text{Approx.}}(A)\right\rangle \otimes \left|\Psi^{\text{Approx.}}(B)\right\rangle. \tag{1.57}$$

A related property, defined by Bartlett [127], is *size-extensivity*, which dictates that any method should produce an energy that scales linearly with the number of electrons, or the size of the system. Truncated CI methods are neither size-consistent nor size-extensive.

1.1.2.4 Nonvariational post Hartree-Fock methods

The other of class post Hartree-Fock methods does not rely on the variational principle. Instead, optimal coefficients are derived by projection of the Hamiltonian onto an appropriate many-body subspace.

The cheapest method of this class is *many-body perturbation theory* (MBPT), for example, the Rayleigh-Schrödinger perturbation theory. The essence of this theory is the splitting of a many-body Hamiltonian into two summands, where one part (the unperturbed Hamiltonian) $\hat{H}_0$ should be easily solvable, and provide a qualitative description of the electronic structure, while another part (the perturbation), $\hat{V}$, should account for a small correction to the $\hat{H}_0$, hence the name perturbation theory. Then, the relevant equations are developed by considering the following auxiliary Hamiltonian, dependent on a coupling constant λ,

$$\hat{H}^{\lambda} = \hat{H}_0 + \lambda\hat{V}, \tag{1.58}$$

where λ ranges from 0 to 1. This way, the "physical" Hamiltonian corresponds to $\lambda = 1$, *i.e.* $\hat{H}^{\lambda=1} = \hat{H} = \hat{H}_0 + \hat{V}$, and the unperturbed Hamiltonian to $\lambda = 0$, *i.e.* $\hat{H}^{\lambda=0} = \hat{H}_0$. The solutions to $\hat{H}_0$, $\{\Psi_I^{(0)}\}_I$, can be used as a basis for expansion of exact solutions (to $\hat{H}^{\lambda=1}$). In this general procedure, the ground state and ground-state energy of $\hat{H}^\lambda$ are written as Taylor expansions about $\lambda = 0$ as follows,

$$E_0^\lambda \approx E_0^{(0)} + \left.\frac{dE_0^\lambda}{d\lambda}\right|_{\lambda=0} \lambda + \frac{1}{2}\left.\frac{d^2E_0^\lambda}{d\lambda^2}\right|_{\lambda=0} \lambda^2 + \ldots, \tag{1.59}$$

$$\left|\Psi_0^\lambda\right\rangle \approx \left|\Psi_0^{(0)}\right\rangle + \left.\frac{d\left|\Psi_0^\lambda\right\rangle}{d\lambda}\right|_{\lambda=0} \lambda + \frac{1}{2}\left.\frac{d^2\left|\Psi_0^\lambda\right\rangle}{d\lambda^2}\right|_{\lambda=0} \lambda^2 + \ldots, \tag{1.60}$$

for any $0 \leq \lambda \leq 1$. The derivatives, $d^k E_0^\lambda / d\lambda^k$ and $d^k \left|\Psi_0^\lambda\right\rangle / d\lambda^k$ can be expressed analytically in terms of the unperturbed solutions. Usually, the terms up to second order for the energy and up to first order for the ground state are considered,

$$E_0 \approx E_0^{(0)} + \langle\Psi_0^{(0)}|\hat{V}|\Psi_0^{(0)}\rangle - \sum_{I\neq 0} \frac{|\langle\Psi_0^{(0)}|\hat{V}|\Psi_I^{(0)}\rangle|^2}{E_I^{(0)} - E_0^{(0)}}, \tag{1.61}$$

$$|\Psi_0\rangle \approx |\Psi_0^{(0)}\rangle - \sum_{I\neq 0} \frac{\langle\Psi_0^{(0)}|\hat{V}|\Psi_I^{(0)}\rangle}{E_I^{(0)} - E_0^{(0)}} |\Psi_I^{(0)}\rangle. \tag{1.62}$$

If we chose as unperturbed Hamiltonian the Fock operator, *i.e.* $\hat{H}_0 = \hat{F}$, then the perturbation part $\hat{V} = \hat{H}_\mathrm{e} - \hat{F}$ is known as the fluctuation potential, and the perturbation theory is known as the *Møller-Plesset* (MP) perturbation theory. In relation to the HF method, the correlation energy comes at the second order in energy perturbation expansion, which is a very cheap correction to add to the Hartree-Fock energy. It is known as the *Møller-Plesset second-order* (MP2) method, which gives,

$$E_\mathrm{el}^\mathrm{MP2} = E_\mathrm{HF} - \sum_{i,j}^{occ.} \sum_{a,b}^{virt.} \frac{\langle ij|ab\rangle \left(2\langle ab|ij\rangle - \langle ab|ji\rangle\right)}{\varepsilon_a + \varepsilon_b - \varepsilon_i - \varepsilon_j}. \tag{1.63}$$

As we can see in the above equation, computing the MP2 energy requires both occupied and virtual HF orbitals, which can be shown to formally scale as $\mathcal{O}(K^5)$ [112]. Also, from the denominator of the second term, we can deduce that the correlation energy of the MP2 method is negative. There is one potential problem though. If the gap between occupied and virtual orbitals becomes small, then the MP2 correlation energy $E_\mathrm{c}^\mathrm{MP2} = E_\mathrm{el}^\mathrm{MP2} - E_\mathrm{HF}$ goes to $-\infty$, which is a serious error. Moreover,

the MP2 method is not variational, meaning that the correlation energy can get below the FCI result. However, it is size-consistent at each order of perturbation [28].

Another size-consistent nonvariational method is the *coupled cluster* (CC) method [128, 129]. The reason for size-consistency of this method comes from clever parametrization of the wavefunction, which is called the *exponential ansatz*. In the CC method, the set of coefficients for expanding the many-body state, also known as *cluster amplitudes*, $\mathbf{t} = \{t_I\}_I$, is collected in the *cluster operator*, which is written as,

$$\hat{T} = \sum_{k=1}^{N} \hat{T}_k, \tag{1.64}$$

where $\hat{T}_k$ are the excitation operator components for different excitation levels, starting with single excitations, doubles and so on,

$$\hat{T}_1 = \sum_i \sum_a t_i^a \hat{c}_a^\dagger \hat{c}_i, \tag{1.65}$$

$$\hat{T}_2 = \frac{1}{4} \sum_{i,j} \sum_{a,b} t_{ij}^{ab} \hat{c}_a^\dagger \hat{c}_b^\dagger \hat{c}_j \hat{c}_i. \tag{1.66}$$

Then, the exponential ansatz consists of applying the matrix exponential of the cluster operator

$$e^{\hat{T}} = \mathbb{1} + \hat{T} + \frac{1}{2}\hat{T}^2 + \ldots, \tag{1.67}$$

to the Hartree-Fock reference determinant,

$$|\Psi_{\mathrm{CC}}(\mathbf{t})\rangle = e^{\hat{T}} |\Phi_{\mathrm{HF}}\rangle, \tag{1.68}$$

The advantage of this parametrization, compared to the linear parametrization of the CI method is that it produces all possible Slater determinants one can get from exciting the occupied electrons in the HF reference even if the cluster operator is truncated, which is precisely what is done in approximate CC methods. This can best be seen by comparing the two parametrizations. If we reintroduce the CI expansion in Eq. (1.49) in terms of operators for single, double and higher excitations as $\hat{C}_S$, $\hat{C}_D$, and so on, we can relate them to the cluster operator components, for

which the lowest three orders read as,

$$\begin{aligned}\hat{C}_S &= \hat{T}_1, \\ \hat{C}_D &= \hat{T}_2 + \frac{1}{2}\hat{T}_1^2, \\ \hat{C}_T &= \hat{T}_3 + \hat{T}_1\hat{T}_2 + \frac{1}{6}\hat{T}_1^3.\end{aligned} \tag{1.69}$$

As we can see, double and higher excitations can be produced by different kinds of processes, which correspond to different products of cluster operator components. For instance, double excitations from the HF reference can be reached by simultaneous excitations of two electrons (described by $\hat{T}_2$), or by products of single excitations (described by $\hat{T}_1^2$). Hence, the $\hat{C}_D$ coefficients and cluster amplitudes are related to the cluster amplitudes by,

$$C_{ij}^{ab} = t_{ij}^{ab} + t_i^a t_j^b - t_j^a t_i^b, \tag{1.70}$$

A similar analysis can be done for triple and higher excitations.

In practice, the CC energy is obtained from the similarity-transformed Hamiltonian $e^{-\hat{T}}\hat{H}_{\mathrm{e}}e^{\hat{T}}$ by projecting into the HF reference,

$$E_{\mathrm{CC}} = \langle\Phi_{\mathrm{HF}}|e^{-\hat{T}}\hat{H}_{\mathrm{e}}e^{\hat{T}}|\Phi_{\mathrm{HF}}\rangle, \tag{1.71}$$

while the amplitudes are obtained by projections into the subspaces of excited determinants,

$$\begin{aligned}\langle\Phi_S|e^{-\hat{T}}\hat{H}_{\mathrm{e}}e^{\hat{T}}|\Phi_{\mathrm{HF}}\rangle &= 0, \\ \langle\Phi_D|e^{-\hat{T}}\hat{H}_{\mathrm{e}}e^{\hat{T}}|\Phi_{\mathrm{HF}}\rangle &= 0, \\ \langle\Phi_T|e^{-\hat{T}}\hat{H}_{\mathrm{e}}e^{\hat{T}}|\Phi_{\mathrm{HF}}\rangle &= 0,\end{aligned} \tag{1.72}$$

and so on, where the number of such equations depends on the order of truncation of the cluster operator $\hat{T}$. This is also known as the *linked CC formulation*, where each equation for the unknown amplitudes in Eq. (1.72) terminates at the fourth order in $\hat{T}$ (when $\hat{T}$ is expanded using Eq. (1.67)), thus giving quite compact expressions. This is because $\hat{H}_{\mathrm{el}}$ contains at most two-electron operators. Another advantage of the CC is that it is size-consistent. If we consider again the hypothetical molecule $A \cup B$ (see Eqs. (1.56) and (1.57)) at $R \to \infty$, the cluster operator becomes additively separable, *i.e.* $\lim_{R\to\infty} \hat{T}(A \cup B, R) = \hat{T}(A) + \hat{T}(B)$, which, it can be shown, ensures

that the CC energy is additively separable as in Eq. (1.56), and the CC wavefunction is multiplicatively separable as in Eq. (1.57).

The coupled cluster methods are some of the most accurate single-reference post-HF methods to date for molecules, which are often used as benchmarks for testing more approximate and newer methods. One major drawback is that most implementations are very expensive. The most commonly used is the *coupled cluster with singles and doubles* (CCSD) method [130], in which the cluster operator is truncated up to double excitations, *i.e.* $\hat{T} = \hat{T}_1 + \hat{T}_2$. It scales as $\mathcal{O}(K^6)$ [112], and is highly accurate for situations where most of the correlation is dynamical. The even more accurate *coupled cluster with singles, doubles and triples* (CCSDT) method, which uses $\hat{T} = \hat{T}_1 + \hat{T}_2 + \hat{T}_3$, is already extremely expensive since it scales as $\mathcal{O}(K^8)$ [112]. The most accurate method that is still commonly used at least for small molecules (up to 10 atoms [28]) is CCSD(T) (with $\mathcal{O}(K^7)$ scaling), which stands for *coupled cluster with singles, doubles and perturbative triples*, where the triple excitations are treated perturbatively with the MP method [130, 131]. Nevertheless, CCSD and CCSD(T) methods can suffer from poor description of situations with strong or static correlation, which was found to be the case for several molecules in bond-dissociation limits [132, 133, 134]. In order to treat strong correlation, one possible solution is the computationally expensive addition of higher excitations (CCSDT and beyond). Another possibility is the *multireference coupled cluster* (MRCC) method [39, 40, 41, 42, 43], which is based on a multiconfigurational wavefunction instead of the HF reference (see below). Alternatively, both obstacles (*i.e.* computational cost and strong correlation) can be tackled simultaneously with quantum embedding methods (introduced in Section 1.3), which facilitate the application of highly accurate CC methods (and FCI) even on larger and strongly correlated molecules by means of reducing full-size systems into easily solvable embedding clusters.

1.1.2.5 Multiconfigurational and multireference methods

So far, all the wavefunction-based methods, described in this chapter, are based on the HF determinant as the reference point for the improvement of the electronic structure description of correlated electrons. The HF reference point is most suitable when electron correlation is essentially dynamical. However, in cases where static correlation is important, like, for example in stretched molecules, close or at conical intersections, or at equilibrium geometries of certain molecules such as ozone (see Ref. [27] and references therein), the HF reference is not qualitatively correct, because several HF (occupied and virtual) orbitals can become degenerate, or nearly degenerate. In such cases, it becomes necessary to reoptimize the orbitals in the CI expansion, which leads to the *multiconfigurational self-consistent field* (MCSCF) method. Practically speaking, the first step in MCSCF is the identification of the dominant electronic configurations in the wavefunction, which are usually obtained by considering all possible excitations within some orbital subspace. In the parlance of MCSCF, such a subspace is called the *active orbital space*, and it is usually chosen judiciously for a problem at hand, guided by chemical intuition. More recently, an automated selection of relevant active spaces according to entropy-based orbital entanglement measures has been proposed by Stein and Reiher [135]. The remaining orbitals are either fully (doubly) occupied or empty (virtuals). Reframing this idea within the variational principle, it means that both molecular orbitals and CI coefficients are optimized together. There are two versions of MCSCF, namely the *state-specific MCSCF* (SS-MCSCF) and *state-averaged MCSCF* (SA-MCSCF) version. The latter is more suitable for excited states and is described in Section 4.1. In SS-MCSCF, which is introduced here, the trial wavefunction is expanded as a linear combination of Slater determinants or *configuration state functions* (CSFs) as follows [28],

$$|\Psi(\boldsymbol{\kappa}, \mathbf{C})\rangle = e^{-\hat{\boldsymbol{\kappa}}} \sum_I C_I \, |\Phi_I\rangle \,, \tag{1.73}$$

where the exponential term rotates orbitals, and the summand I runs over the configurations, generated from the active orbital space and the number of (so-called active) electrons distributed in that space. The MCSCF energy is then obtained

variationally as,

$$E^{\mathrm{MCSCF}}(\boldsymbol{\kappa}, \mathbf{C}) = \frac{\langle \Psi(\boldsymbol{\kappa}, \mathbf{C}) | \hat{H}_{\mathrm{e}} | \Psi(\boldsymbol{\kappa}, \mathbf{C}) \rangle}{\langle \Psi(\boldsymbol{\kappa}, \mathbf{C}) | \Psi(\boldsymbol{\kappa}, \mathbf{C}) \rangle}, \tag{1.74}$$

with the stationarity conditions given as,

$$\left. \frac{\partial E^{\mathrm{MCSCF}}(\boldsymbol{\kappa}, \mathbf{C})}{\partial \kappa_{ij}} \right|_{\boldsymbol{\kappa}=\boldsymbol{\kappa}_0} = \left. \frac{\partial E^{\mathrm{MCSCF}}(\boldsymbol{\kappa}, \mathbf{C})}{\partial C_I} \right|_{\mathbf{C}=\mathbf{C}_0} = 0. \tag{1.75}$$

Several multiconfigurational methods have been proposed, which differ in the way the orbitals are reoptimized and the active space is divided. In the *complete active space self-consistent field* (CASSCF) method [13], all orbitals (doubly occupied, active, and virtual) are reoptimized, and the FCI expansion within the active space is performed. In some programs, such as Molcas [136], one can further divide the doubly occupied and virtual orbitals into those which are reoptimized (inactive, and virtual, respectively), and those that are left out (frozen and deleted, respectively). The active space can also be further divided into several subspaces with restrictions on electron excitations, which gives the *restricted active space self-consistent field* (RASSCF) method [29, 30, 31]. In most RASSCF implementations, the active space is divided into three subspaces - RAS1 (only doubly occupied orbitals with a fixed number of holes), RAS2 (all excitations - and consequently all occupations allowed) and RAS3 (only empty orbitals with a fixed number of particles). An even cheaper approach is to skip the orbital optimization entirely, and perform the FCI expansion within the active space, composed of the HF orbitals. This corresponds to the *complete active space configuration interaction* (CASCI) method. Figure 1.1 depicts the different subspaces of (spin-)orbitals for the HF, FCI, CASSCF and CASCI methods. All in all, multiconfigurational methods serve to provide a qualitatively correct description of the electronic structure when static correlation is important.

In order to recover dynamical correlation, multireference perturbation-theory methods such as the *complete active space second-order perturbation theory* (CASPT2) [32] and *N-electron valence state second-order perturbation theory* (NEVPT2) [33, 34, 35], are commonly applied on top of a multiconfigurational method. Compared to MP2, CASPT2 and NEVPT2 start from the complete active space zeroth order wavefuncion $|\Psi_{\mathrm{CAS}}\rangle$ (obtained variationally from Eq. (1.74)), and with zeroth order Hamiltonians $\hat{H}_0$ that are much more involved. In both methods, one takes into account a set of perturber functions $\{\Psi_K\}_K$ that interact with $|\Psi_{\mathrm{CAS}}\rangle$

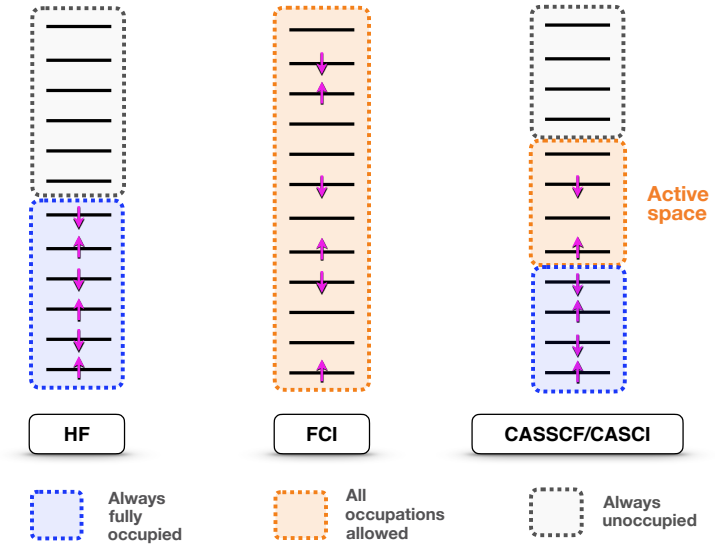

Figure 1.1: Schematic representation of spin-orbital subspaces in different variational methods.

through the first order, *i.e.* $\langle \Psi_{\text{CAS}} | \hat{H}_{\text{el}} | \Psi_K \rangle \neq 0$ (see Eq. (1.62)), to build the so-called *first-order interacting space* (FOIS), and then considers a model Hamiltonian. In CASPT2 the model Hamiltonian is a generalized Fock-like operator $\hat{F}$, while in NEVPT2 it is the Dyall Hamiltonian $\hat{H}^D$, which contains one- and two-electron operators [137]. There exist two versions of NEVPT2, namely the *partially contracted NEVPT2* (PC-NEVPT2) and the *strongly contracted NEVPT2* (SC-NEVPT2), with different dimensions of the FOIS. In CASPT2, and PC-NEVPT2, the FOIS is divided into eight subspaces. The latter can be labelled as $S_l^{(k)}$ according to the pattern l of excitations involving inactive (i, j) and/or virtual (a, b) electrons from $|\Psi_{\text{CAS}}\rangle$, and the number k of electrons excited into or out of the active space [138]. For example, the space with label $S_{ij}^{(+2)}$ has two inactive electrons promoted to the active space, and comprises wavefunctions of the form $\{\hat{E}_{ui}\hat{E}_{vj}\,|\Psi_{\text{CAS}}\rangle\}_{i\leq j, u\leq v}$, where u, v are indices of active space spin-orbitals, and $\hat{E}_{ij} = \hat{c}_{i\uparrow}^\dagger \hat{c}_{j\uparrow} + \hat{c}_{i\downarrow}^\dagger \hat{c}_{j\downarrow}$. The seven remaining subspaces are $S_{ab}^{(-2)}$, $S_i^{(+1)}$, $S_{ij,a}^{(+1)}$, $S_a^{(-1)}$, $S_{i,ab}^{(-1)}$, $S_{i,a}^{(0)}$ and $S_{ij,ab}^{(0)}$. Taking these details into consideration, the zeroth order Hamiltonians of CASPT2 and

PC-NEVPT2 are built as follows,

$$\begin{aligned} \hat{H}_0^{\mathrm{CASPT2}} &= \hat{P}_{\Psi_{\mathrm{CAS}}} \hat{F} \hat{P}_{\Psi_{\mathrm{CAS}}} + \sum_{k,l} \hat{P}_{S_l^{(k)}} \hat{F} \hat{P}_{S_l^{(k)}}, \\ \hat{H}_0^{\mathrm{PC-NEVPT2}} &= \hat{P}_{\Psi_{\mathrm{CAS}}} \hat{H}^D \hat{P}_{\Psi_{\mathrm{CAS}}} + \sum_{k,l} \hat{P}_{S_l^{(k)}} \hat{H}^D \hat{P}_{S_l^{(k)}}, \end{aligned} \tag{1.76}$$

where $\hat{P}_{\Psi_{\mathrm{CAS}}} = |\Psi_{\mathrm{CAS}}\rangle\langle\Psi_{\mathrm{CAS}}|$, and $\hat{P}_{S_l^{(k)}}$ is the projector onto subspace $S_l^{(k)}$. Then, the first-order (FOIS) wavefunction corrections, and the second-order energy corrections are obtained by the standard RSPT equations, with some modifications (for more details, see Ref. [139]).

Besides CASPT2 and NEVPT2, there are other multireference methods for describing dynamical correlation. The *multireference configuration interaction* (MRCI) [36, 37, 38] is an extension of the CI method which uses $|\Psi_{\mathrm{CAS}}\rangle$ as the reference state. Depending on the level of truncation, MRCI involves single, double, and/or higher excitations out of all the determinants in $|\Psi_{\mathrm{CAS}}\rangle$. However, like in the CI method, truncation in MRCI gives rise to size-inconsistency problems. Similarly, the *multireference coupled cluster* (MRCC) [39, 40, 41, 42, 43] method is an extension of the single-reference CC method, which uses $|\Psi_{\mathrm{CAS}}\rangle$ as the reference state for applying the exponential ansatz (see Eq. (1.67)).

Nowadays, multiconfigurational methods, and multireference methods for recovering dynamical correlation, are widely used in many areas of research, such as excited states [140, 141], photochemistry [142], catalysis [143], and actinide chemistry [144], to name a few. However, the exponential scaling with the size of the active space makes these methods prohibitive in many situations. The limit of many CASSCF implementations today is 18 electrons in 18 orbitals [145, 136], which can be insufficient for even qualitative descriptions of many interesting systems with strong correlation, such as transition metal complexes [146], although an implementation using graphical processing units (GPUs) has allowed to perform computations on systems with more than one thousand atoms [147]. Besides, in order to lessen the burden of exponential scaling, new techniques have emerged in recent decades, such as the *density matrix renormalization group* (DMRG) method [148, 149], and the *density matrix embedding theory* (DMET) [15, 16]. The focus of these methods is no longer on approximately solving the full system, but on reducing the size of the system in a certain smart way, and applying exact (*i.e.* FCI) or at least highly accu-

rate solvers on smaller effective systems. In the DMET method, the latter (effective systems) are called *embedding clusters*, and are generated from the active space of "local fragment + delocalized bath" spin-orbitals. In this sense, the wavefunction in DMET is very similar to that in multiconfigurational methods, differing mainly in the type of single-electron spin-orbitals inside the active space. This method, which is central to one of my PhD projects, will be discussed in more detail in Subsection 1.3.2, which is dedicated to quantum embedding. Before that, let us introduce another solution to computational costs, the well-known *density-functional theory* (DFT), which is a completely different paradigm from the wavefunction theory.

1.2 Density Functional Theory

1.2.1 Briefly on reduced quantity theories

The wavefunction, which has been our object of interest so far, contains all the information on the system, including its energy and other physical properties. This is a fundamental postulate of quantum mechanics. However, for most practical purposes, it is a thoroughly complicated object which is unwieldy and difficult to store. In addition, because electrons are indistinguishable, and due to the presence of at most two-electron operators in the electronic Hamiltonian, it can be shown that the wavefunction is not necessary for computing the energy. For these reasons, immense effort has been directed by physicists and chemists toward the development of theories and methods that use simpler, *reduced* quantities.

In order to begin our discussion of reduced quantity theories, let us define the N-electron density matrix operator,

$$\hat{\Gamma}^{(N)} := |\Psi\rangle\langle\Psi| \,, \tag{1.77}$$

describing the same quantum state as the wavefunction Ψ. It also says that the system of interest is in a precisely known state, that is, it represents a "pure state"[7]. In the position representation, the matrix elements of $\hat{\Gamma}^{(N)}$ read as,

$$\begin{aligned} \Gamma^{(N)}(\mathbf{x}_1, \ldots, \mathbf{x}_N; \mathbf{x}'_1, \ldots, \mathbf{x}'_N) &= \langle \mathbf{x}_1, \ldots, \mathbf{x}_N | \Psi \rangle \, \langle \Psi | \mathbf{x}'_1, \ldots, \mathbf{x}'_N \rangle \\ &= \Psi(\mathbf{x}_1, \ldots, \mathbf{x}_N) \Psi^*(\mathbf{x}'_1, \ldots, \mathbf{x}'_N). \end{aligned} \tag{1.80}$$

[7]More generally, in a realistic physical situation, in a given system, if we applied repeated measurements, we could get different outcomes with certain probabilities. The outcomes could be of many sorts, including excited states due to thermal or photochemical transfer of energy, or states with different numbers of particles. The collection of all possible measurable states $|\Psi_i\rangle$ with their probabilities p_i is called *statistical ensemble*, which is defined as density matrix operator,

$$\hat{\Gamma}^{(N,p_1,p_2\cdot,,,)} := \sum_i p_i \, |\Psi_i\rangle\langle\Psi_i| \,. \tag{1.78}$$

A pure state is then just an ensemble with $p_1 = 1$ and $p_i \overset{i\geq 1}{=} 0$. For a given operator $\hat{O}$, its ensemble-averaged expectation value is defined as,

$$\langle O \rangle_{\hat{\Gamma}^{(N,p_1,p_2\cdot,,,)}} = \sum_i p_i \langle \Psi_i | \hat{O} | \Psi_i \rangle = \mathrm{Tr}\left[\hat{\Gamma}^{(N,p_1,p_2\cdot,,,)} \hat{O}\right]. \tag{1.79}$$

More on ensembles will be discussed in the Chapters 4 and 5.

The quantity $\Gamma^{(N)}$ is also called the N-electron density matrix, to distinguish it from the operator $\hat{\Gamma}^{(N)}$ in Eq. (1.77). Based on the above equation, we now define the k-electron reduced density matrix (kRDM) as,

$$\begin{aligned}\Gamma^{(k)}(\mathbf{x}_1,\ldots,\mathbf{x}_k;\mathbf{x}'_1,\ldots,\mathbf{x}'_k) := k!\binom{N}{k}\int d\mathbf{x}_{k+1}\cdots\int d\mathbf{x}_N \times \\ \Gamma^{(N)}(\mathbf{x}_1,\ldots,\mathbf{x}_k,\mathbf{x}_{k+1},\ldots,\mathbf{x}_N\ ;\ \mathbf{x}'_1,\ldots,\mathbf{x}'_k,\mathbf{x}_{k+1},\ldots,\mathbf{x}_N),\end{aligned} \tag{1.81}$$

which is nothing but the partial trace of the N-electron density matrix $\Gamma^{(N)}$ over $N-k$ electronic coordinates. In other words, we reduce the information contained in $\Gamma^{(N)}$ by tracing out (integrating over) $N-k$ electrons. The binomial factor in front of the integral is due to the indistinguishability of the electrons (Pauli's principle). It can be shown that, for the electronic Hamiltonian, the ground-state energy is a functional of the one-body $\gamma \equiv \Gamma^{(1)}$ and two-body $\Gamma^{(2)}$ reduced density matrices,

$$\begin{aligned}E_{\mathrm{e}}[\gamma,\Gamma^{(2)}] &= T[\gamma] + W_{\mathrm{ee}}[\Gamma^{(2)}] + V_{\mathrm{ne}}[\gamma] \\ &= \int\int d\mathbf{x}d\mathbf{x}'\left(-\delta(\mathbf{x}-\mathbf{x}')\frac{1}{2}\nabla^2_{\mathbf{r}} + v_{\mathrm{ne}}(\mathbf{r})\right)\gamma(\mathbf{x},\mathbf{x}') \\ &+ \int\int d\mathbf{x}d\mathbf{x}'\frac{\Gamma^{(2)}(\mathbf{x},\mathbf{x};\mathbf{x}',\mathbf{x}')}{|\mathbf{r}-\mathbf{r}'|}.\end{aligned} \tag{1.82}$$

In fact, E_{e} is a functional of the 2RDM only, because all lower-order kRDMs are obtained from higher-order ones with a recursive relation that can be derived from Eq.(1.81),

$$\begin{aligned}&\Gamma^{(k-1)}(\mathbf{x}_1,\ldots,\mathbf{x}_{k-1};\mathbf{x}'_1,\ldots,\mathbf{x}'_{k-1}) = \\ &\frac{1}{N-k+1}\int d\mathbf{x}_k\,\Gamma^{(k)}(\mathbf{x}_1,\ldots,\mathbf{x}_{k-1},\mathbf{x}_k;\mathbf{x}'_1,\ldots,\mathbf{x}'_{k-1},\mathbf{x}_k).\end{aligned} \tag{1.83}$$

Thus, the 2RDM is all that is required for computing the energy. In principle, we could obtain the ground-state energy by variationally minimizing over those 2RDMs that can be constructed from pure quantum states (that are pure-state N-representable). However, the set of pure-state N-representable 2RDMs is not known exactly (although some necessary conditions were derived by Mazziotti [150]), which hinders the development of functionals based on this variable. The problem is that, if we naively tried to minimize Eq. (1.82) with respect to the 2RDM, the minimizing solution would not necessarily correspond to the one that is obtained from the physical ground-state wavefunction. For this reason, simpler reduced variables, for

which precise representability conditions are known, are preferred. For example, in *one-electron reduced density matrix functional theory* (1RDMFT), the energy is described as a functional of the 1RDM only [113, 151, 152]. In *density-functional theory* (DFT), to which we now turn our attention, the even simpler electron density $n(\mathbf{x}) = \gamma(\mathbf{x}, \mathbf{x})$ is used as basic variable. The price we have to pay in 1RDMFT and DFT is that the energy (and other observables) are no longer explicit functionals of the reduced quantities of interest, and we must necessarily resort to developing functional approximations.

1.2.2 Density-functional theory - historical background and explicit density functionals

Density-functional theory (DFT) is the most widely used *ab initio* quantum mechanical method in quantum chemistry and solid-state physics. Testament to this claim are the wide variety of computational packages, the Nobel Prize shared by W. Kohn and J. Pople in 1998, and the rapid increase in number of scientific papers involving the use of DFT with each passing year [153].

The basic variable in DFT is the electron density, which is obtained by integrating (tracing out) the N-electron density matrix over all degrees of freedom of $N-1$ electrons, and all spin degrees of freedom of N electrons, leaving just a function of 3 spatial coordinates - an enormously simplified variable compared to the wavefunction,

$$n(\mathbf{r}) = N \sum_{\sigma=\uparrow,\downarrow} \int d\mathbf{x}_2 \int d\mathbf{x}_3 \cdots \int d\mathbf{x}_N \Psi^*(\mathbf{r}, \sigma, \mathbf{x}_2, \ldots, \mathbf{x}_N)\Psi(\mathbf{r}, \sigma, \mathbf{x}_2, \ldots, \mathbf{x}_N). \quad (1.84)$$

By construction, it integrates to the number of electrons N. The roots of DFT lie very early in the 20th century with the introduction of the so-called *Thomas-Fermi* (TF) model [44, 45]. The TF model assumes that the electron density in atoms can be locally approximated as a uniform cloud of free (noninteracting) electrons. In this respect, the first density functional[8] that was derived, is that of the kinetic energy of free electrons,

$$T_{\mathrm{TF}}[n] = C_{\mathrm{TF}} \int d\mathbf{r}\, n(\mathbf{r})^{5/3}, \quad (1.85)$$

[8]For more on functionals, see Appendix C.

where $C_{\mathrm{TF}} = 3(3\pi^2)^{2/3}/10$ is the Thomas-Fermi constant in atomic units. Adding the (classical) Coulomb repulsion and external potential contribution results in the Thomas-Fermi energy,

$$E_{\mathrm{TF}}[n] = T_{\mathrm{TF}}[n] + \frac{1}{2}\int d\mathbf{r}\int d\mathbf{r}'\frac{n(\mathbf{r})n(\mathbf{r}')}{|\mathbf{r}-\mathbf{r}'|} + \int d\mathbf{r} v_{\mathrm{ext}}(\mathbf{r})n(\mathbf{r}). \tag{1.86}$$

Minimizing this functional under the constraint of conserved electrons $\int d\mathbf{r}\, n(\mathbf{r}) = N$ gives the Thomas-Fermi differential equation, which governs nonuniform density distribution in "realistic" systems. Although much simpler than wavefunction theory, the applicability of TF model is limited, since it cannot predict shell structure in atoms and molecular bonding, as the energy of a molecule is shown to be higher than the sum of energies of individual atoms [154]. The first improvement over TF model was achieved by Dirac [155], who derived the density functional expression of the exchange energy,

$$E_{\mathrm{x,\,D}}[n] = C_{\mathrm{x}}\int d\mathbf{r}\, n(\mathbf{r})^{4/3}, \tag{1.87}$$

where $C_{\mathrm{x}} = -3(3\pi^2)^{1/3}/4$ (atomic units). Adding this term to the total energy in Eq. (1.86) gives the Thomas-Fermi-Dirac model.

Another notable improvement is the correction by von Weizsäcker in 1935 [156], which is exact for a closed-shell noninteracting 2-electron system,

$$T_{\mathrm{vW}}[n] = \frac{1}{8}\int d\mathbf{r}\,\frac{|\nabla n(\mathbf{r})|^2}{n(\mathbf{r})} \tag{1.88}$$

and represents the first step toward modeling inhomogeneity in electron density. It guarantees some density features such as the exponential decay far away from the system, and the cusp condition at nuclei, but still fails to describe shell structures [157]. The TF model and subsequent explicit density functionals, although inaccurate for practical applications in chemistry, have regained some interest in recent years with the emergence of orbital-free density-functional theory [158]. Notwithstanding, the issue of applicability of density functionals begets an even more fundamental question, namely, "Given a density with certain distribution in space, can we *uniquely* determine to which system it belongs?" The answer to this theoretical question, together with its most successful practical implementation were addressed some 30 years after the TF model, which led to the development of Kohn-Sham DFT.

1.2.3 Exact density-functional theory for ground states

1.2.3.1 Hohenberg-Kohn theorems

The rigorous foundations of density-functional theory were solidified in 1964 [46], when Hohenberg and Kohn presented two theorems establishing the uniqueness of ground-state energy as a functional of ground-state density. To begin the discussion, let us consider the electronic Hamiltonian expressed in first quantization as follows,

$$\hat{H}_{\mathrm{e}} = \hat{T} + \hat{W} + \int d\mathbf{r}\, \hat{n}(\mathbf{r}) v_{\mathrm{ext}}(\mathbf{r}) \tag{1.89}$$

where $\hat{n}(\mathbf{r}) = \sum_{i=1}^{N} \delta(\mathbf{r} - \mathbf{r}_i)$ is the density operator, and $v_{\mathrm{ext}}(\mathbf{r})$ is now any multiplicative external (not necessarily Coulomb) potential. For simplicity, we assume that the ground state of the Hamiltonian in Eq. (1.89) is nondegenerate. What follows are statements of the two Hohenberg-Kohn theorems. Both theorems are simple to prove with *reductio ad absurdum*, and their proofs are given in Appendix B.

First Hohenberg-Kohn theorem (HKI): The ground-state density $n_{\Psi_0[v_{\mathrm{ext}}]}(\mathbf{r})$ determines up to a constant the external potential $v_{\mathrm{ext}}(\mathbf{r})$. The statement of HKI given here consists of two parts, one for the map $v_{\mathrm{ext}}(\mathbf{r}) \to |\Psi_0[v_{\mathrm{ext}}]\rangle$ and another for the map $|\Psi_0[v_{\mathrm{ext}}]\rangle \to n_{\Psi_0[v_{\mathrm{ext}}]}(\mathbf{r})$.

HKI, part 1: Any two Hamiltonians in Eq. (1.89) with external potentials that differ by more than a constant, *i.e.* $v'_{\mathrm{ext}}(\mathbf{r}) - v_{\mathrm{ext}}(\mathbf{r})$ varies with $\mathbf{r}$, give rise to different ground states[9], $|\Psi_0[v'_{\mathrm{ext}}]\rangle \neq |\Psi_0[v_{\mathrm{ext}}]\rangle$.

HKI, part 2: Two different ground states $|\Psi_0[v_{\mathrm{ext}}]\rangle$ and $|\Psi_0[v'_{\mathrm{ext}}]\rangle$ that correspond to different external potentials (as in part 1), give rise to different electron densities, $n_{\Psi_0[v_{\mathrm{ext}}]} \neq n_{\Psi_0[v'_{\mathrm{ext}}]}$.

The consequence of HKI is that the map between v_{ext} and $n_0 = n_{\Psi_0[v_{\mathrm{ext}}]}$ is bijective, such that the ground state, and also the external potential, are functionals of the ground-state density: $|\Psi_0\rangle = |\Psi[v_{\mathrm{ext}}]\rangle = |\Psi[n_0]\rangle$ and $v_{\mathrm{ext}}(\mathbf{r}) = v_{\mathrm{ext}}[n_0](\mathbf{r})$. This implies that the variational principle can be reformulated as a minimization

[9] that differ by more than a global phase factor, $|\Psi_0[v'_{\mathrm{ext}}]\rangle \neq e^{i\phi}|\Psi_0[v_{\mathrm{ext}}]\rangle$ [159]. Otherwise, they would still give the same energy and other observables $\langle\Psi_0[v'_{\mathrm{ext}}]|\hat{O}|\Psi_0[v'_{\mathrm{ext}}]\rangle = e^{-i\phi}e^{i\phi}\langle\Psi_0[v_{\mathrm{ext}}]|\hat{O}|\Psi_0[v_{\mathrm{ext}}]\rangle = \langle\Psi_0[v_{\mathrm{ext}}]|\hat{O}|\Psi_0[v_{\mathrm{ext}}]\rangle$.

over densities. For this purpose, the universal Hohenberg-Kohn density functional has been introduced [46],

$$F_{\mathrm{HK}}[n] := \langle \Psi[n] | \hat{T} + \hat{W}_{\mathrm{ee}} | \Psi[n] \rangle, \tag{1.90}$$

which is universal in the sense that it is independent of the external potential v_{ext}. Then, the HK energy functional is defined as,

$$E_{\mathrm{HK}}[v_{\mathrm{ext}}, n] := F_{\mathrm{HK}}[n] + \int d\mathbf{r}\, v_{\mathrm{ext}}(\mathbf{r}) n(\mathbf{r}), \tag{1.91}$$

which leads us to the second Hohenberg-Kohn theorem:

Second Hohenberg-Kohn theorem (HKII): The minimum of the $E_{\mathrm{HK}}[v_{\mathrm{ext}}, n]$ density functional, which is the ground-state energy for a given v_{ext}, is attained at the ground-state density $n_0 = n_{\Psi_0[v_{\mathrm{ext}}]}$,

$$E_0[v_{\mathrm{ext}}] = E_0[n_0] = \min_n \left\{ E_{\mathrm{HK}}[v_{\mathrm{ext}}, n] \right\}. \tag{1.92}$$

1.2.3.2 Universal density functional - different formulations

Taking a closer look at the HK theorems, and the DFT version of the variational principle in Eq. (1.92), it is evident that so far, the theory is defined only for densities that come from solving the eigenvalue problem of a Hamiltonian with v_{ext}. Such densities are called interacting v-representable. This is problematic, since the set of interacting v-representable densities is not known explicitly. A resolution was achieved by Levy [47, 48], and later Lieb [49], who redefined the universal density functional $F_{\mathrm{HK}}[n]$ in a constrained minimization over all wavefunctions Ψ that yield a desired density n,

$$F_{\mathrm{LL}}[n] := \min_{\Psi \to n} \langle \Psi | \hat{T} + \hat{W}_{\mathrm{ee}} | \Psi \rangle = \langle \Psi[n] | \hat{T} + \hat{W}_{\mathrm{ee}} | \Psi[n] \rangle. \tag{1.93}$$

This definition is commonly referred to as the Levy-Lieb constrained search formulation. The set of admissible densities $\mathcal{D}$ in the domain of $F_{\mathrm{LL}}[n]$ is known as the set of N-representable densities, the properties of which are determined from requirements of nonnegativity, integrability, and finite von Weizsäcker kinetic energy [159],

$$\mathcal{D} = \left\{ n \in L^1(\mathbb{R}^3) \;\middle|\; n \geq 0,\, \int d\mathbf{r}\, n(\mathbf{r}) = N,\, \sqrt{n} \in H^1(\mathbb{R}^3) \right\}, \tag{1.94}$$

where $H^1(\mathbb{R}^3) = \{f | f \in L^2(\mathbb{R}^3),\ \nabla f \in L^2(\mathbb{R}^3)\}$ is a Sobolev space. Hence, the variational principle for the electronic energy can be broken down into a two-step minimization procedure,

$$\begin{aligned} E_0[v_{\text{ext}}] &= \min_{\Psi} \left\{ \langle \Psi | \hat{T} + \hat{W}_{\text{ee}} + \hat{V}_{\text{ext}} | \Psi \rangle \right\} \\ &= \min_{n \in \mathcal{D}} \left\{ \min_{\Psi \to n} \langle \Psi | \hat{T} + \hat{W}_{\text{ee}} | \Psi \rangle + \int d\mathbf{r}\, v_{\text{ext}}(\mathbf{r}) n(\mathbf{r}) \right\} \\ &= \min_{n \in \mathcal{D}} \left\{ F_{\text{LL}}[n] + \int d\mathbf{r}\, v_{\text{ext}}(\mathbf{r}) n(\mathbf{r}) \right\}. \end{aligned} \tag{1.95}$$

In contrast to $F_{\text{HK}}[n]$, $F_{\text{LL}}[n]$ is well-defined for any N-representable density n in the neighborhood of some ground-state density n_0, which solves the problem of v-representability. There exists an even more general definition of the universal functional, which was provided by Lieb [49] (see also Ref. [160] for a related work on the universal functional of 1RDMs by Valone). In Lieb's formulation, the domain of $F_{\text{LL}}[n]$ is extended from pure states to ensembles $\hat{\Gamma}$ that yield a prescribed density n,

$$F_{\text{L}}[n] := \min_{\hat{\Gamma} \to n} \text{Tr} \left[\hat{\Gamma} \left(\hat{T} + \hat{W}_{\text{ee}} \right) \right], \tag{1.96}$$

with the density matrix operators $\hat{\Gamma}$ and electron density $n(\mathbf{r})$ constructed as,

$$\begin{aligned} &\hat{\Gamma} = \sum_k \lambda_k \left| \Psi_k \right\rangle \!\left\langle \Psi_k \right|, \quad 0 \leq \lambda_k \leq 1, \quad \sum_k \lambda_k = 1, \quad \langle \Psi_k | \Psi_l \rangle = \delta_{kl}, \\ &n(\mathbf{r}) = \text{Tr} \left[\hat{\Gamma} \hat{n}(\mathbf{r}) \right]. \end{aligned} \tag{1.97}$$

where $\{\Psi_k\}_k$ is a set of orthonormal wavefunctions in the N-electron Hilbert space. Lieb's functional rests on the rigorous mathematical foundation of convex analysis. Based on the property that the ground-state energy $E_0[v]$ is concave on the set of all possible potentials v[10], Lieb showed that $F_{\text{L}}[n]$ is the Legendre-Fenchel transform of

[10]The concavity of ground-state energy, is a property such that for any two v_{ext} and v'_{ext} and any $0 \leq \alpha \leq 1$,

$$E_0[(1-\alpha)v_{\text{ext}} + \alpha v'_{\text{ext}}] \geq (1-\alpha) E_0[v_{\text{ext}}] + \alpha E_0[v'_{\text{ext}}]. \tag{1.98}$$

This is easily verified from variational principle and linearity of Eq. (1.89) with v_{ext}. It remains to specify what are the admissible v_{ext}. More precisely, Lieb introduced the spaces of all functions v and n that make the integral $\int d\mathbf{r}\, n(\mathbf{r}) v(\mathbf{r})$ finite. It can be shown [159] that any N-representable function n also belongs to $X = L^1(\mathbb{R}^3) \cap L^3(\mathbb{R}^3)$. Then, $\int d\mathbf{r}\, n(\mathbf{r}) v(\mathbf{r})$ is finite for all v belonging

$E_0[v]$,

$$F_{\rm L}[n] \equiv \sup_v \left\{ E_0[v] - \int d\mathbf{r}\, v(\mathbf{r}) n(\mathbf{r}) \right\}. \tag{1.100}$$

This construction is also called Lieb maximization. The advantage of $F_{\rm L}[n]$ over $F_{\rm LL}[n]$ is that it is convex on the set of N-representable densities in Eq. (1.94) (see footnote 10). In fact, it is a convex envelope of $F_{\rm LL}[n]$ with the property $F_{\rm L}[n] \leq F_{\rm LL}[n]$. While $F_{\rm LL}[n]$ is simpler to use in formal theory, $F_{\rm L}[n]$ (with the Lieb maximization form) is very convenient to use when deriving density-functional approximations in model systems like the Hubbard dimer [98, 76], as will be shown in later chapters.

1.2.4 Kohn-Sham Equations

The universal functional $F[n]$ introduced previously in its various formulations, holds, in principle, all the information of any system of interest, thanks to the Hohenberg-Kohn theorem. However, its practical use is rather limited, because it entails knowledge of interacting many-body systems. In light of this problem, Kohn and Sham in 1965 proposed a clever solution. The suggestion comes from considering the following question. "Given the ground-state density of some interacting system, can we find or envision a system of noninteracting electrons with exactly the same ground-state density?" In other words, we would like to have a density that is both interacting and noninteracting v-representable. The definite answer to this question is debatable, but if it turns out to be "yes", then the problem of solving the many-electron Schrödinger equation can be bypassed altogether. This thought experiment is the basis of *Kohn-Sham density-functional theory* (KS-DFT) [11]. In

to $X^* = L^{3/2}(\mathbb{R}^3) + L^\infty(\mathbb{R}^3)$, where $L^\infty(\mathbb{R}^3)$ is the space of all bounded functions,

$$L^\infty(\mathbb{R}^3) := \left\{ v(\mathbf{r}) \middle| \sup_{\mathbf{r}\in\mathbb{R}^3} |v(\mathbf{r})| < M \right\}. \tag{1.99}$$

The space X^* includes many, in particular Coulomb potentials. It can also be shown that X^* is a dual space of X (and vice-versa), which a is critical property for preserving convexity (or concavity) of functionals on X and X^*. Then, since $E_0[v]$ is concave for $v \in X^*$, it follows that the Lieb functional $F_{\rm L}[n]$ in Eq. (1.100) is convex on X, which means a global minimum can be found.

KS-DFT, the universal density functional is split into two contributions as follows,

$$F[n] = T_{\rm s}[n] + E_{\rm Hxc}[n], \tag{1.101}$$

where the first term, $T_{\rm s}[n]$, is the noninteracting kinetic energy density functional. It can be obtained from $F[n]$ (with any formalism), by setting the interaction energy operator $\hat{W}_{\rm ee}$ to zero. In the Levy-Lieb formalism, it is written as,

$$T_{\rm s}[n] = \min_{\Psi\to n} \langle\Psi|\hat{T}|\Psi\rangle = \langle\Psi[n]|\hat{T}|\Psi[n]\rangle. \tag{1.102}$$

In the Lieb formalism, it is defined similarly to Eq. (1.100) as a Legendre-Fenchel transform,

$$T_{\rm s}[n] = \sup_{v} \left\{ \mathcal{E}_0[v] - \int d\mathbf{r}\, v(\mathbf{r}) n(\mathbf{r}) \right\}, \tag{1.103}$$

where $\mathcal{E}_0[v]$ is the ground-state energy of the noninteracting Hamiltonian $\hat{T} + \int d\mathbf{r}\, v(\mathbf{r})\hat{n}(\mathbf{r})$. The remaining term in Eq. (1.101), $E_{\rm Hxc}[n]$, is called the *Hartree-exchange-correlation* (Hxc) functional. Usually, it is further split into the three terms,

$$E_{\rm Hxc}[n] = E_{\rm H}[n] + E_{\rm x}[n] + E_{\rm c}[n], \tag{1.104}$$

where the first term is the Hartree energy, which represents classical Coulomb repulsion of continuous charge density $n(\mathbf{r})$,

$$E_{\rm H}[n] = \frac{1}{2}\int d\mathbf{r} \int d\mathbf{r}' \frac{n(\mathbf{r})n(\mathbf{r}')}{|\mathbf{r}-\mathbf{r}'|}. \tag{1.105}$$

The second term in Eq. (1.104) is called the exchange energy, which is formally defined as,

$$E_{\rm x}[n] = \langle\Phi[n]|\hat{W}_{\rm ee}|\Phi[n]\rangle - E_{\rm H}[n]. \tag{1.106}$$

As we see, it is an implicit density functional[11] because it depends on the occupied orbitals in $\Phi[n]$ (see the exchange integrals HF theory in Eq. (1.24)), which in turn depend on the density (due to the HK theorems for noninteracting electrons). Using explicit density-functional approximations in place of exact exchange produces *self-interaction errors* (SIE)[12] which will be discussed in Subsection 1.2.5.

[11] Except for two electrons, where $E_{\rm x}[n] = -\frac{1}{2}E_{\rm H}[n]$.

[12] For exact (orbital-dependent) exchange, the sum of Hartree and exchange terms,

$$E_{\rm H}[n_\Phi] + E_{\rm x}[\Phi] = \langle\Phi|\hat{W}_{\rm ee}|\Phi\rangle = \sum_{i=1}^{N/2}\sum_{j=1}^{N/2} \frac{2\langle\varphi_i\varphi_i|\varphi_j\varphi_j\rangle - \langle\varphi_i\varphi_j|\varphi_j\varphi_i\rangle}{|\mathbf{r}-\mathbf{r}'|} \tag{1.107}$$

The last term in Eq. (1.104), also an implicit density functional, is the correlation energy, which encodes all the many-electron effects beyond the mean-field level of calculation, such as kinetic energy and Coulomb repulsion of interacting electrons. It contains kinetic and two-electron interaction contributions,

$$\begin{aligned} E_{\mathrm{c}}[n] &= \langle\Psi[n]|\hat{T}+\hat{W}_{\mathrm{ee}}|\Psi[n]\rangle - \langle\Phi[n]|\hat{T}+\hat{W}_{\mathrm{ee}}|\Phi[n]\rangle \\ &= \Big[\langle\Psi[n]|\hat{T}|\Psi[n]\rangle - \langle\Phi[n]|\hat{T}|\Phi[n]\rangle\Big] \\ &+ \Big[\langle\Psi[n]|\hat{W}_{\mathrm{ee}}|\Psi[n]\rangle - \langle\Phi[n]|\hat{W}_{\mathrm{ee}}|\Phi[n]\rangle\Big] \\ &= T_{\mathrm{c}}[n] + U_{\mathrm{c}}[n]. \end{aligned} \tag{1.108}$$

$E_{\mathrm{c}}[n] \leq 0$, because according to the HK theorems,

$$\begin{aligned} &\langle\Psi[n]|\ \hat{T}+\hat{W}_{\mathrm{ee}} + \int d\mathbf{r}\ \hat{n}(\mathbf{r})v_{\mathrm{ext}}[n](\mathbf{r})\ |\Psi[n]\rangle \\ &\leq \langle\Phi[n]|\ \hat{T}+\hat{W}_{\mathrm{ee}} + \int d\mathbf{r}\ \hat{n}(\mathbf{r})v_{\mathrm{ext}}[n](\mathbf{r})\ |\Phi[n]\rangle. \end{aligned} \tag{1.109}$$

Finally, we can rewrite the variational principle with the KS decomposition. This allows us to restrict the minimization to densities that come from Slater determinants,[13]

$$\begin{aligned} E_0 &= \min_n \min_{\Psi\to n}\Big\{\langle\Psi|\hat{T}+\hat{V}_{\mathrm{ext}}|\Psi\rangle + E_{\mathrm{Hxc}}[n_\Psi]\Big\} \\ &= \min_{\Psi}\Big\{\langle\Psi|\hat{T}+\hat{V}_{\mathrm{ext}}|\Psi\rangle + E_{\mathrm{Hxc}}[n_\Psi]\Big\} \\ &= \min_{\Phi}\Big\{\langle\Phi|\hat{T}+\hat{V}_{\mathrm{ext}}|\Phi\rangle + E_{\mathrm{Hxc}}[n_\Phi]\Big\} \\ &= \langle\Phi_{\mathrm{KS}}|\hat{T}+\hat{V}_{\mathrm{ext}}|\Phi_{\mathrm{KS}}\rangle + E_{\mathrm{Hxc}}[n_{\Phi_{\mathrm{KS}}}]. \end{aligned} \tag{1.110}$$

The minimizing solution $|\Phi_{\mathrm{KS}}\rangle$ consists of orbitals that solve the Kohn-Sham (KS) equations[14],

$$\left(-\frac{\nabla^2_{\mathbf{r}}}{2} + v_{\mathrm{ext}}(\mathbf{r}) + v_{\mathrm{Hxc}}[n_{\Phi_{\mathrm{KS}}}]\right)\varphi_i(\mathbf{r}) = \varepsilon_i\varphi_i(\mathbf{r}), \tag{1.111}$$

gives correct number of Coulomb integrals for $i=j$: $\langle\varphi_i\varphi_i|\varphi_i\varphi_i\rangle$, which is that of the opposite-spin electrons interacting with each other in the same spatial orbital. This is no longer the case if we use density-functional approximations (DFAs) such as the local-density approximation (LDA) in place of $E_{\mathrm{x}}[\Phi]$, which means that there will be some residual interaction of electrons with themselves due to the product form of the Hartree term.

[13]This will lead to a minimum assuming, of course, that the ground-state density is both interacting and noninteracting v-representable.

[14]The KS equations can be derived similarly to the HF ones, either via a Lagrangian or orbital rotation techniques.

where

$$v_{\mathrm{Hxc}}[n_{\Phi_{\mathrm{KS}}}] = \left.\frac{\delta E_{\mathrm{Hxc}}[n]}{\delta n(\mathbf{r})}\right|_{n=n_{\Phi_{\mathrm{KS}}}} \tag{1.112}$$

is the Hartree-exchange-correlation potential. The ground-state electron density is, in principle, exactly reproduced by the KS orbitals as follows,

$$n_{\Phi_{\mathrm{KS}}}(\mathbf{r}) = 2\sum_{i=1}^{N/2} |\varphi_i(\mathbf{r})|^2 = n_{\Psi_0}(\mathbf{r}). \tag{1.113}$$

In practice, once a particular *density-functional approximation* (DFA) to the Hxc energy functional is chosen, the KS equations are solved in a self-consistent manner, with the same procedure as described for Roothaan-Hall equations in HF theory.

1.2.5 Density-Functional Approximations

As shown previously, the exchange and correlation functionals are the only functionals that do not have an explicit density dependence, and have to be approximated in practice. What follows is a quick glance at different DFAs. For a more detailed discussion, the reader is referred to a recent comprehensive review of DFAs by Toulouse [161].

The standard approximations are usually sorted in an order of increasing mathematical complexity, commonly referred to as the Jacob's ladder of DFAs [162]. At the bottom of the ladder sits the *local density approximation* (LDA), which is introduced in the same paper as KS-DFT [11]. The idea of LDA, which was already used in Thomas-Fermi theory, is that the electron density $n(\mathbf{r})$ in an infinitesimal volume around some location $\mathbf{r}$ resembles that of the infinite *uniform electron gas* [163] (UEG) with the same density n. The LDA exchange-correlation functional is then approximated by integrating these infinitesimal local UEG energy contributions,

$$E_{\mathrm{xc}}^{\mathrm{LDA}}[n] = \int d\mathbf{r}\, n(\mathbf{r})\, \varepsilon_{\mathrm{xc}}(n(\mathbf{r})), \tag{1.114}$$

where $\varepsilon_{\mathrm{xc}}(n) = \varepsilon_{\mathrm{x}}(n) + \varepsilon_{\mathrm{c}}(n)$ is the xc energy per particle of the UEG with density n. While the exchange part, $\varepsilon_{\mathrm{x}}(n) = C_{\mathrm{x}} n^{1/3}$ has an analytical expression (see Eq. (1.87)), the correlation part $\varepsilon_{\mathrm{c}}(n)$ is only obtainable numerically using, for example, quantum Monte Carlo calculations. Two commonly used parametrizations for the correlation part are VWN [164] and PW92 [165] functionals. Next in order

are *generalized gradient approximations* (GGA) [11, 166], where, in contrast to the LDA, the xc functional attempts to "step away" from locality via the inclusion of density gradients,

$$E_{\mathrm{xc}}^{\mathrm{GGA}}[n] = \int d\mathbf{r}\, e_{\mathrm{xc}}^{\mathrm{GGA}}(n(\mathbf{r}), \|\nabla n(\mathbf{r})\|). \tag{1.115}$$

Some commonly used GGA density functionals are B88 [167], LYP [168], PW91 [169, 170, 171] and PBE [172]. After GGA come meta-GGA functionals, which include even more information on the variation of the density through Laplacians (see the von Weizsäcker kinetic energy in Eq. (1.88)),

$$E_{\mathrm{xc}}^{\mathrm{mGGA}}[n] = \int d\mathbf{r}\, e_{\mathrm{xc}}^{\mathrm{mGGA}}(n(\mathbf{r}), \|\nabla n(\mathbf{r})\|, \nabla^2 n(\mathbf{r}), \sum_{i=1}^{N/2} |\nabla \phi_i(\mathbf{r})|^2). \tag{1.116}$$

Some commonly used mGGA functionals are TPSS [173] and SCAN [174]. The functionals from the aforementioned three classes are explicit density functionals[15], for which the Hxc potential is a local multiplicative operator that can be derived from Eq. (1.112). However, in the case of LDA/GGA functionals, the price to pay is that SIE from the Hartree functional is never completely removed and is in part responsible for the deviation from the correct piecewise linearity of the energy with respect to electron number[16]. This deviation of (semi-)local LDA/GGA functionals is a measure for the *delocalization error*, which gives rise to issues such as incorrect dissociation of radical cations [175], lowering of barrier heights [176], and too small fundamental gaps [177, 178]. Conversely, in HF theory, the deviation from piecewise linearity tends toward the opposite direction, leading to *localization error* [178]. In this respect, several approaches have been developed for correcting this issue, one of which is the development of so-called hybrid functionals. One of the hybrid functionals is the Becke 3-parameter hybrid [179], which includes a combination of exact exchange energy with GGA density functionals [180],

$$\begin{aligned} E_{\mathrm{xc}}^{\mathrm{B3}}[n] = E_{\mathrm{xc}}^{\mathrm{LDA}}[n_\Phi] + a(E_{\mathrm{x}}[\Phi] - E_{\mathrm{x}}^{\mathrm{LDA}}[n_\Phi]) + b(E_{\mathrm{x}}^{\mathrm{GGA}}[n_\Phi] - E_{\mathrm{x}}^{\mathrm{LDA}}[n_\Phi]) \\ + c(E_{\mathrm{c}}^{\mathrm{GGA}}[n_\Phi] - E_{\mathrm{c}}^{\mathrm{LDA}}[n_\Phi]). \end{aligned} \tag{1.117}$$

[15] With the exception of mGGA functionals, which are partly orbital-dependent. A simple solution would be to solve the KS equations only with the density-dependent part, and then evaluate the orbital-dependent part *a posteriori*. In practice, orbital dependence of mGGA is best treated within the Generalized KS formalism (see main text).

[16] See the discussion on the Perdew-Parr-Levy-Balduz (PPLB) approach in Subection 5.2.2.

The most well-known (semi-empirical) instance of this functional is B3LYP, which uses B88 exchange and LYP correlation (semi-)local functionals, and the three parameters are $a = 0.20$, $b = 0.71$, $c = 0.81$, which were obtained by least-squares fitting to a dataset of atomization energies, ionization potentials, proton affinities, and total atomic energies [179]. The other family of hybrid functionals are *range-separated hybrids* [181, 182, 183], in which the electron repulsion $|\mathbf{r}_1 - \mathbf{r}_2|^{-1}$ is split into different terms for short and long ranges, and similarly, combinations of DFAs with exact exchange are used. A popular example of range-separated hybrid is CAM-B3LYP [183, 184]. Due to their orbital dependence, B3LYP and CAM-B3LYP represent a departure from KS-DFT, because the orbitals have to be optimized with a nonlocal potential, like in HF theory[17]. In fact, hybrids have their own rigorous framework, known as *generalized Kohn-Sham* (GKS) theory [185].

A more straightforward approach for correcting the SIE was proposed by Perdew and Zunger in 1981, with the so-called *self-interaction correction* (SIC), which subtracts the self-interaction of each occupied spin-orbital in Φ_{KS}. It is written with the spin-resolved xc functional as follows,

$$E_{\mathrm{xc}}^{\mathrm{SIC}}[n_\uparrow, n_\downarrow] = E_{\mathrm{xc}}^{\mathrm{DFA}}[n_\uparrow, n_\downarrow] - \sum_{i=1}^{N/2} \sum_{\sigma\in\{\uparrow,\downarrow\}} \left(E_{\mathrm{H}}[n_{i\sigma}] + E_{\mathrm{xc}}^{\mathrm{DFA}}[n_{i\sigma}] \right), \tag{1.118}$$

where $n_{i\sigma} = |\varphi_{i\sigma}(\mathbf{r})|^2$ is the density of the i-th occupied spin-orbital of spin σ, and $n_\sigma = \sum_{i=1}^{N/2} n_{i\sigma}$ is the total electron density of spin σ.

Another approach to solving deficiencies related to SIE is to use only exact exchange (see Eq. (1.106)). Although the orbital dependence of exact $E_{\mathrm{x}}[\Phi]$ prevents a straightforward differentiation with respect to the density, obtaining the local exchange potential $v_{\mathrm{x}}[n](\mathbf{r}) = \delta E_{\mathrm{x}}[n]/\delta n(\mathbf{r})$ is still possible in an indirect way, *i.e.* via the one-to-one correspondence between densities and KS potentials due to the HK1 theorem for noninteracting electrons. This leads to the equivalence

$$n \to n + \delta n \Leftrightarrow v_{\mathrm{s}} \to v_{\mathrm{s}} + \delta v_{\mathrm{s}}, \tag{1.119}$$

from which we obtain the chain rule,

$$\frac{\delta E_{\mathrm{x}}}{\delta v_{\mathrm{s}}(\mathbf{r})} \equiv \int d\mathbf{r}' \, \frac{\delta E_{\mathrm{x}}[n]}{\delta n(\mathbf{r}')} \chi_{\mathrm{s}}(\mathbf{r}', \mathbf{r}), \tag{1.120}$$

[17] Strictly speaking, the use of a nonlocal exchange potential is already discussed in the 1965 paper by Kohn and Sham (see Eqs. (2.22) to (2.24) in Ref. [11]).

where

$$\chi_{\mathrm{s}}(\mathbf{r}', \mathbf{r}) = \frac{\delta n(\mathbf{r}')}{\delta v_{\mathrm{s}}(\mathbf{r})} = -2 \sum_{i}^{occ.} \sum_{a}^{virt.} \left(\frac{\varphi_i^*(\mathbf{r}')\varphi_a^*(\mathbf{r})\varphi_a(\mathbf{r}')\varphi_i(\mathbf{r})}{\varepsilon_a - \varepsilon_i} + \text{c.c.} \right) \tag{1.121}$$

is the KS static linear response function, which can be obtained from the KS equations by applying the perturbation $v_{\mathrm{s}} \to v_{\mathrm{s}} + \delta v_{\mathrm{s}}$ to the KS potential. However, solving for exchange potential in Eq. (1.120) has to be done numerically in a procedure, known as *optimized effective potential* (OEP) [186, 187, 188]. Due to the presence of unoccupied KS orbitals, the computation of OEP is quite involved, and as such not routinely done.

DFT also encounters difficulties elsewhere, such as systems with prevalent van der Waals forces (not discussed in this thesis), and strongly correlated systems like transition metal oxides with partially filled d- or f-orbitals [189]. For the former, van der Waals forces, several strategies have been proposed, such as using semiempirical corrections [190, 191, 192, 193, 194, 195], and new classes of hybrid functionals, such as double hybrid [196, 197, 198] and range-separated double hybrid [199] functionals which include a fraction of MP2-based correlation energy. For the latter, strongly correlated systems, which are central to this thesis, the regular single-configuration KS scheme does not provide an adequate description of the electronic structure. For solids, several extensions have been proposed, such as DFT+U [200, 201, 202] (with U taken from the Hubbard model, see Chapter 2) which uses an orbital-dependent exchange functional, and DFT+DMFT (see refs. in [203]), where DMFT stands for *dynamical mean-field theory* (see Section 1.3). Alternatively, the single-configuration formalism of KS-DFT was merged with *density matrix embedding theory* (DMET) in the *local potential functional embedding theory* (LPFET) [204] method (see also *density embedding theory* (DET) by Bulik *et al.* [205, 206] and *self-consistent density-functional embedding* (SDE) by Mordovina *et al.* [207] for similar approaches). Strictly speaking, LPFET makes use of the KS formalism on a lattice, or in the basis of localized molecular orbitals (see 18), so in this respect, it is a *site occupation functional theory* (SOFT) [208, 209]. In LPFET, the KS system "learns" about the Hxc potential from the correlated embedding cluster of DMET in a self-consistent fashion. In quantum chemistry, different strategies for strong correlation which make use of DFT have been proposed. Some of them are listed in Subsection 1.3.1 of the next section, which discusses quantum embedding.

1.3 Quantum embedding and density matrix embedding theory

1.3.1 Introduction

The quantum chemical wavefunction methods we have been discussing so far, although highly developed and very accurate for providing electronic structure details, are generally expensive. The exponential scaling of the number of configurations with the size of the system (see Eq. (1.53)) limits the applicability of highly-accurate wavefunction methods (such as FCI and CCSD(T)) to small molecules [28]. On the other hand, the computationally affordable *Kohn-Sham density-functional theory* (KS-DFT) is routinely used in studying molecules and materials of different sizes and complexities. However, it fails to describe strong electron correlation, which plays an important role in many systems of interest to physicists and chemists. In this respect, one of the solutions is *quantum embedding* (QE), the idea of which is to partition the system under study into smaller fragments. Each fragment is then coupled with the rest of the system through a small number of representative degrees of freedom, usually called "quantum bath", and solved with an accurate "high-level" method. The remaining part is treated at a "low level", usually at the mean-field level. As a refining step, a consistency criterion may be imposed to match some quantity (*e.g.* the wavefunction, Green's function, 1RDM or electron density) of the high-level description to the mean-field one. This way, the computational cost of treating the full system with a high-level method is significantly reduced. Based on the quantity of choice, and the representation of degrees of freedom used in the partitioning, several embedding techniques have been proposed. In quantum chemistry, *frozen-density embedding* (FDE) [50, 51] and subsystem density-functional theory [52, 53] are examples of embedding methods that use real-space partitioning and electron density of DFT as the basic variable. WFT-in-DFT embedding has also been proposed [54, 55, 56, 57, 58], wherein a WFT-based method is (often) used to treat chemically relevant parts of the full the system, and the environment is treated with DFT. *Dynamical mean-field theory* (DMFT) [59, 60, 61, 62, 63, 64, 65, 66, 67] and the more recent *density-matrix embedding theory* (DMET) [15, 16, 17, 68], which were initially applied in condensed-matter physics, operate with a local orbital ba-

sis (also called *lattice basis*)[18]. They use the one-electron Green's function and the *one-electron reduced density matrix* (1RDM), respectively, as basic variables. As one project of my thesis deals with extending DMET toward excited states (see Chapter 8), this technique will be presented in more detail in the following.

1.3.2 Density matrix embedding theory

1.3.2.1 Overview

Density matrix embedding theory (DMET) was introduced by Knizia and Chan in 2012[15]. It was proposed as a static (*i.e.* frequency-independent) alternative to DMFT for describing lattice systems with strong local correlations. The general approach in DMET can be broken down into two steps:

1. Split the full many-body system into nonoverlapping local fragments in the localized orbital basis, and for each fragment, find the effective *quantum bath* degrees of freedom from the environment. The many-body fragment+bath space forms the reduced in size *embedding cluster*.

2. Solve an effective Schrödinger equation inside the previously obtained cluster. Use the cluster ground-state solution to obtain approximate local contributions to the ground-state energy and other properties of the full system.

In practical implementations of DMET, both steps inevitably involve approximations. For the sake of simplicity and clarity, the remainder of this section limits the discussion to a general introduction to DMET, and a more detailed exposition of the embedding of a single impurity, which is also used in the embedding strategy for excited states presented in Chapter 8.

[18]By local (orbital or lattice) basis I mean a basis of orbitals which are localized in space and orthonormal. In finite systems such as molecules, these can be, for example, Löwdin's orthogonal atomic orbitals (OAOs) [210, 211, 212]. In extended systems, local orbitals are represented by Wannier functions, which in simplified models such as the Hubbard model, become lattice sites (see Chapter 2).

1.3.2.2 Exact embedding: Construction of a many-body bath in DMET

In the original work of Knizia and Chan [15, 16], DMET is introduced from the many-body point of view, where the Hamiltonian of the full system is exactly mapped onto an effective Hamiltonian obtained by projection onto a smaller subspace. The mapping is achieved thanks to the so-called *Schmidt decomposition* of the full-size waevefunction, a technique well known in quantum information theory [213], which makes use of the *Singular value decomposition* (SVD). SVD is also a basic ingredient in the DMRG method [148, 149]. The procedure in DMET is described as follows: Considering the full lattice system of L sites (or localized orbitals), nothing prevents us from splitting it into two parts that we call the fragment F, containing L_F sites (or orbitals), and the environment E, containing $L_E = L - L_F$ sites (or orbitals). Then, from the fragment, we can construct $\mathcal{L}_F = 4^{L_F}$ possible many-body states[19], and from the environment $\mathcal{L}_E = 4^{L_E}$ states. If we also assume that $L_F < L_E$, then the FCI expansion of the ground-state wavefunction Ψ_0 of the full system can be written as,

$$|\Psi_0\rangle = \sum_{i=1}^{\mathcal{L}_F} \sum_{j=1}^{\mathcal{L}_E} C_{ij} \, |A_i\rangle \, |B_j\rangle \,, \tag{1.122}$$

where $|A_i\rangle$ and $|B_j\rangle$ are the fragment and environment many-body states, respectively. The FCI coefficients C_{ij} can be stored in a matrix of dimension $\mathcal{L}_F \times \mathcal{L}_E$. By applying the *singular value decomposition* technique, any such matrix can be factorized as a product of three components,

$$\mathbf{C} = \mathbf{U}\mathbf{\Sigma}\mathbf{V}^\dagger, \tag{1.123}$$

where

$$\mathbf{U} = \begin{bmatrix} | & & | \\ \mathbf{u}_1 & \dots & \mathbf{u}_{\mathcal{L}_F} \\ | & & | \end{bmatrix} \quad \mathbf{\Sigma} = \begin{bmatrix} \sigma & \mathbf{0}_{\mathcal{L}_F \times (\mathcal{L}_E - \mathcal{L}_F)} \end{bmatrix} \quad \mathbf{V}^\dagger = \begin{bmatrix} — & \mathbf{v}_1^\dagger & — \\ & \vdots & \\ — & \mathbf{v}_{\mathcal{L}_E}^\dagger & — \end{bmatrix}. \tag{1.124}$$

$\mathbf{U}$ is a unitary matrix of dimensions $\mathcal{L}_F \times \mathcal{L}_F$, $\sigma = \mathrm{diag}(\sigma_1, \dots, \sigma_{\mathcal{L}_F})$, and $\mathbf{V}$ is a unitary $\mathcal{L}_E \times \mathcal{L}_E$ matrix. Then, the $\mathcal{L}_F \times \mathcal{L}_E$ expansion in Eq. (1.122) can be

[19] That is because each site has four possible states, *i.e.* $\{|vac_i\rangle, |\chi_{i\uparrow}\rangle, |\chi_{i\downarrow}\rangle, |\chi_{i\uparrow}\chi_{i\downarrow}\rangle\}_{1 \le i \le L_F + L_E}$.

simplified to an expansion involving only $\mathcal{L}_F$ terms as follows,

$$\begin{aligned}|\Psi_0\rangle &= \sum_{i=1}^{\mathcal{L}_F}\sum_{j=1}^{\mathcal{L}_E}\sum_{a=1}^{\mathcal{L}_F} U_{ia}\sigma_a V_{aj}^\dagger |A_i\rangle |B_j\rangle \\ &= \sum_{a=1}^{\mathcal{L}_F}\sigma_a \left(\sum_{i=1}^{\mathcal{L}_F} U_{ia}|A_i\rangle\right)\left(\sum_{i=1}^{\mathcal{L}_E} V_{aj}^\dagger |B_j\rangle\right) \\ &= \sum_{a=1}^{\mathcal{L}_F}\sigma_a |\tilde{A}_a\rangle|\tilde{B}_a\rangle.\end{aligned} \tag{1.125}$$

Eq. (1.125) is also known as the *Schmidt decomposition* of $|\Psi_0\rangle$. The new orthonormal many-body states $|\tilde{A}_a\rangle$ and $|\tilde{B}_a\rangle$ are the *rotated fragment* and the so-called DMET *bath* states[20], the latter of which are of interest here because they represent the most compact description of the entanglement between the fragment and its environment. If we define the Schmidt projector as

$$\hat{P} = \sum_{a=1}^{\mathcal{L}_F}\sum_{b=1}^{\mathcal{L}_F} |\tilde{A}_a\tilde{B}_b\rangle\langle\tilde{A}_a\tilde{B}_b|, \tag{1.126}$$

it is trivial to show that the ground states of the full-size Hamiltonian $\hat{H}_\mathrm{e}$ and of the effective Hamiltonian that acts only on the Schmidt subspace $\hat{H}_\mathrm{eff} = \hat{P}\hat{H}_\mathrm{e}\hat{P}$, are exactly the same. Since according to Eq. (1.125), $\hat{P}$ leaves $|\Psi_0\rangle$ unchanged, we have

$$\begin{aligned}\hat{H}_\mathrm{eff}|\Psi_0\rangle &= \hat{P}\hat{H}_\mathrm{e}\hat{P}|\Psi_0\rangle \\ = \hat{P}\hat{H}_\mathrm{e}|\Psi_0\rangle &= E_0\hat{P}|\Psi_0\rangle \\ &= E_0|\Psi_0\rangle.\end{aligned} \tag{1.127}$$

This is the rationale for exact DMET.

1.3.2.3 Embedding in practice, step 1: Construction of approximate one-electron bath

In practice, since we do not have access to the true wavefunction (otherwise there would be no point in performing an embedding), the exact projector $\hat{P}$ is unknown, so in the first step of DMET, the wavefunction is approximated with a mean-field (*e.g.* HF or KS) description of the full system, where the ground state is a Slater determinant,

$$|\Psi_0\rangle \approx |\Phi_0\rangle. \tag{1.128}$$

[20]Not to be confused with bath spin-orbitals (see 1.3.2.3).

In this case, the bath states in Eq. (1.125) can be constructed directly from single-electron bath spin-orbitals, which in turn allows us to construct an approximate projector $\hat{\mathcal{P}}$.

For the remainder of this section, we will focus on the simplest case of a *single-impurity embedding*, *i.e.* $L_F = 1$ [105]. We begin with a basis of orthonormal local spin-orbitals in a restricted formalism, $\{|\chi_{i\sigma}\rangle = |\chi_i\rangle\,|\sigma\rangle = \hat{c}^\dagger_{i\sigma}|vac\rangle\}_{1\leq i\leq L,\,\sigma\in\{\uparrow,\downarrow\}}$, where the spin-orbitals $\{|\chi_{1\sigma}\rangle\}_{\sigma\in\{\uparrow,\downarrow\}}$ are the *impurities*, and the remaining spin-orbitals span the *fragment's environment* one-electron subspace. Furthermore, in the present case, the target of interest is the singlet ground state. Then, the central quantity that is considered in DMET is the 1RDM [15, 16, 17], which will be the same for both spins, *i.e.* $\gamma_{ij} = \langle\Phi_0|\hat{c}^\dagger_{i\uparrow}\hat{c}_{j\uparrow}|\Phi_0\rangle = \langle\Phi_0|\hat{c}^\dagger_{i\downarrow}\hat{c}_{j\downarrow}|\Phi_0\rangle$. The critical property that allows for the construction of an exact bath spin-orbital subspace from the 1RDM is idempotency property of the latter, *i.e.* $\boldsymbol{\gamma}^2 = \boldsymbol{\gamma}$, which is fulfilled if $\boldsymbol{\gamma}$ comes from Φ_0[21] [214].

In more detail, in the local basis (dropping the spin label for simplicity),

$$\{|\chi_i\rangle\}_{1\leq i\leq L} = |\chi_1\rangle \oplus \{|\chi_e\rangle\}_{2\leq e\leq L}, \tag{1.129}$$

$\boldsymbol{\gamma}$ has the following structure,

$$\boldsymbol{\gamma} = \begin{bmatrix} \gamma_{11} & \boldsymbol{\gamma}^\dagger_{e1} \\ \boldsymbol{\gamma}_{e1} & \boldsymbol{\gamma}_{ee} \end{bmatrix}. \tag{1.130}$$

The goal is now to change the representation to another orthonormal basis $\boldsymbol{\gamma} \to \tilde{\boldsymbol{\gamma}}$ with a unitary transformation $\mathbf{P}$ that leaves γ_{11} unchanged,

$$\mathbf{P} = \begin{bmatrix} 1 & \mathbf{0}^\dagger_{e1} \\ \mathbf{0}_{e1} & \mathbf{P}_{ee} \end{bmatrix}, \tag{1.131}$$

and reduces the number of couplings between impurity γ_{11} and environment block $\boldsymbol{\gamma}_{ee}$ to just one element. That is, in the transformed matrix

$$\tilde{\boldsymbol{\gamma}} = \mathbf{P}^\dagger\boldsymbol{\gamma}\mathbf{P} = \begin{bmatrix} \gamma_{11} & \boldsymbol{\gamma}^\dagger_{e1}\mathbf{P}_{ee} \\ \mathbf{P}^\dagger_{ee}\boldsymbol{\gamma}_{e1} & \mathbf{P}^\dagger_{ee}\boldsymbol{\gamma}_{ee}\mathbf{P}_{ee} \end{bmatrix}, \tag{1.132}$$

the vector $\boldsymbol{\gamma}^\dagger_{e1}$ in Eq. (1.130) should transform to $\boldsymbol{\gamma}^\dagger_{e1}\mathbf{P}_{ee}$ in Eq. (1.132) as follows,

$$\boldsymbol{\gamma}^\dagger_{e1} = \begin{bmatrix} \gamma_{12} & \gamma_{13} & \dots & \gamma_{1L} \end{bmatrix} \longrightarrow \boldsymbol{\gamma}^\dagger_{e1}\mathbf{P}_{\text{ee}} = \begin{bmatrix} \xi & 0 & \dots & 0 \end{bmatrix}. \tag{1.133}$$

[21] This is the case because, when diagonalized (for instance in the canonical spin-orbital basis), $\boldsymbol{\gamma}_{\Phi_0}$ has eigenvalues 1 for spin-orbitals occupied in Φ_0 and 0 for spin-orbitals not occupied in Φ_0.

There are many possibilities for obtaining $\mathbf{P}$. For instance, in one version of DMET implementations [215], one would apply the SVD (as in Eq. (1.123)) to $\boldsymbol{\gamma}_{e1}^{\dagger}$, and use the $\mathbf{V}$ matrix as $\mathbf{P}_{ee}$. Alternatively, in *Householder-transformed density matrix functional embedding theory* (Ht-DMFET), the Householder transformation [18] has been applied to $\boldsymbol{\gamma}$ [105, 111]. In the special case of a single-impurity embedding, either way gives the same result [105]. The Householder transformation is defined as [19],

$$P_{ij} \underset{1\leq i,j\leq L}{=} \delta_{ij} - 2v_i v_j, \tag{1.134}$$

where

$$\begin{aligned} v_1 &= 0, \\ v_2 &= \frac{\gamma_{21} - \xi}{\sqrt{2\xi(\xi - \gamma_{21})}}, \\ v_j &\underset{j\geq 3}{=} \frac{\gamma_{j1}}{\sqrt{2\xi(\xi - \gamma_{21})}}, \end{aligned} \tag{1.135}$$

and ξ is the only nonzero element of $\boldsymbol{\gamma}_{e1}^{\dagger}\mathbf{P}_{\mathrm{ee}}$ in Eq. (1.133):

$$\xi = -\operatorname{sign}(\gamma_{21})\sqrt{\sum_{j>1}^{L} |\gamma_{j1}|^2}. \tag{1.136}$$

Geometrically, the Householder transformation is a reflection, which implies that it is unitary and Hermitian $\mathbf{P}^{\dagger} = \mathbf{P}^{-1} = \mathbf{P}$. The Householder-transformed 1RDM $\tilde{\boldsymbol{\gamma}}$ has the following structure,

$$\tilde{\boldsymbol{\gamma}} = \begin{bmatrix} \gamma_{11} & \xi & \mathbf{0}_{\mathcal{E}1}^{\dagger} \\ \xi & \tilde{\gamma}_{22} & \tilde{\boldsymbol{\gamma}}_{\mathcal{E}2}^{\dagger} \\ \mathbf{0}_{\mathcal{E}1} & \tilde{\boldsymbol{\gamma}}_{\mathcal{E}2} & \tilde{\boldsymbol{\gamma}}_{\mathcal{E}\mathcal{E}} \end{bmatrix}, \tag{1.137}$$

where we used the following notation for the Householder-transformed basis,

$$\{|\tilde{\chi}_i\rangle\}_{1\leq i\leq L} = |\chi_1\rangle \oplus |\tilde{\chi}_2\rangle \oplus \{|\tilde{\chi}_{\mathcal{E}}\rangle\}_{3\leq \mathcal{E}\leq L}. \tag{1.138}$$

The impurity is now exclusively entangled with the bath spin-orbital, $|\tilde{\chi}_2\rangle$, which is a functional of $\boldsymbol{\gamma}$. In fact, using Eqs. (1.134), (1.135) and (1.136), we find that

$$P_{22} = 1 - 2v_2^2 = 1 - \frac{(\gamma_{21} - \xi)^2}{\xi(\xi - \gamma_{21})} = 1 - \frac{(\xi - \gamma_{21})}{\xi} = \frac{\gamma_{21}}{\xi}, \tag{1.139}$$

and

$$P_{i2} \overset{i\geq 2}{=} -2v_i v_2 = -2\frac{(\gamma_{21} - \xi)\gamma_{i1}}{2\xi(\xi - \gamma_{21})} = \frac{\gamma_{i1}}{\xi}, \tag{1.140}$$

which implies that the bath spin-orbital, $|\tilde{\chi}_2\rangle$, is simply the renormalized $\boldsymbol{\gamma}_{e1}$ vector [214],

$$|\tilde{\chi}_2\rangle = \sum_{i=2}^{L} P_{i2}\,|\chi_i\rangle = \sum_{i=2}^{L} \frac{\gamma_{i1}}{\sqrt{\boldsymbol{\gamma}_{e1}^{\dagger}\boldsymbol{\gamma}_{e1}}}\,|\chi_i\rangle\,. \tag{1.141}$$

At this point, we choose the subspace $|\chi_1\rangle \oplus |\tilde{\chi}_2\rangle$ to define the *embedding cluster*, while the remainder, $\{|\tilde{\chi}_{\mathcal{E}}\rangle\}_{3\leq\mathcal{E}\leq L}$, is designated as the *cluster's environment* (not to be confused with *fragment's environment*!). The construction of the cluster and its environment is depicted in Figure 1.2. Unfortunately, there is in general a buffer sector $\tilde{\boldsymbol{\gamma}}_{\mathcal{E}2}$, connecting the cluster to its environment through the bath orbital, which is not convenient for our purposes, because the desired outcome is strict disentanglement of the cluster from its environment. However, when $\mathbf{P}$ is applied to an idempotent matrix, $\tilde{\boldsymbol{\gamma}}_{\mathcal{E}2}$ vanishes, which is exactly what we want. This is easily verified from Eq. (1.137) by setting $\tilde{\boldsymbol{\gamma}}^2 = \tilde{\boldsymbol{\gamma}}$,

$$\begin{bmatrix} \gamma_{11}^2+\xi^2 & \xi(\gamma_{11}+\tilde{\gamma}_{22}) & \xi\tilde{\boldsymbol{\gamma}}_{\mathcal{E}2}^{\dagger} \\ \xi(\gamma_{11}+\tilde{\gamma}_{22}) & \tilde{\gamma}_{22}^2+\xi^2 & \tilde{\gamma}_{22}\tilde{\boldsymbol{\gamma}}_{\mathcal{E}2}^{\dagger}+\tilde{\boldsymbol{\gamma}}_{\mathcal{E}2}^{\dagger}\tilde{\boldsymbol{\gamma}}_{\mathcal{E}\mathcal{E}} \\ \xi\tilde{\boldsymbol{\gamma}}_{\mathcal{E}2} & \tilde{\boldsymbol{\gamma}}_{\mathcal{E}2}\tilde{\gamma}_{22}+\tilde{\boldsymbol{\gamma}}_{\mathcal{E}\mathcal{E}}\tilde{\boldsymbol{\gamma}}_{\mathcal{E}2} & \tilde{\boldsymbol{\gamma}}_{\mathcal{E}2}\tilde{\boldsymbol{\gamma}}_{\mathcal{E}2}^{\dagger}+\tilde{\boldsymbol{\gamma}}_{\mathcal{E}\mathcal{E}}^2 \end{bmatrix} = \begin{bmatrix} \gamma_{11} & \xi & \mathbf{0}_{\mathcal{E}1}^{\dagger} \\ \xi & \tilde{\gamma}_{22} & \tilde{\boldsymbol{\gamma}}_{\mathcal{E}2}^{\dagger} \\ \mathbf{0}_{\mathcal{E}1} & \tilde{\boldsymbol{\gamma}}_{\mathcal{E}2} & \tilde{\boldsymbol{\gamma}}_{\mathcal{E}\mathcal{E}} \end{bmatrix}, \tag{1.142}$$

and making elementwise comparison. Since $\xi \neq 0$ (otherwise, the fragment would already be disentangled from its environment, and there would be no need for performing a transformation), this implies among other things,

$$\begin{aligned} \xi\tilde{\boldsymbol{\gamma}}_{\mathcal{E}2} = \mathbf{0}_{\mathcal{E}1} \;&\Rightarrow\; \tilde{\boldsymbol{\gamma}}_{\mathcal{E}2} = \mathbf{0}_{\mathcal{E}2}, \\ \xi(\gamma_{11}+\tilde{\gamma}_{22}) = \xi \;&\Rightarrow\; \gamma_{11}+\tilde{\gamma}_{22} = 1. \end{aligned} \tag{1.143}$$

Therefore, any mean-field 1RDM will have a block-diagonal structure in the transformed basis,

$$\tilde{\boldsymbol{\gamma}}_{\Phi_0} = \begin{bmatrix} \gamma_{11} & \xi & \mathbf{0}_{\mathcal{E}1}^{\dagger} \\ \xi & 1-\gamma_{11} & \mathbf{0}_{\mathcal{E}2}^{\dagger} \\ \mathbf{0}_{\mathcal{E}1} & \mathbf{0}_{\mathcal{E}2} & \tilde{\boldsymbol{\gamma}}_{\mathcal{E}\mathcal{E}} \end{bmatrix}, \tag{1.144}$$

where the embedding cluster will be a closed subsystem (with one electron per spin, *i.e.* two in total), completely disentangled from its environment.

Judging from the structure of the matrix in Eq. (1.144), we can show[22] that $|\Phi_0\rangle$ has a structure similar to that of a CASCI wavefunction. Firstly, from the

[22] See Eqs. (33) - (36) in Ref. [105], and the discussion therein.

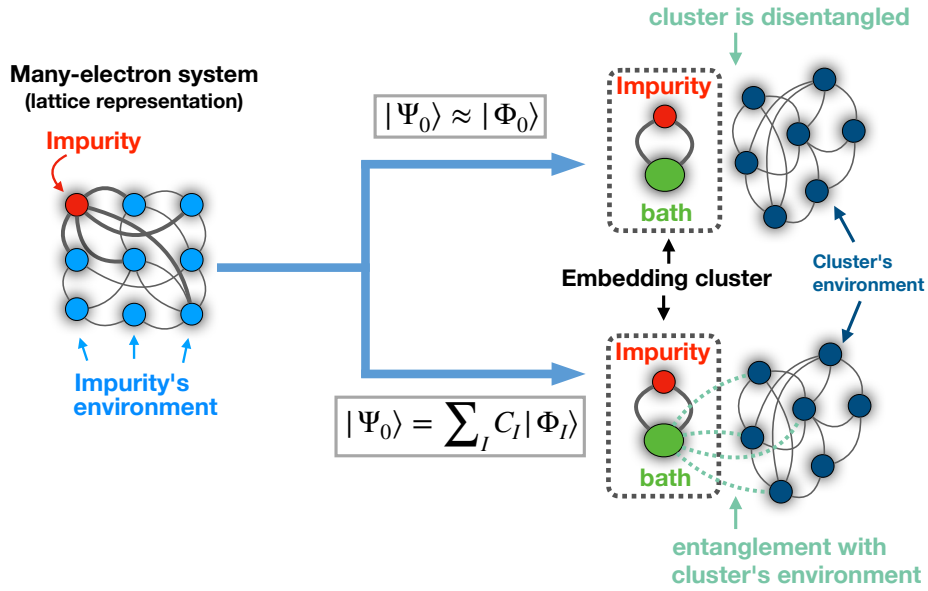

Figure 1.2: Construction of the embedding cluster for a mean-field description (top right) and a general (*e.g.* FCI) description of the full system (bottom right).

cluster spin-orbitals $\{|\chi_1\rangle, |\tilde{\chi}_2\rangle\}$ we form the analog of an active space in $|\Phi_0\rangle$. If we also diagonalize $\tilde{\gamma}_{\mathcal{E}\mathcal{E}}$, we obtain a new set of *cluster's environment* spin-orbitals $\{|\breve{\chi}_\varepsilon\rangle\}_{1\leq\varepsilon\leq L-2}$. For a given spin, the first $N/2-1$ of these will be fully occupied in $|\Phi_0\rangle$, forming the so-called *unentangled occupied environment* or *core* spin-orbitals, while rest, $L-N/2$, belong to *unentangled unoccupied environment* spin-orbital subspace. Then, $|\Phi_0\rangle$ can be factorized exactly,

$$|\Phi_0\rangle = |\Phi^{\mathcal{C}}\rangle|\Phi^{\mathcal{E}}\rangle, \tag{1.145}$$

where $|\Phi^{\mathcal{C}}\rangle$ is the embedding cluster wavefunction, which can be written either as a single Slater determinant from the occupied spin-orbitals in $|\Phi_0\rangle$ that diagonalize the cluster's 1RDM (*i.e.* the top-left subblock of Eq. (1.144)), or expanded in the "impurity+bath" representation directly as follows [105],

$$|\Phi^{\mathcal{C}}\rangle = \frac{\xi^2}{1-\gamma_{11}}|\chi_{1\uparrow}\chi_{1\downarrow}\rangle + (1-\gamma_{11})|\tilde{\chi}_{2\uparrow}\tilde{\chi}_{2\downarrow}\rangle + \xi\left(|\chi_{1\uparrow}\tilde{\chi}_{2\downarrow}\rangle + |\tilde{\chi}_{2\uparrow}\chi_{1\downarrow}\rangle\right), \tag{1.146}$$

and $|\Phi^{\mathcal{E}}\rangle$ is the cluster's environment wavefunction, given as a Slater determinant from the *unentangled occupied environment* spin-orbitals,

$$|\Phi^{\mathcal{E}}\rangle = |\breve{\chi}_{1\uparrow}\breve{\chi}_{1\downarrow}\breve{\chi}_{2\uparrow}\breve{\chi}_{2\downarrow}\cdots\breve{\chi}_{(N/2-1)\uparrow}\breve{\chi}_{(N/2-1)\downarrow}\rangle. \tag{1.147}$$

For comparison, different representations of $|\Phi_0\rangle$, together with their transformations, are shown in Figure 1.3.

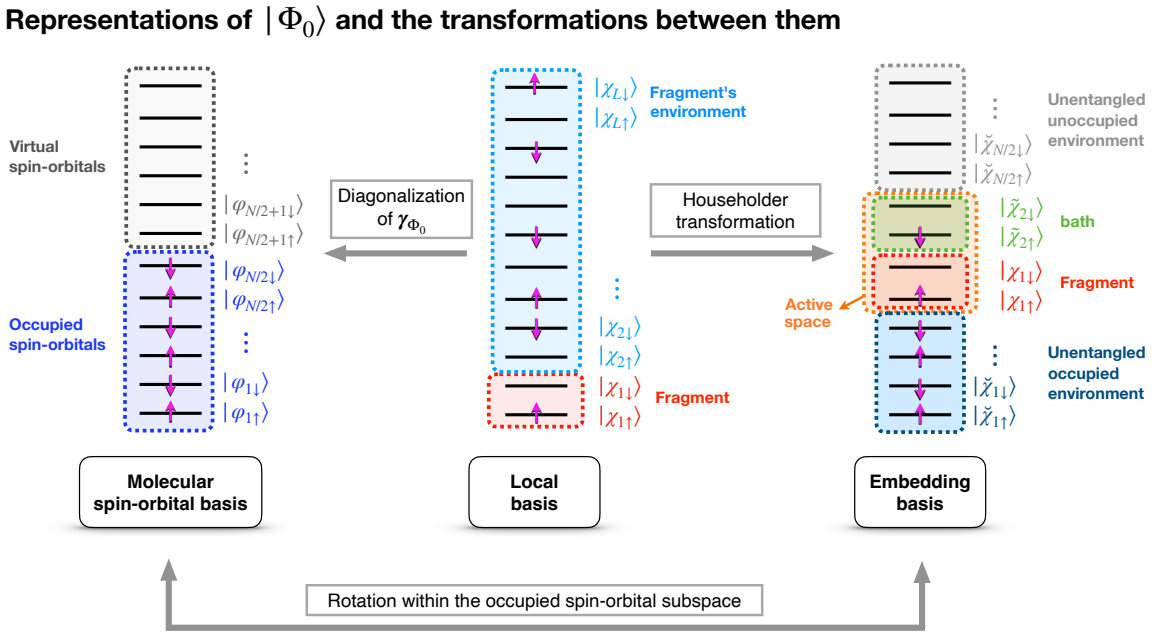

Figure 1.3: Representations of the Slater determinant different spin-orbital bases (inspired by Figure 3 in Ref. [17]). In the molecular spin-orbital basis (left, Aufbau ordering), $|\Phi_0\rangle$ is a genuine Slater determinant. In the local basis (middle), $|\Phi_0\rangle$ has a linear expansion in all possible configurations (like CI, but with localized spin-orbitals). This means that both fragment (middle, red) and environment (middle, blue) actually span several Slater determinants (like in Eq. (1.122)). In the embedding basis (right), $|\Phi_0\rangle$ is fully expanded in the Slater determinant basis consisting of spin-orbital combinations from the impurity+bath "active space" (orange box in the figure), with all determinants sharing the same set of fully occupied orbitals (right, blue), just like CASCI (cf. Figure 1.1).

Once we have obtained the disentangled embedding cluster using the Householder transformation on an idempotent $\boldsymbol{\gamma}$, we may project any operator inside the cluster. This is straightforwardly expressed in the second quantization formalism by changing the creation/annihilation operators to the transformed basis (using Eq. (1.131)),

$$\hat{d}^\dagger_{i\sigma} = \sum_{j=1}^{L} P_{ji}\hat{c}^\dagger_{j\sigma} \qquad \hat{d}_{i\sigma} = \sum_{j=1}^{L} P_{ji}\hat{c}_{j\sigma} \tag{1.148}$$

and keeping only the impurity and bath operators $\{\hat{c}^\dagger_{1\sigma} = \hat{d}^\dagger_{1\sigma}, \hat{c}_{1\sigma} = \hat{d}_{1\sigma}, \hat{d}^\dagger_{2\sigma}, \hat{d}_{2\sigma}\}$.

1.3.2.4 Embedding in practice, step 2: Solving the effective Hamiltonian and obtaining the energy

The exact decomposition for a mean-field (or non-interacting) system in Eq. (1.144) provides a basis for an approximate embedding of interacting systems. The idea is to restore the electron interactions either inside the entire impurity+bath cluster (this is referred to as the interacting bath - IB approach), or only on the impurity (noninteracting bath - NIB approach), while the cluster's environment is kept as a mean field. The interacting cluster wavefunction is then obtained by solving the embedding Schrödinger equation,

$$\hat{\mathcal{H}}^{\text{emb.}}|\Psi^{\mathcal{C}}\rangle = \mathcal{E}^{\mathcal{C}}|\Psi^{\mathcal{C}}\rangle. \tag{1.149}$$

The embedding Hamiltonian with IB reads as,

$$\begin{aligned}\hat{\mathcal{H}}^{\text{emb.}} = &\sum_{i,j=1}^{2}\sum_{\sigma\in\{\uparrow,\downarrow\}}(\tilde{h}_{ij} - \mu^{\text{imp}}\delta_{ij}\delta_{i1})\,\hat{d}^{\dagger}_{i\sigma}\hat{d}_{j\sigma} \\ &+ \frac{1}{2}\sum_{i,j,k,l=1}^{2}\sum_{\sigma,\sigma'\in\{\uparrow,\downarrow\}^2}\tilde{g}_{ijkl}\,\hat{d}^{\dagger}_{i\sigma}\hat{d}^{\dagger}_{j\sigma'}\hat{d}_{l\sigma'}\hat{d}_{k\sigma},\end{aligned} \tag{1.150}$$

where the one- and two-electron integrals in the above equation are expressed in the Householder-transformed basis $\{|\tilde{\chi}_i\rangle\}_{1\leq i\leq L}$. Note that interactions with the *unentangled occupied environment* orbitals can be added to the one-electron integrals,

$$\tilde{h}_{ij} \longleftarrow \tilde{h}_{ij} + \sum_{\mathcal{E}=1}^{N/2-1}\Big[2\,\langle\tilde{\chi}_i\breve{\chi}_{\mathcal{E}}|\tilde{\chi}_j\breve{\chi}_{\mathcal{E}}\rangle - \langle\tilde{\chi}_i\breve{\chi}_{\mathcal{E}}|\breve{\chi}_{\mathcal{E}}\tilde{\chi}_j\rangle\Big]. \tag{1.151}$$

The chemical potential μ^{imp} is introduced as an *ad-hoc* variable which corrects the occupation of the impurity (lattice site with index 1), such that the following constraint is fulfilled,

$$\langle\Psi^{\mathcal{C}}(\mu^{\text{imp}})|\hat{n}_1|\Psi^{\mathcal{C}}(\mu^{\text{imp}})\rangle = \langle\Phi_0|\hat{n}_1|\Phi_0\rangle, \tag{1.152}$$

where Φ_0 is the full-size reference Slater determinant. Then, once we have performed the embedding calculation on site 1, we repeat the same process for other lattice sites. For each site $1 \leq i \leq L$, we obtain the interacting cluster wavefunction $\Psi^{\mathcal{C}_i}$ that fulfills the constraint in Eq. (1.152), which then implies that the total number of electrons, when summed up from all the interacting clusters, should be conserved,

$$\sum_{i=1}^{L}\langle\Psi^{\mathcal{C}_i}(\mu^{\text{imp}})|\hat{n}_i|\Psi^{\mathcal{C}_i}(\mu^{\text{imp}})\rangle = N. \tag{1.153}$$

Note that in systems with symmetry, it is sufficient to restrict the embedding calculations to the asymmetric unit. For example, in Ht-DMFET of the uniform 1D Hubbard lattice, due to translational invariance, only a single embedding calculation with chemical potential μ^{imp} that ensures correct lattice filling $n = N/L$ is necessary [105].

Recently, in *local potential functional embedding theory* (LPFET) [204], which established a formally exact link between DMET and KS-DFT for Hubbard lattices, μ^{imp} was related to the Hxc potential of the KS lattice. In the approximate LPFET scheme,

$$\mu^{\text{imp}}(n) \approx v_{\text{Hxc}}(n) \tag{1.154}$$

is the constraint that is made, which is fulfilled self-consistently, such that the uniform KS Hubbard Hamiltonian and the embedding Hamiltonian reproduce the same lattice filling n. In second quantization, the uniform KS Hubbard Hamiltonian with the Hxc potential $v_{\text{Hxc}}(n)$ reads as,

$$\hat{H}_{\text{KS}}^{\text{Hubb.}} = -t \sum_{i=1}^{L} \sum_{\sigma\in\{\uparrow,\downarrow\}} (\hat{c}_{i\sigma}^{\dagger}\hat{c}_{i+1\sigma} + \hat{c}_{i+1\sigma}^{\dagger}\hat{c}_{i\sigma}) - (\mu - v_{\text{Hxc}}(n)) \sum_{i=1}^{L} \sum_{\sigma\in\{\uparrow,\downarrow\}} \hat{c}_{i\sigma}^{\dagger}\hat{c}_{i\sigma} \tag{1.155}$$

where t is the hopping integral, and μ is the physical chemical potential of the lattice (see Eq. (2.6), and the discussion afterwards). In LPFET, which was designed in the noninteracting bath (NIB) formalism, the embedding Hamiltonian reads as,

$$\hat{\mathcal{H}}^{\text{emb.}} = \sum_{i,j=1}^{2} \sum_{\sigma\in\{\uparrow,\downarrow\}} (\tilde{h}_{ij}(n) - \mu^{\text{imp}}(n)\delta_{ij}\delta_{i1})\, \hat{d}_{i\sigma}^{\dagger}\hat{d}_{j\sigma} + U\hat{d}_{1\uparrow}^{\dagger}\hat{d}_{1\uparrow}\hat{d}_{1\downarrow}^{\dagger}\hat{d}_{1\downarrow}^{\dagger}, \tag{1.156}$$

where $\tilde{h}_{ij}(n)$ are now the Householder-transformed kinetic energy integrals (first term on the right-hand side of Eq. (1.155)). LPFET presents a way to describe strong correlation within the KS-DFT formalism, which is a challenge for approximate functionals in DFT (see Subsection 1.2.5). Let us mention that there are similar methods to LPFET, which make use of the KS-DFT formalism and embedding, namely the *density embedding theory* (DET) by Bulik *et al.* [205, 206] and *self-consistent density-functional embedding* (SDE) by Mordovina *et al.* [207]. Such a connection between DFT and embedding will also be discussed later on in Chapter 8 for the description of excited states.

Finally, once the embedding strategy of choice converges, we may compute approximations for 1RDM and 2RDM elements, which are building blocks for evaluating the ground-state energy. In the *democratic partitioning* approach [17, 216], a given RDM element is approximated as an average over all embedding clusters from which we can extract it. For example, a 1RDM element γ_{ij} of the interacting system can be approximately obtained either from the cluster based on lattice site i or the one based on lattice site j,

$$\gamma_{ij} \approx \langle \Psi^{\mathcal{C}_i} | \hat{c}^\dagger_{i\sigma} \hat{c}_{j\sigma} | \Psi^{\mathcal{C}_i} \rangle, \quad \text{or} \quad \gamma_{ij} \approx \langle \Psi^{\mathcal{C}_j} | \hat{c}^\dagger_{i\sigma} \hat{c}_{j\sigma} | \Psi^{\mathcal{C}_j} \rangle. \tag{1.157}$$

Then, the value of γ_{ij} that is used in DMET expectation values is obtained as the arithmetic average,

$$\gamma_{ij} \approx \frac{1}{2} \sum_{t \in \{i,j\}} \langle \Psi^{\mathcal{C}_t} | \hat{c}^\dagger_{i\sigma} \hat{c}_{j\sigma} | \Psi^{\mathcal{C}_t} \rangle. \tag{1.158}$$

An analogous approach is made for the 2RDM elements, where now the average is over four possible clusters (due to four-index elements),

$$\Gamma^{(2)}_{ijkl} \approx \frac{1}{4} \sum_{t \in \{i,j,k,l\}} \sum_{\sigma,\sigma' \in \{\uparrow,\downarrow\}^2} \langle \Psi^{\mathcal{C}_t} | \hat{c}^\dagger_{i\sigma} \hat{c}^\dagger_{j\sigma'} \hat{c}_{l\sigma'} \hat{c}_{k\sigma} | \Psi^{\mathcal{C}_t} \rangle. \tag{1.159}$$

1.3.2.5 Further discussions on DMET

The single-impurity strategy presented here extends seamlessly to multiple-impurity fragments [111], either with the use of the SVD as in original DMET [215], or with the Block-Householder transformation [217], which is a generalization of the regular Householder transformation. In any case, for L_F fragment spin-orbitals, one obtains the same amount (L_F) of bath spin-orbitals, and, in the idempotent 1RDM, a disentangled cluster containing L_F electrons in total. Although the multiple-impurity versions of the two transformations no longer coincide, it was shown recently that the bath spin-orbitals afforded by either transformation span the same subspace [111], even when the full-size reference 1RDM is not idempotent anymore [214].

Regarding the self-consistency of the approach, the single-shot embedding with impurity occupation matching is just the simplest possibility. Apart from the scheme of LPFET [204] (see also DET[205, 206] and SDE [207] mentioned above), embedding can be made self-consistent by enforcing different constraints. In the standard

implementation of DMET, one tries to match the "high-level" interacting cluster and "low-level" mean-field 1RDM elements in the fragment subspace by introducing a non-local correlation potential to the full-size mean-field Hamiltonian [17]. Energetics may be improved, but this is an ill-conditioned problem, since the 1RDM of an interacting system is non-idempotent, which means that it is not representable by a mean-field 1RDM. Also, the democratic partitioning in Eqs. (1.158) and (1.159) is not the only possible solution for computing approximate energies. There is actually no clear consensus on how to best reconstruct global expectation values from local fragments. In this respect, a recent review by Nusspickel *et al.* [218] presents some alternative approaches with better convergence properties with respect to cluster size than the democratic partitioning. Concerning improvements of the convergence, modifications of DMET with different fragmentations and matching constraints have also been proposed. For example, *Bootstrap embedding* (BE) [219, 220, 221] strives to ameliorate errors arising from fragment edges by using overlapping fragments, and matching local properties from different partitionings.

DMET is a recent and promising method, undergoing active research in last years. Several studies and extensions of DMET for specific systems and regimes have been published, such as spin systems [222, 223, 224], single-ion magnets [225], non-equilibrium dynamics [226], excited states [106, 227] and finite temperature [216], to name a few. It has also been rigorously investigated from a mathematical point of view [228, 229]. In addition, is worth mentioning, that quite recently, methods that are similar in spirit to DMET but are derived from the exact factorization approach of the electronic wavefunction, have been proposed [230, 231]. We can expect more novel applications of DMET (and similar methods) in the near future. In my opinion, it would be interesting to apply DMET to chemical compounds with emerging potential for industrial applications in the next decades. For instance, a DMET study of Frustrated Lewis Pairs [232, 233, 234], which have been gaining interest as possible metal-free catalysts, could be illuminating with regard to gaining new insights in chemistry, and on performance of the method.

Chapter 2

Model systems and Model Hamiltonians

This short chapter is reserved for introducing model systems, which are extensively used in the later chapters of this thesis work (see Chapters 6, 7 and 8). Firstly, what are model systems and why are they useful? The main focus of most of the methods introduced in the previous chapter is solving the *ab initio* electronic structure problem described by the electronic Hamiltonian within the Born-Oppenheimer approximation (Eq. (1.7)). As explained in that chapter, computationally affordable standard methods, such as HF and KS-DFT, which reduce the electronic structure problem to a set of single-electron equations, are inadequate for describing strongly correlated systems of interest to chemistry and physics. On the other hand, standard wavefunction methods that are more suitable for dealing with various complexities of the many-electron problem, such as CASSCF in quantum chemistry, are usually expensive, and a great deal of effort has gone into the development of quantum embedding methods which aim at cleverly combining different approaches, like FCI for the embedding cluster and HF for the full system. In order to facilitate the development of new methods, it is crucial to look for model systems, which are simplified versions of "real-life" systems, containing only those features that are essential for the description the problem we are interested in. One such example we have already mentioned in Subsection 1.3.2 are lattice models, which are introduced in more detail here. It turns out that even very simple models with only a handful of tunable parameters offer surprising theoretical insights into properties of molecules

and materials.

Let us now gradually develop the discussion about models, starting from the *ab initio* electronic Hamiltonian in Eq. (1.7). Using the second quantization formalism, we can write a more compact representation as follows [28],

$$\hat{H}_{\mathrm{e}} \equiv \sum_{ij} h_{ij} \sum_{\sigma\in\{\uparrow,\downarrow\}} \hat{c}^{\dagger}_{i\sigma}\hat{c}_{j\sigma} + \frac{1}{2}\sum_{ijkl} g_{ijkl} \sum_{\sigma,\sigma'\in\{\uparrow,\downarrow\}^2} \hat{c}^{\dagger}_{i\sigma}\hat{c}^{\dagger}_{j\sigma'}\hat{c}_{l\sigma'}\hat{c}_{k\sigma}, \tag{2.1}$$

where i now refers to an orbital (not a spin orbital) in an arbitrary orthonormal basis, and

$$h_{ij} = \int d\mathbf{r}\, \chi^{*}_{i}(\mathbf{r}) \left(-\frac{1}{2}\nabla^{2}_{\mathbf{r}} - \sum_{A=1}^{M} \frac{Z_A}{|\mathbf{r}-\mathbf{R}_A|} \right) \chi_j(\mathbf{r}), \tag{2.2}$$

and

$$g_{ijkl} = \int d\mathbf{r} \int d\mathbf{r}'\, \frac{\chi^{*}_{i}(\mathbf{r})\chi^{*}_{j}(\mathbf{r}')\chi_k(\mathbf{r})\chi_l(\mathbf{r}')}{|\mathbf{r}-\mathbf{r}'|}, \tag{2.3}$$

are known as one- and two-electron integrals, respectively. As we see, the representation of the electronic Hamiltonian in Eq. (2.1) depends on the basis of single-electron orbitals $\{\chi_k(\mathbf{r})\}_k$. This is especially useful for deriving model Hamiltonians, where based on a small number of assumptions, certain integrals are omitted and others simplified.

For example, in single-orbital lattices, which are simplifications of bulk solids, the basis is given by lattice sites (more precisely Wannier functions, or localized orbitals for chemists). One of the well-known models is the Hubbard model [69, 70, 71, 72], which is used in condensed-matter physics for studying metal-insulator transitions and high-temperature superconductivity. In this model, two assumptions are made,

1. Based on overlap arguments, one-electron integrals beyond nearest neighbors are omitted. Nearest-neighbor couplings describe electron delocalization across the lattice, which favors metallic behavior.

2. Electrons have only (super) short range interactions, *i.e.*, when they are on the same site. Longer-range interactions are neglected. This favors insulating behavior in the model by pushing the electrons to localize one on each site.

This minimal set of assumptions turns out to be essential for describing the Mott metal-insulator transition, which cannot be described by the conventional band

structure theory. This effect is most easily seen in the one-dimensional (1D) Hubbard model, whose one- and two-electron integrals are simplified as,

$$h_{ij} = -t(\delta_{j(i+1)} + \delta_{j(i-1)}) \;\; ; \;\; t > 0, \tag{2.4}$$

$$g_{ijkl} = U\delta_{ij}\delta_{ik}\delta_{il}. \tag{2.5}$$

The uniform 1D Hubbard Hamiltonian is given as,

$$\begin{aligned} \hat{H}_{\text{Hubb.}} &= \hat{\mathcal{T}} + \hat{\mathcal{U}} - \mu\hat{\mathcal{N}} \\ &\overset{1D}{\equiv} -t\sum_{i=1}^{L}\sum_{\sigma\in\{\uparrow,\downarrow\}}(\hat{c}^{\dagger}_{i\sigma}\hat{c}_{i+1\sigma} + \hat{c}^{\dagger}_{i+1\sigma}\hat{c}_{i\sigma}) + U\sum_{i=1}^{L}\hat{n}_{i\uparrow}\hat{n}_{i\downarrow} - \mu\sum_{i=1}^{L}\sum_{\sigma\in\{\uparrow,\downarrow\}}\hat{n}_{i\sigma}, \end{aligned} \tag{2.6}$$

where t is called the hopping integral, which represents delocalization between nearest neighboring sites (model version of the kinetic energy operator), U is called the on-site repulsion, μ is the chemical potential (which controls the lattice filling), and $\hat{n}_{i\sigma} = \hat{c}^{\dagger}_{i\sigma}\hat{c}_{i\sigma}$ is the spin-density operator for the site i. In the thermodynamic limit $L \to \infty$, there exists an exact ground-state solution to the Hubbard Hamiltonian, which is known as the Bethe Ansatz [235] solution. The exact solution shows that the half-filled model ($N = L$) is insulating for any nonvanishing site repulsion ($U > 0$), with each site accommodating exactly one electron. For the non-interacting limit ($U = 0$) and any lattice filling ($n = N/L$), the model reduces to the tight-binding (or Hückel) model, in which electrons are allowed to freely flow across lattice sites as in a metal. Metallic behavior is also present in the interacting ($U > 0$) model away from half-filling. Different boundary conditions can be imposed, such as periodic $\hat{c}_{L+1\,\sigma} = \hat{c}_{1\sigma}$, antiperiodic $\hat{c}_{L+1\,\sigma} = -\hat{c}_{1\sigma}$, and open $\hat{c}_{L+1\,\sigma} = 0$ boundary conditions. For finite $L < \infty$ models, each condition leads to different energies and degeneracies in the non-interacting limit. An example of such a model used in this thesis is a 6-site Hubbard model with 6 electrons and open boundary conditions, which will be used in Chapter 8 on embedding ensembles of ground and excited states.

Also a very popular model is the two-site Hubbard model, known as the Hubbard dimer, with the Hamiltonian that reads,

$$\hat{H}_{\text{Hdim}} \equiv -t\sum_{\sigma\in\{\uparrow,\downarrow\}}(\hat{c}^{\dagger}_{0\sigma}\hat{c}_{1\sigma} + \hat{c}^{\dagger}_{1\sigma}\hat{c}_{0\sigma}) + U\sum_{i=0}^{1}\hat{n}_{i\uparrow}\hat{n}_{i\downarrow} + \frac{\Delta v}{2}(\hat{n}_1 - \hat{n}_0), \tag{2.7}$$

where $\hat{n}_i = \hat{n}_{i\uparrow} + \hat{n}_{i\downarrow}$. Adding a site-dependent potential $\Delta v \neq 0$ (often labelled as Δv_{ext} in analogy with the *ab initio* external potential, see Eq. (1.89)) turns it into an asymmetric dimer, which makes it useful as a toy system for studying exact and approximate DFT, and introduces additional physics, such as charge-transfer excitations. In recent years, the Hubbard dimer has been the model of choice for studying features and limitations of DFT and TD-DFT, and also for investigating new concepts [73, 74, 75, 76, 77, 78]. It is also used extensively throughout this thesis in the context of ensemble DFT (see Chapters 6,and 7).

Chapter 3

Time-dependent approaches to electronic excitations

In the present chapter, we turn our attention to electronic excited states. For a large part of the last decades, development of successful theories and efficient computational methods for targeting excited states was lagging behind ground-state counterparts. As we have discussed in chapter 1, there is no one-size-fits-all method for solving ground-state problems. In the world of excited states, the diversity of methods is even greater, largely because of different types of excitations of interest to physicists and chemists. One possible distinction we can make, is that between neutral and charged electronic excitations. In neutral excitations, the system has the same number of electrons before and after the transition between stationary states. In molecules, transitions between low-lying states are crucial for describing, for example, photochemical activities. In insulators and semiconductors, an electron can be excited by a photon of just enough energy to make an *exciton* - a bound electron-hole pair. Neutral excitation energies can be obtained experimentally from many spectroscopy measurements, as diverse as absorption specroscopy (for example, UV-visible spectroscopy, which is routinely used for conjugated molecules in organic chemistry [236, 237]), or scattering experiments, such as inelastic X-ray scattering, which is intensively used for studying electronic properties of solids [9]. In charged processes, the system either loses (ionization) or gains an electron (affinity). Ionization is measured via photoemission [238], where photons of high-enough energy to produce an unbound electron-hole pair are directed at the experimental

sample. In contrast, affinity is measured by directing a beam of electrons of certain energy in the inverse photoemission experiment [239].

A large variety of computational methods have been developed for targeting neutral and/or charged excitations, based on either time-dependent or time-independent theoretical formalisms. Although the two types of excitations are, from an experimental point of view, very different phenomena occuring under distinct conditions, we will later see that theoretically, it is possible to develop an ensemble DFT formalism that unifies the description of both processes (see Chapters 5 and 7). Although the ensemble formalism is attractive from a computational point of view, it is currently not routinely used due to several formal and practical challenges, which are discussed in Chapters 6.

This chapter is reserved for an overview of two commonly used time-dependent methods for electronic excitations. In Section 3.1, we review the *time-dependent density-functional theory* (TD-DFT) which is nowadays the workhorse for computing neutral excitations in molecules and solids [2, 79, 80]. In Section 3.2, we introduce the formalism of many-body Green's functions, which is well-known in physics, and discuss two standard Green's function methods for charged and neutral excitations, namely the GW method and the Bethe-Salpeter equation method, respectively. Time-independent approaches for excitations are not covered here, but are instead reserved for Chapters 4 and 5.

3.1 Time-dependent Density-Functional Theory

3.1.1 Introduction

Time-dependent density-functional theory (TD-DFT) is the most popular method for describing neutral excitations and studying time-dependent phenomena. Similarly to DFT for ground states, it relies on a rigorous foundation known as the Runge-Gross (RG) theorem [1] that establishes observables as functionals of the time-dependent density and initial wavefunction. In traditional TD-DFT, the dependence on time is introduced into the electronic Hamiltonian via a (scalar) external potential,

$$\hat{H}(t) = \hat{T} + \hat{W}_{\text{ee}} + \int d\mathbf{r}\, v_{\text{ext}}(\mathbf{r}, t)\hat{n}(\mathbf{r}). \tag{3.1}$$

We consider the corresponding time-dependent (td) Schrödinger equation,

$$i\frac{\partial \left|\Psi(t)\right\rangle}{\partial t} = \hat{H}(t)\left|\Psi(t)\right\rangle, \tag{3.2}$$

which governs the evolution of the system with time, given some initial state $|\Psi(t_0)\rangle$. Furthermore, we will assume that the external potential does not contain any derivatives with respect to time (this is true for scalar potential of uniform electric field, but not with vector potential of magnetic field). It is elementary to show that if two such potentials differ by a purely td function, in the sense that $v'_{\text{ext}}(\mathbf{r}, t) = v_{\text{ext}}(\mathbf{r}, t) + Q(t)$, the corresponding td states differ by a global phase factor, $\Psi[v'_{\text{ext}}](t) = e^{-i\Theta(t)}\Psi[v_{\text{ext}}](t)$, where $\Theta(t) = \int_0^t Q(\tau)d\tau$. A more general td Hamiltonian would include couplings to both external electric and magnetic fields. However, since magnetic effects are much smaller in physical phenomena involving molecules [2], we will limit our discussion to Hamiltonians with time-dependence coming only from uniform electric fields, for which the RG theorem was initially developed.

3.1.2 Runge-Gross Theorem

As we saw for ground-state DFT, there exists an invertible map between external potentials and ground-state densities: $n_0 = n_{\Psi_0[v_{\text{ext}}]}$. In 1984, Runge and Gross [1] have shown that a similar relation exists between time-dependent scalar external

potentials, and time-dependent densities, provided that an initial quantum state $|\Psi_0\rangle$ of the system is given. Similarly to the HK theorems, the proof of the RG theorem consists of two steps, the only difference being the use of the current density in place of the ground-state wavefunction as intermediate quantity between td potentials and densities. Furthermore, it assumes $v_{\text{ext}}(\mathbf{r}, t)$ is Taylor-expandable around the initial time. Briefly, in the first step, it is shown that for two td potentials that differ by more than a time-dependent, but spatially-independent constant, $v'_{\text{ext}}(\mathbf{r}, t) - v_{\text{ext}}(\mathbf{r}, t) \neq Q(t)$, the corresponding current densities are different, $\mathbf{j}(\mathbf{r}, t) \neq \mathbf{j}'(\mathbf{r}, t)$. In the second step, it is shown, using current densities and their gradients, that if $v'_{\text{ext}}(\mathbf{r}, t) - v_{\text{ext}}(\mathbf{r}, t) \neq Q(t)$, then the td densities cannot be the same, $n'(\mathbf{r}, t) \neq n(\mathbf{r}, t)$. This establishes the invertible map: $n(\mathbf{r}, t) = n[v_{\text{ext}}, \Psi_0](\mathbf{r}, t) \longleftrightarrow v_{\text{ext}}(\mathbf{r}, t) = v_{\text{ext}}[n, \Psi_0](\mathbf{r}, t)$, and builds the foundation of TD-DFT.

3.1.3 Linear Response TD-DFT and Casida Equations

3.1.3.1 Time-dependent perturbation theory and linear response function

Most practical applications of TD-DFT are implemented in the *linear response* regime (LR-TD-DFT). More generally, linear response theory deals with systems whose output - the linear response, is proportional with respect to the external input. In the context of TD-DFT, the input is the td external potential, which is switched on at a certain time, while the output of interest is the td density. As we will show, relevant equations can be derived within perturbation theory[1]. We write our td Hamiltonian as,

$$\hat{H}(t) = \hat{H}_0 + \hat{V}_1(t), \tag{3.3}$$

where $\hat{H}_0$ is any static (time-independent) Hamiltonian, and $\hat{V}_1$ is any td external perturbation. We will consider the external field sufficiently weak such that we can expand the td wavefunction of the fully perturbed system in a power series of the unperturbed wavefunctions. The idea is that the system is in its ground state at $t = 0$, and then, we probe it gently with the external field. Quantum

[1]For reference, see the chapter on Time-Dependent Perturbation Theory in *Principles of Quantum Mechanics* by R. Shankar [240]. See also the chapter on TD-DFT in Ref. [159].

mechanical problems with one time-independent component and a td perturbation are best tackled within the "interaction picture". It means that all the operators are transformed by a unitary transformation: $\hat{O}^{(I)}(t) = e^{i\hat{H}_0 t}\hat{O}(t)e^{-i\hat{H}_0 t}$, and similarly wavefunctions, $\left|\Psi^{(I)}(t)\right\rangle = e^{i\hat{H}_0 t}\left|\Psi(t)\right\rangle$. Then it is simple to show that the time-evolution in the interaction picture is governed by a modified Schrödinger equation,

$$i\frac{\partial\left|\Psi^{(I)}(t)\right\rangle}{\partial t} = \hat{V}_1^{(I)}(t)\left|\Psi^{(I)}(t)\right\rangle. \tag{3.4}$$

For the remainder of this section, superscripts (I) are dropped unless necessary. The td wavefunction is then given by the time-ordered unitary evolution operator acting on the ground state of isolated system,

$$\left|\Psi(t)\right\rangle = \mathcal{T}e^{-i\int_0^t \hat{V}_1(t')dt'}\left|\Psi_0\right\rangle. \tag{3.5}$$

In linear response theory, the expansion of this operator only to first order is considered,

$$\left|\Psi(t)\right\rangle \approx (\mathbb{1} - i\int_0^t \hat{V}_1(t')dt')\left|\Psi_0\right\rangle. \tag{3.6}$$

Consequently the time evolution of any observable $\hat{O}(t)$, will be approximated as

$$\begin{aligned}\langle\hat{O}(t)\rangle_{\Psi(t)} &\approx \langle\hat{O}(t)\rangle_{\Psi_0} - i\int_0^t dt'\langle\Psi_0|[\hat{O}(t),\hat{V}_1(t')]|\Psi_0\rangle \\ &= \langle\hat{O}(t)\rangle_{\Psi_0} - i\int_0^\infty dt'\theta(t-t')\langle\Psi_0|[\hat{O}(t),\hat{V}_1(t')]|\Psi_0\rangle,\end{aligned} \tag{3.7}$$

where $\theta(x)$ is the Heaviside step function. In particular, if $\hat{O}(t) = \hat{n}(\mathbf{r},t) = e^{i\hat{H}_0 t}\hat{n}(\mathbf{r})e^{-i\hat{H}_0 t}$ and the external perturbation operator is multiplicative, *i.e.* $\hat{V}_1(t) = \int d\mathbf{r}\, v_1(\mathbf{r},t)\,\hat{n}(\mathbf{r},t)$, we obtain the following formula for the first-order approximation to the td density response,

$$\begin{aligned}\Delta n(\mathbf{r},t) &= n(\mathbf{r},t) - n_{\Psi_0}(\mathbf{r}) \\ &\approx -i\int_0^\infty dt'\int d\mathbf{r}'\,\theta(t-t')\langle\Psi_0|[\hat{n}(\mathbf{r},t),\hat{n}(\mathbf{r}',t')]|\Psi_0\rangle v_1(\mathbf{r}',t') \\ &= \int_0^\infty dt'\int d\mathbf{r}'\chi(\mathbf{r},t,\mathbf{r}',t')v_1(\mathbf{r}',t'),\end{aligned} \tag{3.8}$$

which becomes exact in the limit of an infinitesimally small perturbation $v_1 \to \delta v_1$, such that $\Delta n \to \delta n$,

$$\delta n(\mathbf{r},t) = \int_0^\infty dt'\int d\mathbf{r}'\chi(\mathbf{r},t,\mathbf{r}',t')\delta v_1(\mathbf{r}',t'). \tag{3.9}$$

The above equation can be seen as a matrix multiplication $\delta n = \chi \delta v_1$, where the operator χ, acting on δv_1, is defined as the *linear response function* or *susceptibility*[2],

$$\chi(\mathbf{r}, t, \mathbf{r}', t') = \left.\frac{\delta n(\mathbf{r}, t)}{\delta v_1(\mathbf{r}', t')}\right|_{v_1=0} = -i\theta(t-t')\langle\Psi_0|[\hat{n}(\mathbf{r}, t), \hat{n}(\mathbf{r}', t')]|\Psi_0\rangle. \tag{3.10}$$

The response function carries information about many properties, in particular, excitation energies of the system. In practice, we just have to transform it to the more useful frequency domain. Expanding the commutator, and inserting the resolution of the identity for the unperturbed states $\{\Psi_I\}_I$ between density operators, we obtain,

$$\begin{aligned}\chi(\mathbf{r}, t, \mathbf{r}', t') = &- i\theta(t-t')\sum_I \langle\Psi_0|\hat{n}(\mathbf{r}, t)|\Psi_I\rangle\langle\Psi_I|\hat{n}(\mathbf{r}', t')|\Psi_0\rangle \\ &+ i\theta(t-t')\sum_I \langle\Psi_0|\hat{n}(\mathbf{r}', t')|\Psi_I\rangle\langle\Psi_I|\hat{n}(\mathbf{r}, t)|\Psi_0\rangle.\end{aligned} \tag{3.11}$$

By plugging in the density operators in the interaction representation, $\hat{n}(\mathbf{r}, t) = e^{i\hat{H}_0 t}\hat{n}(\mathbf{r})e^{-i\hat{H}_0 t}$, and rearranging the phases $e^{\pm iE_I t}$, we can show that the linear response depends only on the time difference $\tau = t - t'$,

$$\begin{aligned}\chi(\mathbf{r}, \mathbf{r}', \tau) = &- i\theta(\tau)\sum_I \langle\Psi_0|\hat{n}(\mathbf{r})|\Psi_I\rangle\langle\Psi_I|\hat{n}(\mathbf{r}')|\Psi_0\rangle e^{-i\omega_I\tau} \\ &+ i\theta(\tau)\sum_I \langle\Psi_0|\hat{n}(\mathbf{r}')|\Psi_I\rangle\langle\Psi_I|\hat{n}(\mathbf{r})|\Psi_0\rangle e^{i\omega_I\tau},\end{aligned} \tag{3.12}$$

where $\omega_I = E_I - E_0$ is the neutral excitation energy of the isolated system (which is described by $\hat{H}_0$). Changing to the frequency domain can now be done with Fourier transform. The convolution theorem allows us to obtain the frequency-dependent density response,

$$\delta n(\mathbf{r}, \omega) = \int d\mathbf{r}' \chi(\mathbf{r}, \mathbf{r}', \omega)\delta v_1(\mathbf{r}, \omega), \tag{3.13}$$

where the linear response function in Fourier space looks like (see Appendix D for relevant integrals),

$$\begin{aligned}\chi(\mathbf{r}, \mathbf{r}', \omega) = &\sum_I \frac{\langle\Psi_0|\hat{n}(\mathbf{r})|\Psi_I\rangle\langle\Psi_I|\hat{n}(\mathbf{r}')|\Psi_0\rangle}{\omega - \omega_I + i0^+} \\ &- \sum_I \frac{\langle\Psi_0|\hat{n}(\mathbf{r}')|\Psi_I\rangle\langle\Psi_I|\hat{n}(\mathbf{r})|\Psi_0\rangle}{\omega + \omega_I + i0^+}.\end{aligned} \tag{3.14}$$

[2]In fact, $\chi(\mathbf{r}, t, \mathbf{r}', t')$ is also called *retarded* response function, which is nonzero strictly for $t' \leq t$, that is, when effect at time t (response) follows the cause (external field) at previous times t'.

As we can see, the poles of χ coincide with excitation and de-excitation energies. This expression for linear response is valid for any system. In particular, for a noninteracting KS system, the linear response contains excitations from the KS ground state, Φ_0. Since $\hat{n}(\mathbf{r})$ is a one-electron operator, only single excitations "survive", *i.e.*,

$$\begin{aligned}\chi_{\mathrm{KS}}(\mathbf{r},\mathbf{r}',\omega) =& 2\sum_{i}^{occ.}\sum_{a}^{virt.}\frac{\varphi_i^*(\mathbf{r})\varphi_a(\mathbf{r})\varphi_a^*(\mathbf{r}')\varphi_i(\mathbf{r}')}{\omega-(\varepsilon_a-\varepsilon_i)+i0^+} \\ &- 2\sum_{i}^{occ.}\sum_{a}^{virt.}\frac{\varphi_i^*(\mathbf{r}')\varphi_a(\mathbf{r}')\varphi_a^*(\mathbf{r})\varphi_i(\mathbf{r})}{\omega+(\varepsilon_a-\varepsilon_i)+i0^+},\end{aligned} \tag{3.15}$$

and the excitation energies reduce to orbital energy differences.

3.1.3.2 Connection between response functions and the Casida equation

Just like in the ground-state DFT, TD-DFT is made practical by connecting the true interacting system to the KS one. In LR-TD-DFT, the linear density response of both systems is the same, *i.e.* $\delta n(\mathbf{r},\omega) = \delta n_{\mathrm{KS}}(\mathbf{r},\omega)$, if the mapping is exact. According to Eq. (3.13), this implies

$$\int d\mathbf{r}'\chi(\mathbf{r},\mathbf{r}',\omega)\delta v_1(\mathbf{r},\omega) = \int d\mathbf{r}'\chi_{\mathrm{KS}}(\mathbf{r},\mathbf{r}',\omega)\delta v_{\mathrm{KS}}(\mathbf{r},\omega), \tag{3.16}$$

where $\delta v_{\mathrm{KS}}(\mathbf{r},\omega)$ is the perturbation to the ground-state KS potential. To make the above equation workable, we turn to the KS system. Assuming the time evolution starts from a nondegenerate ground state[3], the td KS equations read as,

$$\left(-\frac{\nabla_{\mathbf{r}}^2}{2}+v_{\mathrm{KS}}[n](\mathbf{r},t)\right)\varphi_k(\mathbf{r},t) = i\frac{\partial\varphi_k(\mathbf{r},t)}{\partial t}, \tag{3.17}$$

where the td KS potential and density at time t read as,

$$v_{\mathrm{KS}}[n](\mathbf{r},t) = v_{\mathrm{ext}}(\mathbf{r}) + v_1(\mathbf{r},t) + v_{\mathrm{Hxc}}[n](\mathbf{r},t), \tag{3.18}$$

and

$$n(\mathbf{r},t) = \sum_{k=1}^{N}|\varphi_k(\mathbf{r},t)|^2. \tag{3.19}$$

[3]In general, the td KS potential will depend not only on the td density, but also on initial states of the interacting and KS system, *i.e.* $v_{\mathrm{KS}} = v_{\mathrm{KS}}[n,\Psi_0,\Phi_0]$. If initial state is a nondegenerate ground state such that $n_{\Psi_0} = n_{\Phi_0}$, then the potential only depends on density $v_{\mathrm{KS}} = v_{\mathrm{KS}}[n]$.

Unlike the td potential of the interacting sytem, which depends on time t, the td KS potential also depends, through the density, on previous times $t' \leq t$ (memory effect). Therefore, to find the relation between the response functions χ and $\chi_{\rm KS}$, we go back to the time domain, and make use of the chain rule of differentiation. First of all, because the interacting and KS td densities are the same, (in the time domain, $\delta n(\mathbf{r},t) = \delta n_{\rm KS}(\mathbf{r},t)$) we realize that,

$$\chi(\mathbf{r},t,\mathbf{r}',t') = \frac{\delta n(\mathbf{r},t)}{\delta v_1(\mathbf{r}',t')} = \frac{\delta n_{\rm KS}(\mathbf{r},t)}{\delta v_1(\mathbf{r}',t')}. \tag{3.20}$$

By the chain rule, the rightmost term of the above equation reads,

$$\begin{aligned}\frac{\delta n_{\rm KS}(\mathbf{r},t)}{\delta v_1(\mathbf{r}',t')} = \int d\mathbf{r}'' \int dt'' \, \frac{\delta n_{\rm KS}(\mathbf{r},t)}{\delta v_{\rm KS}(\mathbf{r}'',t'')} \cdot \Bigg(\frac{\delta v_{\rm KS}(\mathbf{r}'',t'')}{\delta v_1(\mathbf{r}',t')} \\ + \int d\mathbf{r}''' \int dt''' \frac{\delta v_{\rm Hxc}[n](\mathbf{r}'',t'')}{\delta n(\mathbf{r}''',t''')} \cdot \frac{\delta n(\mathbf{r}''',t''')}{\delta v_1(\mathbf{r}',t')} \Bigg),\end{aligned} \tag{3.21}$$

where

$$\frac{\delta v_{\rm KS}(\mathbf{r},t)}{\delta v_1(\mathbf{r}',t')} = \delta(\mathbf{r}-\mathbf{r}')\delta(t-t'), \tag{3.22}$$

and the functional derivative of the Hxc potential with respect to the td density is defined as the Hartree-exchange-correlation (Hxc) kernel[4],

$$f_{\rm Hxc}(\mathbf{r},t,\mathbf{r}',t') := \frac{\delta v_{\rm Hxc}[n](\mathbf{r},t)}{\delta n(\mathbf{r}',t')}. \tag{3.23}$$

By plugging the functional derivative definitions $\chi(\mathbf{r},t,\mathbf{r}',t') = \delta n(\mathbf{r},t)/\delta v_1(\mathbf{r}',t')$ and $\chi_{\rm KS}(\mathbf{r},t,\mathbf{r}',t') = \delta n_{\rm KS}(\mathbf{r},t)/\delta v_{\rm KS}(\mathbf{r}',t')$ into Eq. (3.21), we obtain a Dyson-like equation relating the two response functions,

$$\begin{aligned}\chi(\mathbf{r},t,\mathbf{r}',t') = \int d\mathbf{r}'' \int dt'' \, \chi_{\rm KS}(\mathbf{r},t,\mathbf{r}'',t'') \cdot \Bigg(\delta(\mathbf{r}''-\mathbf{r}')\delta(t''-t') \\ + \int d\mathbf{r}''' \int dt''' f_{\rm Hxc}(\mathbf{r}'',t'',\mathbf{r}''',t''') \cdot \chi(\mathbf{r}''',t''',\mathbf{r}',t') \Bigg).\end{aligned} \tag{3.24}$$

[4]Just like response functions, the Hxc kernel should depend only on time difference (causality), *i.e.* $f_{\rm Hxc}(\mathbf{r},t,\mathbf{r}',t') = f_{\rm Hxc}(\mathbf{r},\mathbf{r}',t-t')$. However, this makes it difficult do define it as a second functional derivative of some Hxc density functional. One possibility for is to start from the Frenkel-Dirac action [155, 241], which however has problems associated with causality. There have been many rigorous redefinitions of the action such as Keldysh pseudo-time formalism [242, 243], or actions with the Berry phase [244], all of which attempt to derive causal equations of motion.

In the frequency domain, it reads,

$$\begin{aligned}\chi(\mathbf{r},\mathbf{r}',\omega) &= \chi_{\mathrm{KS}}(\mathbf{r},\mathbf{r}',\omega) \\ &+ \int d\mathbf{r}'' \int d\mathbf{r}''' \chi_{\mathrm{KS}}(\mathbf{r},\mathbf{r}'',\omega) f_{\mathrm{Hxc}}(\mathbf{r}'',\mathbf{r}''',\omega)\chi(\mathbf{r}''',\mathbf{r}',\omega).\end{aligned} \tag{3.25}$$

Casida has shown [10] that Eq. (3.25) can be recast into a matrix representation in the occupied-virtual product (ia, jb) space of KS orbitals, also known as transition space. The so-called Casida equation looks like[5],

$$\begin{bmatrix} \mathbf{A}(\omega) & \mathbf{B}(\omega) \\ \mathbf{B}^*(\omega) & \mathbf{A}^*(\omega) \end{bmatrix} \begin{bmatrix} \mathbf{X}(\omega) \\ \mathbf{Y}(\omega) \end{bmatrix} = \omega \begin{bmatrix} -1 & 0 \\ 0 & 1 \end{bmatrix} \begin{bmatrix} \mathbf{X}(\omega) \\ \mathbf{Y}(\omega) \end{bmatrix}, \tag{3.26}$$

where the $\mathbf{A}$ and $\mathbf{B}$ matrix elements read,

$$\begin{aligned}\mathbf{A}_{ia,jb}(\omega) &= \delta_{ij}\delta_{ab}(\varepsilon_a - \varepsilon_i) + \langle \varphi_i\varphi_b | f_{\mathrm{Hxc}}(\omega) | \varphi_a\varphi_j \rangle, \\ \mathbf{B}_{ia,jb}(\omega) &= \langle \varphi_i\varphi_j | f_{\mathrm{Hxc}}(\omega) | \varphi_a\varphi_b \rangle.\end{aligned} \tag{3.27}$$

This is a generalized eigenvalue problem, whose solutions are the interacting system's excitation energies ω with response eigenvectors $[\mathbf{X}(\omega), \mathbf{Y}(\omega)]$, and de-excitation energies $-\omega$ with response eigenvectors $[\mathbf{Y}^*(\omega), \mathbf{X}^*(\omega)]$.

The size of the matrix in Eq. (3.26) is equal to $(2 \times N_{occ} \times N_{virt})^2$. The presence of virtuals entails additional computational costs compared to the ground-state KS-DFT calculations, for example. This is also one of the reasons why ensemble DFT, in particular the *Theophilou-Gross-Oliveira-Kohn* (TGOK) DFT [86, 87, 88, 90, 89] is an appealing alternative, which will be discussed in more detail in Chapters 4 and 6. Because of frequency dependence in the Hxc kernel, there are more solutions than the size of the matrix dictates. Thus, in principle, double and higher-order excitations should be recovered even though the KS linear response function explicitly includes only single excitations. However, in most practical applications, the so-called *adiabatic approximation* (AA) is employed, where the bare ground-state Hxc density-functional is employed in place of the Hxc kernel,

$$f_{\mathrm{xc}}^{\mathrm{AA}}(\mathbf{r},\mathbf{r}',t-t') = \left.\frac{\delta^2 E_{\mathrm{Hxc}}[n]}{\delta n(\mathbf{r}')\delta n(\mathbf{r})}\right|_{n=n(\mathbf{r},t)}. \tag{3.28}$$

The latter has no memory effect, hence no frequency dependence. For example, in the *adiabatic local density approximation* (ALDA), f_{Hxc} is directly computed from

[5]For a complete derivation, see the original paper by M. Casida [10], or, for example, the following master's thesis in Ref. [245].

the LDA functional derivative, evaluated at the ground-state density,

$$f_{\mathrm{xc}}^{\mathrm{ALDA}}(\mathbf{r},\mathbf{r}',t-t') = \delta(\mathbf{r}-\mathbf{r}')\delta(t-t')\left.\frac{d^2(n\varepsilon_{\mathrm{xc}}(n))}{dn^2}\right|_{n=n_{\Phi_0}(\mathbf{r})}. \tag{3.29}$$

Consequently, ALDA gives frequency-independent matrix elements in Eq. (3.26), so that only single excitation (and de-excitation) energies are recovered. Furthermore, assuming that we are working with real algebra $\mathbf{A}^* = \mathbf{A}$ and $\mathbf{B}^* = \mathbf{B}$, and $\mathbf{A}-\mathbf{B}$ is positive-definite [246], the generalized eigenvalue problem can be transformed into a half-size symmetric eigenvalue problem,

$$\boldsymbol{\Omega}\mathbf{F} = \omega^2\mathbf{F}, \tag{3.30}$$

where $\boldsymbol{\Omega} = (\mathbf{A}-\mathbf{B})^{1/2}(\mathbf{A}+\mathbf{B})(\mathbf{A}-\mathbf{B})^{1/2}$ and $\mathbf{F} = (\mathbf{A}-\mathbf{B})^{-1/2}(\mathbf{X}+\mathbf{Y})$. If we take $\mathbf{B} = 0$ (excitations and de-excitations are then decoupled), we obtain the *Tamm-Dancoff approximation* (TDA),

$$\mathbf{A}\mathbf{X} = \omega\mathbf{X}, \tag{3.31}$$

which is very similar to the configuration *interaction singles* (CIS) method.
In addition to excitation energies, the Casida equation can be used to extract oscillator strengths, which give information on optical transition intensities. For an excitation $\omega_I = E_I - E_0$, the corresponding oscillator strength is given by,

$$f_I = \frac{2}{3}\omega_I \sum_{q=x,y,z} |\langle\Psi_0|\hat{q}|\Psi_I\rangle|^2. \tag{3.32}$$

Transition matrix elements $\langle\Psi_0|\hat{q}|\Psi_I\rangle$ are obtained by probing the system with uniform electric field in different directions, $\hat{V}_1(t) \equiv \mathcal{E}_q \cos(\omega t)\sum_{i=1}^{N}\hat{q}_i$. Then, from eigenvectors of Eq. (3.30), oscillator strengths can be extracted as [10],

$$f_I = \frac{2}{3}\sum_{\mathbf{q}=\mathbf{x},\mathbf{y},\mathbf{z}} |\mathbf{q}^\dagger(\mathbf{A}-\mathbf{B})^{-1/2}\mathbf{F}_I|^2, \tag{3.33}$$

where $\mathbf{q}_{ia} = \int d\mathbf{r}\,\varphi_i^*(\mathbf{r})\hat{q}\varphi_a(\mathbf{r})$.

3.1.3.3 Challenges in linear response TD-DFT

The success of LR-TD-DFT, as evident in the numbers of cited papers, mirrors that of KS-DFT for ground states. Nonetheless, the method has several drawbacks that

lead to inaccurate predictions, or no predictions at all for some types of excitations. Some drawbacks of LR-TD-DFT are discussed in the following.

As already mentioned, in the commonly used AA, only single (1-particle-1-hole) excitations are explicitly accounted for, with multiple excitations completely missing in the AA spectrum. One explicit way to include multiple excitations is to go beyond the linear response regime, but double excitations do not appear before the KS third-order response function except as sums of single excitations (*i.e.* there is no mixing with other single excitations in the second order) [247]. A more readily accessible improvement is, as mentioned earlier, to replace ALDA by a frequency-dependent kernel, which creates additional solutions in the Casida equation. Many approaches for introducing frequency dependence have been developed, such as dressed TDDFT [248], or methods based on many-body theory [249, 250, 251, 252, 253, 254, 255], which however are not standard. In comparison, Spin-Flip TDDFT [256, 257, 258] tackles 2p2h excitations with frequency independent kernels.

Another class of neutral excitations for which the standard LR-TD-DFT fails are *charge-transfer* (CT) excitations [81, 82, 83]. A simple example suffices to show the issue at hand (see pp.17-18 in Ref. [259] for more details). Consider a well-separated two-level system with φ_0 (donor, doubly occupied) and φ_1 (acceptor, empty) orbitals in the ground state. The CT excitation is given as the difference between donor ionization, acceptor affinity, and resulting ionic Coulomb interaction,

$$\omega_{\mathrm{CT}} \approx I_0 - A_1 - 1/R. \tag{3.34}$$

Within the AA, the same excitation can be approximated as the KS orbital energy difference between the donor and the acceptor, plus a kernel contribution,

$$\omega_{\mathrm{CT}} \approx \varepsilon_1 - \varepsilon_0 + 2\langle\varphi_0\varphi_1|f_{\mathrm{Hxc}}|\varphi_0\varphi_1\rangle. \tag{3.35}$$

However, since the involved orbitals are assumed well-separated with negligible differential overlap $\varphi_0(\mathbf{r})\varphi_1(\mathbf{r}) \approx 0$, the Hxc kernel contribution vanishes (this is the case for standard (semi-)local density functionals such as LDA/GGA), and the result is close to the KS energy difference, $\omega \approx \varepsilon_1 - \varepsilon_0$, which can be a drastic underestimation of the true CT excitation energy. It turns out that using hybrids and range-separated hybrid functionals can be beneficial for describing CT

excitations [260, 261, 262, 79]. Firstly, this is because the two classes of hybrids afford a better description of the KS orbital energies than standard (semi-)local ground-state density functionals. The poor orbital energy description of the latter is related to the missing derivative discontinuity [79], which is a fundamental concept of (time-independent) DFT for charged excitations [102], and also the more recent N-centered ensemble DFT [91] (see Chapter 5 for a detailed discussion on the derivative discontinuity and the N-centered eDFT, and Chapter 7 for the recent work on exactification of the KS orbital energies). Secondly, the Hxc kernel of hybrid functionals partially accounts for the $-1/R$ asymptotic behavior of the exact charge-transfer excitation [263, 79].

LR-TD-DFT with (semi-local) functionals also fails for other cases, such as Rydberg excitations [2, 264], and band gaps in solids [265] (as the asymptotic limit of Rydberg series), and conical intersections [84, 85]. In the latter (conical intersections), a balanced treatment of low-lying excited states is critical, which cannot be expected from LR-TD-DFT as it relies on orbitals from a ground-state DFT calculation. By comparison, in TGOK-DFT, which is one of the central methods of this thesis work, the orbitals are optimized for ensembles of ground and low-lying excited states (each of which are described by configuration-state functions in the ensemble KS scheme, much like in state-averaged CASSCF in Section 4.1), with the constraint that they (orbitals) reproduce the ensemble density of the true interacting system. TGOK-DFT will be discussed in more detail in Chapters 4 and 5. In addition, an embedding strategy for multiple states with the formalism of TGOK ensembles is proposed in this thesis work, which is which is the topic of Chapter 8. The latter strategy was successful in describing conical intersections and avoided crossings in finite model systems.

3.1.4 Further discussion, extensions, and alternative approaches

Originally, the TD-DFT method that we discussed in this section, has been formulated for scalar electric potentials $v_{\text{ext}}(\mathbf{r}, t)$ (see Subsection 3.1.2. An extension of TD-DFT with a more general electromagnetic interaction, known as *time-*

dependent current density functional theory (TD-CDFT), includes magnetic field effects through the td vector potential $\mathbf{A}(t)$. In TD-CDFT, whose formal proof was first given by Ghosh and Dhara [266], the mapping of potentials to densities is extended to pairs of variables $(v, \mathbf{A}) \leftrightarrow (n, \mathbf{j})$. This extension makes the RG theorem more general for periodic systems [267], and offers a more suitable route than regular TD-DFT for the development of xc kernels with memory effects [268, 269].

Finally, the usual LR-TD-DFT approach with Casida equation, although nowadays being a standard in most computational chemistry packages, has a moderate computational cost, since the evaluation of the Casida equation requires both occupied and virtual orbitals, which scales roughly as $\mathcal{O}(K^4)$ with the size K of the system (*e.g.* number of atoms in the system). For dealing with the limitations of the Casida equation, an alternative linear response scheme known as the Sternheimer method has been proposed [270, 271], which requires only occupied orbitals for the evaluation of excitations, and can be completely parallelized for perturbations with different frequencies [272]. Outside the scope of TD-DFT, the theory of Green's functions with the *Bethe-Salpeter equation* (BSE) formalism (see Subsection 3.2.3) offers a similar way for targeting neutral excitations, with essentially the same computational cost (without considering the preceding GW calculation [12]). Alternatively, TGOK-DFT, which is a variational and time-independent theory for ensembles of ground and excited states, has been a subject of interest in recent decades due to the prospect of obtaining neutral excitation energies with essentialy the same cost as KS-DFT. The latter will also be explored further in this thesis in various contexts (see Chapters 4 - 8).

3.2 Green's Function Theory

3.2.1 Introduction

The theory of (many-body) Green's functions is another formalism for the description of excitations, which is particularly popular in condensed-matter physics. The Green's function formalism allows for extraction of both neutral and charged excitations, with the GW approximation [4, 5, 6] and the Bethe-Salpeter equation [7, 8], respectively. This section is a brief attempt at summarizing the key concepts about both GW and BSE. Far more comprehensive discussions are available for example in the theses of F. Sottile [273] and F. Bruneval [274] (see also Ref. [246] for a short introduction to Green's functions).

3.2.2 Single-particle Green's function and the GW method

The usual formalism is introduced in position representation in second quantization, using creation $\hat{\Psi}^\dagger$ and annihilation $\hat{\Psi}$ field operators (see Appendix A), taken in the Heisenberg picture (which is the same as the interaction picture introduced in Subsection 3.1.3 when the Hamiltonian is time-independent),

$$\hat{\Psi}(\mathbf{x},t) \equiv e^{i\hat{H}t}\hat{\Psi}(\mathbf{x})e^{-i\hat{H}t}, \quad \hat{\Psi}^\dagger(\mathbf{x},t) \equiv e^{i\hat{H}t}\hat{\Psi}^\dagger(\mathbf{x})e^{-i\hat{H}t}. \tag{3.36}$$

The time-ordered one-particle Green's function at zero-temperature is defined as,

$$\begin{aligned} iG(1,2) &= \langle\Psi_0^N|\mathcal{T}\hat{\Psi}(1)\hat{\Psi}^\dagger(2)|\Psi_0^N\rangle \\ &= \theta(t_1-t_2)\langle\Psi_0^N|\hat{\Psi}(1)\hat{\Psi}^\dagger(2)|\Psi_0^N\rangle - \theta(t_2-t_1)\langle\Psi_0^N|\hat{\Psi}^\dagger(2)\hat{\Psi}(1)|\Psi_0^N\rangle, \end{aligned} \tag{3.37}$$

where $1 \equiv (\mathbf{x}_1,\sigma_1) = (\mathbf{r}_1,t_1,\sigma_1)$, and $|\Psi_0^N\rangle$ is the ground state of the N-electron system under study. The time ordering operator $\mathcal{T}$ ensures that creation/annihilation operators appear chronologically from earlier to later times (when applied from right to left, respectively). This means that the Green's function describes two phenomena. When $t_1 > t_2$, an electron is added to the N-electron system at time t_2 and position $\mathbf{r}_2$ with spin σ_2, and then the removal of an electron at position $\mathbf{r}_1$ with spin σ_1 occurs later at time t_1. On the other hand, if $t_2 > t_1$, an electron is removed from the N-electron system at time t_1 and position $\mathbf{r}_1$ with spin σ_1, followed by the

addition of an electron at position $\mathbf{r}_2$ with spin σ_2 later at time t_2. The one-particle Green's function contains in itself simpler, static reduced quantities, such as the 1RDM and the electron density,

$$\gamma(\mathbf{x}_2, \mathbf{x}_1) = \langle \Psi_0^N | \hat{\Psi}^\dagger(\mathbf{x}_2) \hat{\Psi}(\mathbf{x}_1) | \Psi_0^N \rangle = -iG(\mathbf{x}_1 t_1, \mathbf{x}_2 t_1^+), \tag{3.38}$$

$$n(\mathbf{r}_1) = -i \sum_{\sigma_1 \in \{\uparrow,\downarrow\}} G(\mathbf{r}_1 \sigma_1 t_1, \mathbf{r}_1 \sigma_1 t_1^+), \tag{3.39}$$

where $t_1^+ = t_1 + 0^+$. The one-particle Green's function also contains information about charged excitations. This can be shown, just like for the linear response function in TD-DFT, by transforming Eq. (3.37) to the frequency domain. The only difference is that we need to insert the projectors for $N+1$-electron states $\sum_a |\Psi_a^{N+1}\rangle\langle\Psi_a^{N+1}|$ inside the $t_1 > t_2$ term, and $N-1$-electron states $\sum_i |\Psi_i^{N-1}\rangle\langle\Psi_i^{N-1}|$ inside the $t_1 < t_2$ term. As a result, we arrive at the so-called Lehmann representation for G,

$$G(\mathbf{x}_1, \mathbf{x}_2, \omega) = \sum_a \frac{f_a(\mathbf{x}_1) f_a^*(\mathbf{x}_2)}{\omega - \mathcal{E}_a + i0^+} + \sum_i \frac{f_i(\mathbf{x}_1) f_i^*(\mathbf{x}_2)}{\omega - \mathcal{E}_i + i0^+}, \tag{3.40}$$

where $f_a(\mathbf{x}) = \langle \Psi_0^N | \hat{\Psi}(\mathbf{x}) | \Psi_a^{N+1} \rangle$ and $f_i(\mathbf{x}) = \langle \Psi_i^{N-1} | \hat{\Psi}(\mathbf{x}) | \Psi_0^N \rangle$ are the Lehmann (quasiparticle) amplitudes or Dyson orbitals. The corresponding poles are the exact electron affinities (EA) $A_a^N = E_0^N - E_a^{N+1} = -\mathcal{E}_a$, and ionization potentials (IP), $I_i^N = E_i^{N-1} - E_0^N = -\mathcal{E}_i$. In a noninteracting (or mean-field) Green's function, the amplitudes are replaced by spin-orbitals,

$$G(\mathbf{x}_1, \mathbf{x}_2, \omega) = \sum_a^{\text{virt}} \frac{\varphi_a(\mathbf{x}_1) \varphi_a^*(\mathbf{x}_2)}{\omega - \varepsilon_a + i0^+} + \sum_i^{\text{occ}} \frac{\varphi_i(\mathbf{x}_1) \varphi_i^*(\mathbf{x}_2)}{\omega - \varepsilon_i + i0^+}, \tag{3.41}$$

and EA/IP are given by the orbital energies. For a general, interacting Hamiltonian with the one-electron operator $h(1) \equiv -\nabla_{\mathbf{r}_1}^2/2 + v_{\text{ext}}(\mathbf{r}_1)$, and two-electron operator $w_{\text{ee}}(1,2) \equiv |\mathbf{r}_1 - \mathbf{r}_2|^{-1}$, we do not know *a priori* how to obtain exact amplitudes in Eq. (3.40), apart from solving the Schrödinger equation for N and $N \pm 1$ electrons. Concerning the one-particle Green's function, it is possible to derive a series of coupled equations of motion coupling it to other Green's functions. The first one, connecting G and G_2 (the two-particle Green's function) is given as [246],

$$\left(i\frac{\partial}{\partial t_1} - h(1) \right) G(1,2) + i \int d3\, w_{\text{ee}}(1,3) G_2(1, 3^+; 2, 3^{++}) = \delta(1,2), \tag{3.42}$$

where $3^+, 3^{++}$ means $t_3 + 0^+$ and $t_3 + 0^+ + 0^+$, respectively, and G_2 is defined as,

$$i^2 G_2(1,2;1',2') = \langle \Psi_0^N | \mathcal{T} \hat{\Psi}(1) \hat{\Psi}(2) \hat{\Psi}^\dagger(2') \hat{\Psi}^\dagger(1') | \Psi_0^N \rangle. \tag{3.43}$$

In fact, coupled equations of motion continue for G_2 and G_3, and so on, which means that we have to resort to approximations for practical purposes. For describing charged excitations in this context, we need approximations to G_2, while for neutral excitations, which can be extracted from G_2 (see Subsection 3.2.3), we would need approximations for G_3 [274]. For this purpose, the self-energy operator Σ_{Hxc} is formally defined so as to close the recursive dependence on many-particle Green's functions,

$$\int d3\, \Sigma_{\text{Hxc}}(1,3) G(3,2) = -i \int d3\, w_{\text{ee}}(1,3) G_2(1,3^+;2,3^{++}). \tag{3.44}$$

For the noninteracting Green's function G_0, $\Sigma_{\text{Hxc}} = 0$. Then, we can show that the interacting Green's function G is related to G_0 by a Dyson equation,

$$G(1,2) = G_0(1,2) + \int d34\, G_0(1,3) \Sigma_{\text{Hxc}}(3,4) G(4,2). \tag{3.45}$$

Thus, the self-energy Σ_{Hxc} now contains all the (difficult-to-model) many-electron effects, which is analogous to v_{Hxc} in KS-DFT, except that Σ_{Hxc} nonlocal and dynamical (*i.e.* time-dependent), while v_{Hxc} is local and static. Transforming Eq. (3.42) into the frequency domain, and using the definition of the self energy in Eq. (3.44), we obtain,

$$[\omega - h(\mathbf{r}_1)]\, G(\mathbf{x}_1, \mathbf{x}_2, \omega) - \int d\mathbf{x}_3 \Sigma_{\text{Hxc}}(\mathbf{x}_1, \mathbf{x}_3, \omega) G(\mathbf{x}_1, \mathbf{x}_3, \omega) = \delta(\mathbf{x}_1, \mathbf{x}_2). \tag{3.46}$$

Upon inserting the Lehmann representation of the Green's function, we obtain a set of eigenvalue equations for the Dyson orbitals, coupled through the self energy,

$$h(\mathbf{r}_1) f_k(\mathbf{x}_1) - \int d\mathbf{x}_3 \Sigma_{\text{Hxc}}(\mathbf{x}_1, \mathbf{x}_3, \mathcal{E}_k) f_k(\mathbf{x}_3) = \mathcal{E}_k f_k(\mathbf{x}_1), \tag{3.47}$$

which is analogous to the HF and KS equations[6]. In fact, by inserting the noninteracting functional approximation to the two-particle Green's function into the

[6]To be more precise, in the HF theory, Σ_{Hxc} is static and nonlocal (see main text), while for the KS system, Σ_{Hxc} becomes static and local.

equation of motion: $G_2^{\mathrm{HF}}(1,2;1',2') = G(1,1')G(2,2') - G(1,2')G(2,1')$, and Fourier-transforming, we get the frequency-independent (local) Hartree and exchange self-energy components [246],

$$\Sigma_{\mathrm{H}}(\mathbf{x}_1,\mathbf{x}_2) = \delta(\mathbf{x}_1-\mathbf{x}_2)v_{\mathrm{H}}(\mathbf{r}_1) \quad \Sigma_{\mathrm{x}}(\mathbf{x}_1,\mathbf{x}_2) = \gamma(\mathbf{x}_1,\mathbf{x}_2)w_{\mathrm{ee}}(\mathbf{r}_1,\mathbf{r}_2), \tag{3.48}$$

which, when inserted into Eq. (3.47), give back the HF equations. Thus, if we know the self-energy, we can obtain all the quasiparticle enegies (ionization potentials and electron affinities) of the system. The full self-energy Σ_{Hxc} (including correlation effects) can be obtained, in principle exactly, from Hedin's equations [3], which is a set of five coupled equations including the above Dyson equation, and four other equations for the self-energy (Σ_{Hxc}), the vertex function (Γ), the polarizability (χ) and the screened Coulomb interaction (W). Unfortunately, Hedin's scheme is computationally extremely expensive, so that approximations are usually necessary. One of the most popular approximations in this respect is the GW method [4, 5, 6], which consists in omitting the vertex part of Hedin's scheme. This gives the approximate expression for the xc part of the self-energy as a product of Green's function G and the screened Coulomb interaction W,

$$\Sigma_{\mathrm{xc}} = iG(1,2)W(2,1^+). \tag{3.49}$$

In GW approximation, the polarizability reads,

$$\chi_0(1,2) = -iG(1,2)G(2,1), \tag{3.50}$$

which is known as the *random-phase approximation* (RPA). It is the input for the screened Coulomb interaction,

$$W(1,2) = w_{\mathrm{ee}}(1,2) + \int d34\, w_{\mathrm{ee}}(1,3)\chi_0(3,4)W(4,2). \tag{3.51}$$

The computation of the self-energy proceeds as follows. Firstly, G is taken from a noninteracting system, usually the Kohn-Sham system. Then, χ_0 and the inverse dielectric function $\varepsilon^{-1} = [\mathbb{1} - w_{\mathrm{ee}}\chi_0]^{-1}$ are evaluated, which in turn is used to evaluate the screened Coulomb interaction $W = \varepsilon^{-1}w_{\mathrm{ee}}$. Afterwards, Eq. (3.49) is calculated as a convolution in the frequency domain. In solids, the plasmon-pole model [275, 276] is commonly employed for ε^{-1}, which simplifies the evaluation of the convolution integral for Σ_{xc}.

After obtaining the self-energy, we can use it to calculate quasiparticle energies and band gaps. In the simplest G_0W_0 approach (also called single-shot GW), the G and W are obtained once from the KS ingredients. Also, an assumption is often made that Dyson orbitals are not too different from the KS orbitals, so that approximate quasiparticle energies can be obtained from the perturbation expansion of $(\Sigma_{\mathrm{xc}} - v_{\mathrm{xc}})$ on top of the KS Hamiltonian. The first-order quasiparticle energy corrections read,

$$\mathcal{E}_k^{\mathrm{GW}} = \varepsilon_k^{\mathrm{KS}} + \langle \varphi_k^{\mathrm{KS}} | \Sigma_{\mathrm{xc}}(\mathcal{E}_k^{\mathrm{GW}}) - v_{\mathrm{xc}} | \varphi_k^{\mathrm{KS}} \rangle. \tag{3.52}$$

In order to avoid solving this nonlinear equation for $\mathcal{E}_k^{\mathrm{GW}}$, another approximation is made by considering the Taylor expansion around the KS energies,

$$\Sigma_{\mathrm{xc}}(\mathcal{E}_k^{\mathrm{GW}}) \approx \Sigma_{\mathrm{xc}}(\varepsilon_k^{\mathrm{KS}}) + (\mathcal{E}_k^{\mathrm{GW}} - \varepsilon_k^{\mathrm{KS}}) \left. \frac{\partial \Sigma_{\mathrm{xc}}(\omega)}{\partial \omega} \right|_{\omega = \varepsilon_k^{\mathrm{KS}}}. \tag{3.53}$$

Inserting this back into Eq. (3.52) gives,

$$\mathcal{E}_k^{\mathrm{GW}} \approx \varepsilon_k^{\mathrm{KS}} + Z_k \langle \varphi_k^{\mathrm{KS}} | \Sigma_{\mathrm{xc}}(\varepsilon_k^{\mathrm{KS}}) - v_{\mathrm{xc}} | \varphi_k^{\mathrm{KS}} \rangle, \tag{3.54}$$

where the renormalization factor Z_k is equal to,

$$Z_k = \left[1 - \langle \varphi_k^{\mathrm{KS}} | \left. \frac{\partial \Sigma_{\mathrm{xc}}(\omega)}{\partial \omega} \right|_{\omega = \varepsilon_i^{\mathrm{KS}}} | \varphi_k^{\mathrm{KS}} \rangle \right]^{-1}. \tag{3.55}$$

This linearization, which usually works well near the Fermi level in solids, has been used extensively in the past for correcting KS-predicted energies and band structures in semiconductors and insulators [277, 276, 278, 279], and surfaces [280, 281, 282]. For instance, based on Eq. (3.54), the fundamental gap can be expressed as the bare KS gap plus a GW-based correction [283],

$$\begin{aligned} E_g^N &= I_0^N - A_0^N \\ &\overset{GW}{\approx} \varepsilon_{N+1} - \varepsilon_N + Z_{N+1} \langle \varphi_{N+1}^{\mathrm{KS}} | \Sigma_{\mathrm{xc}}(\varepsilon_{N+1}^{\mathrm{KS}}) - v_{\mathrm{xc}} | \varphi_{N+1}^{\mathrm{KS}} \rangle \\ &\qquad - Z_N \langle \varphi_N^{\mathrm{KS}} | \Sigma_{\mathrm{xc}}(\varepsilon_N^{\mathrm{KS}}) - v_{\mathrm{xc}} | \varphi_N^{\mathrm{KS}} \rangle, \end{aligned} \tag{3.56}$$

This simple perturbative correction may be improved upon by re-calculating G self-consistently from Eq. (3.45), albeit with additional computational costs. For further details on the different self-consistent GW implementations, see a review by Reining [284], and the references therein. Nevertheless, even the G_0W_0 approach is not cheap, with ordinary implementations scaling as $\mathcal{O}(K^4)$ with system size

K [285]. This is one of the reasons why other formalisms are being explored, such as the N-centered ensemble DFT for charged excitations [91], which is introduced Chapter 5. In the latter, the correction to the bare KS gap is given by the weight derivative of the ensemble exchange-correlation (xc) density functional (see Eqs. (5.24), (5.86) and (5.87) in Chapter 5), with essentially the same computational cost as the regular KS-DFT.

3.2.3 Two-particle Green's function and the Bethe-Salpeter equation

The theory of Green's functions can also describe neutral excitations. Within this formalism, they are understood as a two-particle process. When an electron is excited, it leaves its occupied state behind, which creates a hole of net positive charge. Then, the two charged entities interact, forming an *exciton*, followed by rearrangement and screening of the rest of the electrons in the system [274]. Describing a two-particle process requires a two-particle Green's function, which is defined as,

$$i^2 G_2(1,2;1',2') \;\; = \langle \Psi_0^N | \mathcal{T} \hat{\Psi}(1) \hat{\Psi}(2) \hat{\Psi}^\dagger(2') \hat{\Psi}^\dagger(1') | \Psi_0^N \rangle. \tag{3.57}$$

In general, G_2 describes the propagation of either two particles, particle and a hole, or two holes. Usually, the two-particle Green's function is not used directly as such when extracting neutral excitations. Rather, the object known as the *four-point linear response function* is employed, which is defined as,

$$i\chi(1,2;1',2') = i^2 G_2(1,2;1',2') - iG(1,1')iG(2,2'). \tag{3.58}$$

This definition subtracts from the two-particle Green's function any propagation of independent pairs of entities. With the time-ordering choice of $t_1' = t_1 + 0^+$ and $t_2' = t_2 + 0^+$, we arrive at the *particle-hole linear response function* or the *polarization propagator*. The latter depends only on $\tau = t_1 - t_2$, so it can be Fourier-transformed to the Lehmann representation, which reads [246],

$$\begin{aligned} \chi(\mathbf{x}_1, \mathbf{x}_2; \mathbf{x}_1', \mathbf{x}_2', \omega) = &\sum_I \frac{\langle \Psi_0^N | \hat{\Psi}^\dagger(\mathbf{x}_1') \hat{\Psi}(\mathbf{x}_1) | \Psi_I^N \rangle \langle \Psi_I^N | \hat{\Psi}^\dagger(\mathbf{x}_2') \hat{\Psi}(\mathbf{x}_2) | \Psi_0^N \rangle}{\omega - \omega_I + i0^+} \\ &- \sum_I \frac{\langle \Psi_0^N | \hat{\Psi}^\dagger(\mathbf{x}_2') \hat{\Psi}(\mathbf{x}_2) | \Psi_I^N \rangle \langle \Psi_I^N | \hat{\Psi}^\dagger(\mathbf{x}_1') \hat{\Psi}(\mathbf{x}_1) | \Psi_0^N \rangle}{\omega + \omega_I - i0^+}, \end{aligned} \tag{3.59}$$

where the poles now reveal neutral excitation (and de-excitation) energies $\omega_I = E_I^N - E_0^N$. Similarly, for a noninteracting or mean-field system, like in HF theory or KS-DFT, the linear response function can be expressed in terms of the occupied and unoccupied (in the ground state) spin-orbitals,

$$\begin{aligned}\chi_0(\mathbf{x}_1,\mathbf{x}_2;\mathbf{x}_1',\mathbf{x}_2',\omega) = &\sum_i^{occ.}\sum_a^{virt.} \frac{\varphi_i^*(\mathbf{x}_1')\varphi_a(\mathbf{x}_1)\varphi_a^*(\mathbf{x}_2')\varphi_i(\mathbf{x}_2)}{\omega-(\varepsilon_a-\varepsilon_i)+i0^+} \\ &- \sum_i^{occ.}\sum_a^{virt.} \frac{\varphi_i^*(\mathbf{x}_2')\varphi_a(\mathbf{x}_2)\varphi_a^*(\mathbf{x}_1')\varphi_i(\mathbf{x}_1)}{\omega+(\varepsilon_a-\varepsilon_i)-i0^+}.\end{aligned} \tag{3.60}$$

At this point, one may notice the analogy with TD-DFT. In LR-TD-DFT, the linear response function (Eq. (3.14)) is derived from perturbation theory with an external potential $v_{\text{ext}}(\mathbf{r},t)$ that is local in space. Similarly, Eq. (3.59) can be derived from perturbation theory with a nonlocal external potential $u_{\text{ext}}(\mathbf{x},\mathbf{x}',t)$ [8]. If we define the Bethe-Salpeter kernel as $\Xi_{\text{Hxc}}(1,2;1',2') = i\delta\Sigma_{\text{Hxc}}(1,1')/\delta G(2',2)$ (again, see the analogy with the Hxc potential and kernel in TD-DFT), it is possible to show (see Eqs. (4.1) - (4.5) in Ref. [8]) that the two functions, χ and χ_0 are related by the following four-point Dyson equation known as the *Bethe-Salpeter equation*,

$$\begin{aligned}\chi(1,2,1',2') = &\chi_0(1,2,1',2') \\ &- \int d\,3456\chi_0(1,3,1',4)\Xi_{\text{Hxc}}(4,5,3,6)\chi(6,2,5,2').\end{aligned} \tag{3.61}$$

Its inverse relation in the frequency domain reads (where time-ordering for particle-hole propagator is assumed),

$$\chi^{-1}(\mathbf{x}_1,\mathbf{x}_2;\mathbf{x}_1',\mathbf{x}_2',\omega) = \chi_0^{-1}(\mathbf{x}_1,\mathbf{x}_2;\mathbf{x}_1',\mathbf{x}_2',\omega) - \Xi_{\text{Hxc}}(\mathbf{x}_1,\mathbf{x}_2;\mathbf{x}_1',\mathbf{x}_2',\omega). \tag{3.62}$$

The above equation can be recast as a matrix in the transition (ia,jb) space, just like the Dyson equation (or practically speaking, the Casida equation, Eq. (3.26)) from TD-DFT.

Finally, let us look at some common approximations emanating from the BSE formalism. If we use the Bethe-Salpeter kernel derived from the HF self-energy [246],

$$\begin{aligned}\Xi_{\text{Hxc}}^{HF}(\mathbf{x}_1,\mathbf{x}_2;\mathbf{x}_1',\mathbf{x}_2') = w_{\text{ee}}(\mathbf{r}_1,\mathbf{r}_2)[&\delta(\mathbf{x}_1-\mathbf{x}_1')\delta(\mathbf{x}_2-\mathbf{x}_2') \\ &- \delta(\mathbf{x}_1-\mathbf{x}_2')\delta(\mathbf{x}_1'-\mathbf{x}_2)],\end{aligned} \tag{3.63}$$

we obtain the *time-dependent Hartree-Fock* (TD-HF) equations. Omitting the exchange part (second pair of Dirac delta functions in Eq. (3.63)) gives the Dyson

equation for *time-dependent Hartee* (TD-H) which can be contracted to a two-point equation [274].

An improvement over the HF-based kernel is afforded by mixing in the GW method. Using the GW approximation for Σ_{xc} and neglecting the G-dependence of the screened Coulomb interaction W gives the kernel for the BSE@GW method [12],

$$\begin{aligned}\Xi_{\text{Hxc}}^{BSE@GW}(\mathbf{x}_1,\mathbf{x}_2;\mathbf{x}_1',\mathbf{x}_2',\omega) = w_{\text{ee}}(\mathbf{r}_1,\mathbf{r}_2)\delta(\mathbf{x}_1-\mathbf{x}_1')\delta(\mathbf{x}_2-\mathbf{x}_2') \\ -W(\mathbf{r}_1,\mathbf{r}_2,\omega)\delta(\mathbf{x}_1-\mathbf{x}_2')\delta(\mathbf{x}_1'-\mathbf{x}_2).\end{aligned} \tag{3.64}$$

Finally, using the static screening approximation $W(\omega = 0)$ gives the screened TD-HF approximation, which has had several practical applications [286]. The statically-screened BSE@GW kernel has been successful in describing charge-transfer excitations [287, 288, 289], which, as mentioned in previous section, are a challenge in LR-TD-DFT. Both the GW and BSE@GW have also been used for describing (charged and neutral, respectively) excitations in various small molecules [290]. However, just like in AAs for the xc kernel, the consequence of neglecting frequency dependence is that multiple excitations are absent from the BSE spectrum. Thus, developing frequency-dependent BSE kernels (dynamical screening) is one of the key next steps [12, 291]. If we compare LR-TD-DFT and BSE, both methods are very similar and also have their own advantages and disadvantages. While the electron density and its response are simpler to handle than their BSE counterparts, BSE offers clear physical interpretations of the different approximations used in the kernel, and a systematically improvable way of approximating the self-energy. The computational cost of standard implementations both methods is the same once the BSE kernel is obtained, which is a bottleneck of the BSE method, although significant progress in low-scaling GW calculations has been made [12]. Therefore, the same argument as in LR-TD-DFT applies in the case of BSE concerning the motivation for development of TGOK-DFT for neutral excitations.

Chapter 4

Time-independent approaches to neutral electronic excitations

In this chapter, we review time-independent approaches to neutral electronic excitations. In contrast to TD-DFT (see Section 3.1), time-independent methods for neutral excitations are not as commonly used, although several computational packages such as Molcas [136] and ORCA [292, 293, 294, 295] offer highly developed implementations of wavefunction-based methods. One of the main difficulties of targeting excited states in a time-independent way is that contrary to the ground state, there is no minimum principle for a specific excited state, except in the case of the lowest state of a given spatial and spin symmetry. In general, however, excited states are stationary points of the electronic energy landscape, which are far more challenging to locate than energy minima. Some methods, such as the Δ-SCF method [296, 297], and the *equation-of-motion coupled cluster* (EOM-CC) method [298, 299], are designed for individual states, while others, such as the *state-averaged CASSCF* (SA-CASSCF) method [14], are designed for a balanced treatment of multiple states. In recent decades, *ensemble density-functional theory* (eDFT) based on the *Theophilou-Gross-Oliveira-Kohn* (TGOK) variational principle [86, 87, 88, 89, 90] has been proposed as a low-cost alternative to other well-established methods for describing low-lying excited states.

The chapter is organized as follows. In Section 4.1, we begin with a very short overview of wavefunction-based methods used in quantum chemistry for targeting one or several excited states. Following that, in Section 4.2, we give a detailed intro-

duction to TGOK-DFT, with a focus on the exact theory and its KS formulation.

4.1 Brief review of standard time-independent methods in quantum chemistry

Most of the WFT-based methods (and DFT) introduced in the Chapter 1 were at some point also adapted for excited states. Here we mention the ones most commonly used in quantum chemistry, divided into single-configuration methods, which are based on a Slater determinant (or configuration state function) reference, and multiconfigurational methods.

In the *configuration interaction* (CI) method (see Subection 1.1.2), excited states are extracted simply from higher roots of the CI matrix. The simplest of those, the *configuration interaction singles* (CIS) [300] is actually commonly used. In its practical implementation, it is related to *time-dependent Hartree-Fock* (TD-HF), and similar to *time-dependent density-functional theory* (TD-DFT). Although computationally efficient, it only accounts for relaxation of orbitals in the excited states via single excitations. Double and higher excitations are missing, just like in LR-TD-DFT in the adiabatic approximation. Another excited-state method based on the ground-state HF reference that has been gaining increasing interest is the *equation-of-motion coupled cluster* (EOM-CC) method [298, 299], which can describe multiple excitations, but is more expensive than CIS. In addition, different modifications to the SCF procedure (of HF or KS-DFT) for describing individual excited states with a single Slater determinant have been proposed, such as non-Aufbau recipe for occupying orbitals in the Δ-SCF method [296, 297, 301] maximization of the overlap between the occupied orbitals on successive SCF loops in the *maximum overlap method* (MOM) [302], energy variance optimization in σ-the SCF [303, 304] method, and the use of metadynamics-inspired biasing potential technique [305] in SCF metadynamics [306].

As far as multiconfigurational approaches are concerned, the CASSCF method introduced in Subection 1.1.2 may also be used to compute excited state energies and wavefunctions. The possible adaptations for excited states are either state-specific CASSCF [13], which searches for suitable wavefunctions for individual excited states [28], or more commonly used *state-averaged CASSCF* (SA-CASSCF) [14], in which the average energy of an ensemble of wavefunctions of a given spatial and

spin symmetry is optimized, using the same set of orbitals. This way, orthonormal ground and low-lying excited states are obtained, which is convenient for treating (near-)degeneracies.

In SA-CASSCF, we start with a set of $\mathcal{M}$ orthonormal multiconfigurational wavefunctions, which are expanded in the basis of Slater determinants, formed from excitations in the active space,

$$\left\{ |\tilde{\Psi}_I^{(0)}\rangle = \sum_K C_{KI}^{(0)} |\Phi_K\rangle \right\}_{1 \leq I \leq \mathcal{M}} . \tag{4.1}$$

The orthonormality in the optimization process is preserved by introducing the rotation operator in configuration space, in analogy with the orbital rotation,

$$\hat{S} = \sum_{J=1}^{\mathcal{M}} \sum_{K>J} S_{KJ} \left(|\tilde{\Psi}_K^{(0)}\rangle\langle\tilde{\Psi}_J^{(0)}| - |\tilde{\Psi}_J^{(0)}\rangle\langle\tilde{\Psi}_K^{(0)}| \right) . \tag{4.2}$$

Hence, individual wavefunctions in SA-CASSCF are conveniently written using a double exponential parametrization [28],

$$|\tilde{\Psi}_I(\boldsymbol{\kappa}, \mathbf{S})\rangle = e^{-\hat{\kappa}} e^{-\hat{S}} |\tilde{\Psi}_I^{(0)}\rangle. \tag{4.3}$$

The state-averaged energy is then a function of both orbital space $\boldsymbol{\kappa} = \{\kappa_{ij}\}_{i>j}$ (see Eq. (1.28)) and configuration space $\mathbf{S} = \{S_{KJ}\}_{K>J}$ rotation parameters,

$$E(\boldsymbol{\kappa}, \mathbf{S}) = \sum_{I=1}^{\mathcal{M}} w_I \langle \tilde{\Psi}_I(\boldsymbol{\kappa}, \mathbf{S}) | \hat{H}_\mathrm{e} | \tilde{\Psi}_I(\boldsymbol{\kappa}, \mathbf{S}) \rangle, \tag{4.4}$$

where $\{w_I\}_{1 \leq I \leq M}$ are the weight coefficients of individual multiconfigurational states, which are fixed at the beginning of the SA-CASSCF calculation. The stationarity condition is obtained as,

$$\left. \frac{\partial E(\boldsymbol{\kappa}, \mathbf{S})}{\partial \kappa_{ij}} \right|_{\boldsymbol{\kappa}=\boldsymbol{\kappa}_0} = \left. \frac{\partial E(\boldsymbol{\kappa}, \mathbf{S})}{\partial S_{KJ}} \right|_{\mathbf{S}=\mathbf{S}_0} = 0, \tag{4.5}$$

which can be derived analytically from Taylor expansions of the exponentials $e^{-\hat{\kappa}}$ and $e^{-\hat{S}}$. In the most commonly used equal-weight formulation, $w_I = 1/\mathcal{M}$. It is also possible, albeit not common, to use unequally-weighted SA-CASSCF. The mathematical foundation of SA-CASSCF is the *Theophilou-Gross-Oliveira-Kohn* (TGOK) variational principle [86, 87, 88], which will be introduced in Subsection 4.2.2. This method is suitable for describing a small number of low-lying states in molecules,

for example close to conical intersections or avoided crossings, where a balanced optimization of orbitals for ground and excited states is preferable (rather than using orbitals optimized for the ground state). However, just like all multiconfigurational methods, it is computationally involved and requires substantial experience from the user, especially for choosing a proper active space (see also the overview of multiconfigurational methods in the context of ground states in Subsection 1.1.2). Moreover, a post SA-CASSCF treatment is often necessary to recover a proper ordering of the states, for example, and also for retrieving dynamical correlation effects. Examples of the latter are multi-state PT2 methods, such as the *multi-state CASPT2* (MS-CASPT2) [307] and the *quasidegenerate NEVPT2* (QD-NEVPT2) [308] methods.

4.2 Ensemble DFT of neutral excitations (TGOK-DFT)

4.2.1 Introduction

TGOK-DFT has been formulated in the end of the 1980's by Gross, Oliveira, and Kohn [88, 89, 90] and is a generalization of the equiensemble DFT of Theophilou [86, 87]. In contrast to standard DFT, which is a ground-state theory, TGOK-DFT can describe both ground and (neutral) excited states. In this context, the ensemble density is used as a basic variable (in place of the ground-state density). For the description of charged excitations, a similar formalism, referred to as N-centered eDFT, has been derived recently by Senjean and Fromager [91], which will be described in Section 5.1.

The combination of quantum ensemble formalism together with the simplicity of density-functional theory, lends itself to an elegant extension of existing machinery of KS-DFT to neutral and charged excitations. In contrast to TD-DFT and BSE methods, which involve post-KS calculations, the computational cost of eDFT is essentially that of a standard KS-DFT calculation. For example, obtaining accurate optical and fundamental gaps is as simple as adding a correction term from ensemble xc functional to the bare KS gap, which is modelled in the ensemble DFA of choice. Another promising feature of eDFT is that it can in principle describe any kind of excitation, including the double excitations [110, 309] that LR-TD-DFT with the adiabatic approximation misses (see Section 3.1.3.3). The challenging aspect of the theory is now carried by the ensemble version of exchange-correlation (xc) functional, for which the user has to input both electron density and ensemble weights for excitations of choice. As it turns out, there are features and subtleties of ensemble xc functional that are not present in regular ground-state DFT.

The main focus of this section, which is based on the book chapter "Ensemble density functional theory of neutral and charged excitations" [92], is exact theory. Discussion on development of DFAs for the ensemble xc functional from first principles is reserved for the Chapter 6 that follows. TGOK-DFT will be reviewed again in a different context in Chapter 7, titled "Derivative discontinuities in ensemble DFT for neutral electronic excitations: An N-centered perspective", which discusses, for

the time of writing of this thesis, unpublished work.

4.2.2 TGOK ensembles

Before deriving the main equations of TGOK-DFT, let us introduce the exact ensemble theory. We start with the ensemble TGOK energy expression [88]

$$E^{\mathbf{w}} = \sum_I \mathtt{w}_I E_I, \tag{4.6}$$

which is simply a state-averaged energy where $\mathbf{w} = (\mathtt{w}_1, \mathtt{w}_2, \ldots)$ denotes the collection of ensemble weights that are assigned to the *excited* states, and $E_I \equiv E_I^N$ are the energies of the N-electron ground ($I = 0$) and excited ($I > 0$) states $\left|\Psi_I^N\right\rangle$. We assumed in Eq. (4.6) that the full set of weights (which includes the weight $\mathtt{w}_0$ assigned to the ground state) is normalized, *i.e.*, $\mathtt{w}_0 = 1 - \sum_{I>0} \mathtt{w}_I$, so that

$$\begin{aligned} E^{\mathbf{w}} &= \left(1 - \sum_{I>0} \mathtt{w}_I\right) E_0 + \sum_{I>0} \mathtt{w}_I E_I \\ &= E_0 + \sum_{I>0} \mathtt{w}_I \left(E_I - E_0\right). \end{aligned} \tag{4.7}$$

For ordered weights $\mathtt{w}_I \geq \mathtt{w}_{I+1} \geq 0$, with $I \geq 0$, the following (so-called TGOK) variational principle holds [88],

$$E^{\mathbf{w}} \leq \sum_I \mathtt{w}_I \left\langle \tilde{\Psi}_I \right| \hat{H} \left| \tilde{\Psi}_I \right\rangle, \tag{4.8}$$

where $\left\{\tilde{\Psi}_I\right\}$ is a trial set of orthonormal N-electron wave functions. Note that the lower bound $E^{\mathbf{w}}$, which is the exact ensemble energy, is not an observable. It is just an (artificial) auxiliary quantity from which properties of interest, such as the excitation energies, can be extracted. Since it varies *linearly* with the ensemble weights, the extraction of individual energy levels is actually trivial. Indeed, combining the following two relations [see Eq. (4.7)],

$$\frac{\partial E^{\mathbf{w}}}{\partial \mathtt{w}_I} = E_I - E_0, \tag{4.9}$$

and

$$\begin{aligned} E_K &\underset{K\geq 0}{=} E_0 + \sum_{I>0} \delta_{IK}(E_I - E_0) \\ &= E^{\mathbf{w}} + \sum_{I>0} (\delta_{IK} - \mathtt{w}_I)(E_I - E_0), \end{aligned} \tag{4.10}$$

leads to

$$E_K = E^{\mathbf{w}} + \sum_{I>0} (\delta_{IK} - \mathtt{w}_I) \frac{\partial E^{\mathbf{w}}}{\partial \mathtt{w}_I}. \tag{4.11}$$

Despite its simplicity the above expression has not been used until very recently for extracting excited-state energies from a TGOK-DFT calculation [310, 109]. Further details and reformulation of Eq. (4.11) in TGOK-DFT will be given in the following subsections.

4.2.3 DFT of TGOK ensembles

In TGOK-DFT, the ensemble energy is obtained variationally as follows [89],

$$E^{\mathbf{w}} = \min_{n \to N} \left\{ F^{\mathbf{w}}[n] + \int \mathrm{d}\mathbf{r}\, v_{\mathrm{ext}}(\mathbf{r}) n(\mathbf{r}) \right\}, \tag{4.12}$$

where the minimization is restricted to N-electron densities, *i.e.*, $\int d\mathbf{r}\, n(\mathbf{r}) = N$, and the universal TGOK density functional

$$F^{\mathbf{w}}[n] := \sum_I \mathtt{w}_I \left\langle \Psi_I^{\mathbf{w}}[n] | \hat{T} + \hat{W}_{\mathrm{ee}} | \Psi_I^{\mathbf{w}}[n] \right\rangle, \tag{4.13}$$

which is evaluated from the density-functional eigenfunctions $\{\Psi_I^{\mathbf{w}}[n]\}$ that fulfill the density constraint $\sum_I \mathtt{w}_I n_{\Psi_I^{\mathbf{w}}[n]}(\mathbf{r}) = n(\mathbf{r})$, is the analog for TGOK ensembles of the universal Hohenberg–Kohn functional (see Eq. (1.90)). Its construction relies on a potential-ensemble-density map that is established for a *given and fixed* set $\mathbf{w}$ of ensemble weight values. Therefore, the universality of the functional implies, like in ground-state DFT, that it does not depend on the local external potential. However, it does *not* mean that it is ensemble-independent[1] and therefore applicable to any excited state. As discussed in further detail in Secs. 6.1 and 6.2, encoding ensemble dependencies into density functionals is probably the most challenging task in eDFT.

In the standard KS formulation of TGOK-DFT [89], the TGOK functional is split into non-interacting kinetic and Hartree-xc (Hxc) ensemble energy contributions, by

[1] One may ask, why do we need a weight-dependent universal functional, instead of just using the regular HK functional and plugging in the ensemble density, *i.e.* $F_{\mathrm{HK}}[n^{\mathbf{w}}]$? The reason is that a density $n^{\mathbf{w}}$ that integrates to an integer number of electrons N, can be both pure-state and ensemble N-representable at the same time. Therefore, we need additional weight dependence in the functional to ensure that ensemble energy, and not a pure-state one is calculated.

analogy with regular KS-DFT:

$$F^{\mathbf{w}}[n] = T_{\mathrm{s}}^{\mathbf{w}}[n] + E_{\mathrm{Hxc}}^{\mathbf{w}}[n]. \tag{4.14}$$

The non-interacting ensemble kinetic energy functional can be expressed more explicitly as follows within the constrained-search formalism [47],

$$\begin{aligned} T_{\mathrm{s}}^{\mathbf{w}}[n] &= \min_{\hat{\gamma}^{\mathbf{w}} \to n} \left\{ \mathrm{Tr}\left[\hat{\gamma}^{\mathbf{w}} \hat{T}\right] \right\} && (4.15) \\ &\equiv \sum_I \mathtt{w}_I \left\langle \Phi_I^{\mathbf{w}}[n] \right| \hat{T} \left| \Phi_I^{\mathbf{w}}[n] \right\rangle, && (4.16) \end{aligned}$$

where Tr denotes the trace, $\hat{\gamma}^{\mathbf{w}} = \sum_I \mathtt{w}_I \left|\Phi_I\right\rangle \left\langle\Phi_I\right|$ is a trial ensemble density matrix operator that fulfills the density constraint $n_{\hat{\gamma}^{\mathbf{w}}}(\mathbf{r}) \equiv \mathrm{Tr}\left[\hat{\gamma}^{\mathbf{w}} \hat{n}(\mathbf{r})\right] = \sum_I \mathtt{w}_I n_{\Phi_I}(\mathbf{r}) = n(\mathbf{r})$, and $\hat{n}(\mathbf{r}) \equiv \sum_{i=1}^{N} \delta(\mathbf{r} - \mathbf{r}_i)$ is the electron density operator at position $\mathbf{r}$. Combining Eqs. (4.12), (4.14) and (4.15) leads to the final TGOK-DFT variational energy expression

$$\begin{aligned} E^{\mathbf{w}} &= \min_{\{\varphi_p\}} \left\{ \mathrm{Tr}\left[\hat{\gamma}^{\mathbf{w}} \left(\hat{T} + \hat{V}_{\mathrm{ext}}\right)\right] + E_{\mathrm{Hxc}}^{\mathbf{w}}\left[n_{\hat{\gamma}^{\mathbf{w}}}\right] \right\} \\ &= \mathrm{Tr}\left[\hat{\gamma}_{\mathrm{KS}}^{\mathbf{w}} \left(\hat{T} + \hat{V}_{\mathrm{ext}}\right)\right] + E_{\mathrm{Hxc}}^{\mathbf{w}}\left[n_{\hat{\gamma}_{\mathrm{KS}}^{\mathbf{w}}}\right], && (4.17) \end{aligned}$$

where the minimization can be restricted to single-configuration wave functions (determinants or configuration state functions), hence the minimization over orbitals $\{\varphi_p\}$ on the first line of Eq. (4.17). The minimizing KS orbitals $\{\varphi_p^{\mathbf{w}}\}$, from which the KS wave functions $\{\Phi_I^{\mathbf{w}}[n^{\mathbf{w}}] \equiv \Phi_I^{\mathbf{w}}\}$ in the minimizing density matrix operator $\hat{\gamma}_{\mathrm{KS}}^{\mathbf{w}}$ are constructed, fulfill the following self-consistent TGOK-DFT equations,

$$\left(-\frac{\nabla_{\mathbf{r}}^2}{2} + v_{\mathrm{ext}}(\mathbf{r}) + v_{\mathrm{Hxc}}^{\mathbf{w}}[n^{\mathbf{w}}](\mathbf{r})\right) \varphi_p^{\mathbf{w}}(\mathbf{r}) = \varepsilon_p^{\mathbf{w}} \varphi_p^{\mathbf{w}}(\mathbf{r}), \tag{4.18}$$

where

$$v_{\mathrm{Hxc}}^{\mathbf{w}}[n](\mathbf{r}) = \frac{\delta E_{\mathrm{Hxc}}^{\mathbf{w}}[n]}{\delta n(\mathbf{r})} \tag{4.19}$$

is the ensemble Hxc density-functional potential. In the exact theory, the ensemble KS orbitals reproduce the exact (interacting) ensemble density, *i.e.*,

$$\sum_I \mathtt{w}_I n_{\Phi_I^{\mathbf{w}}}(\mathbf{r}) = \sum_I \mathtt{w}_I n_{\Psi_I}(\mathbf{r}) = n^{\mathbf{w}}(\mathbf{r}), \tag{4.20}$$

where the individual KS densities read as

$$n_{\Phi_I^{\mathbf{w}}}(\mathbf{r}) = \sum_p n_p^I \left|\varphi_p^{\mathbf{w}}(\mathbf{r})\right|^2, \tag{4.21}$$

and n_p^I is the (weight-independent) occupation number of the orbital $\varphi_p^{\mathbf{w}}$ in the single-configuration wave function $\Phi_I^{\mathbf{w}}$.

Let us now focus on the ensemble Hxc density functional. By analogy with regular KS-DFT, it can decomposed into Hx and correlation energy contributions as follows,

$$E_{\text{Hxc}}^{\mathbf{w}}[n] = E_{\text{Hx}}^{\mathbf{w}}[n] + E_{\text{c}}^{\mathbf{w}}[n]. \tag{4.22}$$

In the original formulation of TGOK-DFT [89], the Hx functional is further decomposed as follows,

$$E_{\text{Hx}}^{\mathbf{w}}[n] = E_{\text{H}}[n] + E_{\text{x}}^{\mathbf{w}}[n], \tag{4.23}$$

where

$$E_{\text{H}}[n] = \frac{1}{2}\int \mathrm{d}\mathbf{r} \int \mathrm{d}\mathbf{r}' \frac{n(\mathbf{r})n(\mathbf{r}')}{|\mathbf{r}-\mathbf{r}'|} \tag{4.24}$$

is the standard *weight-independent* Hartree functional, and

$$E_{\text{x}}^{\mathbf{w}}[n] = \sum_I \mathtt{w}_I \left\langle \Phi_I^{\mathbf{w}}[n] \right| \hat{W}_{\text{ee}} \left| \Phi_I^{\mathbf{w}}[n] \right\rangle - E_{\text{H}}[n] \tag{4.25}$$

is the exact (complementary and weight-dependent) ensemble exchange functional. Note that $\Phi_I^{\mathbf{w}}[n]$, which describes one of the configurations included into the ensemble, may not be a pure Slater determinant [311]. Other (weight-dependent) definitions for the ensemble Hartree energy, where the explicit dependence on the ensemble density n is lost, have been explored [312]. In the most intuitive one, the ensemble Hartree energy is evaluated as the weighted sum of the individual KS Hartree energies:

$$E_{\text{H}}^{\mathbf{w}}[n] := \sum_I \mathtt{w}_I E_{\text{H}}\left[n_{\Phi_I^{\mathbf{w}}[n]}\right]. \tag{4.26}$$

For the sake of generality, we will keep in the following both Hartree and exchange energies into a single functional $E_{\text{Hx}}^{\mathbf{w}}[n]$ which is defined as

$$E_{\text{Hx}}^{\mathbf{w}}[n] = \sum_I \mathtt{w}_I \left\langle \Phi_I^{\mathbf{w}}[n] \right| \hat{W}_{\text{ee}} \left| \Phi_I^{\mathbf{w}}[n] \right\rangle. \tag{4.27}$$

The remaining weight-dependent correlation energy can then be expressed as follows, according to Eqs. (4.13) and (4.16),

$$\begin{aligned} E_{\rm c}^{\mathbf{w}}[n] &= F^{\mathbf{w}}[n] - T_{\rm s}^{\mathbf{w}}[n] - E_{\rm Hx}^{\mathbf{w}}[n] \\ &= \sum_I \mathtt{w}_I \left(\langle \Psi_I^{\mathbf{w}}[n] | \hat{T} + \hat{W}_{\rm ee} | \Psi_I^{\mathbf{w}}[n] \rangle - \langle \Phi_I^{\mathbf{w}}[n] | \hat{T} + \hat{W}_{\rm ee} | \Phi_I^{\mathbf{w}}[n] \rangle \right) , \end{aligned} \quad (4.28)$$

where the non-interacting KS $\{\Phi_I^{\mathbf{w}}[n]\}$ and interacting $\{\Psi_I^{\mathbf{w}}[n]\}$ wave functions, which both reproduce the (weight-independent here) trial ensemble density n, *whatever* the ensemble weight values $\mathbf{w}$, are in principle weight-dependent [313, 98]. Interestingly, the interacting density-functional wave functions lose their weight dependence when the trial density n matches the exact physical ensemble density $n^{\mathbf{w}}$, *i.e.*, $\Psi_I^{\mathbf{w}}[n^{\mathbf{w}}] = \Psi_I \equiv \Psi_I^N$. However, as shown in Subsection 6.2.2, the KS wave functions remain weight-dependent, even in this special case.

As readily seen from Eqs. (4.14), (4.17) and (4.18), the only (but crucial) difference between regular ground-state KS-DFT and TGOK-DFT is the weight dependence in the ensemble density-functional Hxc energy and potential. The computational cost should essentially be the same in both approaches. The challenge lies in the proper description of the weight-dependent ensemble Hxc density functional. Different approximations have been considered, such as the use of (weight-independent) regular ground-state functionals [93, 101], or the use of an ensemble exact-exchange energy [311, 314, 76] with or without approximate weight-dependent correlation functionals [76, 109, 110]. Note that the expected linearity-in-weight of the ensemble energy is not always reproduced in (approximate) practical TGOK-DFT calculations [101]. As a result, different weights can give different excitation energies, which is a serious issue. This lead to different computation strategies, such as trying to find an optimal value for the weights [315], using Boltzmann weights instead [93], restricting to equiensembles [109, 110], or considering the ground-state $\mathbf{w} = 0$ limit of the theory, like in the *direct ensemble correction* (DEC) scheme [316, 77]. A linear interpolation method has also been proposed [101, 317].

Designing weight-dependent ensemble DFAs that systematically reduce the curvature in weight of the ensemble energy, while providing at the same time accurate

excitation energies, is an important and challenging task. Recent progress in this matter will be extensively discussed in Secs. 6.1 and 6.2.

4.2.4 Extraction of individual state properties

In Subsection 4.2.3, we have shown that both exact ensemble energy and density can be calculated, in principle exactly, within TGOK-DFT. At this point we should stress that the KS and true physical densities are not expected to match individually, even though they both reproduce the same ensemble density [see Eq. (4.20)]. This subtle point will be discussed in more detail in Subsection 6.2.2. Nevertheless, in complete analogy with Eq. (4.11), the exact individual densities can be extracted from the ensemble density as follows [97],

$$n_{\Psi_J}(\mathbf{r}) = n^{\mathbf{w}}(\mathbf{r}) + \sum_{I>0} (\delta_{IJ} - \mathtt{w}_I) \frac{\partial n^{\mathbf{w}}(\mathbf{r})}{\partial \mathtt{w}_I}, \tag{4.29}$$

which, by inserting the expression in Eq. (4.20), leads to the key result [97]

$$n_{\Psi_J}(\mathbf{r}) = n_{\Phi^{\mathbf{w}}_J}(\mathbf{r}) + \sum_{I>0} \sum_{K\geq 0} (\delta_{IJ} - \mathtt{w}_I)\, \mathtt{w}_K \frac{\partial n_{\Phi^{\mathbf{w}}_K}(\mathbf{r})}{\partial \mathtt{w}_I}, \tag{4.30}$$

where, according to Eq. (4.21), the weight derivative of the individual KS densities

$$\frac{\partial n_{\Phi^{\mathbf{w}}_K}(\mathbf{r})}{\partial \mathtt{w}_I} = 2 \sum_p n_p^K \varphi_p^{\mathbf{w}}(\mathbf{r}) \frac{\partial \varphi_p^{\mathbf{w}}(\mathbf{r})}{\partial \mathtt{w}_I} \tag{4.31}$$

can be evaluated from the (static) linear response of the KS orbitals. This can be done, in practice, by solving an ensemble coupled-perturbed equation [318, 97], for example.

Turning to the excitation energies, we obtain from the variational GOK-DFT ensemble energy expression and the Hellmann–Feynman theorem the following expression, where the derivatives of the minimizing (and therefore stationary) KS wave functions do not contribute,

$$\begin{aligned} \frac{\partial E^{\mathbf{w}}}{\partial \mathtt{w}_I} &= \mathrm{Tr}\left[\Delta\hat{\gamma}^{\mathbf{w}}_{\mathrm{KS},I}\left(\hat{T} + \hat{V}_{\mathrm{ext}}\right)\right] + \left.\frac{\partial E^{\mathbf{w}}_{\mathrm{Hxc}}[n]}{\partial \mathtt{w}_I}\right|_{n=n_{\hat{\gamma}^{\mathbf{w}}_{\mathrm{KS}}}} \\ &\quad + \int \mathrm{d}\mathbf{r}\, \frac{\delta E^{\mathbf{w}}_{\mathrm{Hxc}}[n_{\hat{\gamma}^{\mathbf{w}}_{\mathrm{KS}}}]}{\delta n(\mathbf{r})} \mathrm{Tr}\left[\Delta\hat{\gamma}^{\mathbf{w}}_{\mathrm{KS},I}\hat{n}(\mathbf{r})\right], \end{aligned} \tag{4.32}$$

with $\Delta\hat{\gamma}^{\mathbf{w}}_{\mathrm{KS},I} = |\Phi^{\mathbf{w}}_I\rangle\langle\Phi^{\mathbf{w}}_I| - |\Phi^{\mathbf{w}}_0\rangle\langle\Phi^{\mathbf{w}}_0|$. This expression can be further simplified as follows [310]:

$$\frac{\partial E^{\mathbf{w}}}{\partial \mathtt{w}_I} = E_I - E_0 = \mathcal{E}^{\mathbf{w}}_I - \mathcal{E}^{\mathbf{w}}_0 + \left.\frac{\partial E^{\mathbf{w}}_{\mathrm{Hxc}}[n]}{\partial \mathtt{w}_I}\right|_{n=n_{\hat{\gamma}^{\mathbf{w}}_{\mathrm{KS}}}}, \tag{4.33}$$

where $\mathcal{E}^{\mathbf{w}}_I$ denotes the Ith (weight-dependent) KS energy which is obtained by summing up the energies $\{\varepsilon^{\mathbf{w}}_p\}$ of the KS orbitals that are occupied in $\Phi^{\mathbf{w}}_I$. Hence, the excitation energies can all be determined, in principle exactly, from a *single* TGOK-DFT calculation.

As shown by Deur and Fromager [310], individual energy levels can also be extracted (from the KS ensemble) and written in a compact form. For that purpose, we will use the exact expression of Eq. (4.11) where we see, in the light of Eq. (4.33), that it is convenient to express the total ensemble energy [first term on the right-hand side of Eq. (4.11)] in terms of total KS energies. Levy and Zahariev (LZ) made such a suggestion in the context of regular ground-state DFT [319]. For that purpose, they introduced a shift in the Hxc potential that can be trivially generalized to TGOK ensembles as follows [310],

$$\frac{\delta E^{\mathbf{w}}_{\mathrm{Hxc}}[n]}{\delta n(\mathbf{r})} \to \overline{v}^{\mathbf{w}}_{\mathrm{Hxc}}[n](\mathbf{r}) = \frac{\delta E^{\mathbf{w}}_{\mathrm{Hxc}}[n]}{\delta n(\mathbf{r})} + \frac{E^{\mathbf{w}}_{\mathrm{Hxc}}[n] - \int \mathrm{d}\mathbf{r}\, \dfrac{\delta E^{\mathbf{w}}_{\mathrm{Hxc}}[n]}{\delta n(\mathbf{r})} n(\mathbf{r})}{\int \mathrm{d}\mathbf{r}\, n(\mathbf{r})}. \tag{4.34}$$

Note that, if the exact LZ-shifted Hxc potential were known, we would be able to evaluate exact ensemble density-functional Hxc energies as follows,

$$E^{\mathbf{w}}_{\mathrm{Hxc}}[n] = \int \mathrm{d}\mathbf{r}\, \overline{v}^{\mathbf{w}}_{\mathrm{Hxc}}[n](\mathbf{r}) n(\mathbf{r}). \tag{4.35}$$

Once the LZ shift has been applied to the ensemble Hxc potential, the (total N-electron) KS energies will be modified as follows,

$$\mathcal{E}^{\mathbf{w}}_I \to \overline{\mathcal{E}}^{\mathbf{w}}_I = \mathcal{E}^{\mathbf{w}}_I + E^{\mathbf{w}}_{\mathrm{Hxc}}[n_{\hat{\gamma}^{\mathbf{w}}_{\mathrm{KS}}}] - \int \mathrm{d}\mathbf{r}\, \frac{\delta E^{\mathbf{w}}_{\mathrm{Hxc}}[n_{\hat{\gamma}^{\mathbf{w}}_{\mathrm{KS}}}]}{\delta n(\mathbf{r})} n_{\hat{\gamma}^{\mathbf{w}}_{\mathrm{KS}}}(\mathbf{r}), \tag{4.36}$$

and the true ensemble energy will simply read as a weighted sum of (LZ-shifted) KS energies:

$$E^{\mathbf{w}} = \left(1 - \sum_{I>0} \mathtt{w}_I\right) \overline{\mathcal{E}}^{\mathbf{w}}_0 + \sum_{I>0} \mathtt{w}_I \overline{\mathcal{E}}^{\mathbf{w}}_I. \tag{4.37}$$

Note that the KS excitation energies are not affected by the shift:

$$\overline{\mathcal{E}}_I^{\mathbf{w}} - \overline{\mathcal{E}}_0^{\mathbf{w}} = \mathcal{E}_I^{\mathbf{w}} - \mathcal{E}_0^{\mathbf{w}}. \tag{4.38}$$

Thus, by combining Eqs. (4.11), (4.33), (4.37) and (4.38), we recover the exact expression of Ref. [310] for ground- and excited-state energy levels:

$$E_K = \overline{\mathcal{E}}_K^{\mathbf{w}} + \sum_{I>0} (\delta_{IK} - \mathtt{w}_I) \left. \frac{\partial E_{\text{Hxc}}^{\mathbf{w}}[n]}{\partial \mathtt{w}_I} \right|_{n=n_{\hat{\gamma}_{\text{KS}}^{\mathbf{w}}}}. \tag{4.39}$$

As readily seen from Eq. (4.39), applying the LZ shift is not sufficient for reaching an exact energy level. The ensemble weight derivatives of the Hxc density functional are also needed for that purpose.

Finally, it is instructive to consider the general expression of Eq. (4.39) in the ground-state $\mathbf{w} = 0$ limit of the theory, which gives

$$E_I = \overline{\mathcal{E}}_I^{\mathbf{w}=0} + (1 - \delta_{I0}) \left. \frac{\partial E_{\text{Hxc}}^{\mathbf{w}}[n_{\Psi_0}]}{\partial \mathtt{w}_I} \right|_{\mathbf{w}=0}, \tag{4.40}$$

where n_{Ψ_0} is the exact ground-state density. As readily seen from Eq. (4.40), as we start from a pure $I = 0$ ground-state theory (we recover the energy expression of Levy and Zahariev in this case [319]), the inclusion of a given $I > 0$ excited state into the ensemble induces an additional shift in the Hxc potential, which corresponds to the weight derivative $\partial E_{\text{Hxc}}^{\mathbf{w}}[n_{\Psi_0}]/\partial \mathtt{w}_I|_{\mathbf{w}=0}$ and can be interpreted as a derivative discontinuity, as shown in Ref. [104] and extensively discussed in Section 5.2 of the next chapter, in the context of charged excitations.

Chapter 5

Ensemble density-functional theory of charged excitations

A recent adaptation of TGOK-DFT to charged excitations, which is referred to as N-centered eDFT [91], is introduced in the present chapter. As already mentioned at the beginning of Chapter 3, even though the neutral and charged excitations are very different physical processes, their mathematical formulations of TGOK-DFT and N-centered eDFT are very similar, as will be shown in the following.

This chapter is organized as follows. In Section 5.1, we introduce the N-centered ensemble formalism and derive in-principle exact expressions for individual energy levels, as well as the exact ionization potential and electron affinity theorems in the formalism of N-centered eDFT. Then, in Section 5.2, which starts with a detour to the traditional *Perdew-Parr-Levy-Balduz* (PPLB) DFT approach to charged excitations, we discuss the equivalence between the xc derivative discontinuity, which is a fundamental concept in DFT, and the ensemble weight derivative of the xc density functional, which is central in eDFT. For a similar concept of derivative discontinuity in the context of neutral excitations, the reader is referred to Chapter 7. In Section 5.3, we give more details on the connection between PPLB and N-centered pictures. We conclude with Section 5.4, which talks about suppression of the derivative discontinuity (for charged excitations).

5.1 DFT of charged excitations: The N-centered ensemble formalism

5.1.1 N-centered ensembles

The N-centered ensemble [91] can be seen as the "grand canonical" ground-state version of TGOK ensembles. It is constructed from the M-electron ground states where the three possible values of the *integer* $M \in \{N-1, N, N+1\}$ are, like the corresponding ensemble density (see below), centered in N, hence the name "N-centered". The exact N-centered ensemble energy is defined as follows [91],

$$E_0^{\boldsymbol{\xi}} = \xi_- E_0^{N-1} + \xi_+ E_0^{N+1} + \left(1 - \xi_- \frac{N-1}{N} - \xi_+ \frac{N+1}{N}\right) E_0^N, \tag{5.1}$$

where the two N-centered ensemble weights ξ_- and ξ_+, which describe the removal/addition of an electron from/to the N-electron system, respectively, are collected in

$$\boldsymbol{\xi} \equiv (\xi_-, \xi_+)\,. \tag{5.2}$$

Similarly, the N-centered ensemble density reads as

$$n_0^{\boldsymbol{\xi}}(\mathbf{r}) = \xi_- n_{\Psi_0^{N-1}}(\mathbf{r}) + \xi_+ n_{\Psi_0^{N+1}}(\mathbf{r}) + \left(1 - \xi_- \frac{N-1}{N} - \xi_+ \frac{N+1}{N}\right) n_{\Psi_0^N}(\mathbf{r}). \tag{5.3}$$

Designed by analogy with TGOK-DFT (which describes *neutral* excitations), the N-centered ensemble density integrates to the central *integer* number N of electrons:

$$\int \mathrm{d}\mathbf{r}\, n_0^{\boldsymbol{\xi}}(\mathbf{r}) = N. \tag{5.4}$$

In other words, even though we describe charged excitation processes, the number of electrons remains *fixed and equal to the integer* N whatever the value of the ensemble weights $\boldsymbol{\xi}$. This major difference with the conventional DFT for fractional electron numbers [102] has important implications that will be discussed extensively in Section 5.2.

In this context, the ensemble energy can be determined variationally, as a direct consequence of the conventional Rayleigh–Ritz variational principle for a fixed

number of electrons, *i.e.*,

$$\begin{aligned} E_0^{\boldsymbol{\xi}} &\leq \xi_- \left\langle \tilde{\Psi}^{N-1} \middle| \hat{H} \middle| \tilde{\Psi}^{N-1} \right\rangle + \xi_+ \left\langle \tilde{\Psi}^{N+1} \middle| \hat{H} \middle| \tilde{\Psi}^{N+1} \right\rangle \\ &\quad + \left(1 - \xi_- \frac{N-1}{N} - \xi_+ \frac{N+1}{N} \right) \left\langle \tilde{\Psi}^{N} \middle| \hat{H} \middle| \tilde{\Psi}^{N} \right\rangle , \end{aligned} \tag{5.5}$$

where $\{\tilde{\Psi}^M\}$ are trial M-electron normalized wave functions, provided that the (so-called convexity) conditions $\xi_- \geq 0$, $\xi_+ \geq 0$, and $\xi_-(N-1) + \xi_+(N+1) \leq N$ are fulfilled. Like in TGOK-DFT, the ensemble energy $E_0^{\boldsymbol{\xi}}$ varies linearly with the ensemble weights. As a result, charged excitation energies can be extracted through differentiation with respect to the N-centered ensemble weights. For example, since

$$\frac{\partial E_0^{\boldsymbol{\xi}}}{\partial \xi_\pm} = E_0^{N\pm1} - \left(\frac{N \pm 1}{N} \right) E_0^N , \tag{5.6}$$

the exact fundamental gap can be determined as follows,

$$\frac{\partial E_0^{\boldsymbol{\xi}}}{\partial \xi_-} + \frac{\partial E_0^{\boldsymbol{\xi}}}{\partial \xi_+} = E_0^{N-1} + E_0^{N+1} - 2E_0^N = E_{\text{gap}}^{\text{fund}} . \tag{5.7}$$

We can also extract the individual cationic, anionic, and neutral energies, respectively, as follows,

$$E_0^{N-1} = \frac{N-1}{N} \left(E_0^{\boldsymbol{\xi}} - \xi_+ \frac{\partial E_0^{\boldsymbol{\xi}}}{\partial \xi_+} + \left(\frac{N}{N-1} - \xi_- \right) \frac{\partial E_0^{\boldsymbol{\xi}}}{\partial \xi_-} \right) , \tag{5.8}$$

$$E_0^{N+1} = \frac{N+1}{N} \left(E_0^{\boldsymbol{\xi}} - \xi_- \frac{\partial E_0^{\boldsymbol{\xi}}}{\partial \xi_-} + \left(\frac{N}{N+1} - \xi_+ \right) \frac{\partial E_0^{\boldsymbol{\xi}}}{\partial \xi_+} \right) , \tag{5.9}$$

and

$$E_0^N = E_0^{\boldsymbol{\xi}} - \xi_- \frac{\partial E_0^{\boldsymbol{\xi}}}{\partial \xi_-} - \xi_+ \frac{\partial E_0^{\boldsymbol{\xi}}}{\partial \xi_+} . \tag{5.10}$$

Eqs. (5.8)–(5.10) will be used in the following for deriving exact ionization potential and electron affinity theorems.

5.1.2 DFT of N-centered ensembles

In complete analogy with TGOK-DFT, the N-centered ensemble energy can be determined variationally as follows,

$$E_0^{\boldsymbol{\xi}} = \min_{n \to N} \left\{ F^{\boldsymbol{\xi}}[n] + \int \mathrm{d}\mathbf{r}\, v_{\text{ext}}(\mathbf{r}) n(\mathbf{r}) \right\} , \tag{5.11}$$

where, in the KS formulation of the theory [91], the universal N-centered ensemble functional reads as

$$F^{\boldsymbol{\xi}}[n] = T_{\rm s}^{\boldsymbol{\xi}}[n] + E_{\rm Hxc}^{\boldsymbol{\xi}}[n]. \tag{5.12}$$

The non-interacting kinetic energy functional

$$T_{\rm s}^{\boldsymbol{\xi}}[n] = \min_{\hat{\gamma}^{\boldsymbol{\xi}}\to n} \left\{ {\rm Tr}\left[\hat{\gamma}^{\boldsymbol{\xi}}\hat{T}\right]\right\} \tag{5.13}$$

is now determined through a minimization over N-centered density matrix operators

$$\begin{aligned}\hat{\gamma}^{\boldsymbol{\xi}} \equiv\ & \xi_- \left|\Phi^{N-1}\right\rangle\left\langle\Phi^{N-1}\right| + \xi_+ \left|\Phi^{N+1}\right\rangle\left\langle\Phi^{N+1}\right| \\ & + \left(1 - \xi_- \frac{N-1}{N} - \xi_+ \frac{N+1}{N}\right)\left|\Phi^{N}\right\rangle\left\langle\Phi^{N}\right|\end{aligned} \tag{5.14}$$

that fulfill the density constraint $n_{\hat{\gamma}^{\boldsymbol{\xi}}}(\mathbf{r}) = {\rm Tr}\left[\hat{\gamma}^{\boldsymbol{\xi}}\hat{n}(\mathbf{r})\right] = n(\mathbf{r})$. Combining Eqs. (5.11), (5.12) and (5.13) leads to the final ensemble energy expression,

$$\begin{aligned} E_0^{\boldsymbol{\xi}} &= \min_{\{\varphi_p\}} \left\{ {\rm Tr}\left[\hat{\gamma}^{\boldsymbol{\xi}}\left(\hat{T} + \hat{V}_{\rm ext}\right)\right] + E_{\rm Hxc}^{\boldsymbol{\xi}}\left[n_{\hat{\gamma}^{\boldsymbol{\xi}}}\right]\right\} \\ &= {\rm Tr}\left[\hat{\gamma}_{\rm KS}^{\boldsymbol{\xi}}\left(\hat{T} + \hat{V}_{\rm ext}\right)\right] + E_{\rm Hxc}^{\boldsymbol{\xi}}\left[n_{\hat{\gamma}_{\rm KS}^{\boldsymbol{\xi}}}\right], \end{aligned} \tag{5.15}$$

which is mathematically identical to its analog in TGOK-DFT [see Eq. (4.17)], even though the physics it describes is completely different. The orbitals $\{\varphi_p^{\boldsymbol{\xi}}\}$, from which the minimizing single-configuration KS wave functions $\left\{\Phi_0^{M,\boldsymbol{\xi}}\right\}$ in $\hat{\gamma}_{\rm KS}^{\boldsymbol{\xi}}$ are constructed, fulfill self-consistent KS equations that are similar to those of regular (N-electron ground-state) KS-DFT:

$$\left(-\frac{\nabla_{\mathbf{r}}^2}{2} + v_{\rm ext}(\mathbf{r}) + v_{\rm Hxc}^{\boldsymbol{\xi}}[n^{\boldsymbol{\xi}}](\mathbf{r})\right)\varphi_p^{\boldsymbol{\xi}}(\mathbf{r}) = \varepsilon_p^{\boldsymbol{\xi}}\varphi_p^{\boldsymbol{\xi}}(\mathbf{r}). \tag{5.16}$$

The only difference is that the N-centered ensemble Hxc potential $v_{\rm Hxc}^{\boldsymbol{\xi}}[n](\mathbf{r}) = \delta E_{\rm Hxc}^{\boldsymbol{\xi}}[n]/\delta n(\mathbf{r})$ is now employed. In the exact theory, the ensemble KS orbitals are expected to reproduce the interacting N-centered ensemble density, *i.e.*,

$$n_0^{\boldsymbol{\xi}}(\mathbf{r}) = n_{\hat{\gamma}_{\rm KS}^{\boldsymbol{\xi}}}(\mathbf{r}) \tag{5.17}$$

$$\begin{aligned} &= \xi_- n_{\Phi_0^{N-1,\boldsymbol{\xi}}}(\mathbf{r}) + \xi_+ n_{\Phi_0^{N+1,\boldsymbol{\xi}}}(\mathbf{r}) \\ &\quad + \left(1 - \xi_- \frac{N-1}{N} - \xi_+ \frac{N+1}{N}\right) n_{\Phi_0^{N,\boldsymbol{\xi}}}(\mathbf{r}), \end{aligned} \tag{5.18}$$

or, equivalently [91],

$$n_0^{\boldsymbol{\xi}}(\mathbf{r}) = \left(1 + \frac{\xi_- - \xi_+}{N}\right)\sum_{p=1}^{N} |\varphi_p^{\boldsymbol{\xi}}(\mathbf{r})|^2 - \xi_- |\varphi_N^{\boldsymbol{\xi}}(\mathbf{r})|^2 + \xi_+ |\varphi_{N+1}^{\boldsymbol{\xi}}(\mathbf{r})|^2. \tag{5.19}$$

Turning to the N-centered ensemble Hxc density functional, it can be decomposed as $E_{\rm Hxc}^{\boldsymbol{\xi}}[n] = E_{\rm Hx}^{\boldsymbol{\xi}}[n] + E_{\rm c}^{\boldsymbol{\xi}}[n]$, where, by analogy with TGOK-DFT, the exact Hx energy is expressed in terms of the N-centered ensemble density-functional KS wave functions as follows,

$$\begin{aligned} E_{\rm Hx}^{\boldsymbol{\xi}}[n] = {} & \xi_- \left\langle \Phi_0^{N-1,\boldsymbol{\xi}}[n] \middle| \hat{W}_{\rm ee} \middle| \Phi_0^{N-1,\boldsymbol{\xi}}[n] \right\rangle \\ & + \xi_+ \left\langle \Phi_0^{N+1,\boldsymbol{\xi}}[n] \middle| \hat{W}_{\rm ee} \middle| \Phi_0^{N+1,\boldsymbol{\xi}}[n] \right\rangle \\ & + \left(1 - \xi_- \frac{N-1}{N} - \xi_+ \frac{N+1}{N} \right) \left\langle \Phi_0^{N,\boldsymbol{\xi}}[n] \middle| \hat{W}_{\rm ee} \middle| \Phi_0^{N,\boldsymbol{\xi}}[n] \right\rangle , \end{aligned} \tag{5.20}$$

and the complementary correlation functional reads as

$$\begin{aligned} E_{\rm c}^{\boldsymbol{\xi}}[n] &= F^{\boldsymbol{\xi}}[n] - T_{\rm s}^{\boldsymbol{\xi}}[n] - E_{\rm Hx}^{\boldsymbol{\xi}}[n] \\ &= \xi_- \left(\left\langle \hat{T} + \hat{W}_{\rm ee} \right\rangle_{\Psi_0^{N-1,\boldsymbol{\xi}}[n]} - \left\langle \hat{T} + \hat{W}_{\rm ee} \right\rangle_{\Phi_0^{N-1,\boldsymbol{\xi}}[n]} \right) \\ &\quad + \xi_+ \left(\left\langle \hat{T} + \hat{W}_{\rm ee} \right\rangle_{\Psi_0^{N+1,\boldsymbol{\xi}}[n]} - \left\langle \hat{T} + \hat{W}_{\rm ee} \right\rangle_{\Phi_0^{N+1,\boldsymbol{\xi}}[n]} \right) \\ &\quad + \left(1 - \xi_- \frac{N-1}{N} - \xi_+ \frac{N+1}{N} \right) \\ &\quad \times \left[\left\langle \hat{T} + \hat{W}_{\rm ee} \right\rangle_{\Psi_0^{N,\boldsymbol{\xi}}[n]} - \left\langle \hat{T} + \hat{W}_{\rm ee} \right\rangle_{\Phi_0^{N,\boldsymbol{\xi}}[n]} \right] , \end{aligned} \tag{5.21}$$

where $\{\Psi_0^{M,\boldsymbol{\xi}}[n]\}$ denotes the interacting density-functional N-centered ensemble.

When comparison is made with Subsection 4.2.3, it becomes clear that N-centered and TGOK eDFTs are essentially the same theory (they only differ in the definition of the ensemble). From that point of view, we now have a unified eDFT for charged and neutral electronic excitations. As a result, N-centered eDFT can benefit from progress made in TGOK-DFT, and *vice versa*.

5.1.3 Exact ionization potential and electron affinity theorems

We have shown in Subsection 5.1.1 that neutral, anionic, and cationic ground-state energies can be extracted exactly from the N-centered ensemble energy [see Eqs. (5.8), (5.9), and (5.10)]. We can now use the variational density-functional expression of Eq. (5.15) to obtain expressions for the fundamental gap, the ionization potential (IP), and the electron affinity (EA). Note that these quantities are

traditionally derived in the context of DFT for fractional electron numbers [102] (see Section 5.2 for a detailed comparison). According to the Hellmann–Feynman theorem, we can express the weight derivatives of the ensemble energy as follows,

$$\begin{aligned}\frac{\partial E_0^{\boldsymbol{\xi}}}{\partial \xi_\pm} &= \mathrm{Tr}\left[\Delta_\pm \hat{\gamma}_{\mathrm{KS}}^{\boldsymbol{\xi}} \left(\hat{T} + \hat{V}_{\mathrm{ext}}\right)\right] + \left.\frac{\partial E_{\mathrm{Hxc}}^{\boldsymbol{\xi}}[n]}{\partial \xi_\pm}\right|_{n=n_{\hat{\gamma}_{\mathrm{KS}}^{\boldsymbol{\xi}}}} \\ &\quad + \int \mathrm{d}\mathbf{r} \frac{\delta E_{\mathrm{Hxc}}^{\boldsymbol{\xi}}[n_{\hat{\gamma}_{\mathrm{KS}}^{\boldsymbol{\xi}}}]}{\delta n(\mathbf{r})} \mathrm{Tr}\left[\Delta_\pm \hat{\gamma}_{\mathrm{KS}}^{\boldsymbol{\xi}} \hat{n}(\mathbf{r})\right], \end{aligned} \tag{5.22}$$

where $\Delta_\pm \hat{\gamma}_{\mathrm{KS}}^{\boldsymbol{\xi}} = \left|\Phi_0^{N\pm1,\boldsymbol{\xi}}\right\rangle\left\langle\Phi_0^{N\pm1,\boldsymbol{\xi}}\right| - \frac{N\pm1}{N}\left|\Phi_0^{N,\boldsymbol{\xi}}\right\rangle\left\langle\Phi_0^{N,\boldsymbol{\xi}}\right|$. Since the single-configuration M-electron KS wave functions $\Phi_0^{M,\boldsymbol{\xi}}$ are constructed from orbitals that fulfill the KS Eq. (5.16), the above energy derivative can be rewritten in terms of the KS orbital energies as [91]

$$\frac{\partial E_0^{\boldsymbol{\xi}}}{\partial \xi_\pm} = \pm\frac{1}{N}\sum_{p=1}^{N}\left(\varepsilon_{N+\frac{1}{2}\pm\frac{1}{2}}^{\boldsymbol{\xi}} - \varepsilon_p^{\boldsymbol{\xi}}\right) + \left.\frac{\partial E_{\mathrm{Hxc}}^{\boldsymbol{\xi}}[n]}{\partial \xi_\pm}\right|_{n=n_{\hat{\gamma}_{\mathrm{KS}}^{\boldsymbol{\xi}}}}. \tag{5.23}$$

By plugging Eq. (5.23) into Eq. (5.7), we immediately obtain the following exact expression for the fundamental gap:

$$E_{\mathrm{gap}}^{\mathrm{fund}} = \varepsilon_{N+1}^{\boldsymbol{\xi}} - \varepsilon_N^{\boldsymbol{\xi}} + \left.\left(\frac{\partial E_{\mathrm{Hxc}}^{\boldsymbol{\xi}}[n]}{\partial \xi_+} + \frac{\partial E_{\mathrm{Hxc}}^{\boldsymbol{\xi}}[n]}{\partial \xi_-}\right)\right|_{n=n_{\hat{\gamma}_{\mathrm{KS}}^{\boldsymbol{\xi}}}}. \tag{5.24}$$

If we now apply the LZ shift-in-potential procedure [319], by analogy with TGOK-DFT (see Section 4.2.4), *i.e.*,

$$\frac{\delta E_{\mathrm{Hxc}}^{\boldsymbol{\xi}}[n]}{\delta n(\mathbf{r})} \to \overline{v}_{\mathrm{Hxc}}^{\boldsymbol{\xi}}[n](\mathbf{r}) = \frac{\delta E_{\mathrm{Hxc}}^{\boldsymbol{\xi}}[n]}{\delta n(\mathbf{r})} + \frac{E_{\mathrm{Hxc}}^{\boldsymbol{\xi}}[n] - \int \mathrm{d}\mathbf{r}\, \frac{\delta E_{\mathrm{Hxc}}^{\boldsymbol{\xi}}[n]}{\delta n(\mathbf{r})} n(\mathbf{r})}{\int \mathrm{d}\mathbf{r}\, n(\mathbf{r})}, \tag{5.25}$$

we can express both the ensemble energy and its derivatives in terms of the LZ-shifted KS orbital energies $\overline{\varepsilon}_p^{\boldsymbol{\xi}}$, thus leading to the following compact expressions for the ensemble and individual energies [91], respectively:

$$E_0^{\boldsymbol{\xi}} = \left(1 + \frac{\xi_- - \xi_+}{N}\right)\sum_{p=1}^{N}\overline{\varepsilon}_p^{\boldsymbol{\xi}} - \xi_-\overline{\varepsilon}_N^{\boldsymbol{\xi}} + \xi_+\overline{\varepsilon}_{N+1}^{\boldsymbol{\xi}}, \tag{5.26}$$

$$E_0^{N-1} = \sum_{p=1}^{N-1} \overline{\varepsilon}_p^{\boldsymbol{\xi}} + \left(1 - \frac{(N-1)\xi_-}{N}\right) \left.\frac{\partial E_{\text{Hxc}}^{\boldsymbol{\xi}}[n]}{\partial \xi_-}\right|_{n=n_{\hat{\gamma}_{\text{KS}}^{\boldsymbol{\xi}}}} - \frac{(N-1)\xi_+}{N} \left.\frac{\partial E_{\text{Hxc}}^{\boldsymbol{\xi}}[n]}{\partial \xi_+}\right|_{n=n_{\hat{\gamma}_{\text{KS}}^{\boldsymbol{\xi}}}}, \tag{5.27}$$

$$E_0^{N+1} = \sum_{p=1}^{N+1} \overline{\varepsilon}_p^{\boldsymbol{\xi}} + \left(1 - \frac{(N+1)\xi_+}{N}\right) \left.\frac{\partial E_{\text{Hxc}}^{\boldsymbol{\xi}}[n]}{\partial \xi_+}\right|_{n=n_{\hat{\gamma}_{\text{KS}}^{\boldsymbol{\xi}}}} - \frac{(N+1)\xi_-}{N} \left.\frac{\partial E_{\text{Hxc}}^{\boldsymbol{\xi}}[n]}{\partial \xi_-}\right|_{n=n_{\hat{\gamma}_{\text{KS}}^{\boldsymbol{\xi}}}}, \tag{5.28}$$

and

$$E_0^{N} = \sum_{p=1}^{N} \overline{\varepsilon}_p^{\boldsymbol{\xi}} - \xi_- \left.\frac{\partial E_{\text{Hxc}}^{\boldsymbol{\xi}}[n]}{\partial \xi_-}\right|_{n=n_{\hat{\gamma}_{\text{KS}}^{\boldsymbol{\xi}}}} - \xi_+ \left.\frac{\partial E_{\text{Hxc}}^{\boldsymbol{\xi}}[n]}{\partial \xi_+}\right|_{n=n_{\hat{\gamma}_{\text{KS}}^{\boldsymbol{\xi}}}}. \tag{5.29}$$

By subtraction, we immediately obtain in-principle-exact IP and EA theorems:

$$I_0^N = E_0^{N-1} - E_0^N = -\overline{\varepsilon}_N^{\boldsymbol{\xi}} + \left(1 + \frac{\xi_-}{N}\right) \left.\frac{\partial E_{\text{Hxc}}^{\boldsymbol{\xi}}[n]}{\partial \xi_-}\right|_{n=n_{\hat{\gamma}_{\text{KS}}^{\boldsymbol{\xi}}}} + \frac{\xi_+}{N} \left.\frac{\partial E_{\text{Hxc}}^{\boldsymbol{\xi}}[n]}{\partial \xi_+}\right|_{n=n_{\hat{\gamma}_{\text{KS}}^{\boldsymbol{\xi}}}}, \tag{5.30}$$

and

$$A_0^N = E_0^N - E_0^{N+1} = -\overline{\varepsilon}_{N+1}^{\boldsymbol{\xi}} - \left(1 - \frac{\xi_+}{N}\right) \left.\frac{\partial E_{\text{Hxc}}^{\boldsymbol{\xi}}[n]}{\partial \xi_+}\right|_{n=n_{\hat{\gamma}_{\text{KS}}^{\boldsymbol{\xi}}}} + \frac{\xi_-}{N} \left.\frac{\partial E_{\text{Hxc}}^{\boldsymbol{\xi}}[n]}{\partial \xi_-}\right|_{n=n_{\hat{\gamma}_{\text{KS}}^{\boldsymbol{\xi}}}}. \tag{5.31}$$

Interestingly, in the regular ground-state N-electron limit (*i.e.*, when $\boldsymbol{\xi} = 0$), the expression of Levy and Zahariev [319] is recovered for the IP,

$$I_0^N = -\overline{\varepsilon}_N^{\boldsymbol{\xi}=0} + \left.\frac{\partial E_{\text{Hxc}}^{\boldsymbol{\xi}}[n_{\Psi_0}]}{\partial \xi_-}\right|_{\boldsymbol{\xi}=0}, \tag{5.32}$$

where the asymptotic value of the LZ-shifted Hxc potential away from the system [see Ref. [319] and Eq. (5.95)] can now be expressed explicitly, within the N-centered

ensemble formalism, as $\partial E_{\text{Hxc}}^{\boldsymbol{\xi}}[n_{\Psi_0}]/\partial\xi_-\Big|_{\boldsymbol{\xi}=0}$. Similarly, we obtain the following expression for the EA:

$$A_0^N = -\bar{\varepsilon}_{N+1}^{\boldsymbol{\xi}=0} - \left.\frac{\partial E_{\text{Hxc}}^{\boldsymbol{\xi}}[n_{\Psi_0}]}{\partial\xi_+}\right|_{\boldsymbol{\xi}=0} . \tag{5.33}$$

As readily seen from the above expressions, neutral and charged systems cannot be described with the same (LZ-shifted) Hxc potential. As shown in Section 5.2, the additional ensemble weight derivative correction [second term on the right-hand side of Eqs. (5.32) and (5.33)] is actually connected to the concept of derivative discontinuity which manifests in conventional DFT for fractional electron numbers, when crossing an integer [320].

5.2 Review of the regular PPLB approach to charged excitations and the concept of derivative discontinuity

5.2.1 Introduction

The concept of derivative discontinuity originally appeared in the context of DFT for fractional electron numbers [102], which is the conventional theoretical framework for the description of charged excitations. The (xc functional) derivative discontinuities play a crucial role in the evaluation of fundamental gaps [320]. More specifically, they correct the bare KS gap which is only an approximation to the true interacting gap. It is well known that standard (semi)-local DFAs do not contain such discontinuities, which explains why post-DFT methods based on Green functions, for example, are preferred for the computation of accurate gaps [286, 321, 322, 323, 324, 325, 326, 284] (see also Subsection 3.2.2). Their substantially higher computational cost is a motivation for exploring simpler (frequency-independent) strategies. The recently proposed N-centered ensemble formalism [91, 327], which has been introduced in Subsection 5.1.1, is (among others [328, 329, 330, 331, 332, 333, 334, 335]) promising in this respect.

From a more fundamental point of view, it is important to clarify the similarities and differences between N-centered eDFT and the standard formulation of DFT for

charged excitations, which is often referred to as *Perdew–Parr–Levy–Balduz* (PPLB) DFT [102]. More specifically, we should explain what the derivative discontinuity, which is central in PPLB, becomes when switching to the N-centered formalism. This is the purpose of this section.

After a brief review in the present section of the PPLB formalism and its implications, we will show (in Section 5.3), on the basis of Ref. [103], that derivative discontinuities exist also in N-centered eDFT and that they are directly connected to the ensemble weight derivatives of the xc functional, like in TGOK-DFT [104]. Finally, we will explain in Section 5.4 why these discontinuities can essentially be removed from the theory, unlike in PPLB, and discuss the practical implications.

5.2.2 Ensemble formalism for open systems

The key idea in PPLB is to describe electron ionization or affinity processes through a continuous variation of the electron number, hence the need for an extension of DFT to fractional electron numbers. Obviously, fractional charges cannot be physically represented by a closed system with fixed amount of electrons. Instead, they can be understood in statistical sense, *e.g.* an indication that the system is open for an exchange of electrons with environment given some elapsed time. The most appropriate quantity for open systems is thus ensemble of neutral and charged (ground) states. For that purpose, the energy of an artificial (zero-temperature) grand-canonical-type ensemble, which should not be confused with physical finite-temperature grand-canonical ensembles of statistical physics [336], is constructed as follows[1],

$$\mathcal{G}(\mu) = \min_{M} \left\{ E_0^M - \mu M \right\}, \tag{5.34}$$

where we minimize over *integer* numbers M of electrons and E_0^M denotes the exact M-electron ground-state energy of the system. In this formalism, the number of electrons in the system can be arbitrarily fixed by tuning the chemical potential μ. For example, if the following inequalities are fulfilled,

$$E_0^{N-1} - \mu(N-1) > E_0^N - \mu N < E_0^{N+1} - \mu(N+1), \tag{5.35}$$

[1]The minimum in Eq. (5.34) is unique, provided that the ground-state energy E_0^M is convex with respect to electron number [102]. That is, for every M, $E_0^{M+1} + E_0^{M-1} > 2E_0^M$.

or, equivalently,

$$-I_0^N < \mu < -A_0^N, \tag{5.36}$$

then the system contains an integer number N of electrons (it is assumed that the N-electron fundamental gap $E_g^N = I_0^N - A_0^N$ is positive, so that Eq. (5.36) can be fulfilled). In the special case where one of the inequality becomes a strict equality, say

$$E_0^{N-1} - \mu(N-1) = E_0^N - \mu N, \tag{5.37}$$

which means that the chemical potential is exactly equal to minus the N-electron ionization potential,

$$\mu = E_0^N - E_0^{N-1} = -I_0^N, \tag{5.38}$$

the N- and $(N-1)$-electron solutions are *degenerate* (grand-canonical energy wise). Therefore, they can be *mixed* as follows,

$$\begin{aligned}
\mathcal{G}(\mu) &\overset{\mu=-I_0^N}{=} (1-\alpha)\Big(E_0^{N-1} - \mu(N-1)\Big) + \alpha\Big(E_0^N - \mu N\Big) && (5.39)\\
&= \Big((1-\alpha)E_0^{N-1} + \alpha E_0^N\Big) - \mu\Big(N - 1 + \alpha\Big) && (5.40)\\
&\equiv E_0^{\mathcal{N}} - \mu\mathcal{N}, && (5.41)
\end{aligned}$$

where $0 \leq \alpha \leq 1$, thus allowing for a *continuous* variation of the electron number $\mathcal{N}$ (which now becomes fractional) from $N-1$ to N:

$$\mathcal{N} \equiv N - 1 + \alpha. \tag{5.42}$$

This is the central idea in PPLB for describing the ionization of an N-electron system. Ionizing the $(N+1)$-electron system gives access to the N-electron affinity. Interestingly, we recover from Eqs. (5.40), (5.41), and (5.42) the well-known piecewise linearity of the energy with respect to the electron number [102]:

$$E_0^{\mathcal{N}} \equiv (1-\alpha)E_0^{N-1} + \alpha E_0^N = (N-\mathcal{N})E_0^{N-1} + (\mathcal{N} - N + 1)E_0^N. \tag{5.43}$$

In order to establish a clearer connection between the PPLB and N-centered formalisms, we follow the approach of Kraisler and Kronik [328] where the ensemble

weight α is used as a variable, in place of the electron number $\mathcal{N}$. Therefore, in PPLB, the ensemble energy reads as

$$\begin{aligned} E^{\alpha} &= (1-\alpha)E_0^{N-1} + \alpha E_0^N \qquad (5.44) \\ &= (1-\alpha)\left\langle \Psi_0^{N-1}\middle|\hat{T}+\hat{W}_{\rm ee}\middle|\Psi_0^{N-1}\right\rangle + \alpha\left\langle \Psi_0^{N}\middle|\hat{T}+\hat{W}_{\rm ee}\middle|\Psi_0^{N}\right\rangle \\ &\quad + \int d\mathbf{r}\, v_{\rm ext}(\mathbf{r}) n_0^{\alpha}(\mathbf{r}), \qquad (5.45) \end{aligned}$$

where

$$n_0^{\alpha}(\mathbf{r}) = (1-\alpha) n_{\Psi_0^{N-1}}(\mathbf{r}) + \alpha n_{\Psi_0^{N}}(\mathbf{r}) \qquad (5.46)$$

is the exact ground-state ensemble density. Note that, if we introduce the ensemble density matrix operator

$$\hat{\Gamma}_0^{\alpha} = (1-\alpha)\left|\Psi_0^{N-1}\right\rangle\left\langle\Psi_0^{N-1}\right| + \alpha\left|\Psi_0^{N}\right\rangle\left\langle\Psi_0^{N}\right|, \qquad (5.47)$$

the ensemble energy and density can be expressed in a compact way as follows,

$$E^{\alpha} = \mathrm{Tr}\left[\hat{\Gamma}_0^{\alpha}\hat{H}\right] \qquad (5.48)$$

and

$$n_0^{\alpha}(\mathbf{r}) = \mathrm{Tr}\left[\hat{\Gamma}_0^{\alpha}\hat{n}(\mathbf{r})\right], \qquad (5.49)$$

respectively.

5.2.3 DFT for fractional electron numbers

On the basis of the "grand-canonical" ensemble formalism introduced in the previous section, we can extend the domain of definition of the universal Hohenberg–Kohn functional $F[n]$ to densities n that integrate to fractional electron numbers, *i.e.*,

$$\int d\mathbf{r}\, n(\mathbf{r}) = N - 1 + \alpha, \qquad (5.50)$$

as follows,

$$F[n] = (1-\alpha)\left\langle \hat{T}+\hat{W}_{\rm ee}\right\rangle_{\Psi_0^{N-1}[n]} + \alpha\left\langle \hat{T}+\hat{W}_{\rm ee}\right\rangle_{\Psi_0^{N}[n]}, \qquad (5.51)$$

where the ground-state density-functional wave functions fulfill the density constraint

$$(1-\alpha) n_{\Psi_0^{N-1}[n]}(\mathbf{r}) + \alpha n_{\Psi_0^{N}[n]}(\mathbf{r}) = n(\mathbf{r}). \qquad (5.52)$$

From now on we will take α in the range

$$0 < \alpha \leq 1, \tag{5.53}$$

so that the *integer* electron number case systematically corresponds to $\alpha = 1$. Therefore, in the present density-functional PPLB ensemble, the N-electron state will always contribute (even infinitesimally), and

$$N = \lceil \int d\mathbf{r}\, n(\mathbf{r}) \rceil. \tag{5.54}$$

At this point it is essential to realize that, unlike in N-centered eDFT, the ensemble weight α is *not* an independent variable. Indeed, according to Eqs. (5.50) and (5.54), it is an explicit functional of the density:

$$\alpha \equiv \alpha[n] = \int d\mathbf{r}\, n(\mathbf{r}) - \lceil \int d\mathbf{r}\, n(\mathbf{r}) \rceil + 1. \tag{5.55}$$

Therefore, in PPLB, the ensemble is fully determined from the density. The latter remains, like in regular DFT for integer electron numbers, the sole basic variable in the theory. Following Levy and Lieb [47, 48, 49], the extended universal functional of Eq. (5.51) can be expressed in a compact way as follows,

$$F[n] = \min_{\hat{\gamma}^\alpha \to n} \mathrm{Tr}\left[\hat{\gamma}^\alpha \left(\hat{T} + \hat{W}_{\mathrm{ee}}\right)\right], \tag{5.56}$$

where we minimize over grand-canonical ensemble density matrix operators

$$\hat{\gamma}^\alpha \equiv (1-\alpha) \left|\Psi^{N-1}\right\rangle \left\langle\Psi^{N-1}\right| + \alpha \left|\Psi^{N}\right\rangle \left\langle\Psi^{N}\right| \tag{5.57}$$

that fulfill the following density contraint:

$$\mathrm{Tr}\left[\hat{\gamma}^\alpha \hat{n}(\mathbf{r})\right] = n_{\hat{\gamma}^\alpha}(\mathbf{r}) = (1-\alpha) n_{\Psi^{N-1}}(\mathbf{r}) + \alpha n_{\Psi^N}(\mathbf{r}) = n(\mathbf{r}). \tag{5.58}$$

5.2.4 Kohn-Sham PPLB

The commonly used KS formulation of PPLB is recovered when introducing the non-interacting kinetic energy functional

$$T_{\mathrm{s}}[n] = \min_{\hat{\gamma}^\alpha \to n} \mathrm{Tr}\left[\hat{\gamma}^\alpha \hat{T}\right] \tag{5.59}$$

and the in-principle-exact decomposition

$$F[n] = T_{\mathrm{s}}[n] + E_{\mathrm{Hxc}}[n], \tag{5.60}$$

where the Hxc functional now applies to fractional electron numbers. Let us stress that, unlike in N-centered eDFT, the Hxc functional has no ensemble weight dependence because the weight is determined from the density n. Any dependence in α is incorporated into the functional through the density. This is a major difference with N-centered eDFT where the ensemble weight and the density are *independent* variables, like in GOK-DFT. This subtle point will be central later on when comparing the two theories.

According to the variational principle, the exact ensemble energy can be determined, for a given and *fixed* value of α, as follows,

$$E^\alpha = \min_{n \to N-1+\alpha} \left\{ F[n] + \int d\mathbf{r}\, v_{\text{ext}}(\mathbf{r}) n(\mathbf{r}) \right\}, \tag{5.61}$$

where we minimize over densities that integrate to the desired number $N-1+\alpha$ of electrons. According to Eqs. (5.59) and (5.60), the ensemble energy can be rewritten as

$$\begin{aligned} E^\alpha &= \min_{n \to N-1+\alpha} \left\{ \min_{\hat{\gamma}^\alpha \to n} \left\{ \text{Tr}\left[\hat{\gamma}^\alpha \left(\hat{T} + \hat{V}_{\text{ext}} \right) \right] + E_{\text{Hxc}}[n_{\hat{\gamma}^\alpha}] \right\} \right\} \\ &= \min_{\hat{\gamma}^\alpha} \left\{ \text{Tr}\left[\hat{\gamma}^\alpha \left(\hat{T} + \hat{V}_{\text{ext}} \right) \right] + E_{\text{Hxc}}[n_{\hat{\gamma}^\alpha}] \right\} \\ &\equiv \text{Tr}\left[\hat{\gamma}^\alpha_{\text{KS}} \left(\hat{T} + \hat{V}_{\text{ext}} \right) \right] + E_{\text{Hxc}}[n_{\hat{\gamma}^\alpha_{\text{KS}}}], \end{aligned} \tag{5.62}$$

where the minimizing KS density matrix operator

$$\hat{\gamma}^\alpha_{\text{KS}} = (1-\alpha) \left| \Phi_0^{N-1,\alpha} \right\rangle \left\langle \Phi_0^{N-1,\alpha} \right| + \alpha \left| \Phi_0^{N,\alpha} \right\rangle \left\langle \Phi_0^{N,\alpha} \right| \tag{5.63}$$

reproduces the exact ensemble density of Eq. (5.46):

$$n_{\hat{\gamma}^\alpha_{\text{KS}}}(\mathbf{r}) = \text{Tr}\left[\hat{\gamma}^\alpha \hat{n}(\mathbf{r}) \right] = n_0^\alpha(\mathbf{r}). \tag{5.64}$$

The orbitals from which $\Phi_0^{N-1,\alpha}$ and $\Phi_0^{N,\alpha}$ are constructed fulfill self-consistent KS equations,

$$\left(-\frac{1}{2}\nabla^2_{\mathbf{r}} + v_{\text{ext}}(\mathbf{r}) + \frac{\delta E_{\text{Hxc}}[n_{\hat{\gamma}^\alpha_{\text{KS}}}]}{\delta n(\mathbf{r})} \right) \varphi_i^\alpha(\mathbf{r}) = \varepsilon_i^\alpha \varphi_i^\alpha(\mathbf{r}), \tag{5.65}$$

where, as readily seen from the following ensemble density expression,

$$\begin{aligned} n_{\hat{\gamma}^\alpha_{\text{KS}}}(\mathbf{r}) &= (1-\alpha) \sum_{i=1}^{N-1} |\varphi_i^\alpha(\mathbf{r})|^2 + \alpha \sum_{i=1}^{N} |\varphi_i^\alpha(\mathbf{r})|^2 \\ &= \sum_{i=1}^{N-1} |\varphi_i^\alpha(\mathbf{r})|^2 + \alpha |\varphi_N^\alpha(\mathbf{r})|^2, \end{aligned} \tag{5.66}$$

the *highest occupied molecular orbital* (HOMO) [*i.e.*, φ_N^α] is *fractionally* occupied. This is the main difference with conventional DFT calculations for integer electron numbers.

5.2.5 Janak's theorem and its implications

Once the ensemble energy E^α has been determined (variationally), we can evaluate the IP, which is the quantity we are interested in, by differentiation with respect to the ensemble weight α [see Eq. (5.44)], *i.e.*,

$$\frac{dE^\alpha}{d\alpha} = -I_0^N, \tag{5.67}$$

which, according to the Hellmann–Feynman theorem and Eqs. (5.62), (5.63), and (5.65), can be written more explicitly as follows,

$$\begin{aligned}
\frac{dE^\alpha}{d\alpha} &= \left\langle \Phi_0^{N,\alpha} \middle| \hat{T} + \hat{V}_{\text{ext}} \middle| \Phi_0^{N,\alpha} \right\rangle - \left\langle \Phi_0^{N-1,\alpha} \middle| \hat{T} + \hat{V}_{\text{ext}} \middle| \Phi_0^{N-1,\alpha} \right\rangle \\
&\quad + \int d\mathbf{r} \frac{\delta E_{\text{Hxc}}[n_{\hat{\gamma}_{\text{KS}}^\alpha}]}{\delta n(\mathbf{r})} \left(n_{\Phi_0^{N,\alpha}}(\mathbf{r}) - n_{\Phi_0^{N-1,\alpha}}(\mathbf{r}) \right) \qquad (5.68) \\
&\equiv \sum_{i=1}^{N} \varepsilon_i^\alpha - \sum_{i=1}^{N-1} \varepsilon_i^\alpha \\
&= \varepsilon_N^\alpha, \qquad (5.69)
\end{aligned}$$

thus leading to the famous Janak's theorem [337]:

$$I_0^N = -\varepsilon_N^\alpha, \ \ \forall \alpha \in (0,1]. \tag{5.70}$$

As readily seen from Eq. (5.70), the energy ε_N^α of the KS HOMO does not vary with the fraction $\alpha > 0$ of electron that is introduced into the $(N-1)$-electron system. Therefore, it matches the N-electron KS HOMO energy that we simply denote ε_N^N:

$$\varepsilon_N^\alpha = \varepsilon_N^{\alpha=1} \equiv \varepsilon_N^N = -I_0^N. \tag{5.71}$$

Equally, with Janak's theorem, we can evaluate electron affinity. The only difference is that we need to consider a grand-canonical ensemble with N- and $N+1$-electron states,

$$\hat{\gamma}^\alpha \equiv (1-\alpha) \left| \Psi^N \right\rangle \left\langle \Psi^N \right| + \alpha \left| \Psi^{N+1} \right\rangle \left\langle \Psi^{N+1} \right|, \tag{5.72}$$

for which the variationally obtained ensemble energy reads,

$$E^{\alpha} = (1-\alpha)E_0^N + \alpha E_0^{N+1}. \tag{5.73}$$

Differentiating with respect to α gives the negative of electron affinity,

$$\frac{dE^{\alpha}}{d\alpha} = E_0^{N+1} - E_0^N = -A_0^N. \tag{5.74}$$

Similarly to Eq. (5.68), we can equate this with the HOMO energy of the $(N+1)$-electron system in KS PPLB,

$$\begin{aligned}
\frac{dE^{\alpha}}{d\alpha} &= \left\langle \Phi_0^{N+1,\alpha} \middle| \hat{T} + \hat{V}_{\text{ext}} \middle| \Phi_0^{N+1,\alpha} \right\rangle - \left\langle \Phi_0^{N,\alpha} \middle| \hat{T} + \hat{V}_{\text{ext}} \middle| \Phi_0^{N,\alpha} \right\rangle \\
&\quad + \int d\mathbf{r} \frac{\delta E_{\text{Hxc}}[n_{\hat{\gamma}_{\text{KS}}^{\alpha}}]}{\delta n(\mathbf{r})} \left(n_{\Phi_0^{N+1,\alpha}}(\mathbf{r}) - n_{\Phi_0^{N,\alpha}}(\mathbf{r}) \right) \qquad (5.75) \\
&\equiv \sum_{i=1}^{N+1} \varepsilon_i^{\alpha} - \sum_{i=1}^{N} \varepsilon_i^{\alpha} \\
&= \varepsilon_{N+1}^{\alpha}, \qquad (5.76)
\end{aligned}$$

where the minimizing KS density matrix operator is now equal to,

$$\hat{\gamma}_{\text{KS}}^{\alpha} = (1-\alpha) \left| \Phi_0^{N,\alpha} \right\rangle \left\langle \Phi_0^{N,\alpha} \right| + \alpha \left| \Phi_0^{N+1,\alpha} \right\rangle \left\langle \Phi_0^{N+1,\alpha} \right|. \tag{5.77}$$

Thus, giving the Janak's theorem for affinity,

$$A_0^N = -\varepsilon_{N+1}^{\alpha}, \;\; \forall \alpha \in (0,1]. \tag{5.78}$$

And just as before (see Eq. (5.71)), we can match the HOMO energy, now for a $(N+1)$-electron system, to the electron affinity

$$\varepsilon_{N+1}^{\alpha} = \varepsilon_{N+1}^{\alpha=1} \equiv \varepsilon_{N+1}^{N+1} = -A_0^N. \tag{5.79}$$

Therefore, the fundamental gap can be evaluated as a difference between two KS HOMO energies,

$$E_g^N = I_0^N - A_0^N = \varepsilon_{N+1}^{N+1} - \varepsilon_N^N. \tag{5.80}$$

Importantly, as we will show later in Subsection 5.2.6, $\varepsilon_{N+1}^{N+1} \neq \varepsilon_{N+1}^{N}$, since the two energies correspond to different KS potentials. As a consequence, evaluating the fundamental gap with above equation would require two KS calculations. If we are to compute the gap with just one KS calculation for the N-electron system, the approximation $E_g \approx \varepsilon_{N+1}^N - \varepsilon_N^N$ usually drastically underestimates the fundamental gap

by the amount that is known as the "derivative discontinuity" (DD) in traditional PPLB (see Subsection 5.2.6 for a more detailed discussion).

At this point it is also important to mention that, unlike in N-centered eDFT [see Eq. (5.32)], there is no ensemble weight derivative of the Hxc functional involved in Janak's theorem. Such a quantity does not exist in PPLB, simply because the ensemble weight α and the density n cannot vary independently. However, while the number of electrons is artificially held constant in the N-centered formalism, it is not the case in PPLB. Indeed, variations in α induce a change in density [see the third contribution on the right-hand side of Eq. (5.68)] that does not integrate to zero:

$$1 = \int d\mathbf{r} \left(n_{\Phi_0^{N,\alpha}}(\mathbf{r}) - n_{\Phi_0^{N-1,\alpha}}(\mathbf{r}) \right) \neq 0. \tag{5.81}$$

Therefore, it is crucial, when evaluating the functional derivative of the Hxc energy $\delta E_{\text{Hxc}}[n_{\hat{\gamma}_{\text{KS}}^{\alpha}}]/\delta n(\mathbf{r})$ (*i.e.*, the Hxc potential), to consider variations of the density $\delta n(\mathbf{r})$ that do not integrate to zero. This is unnecessary in N-centered eDFT. In PPLB, however, the proper modeling of the xc potential is essential for describing charged excitations. This is clearly illustrated by the fact that the exact xc potential exhibits derivative discontinuities when crossing an integer electron number, as discussed further in Section 5.3.

Let us finally discuss the unicity of the xc potential. We recall that, in the present review, the external potential is simply the (Coulomb) nuclear potential of the molecule under study. It is *fixed* and it vanishes away from the system:

$$v_{\text{ext}}(\mathbf{r}) \underset{|\mathbf{r}|\to+\infty}{\to} 0, \tag{5.82}$$

which we simply denote $v_{\text{ext}}(\infty) = 0$ in the following. As readily seen from Eq. (5.70), when describing a continuous variation of the electron number $\mathcal{N}$ in the range $N - 1 < \mathcal{N} < N$, the KS potential becomes truly unique, not anymore up to a constant. This can be related to the unicity of the chemical potential which allows for fractional electron numbers, as discussed previously in the interacting case [see Eq. (5.38)]. As a result, the xc potential is truly unique. More precisely, as illustrated in Appendix E for a one-dimensional (1D) system, Janak's theorem

implies that [338]

$$\left.\frac{\delta E_{\rm xc}[n_{\hat{\gamma}^\alpha_{\rm KS}}]}{\delta n(\mathbf{r})}\right|_{|\mathbf{r}|\to+\infty} \equiv v^\alpha_{\rm xc}(\infty) = 0. \tag{5.83}$$

5.2.6 Fundamental gap problem

According to Janak's theorem, the fundamental gap can be evaluated in PPLB, in principle exactly, from the HOMO energies as follows,

$$E^N_g = I^N_0 - I^{N+1}_0 = \varepsilon^{N+1}_{N+1} - \varepsilon^N_N. \tag{5.84}$$

What is truly challenging in practice, in particular in solids [339], is the extraction of this gap from a single N-electron calculation. Indeed, the HOMO energy ε^{N+1}_{N+1} of the $(N+1)$-electron system has no reason to match the *lowest unoccupied molecular orbital* (LUMO) energy ε^N_{N+1} of the N-electron system, simply because the infinitesimal addition of an electron to the latter system will affect the density [see Eq. (E.10)] and, consequently, the xc potential. The impact of an electron addition on the xc potential will be scrutinized in Section 5.3, in the context of N-centered eDFT. If we denote

$$\Delta^N_{\rm xc} = \varepsilon^{N+1}_{N+1} - \varepsilon^N_{N+1} \tag{5.85}$$

the deviation in energy between the above-mentioned HOMO and LUMO, we recover the usual expression [320]

$$E^N_g = \varepsilon^N_{N+1} - \varepsilon^N_N + \Delta^N_{\rm xc}, \tag{5.86}$$

where $\Delta^N_{\rm xc}$ can now be interpreted as the difference in gap between the physical and KS systems. As readily seen from the key Eq. (5.24) of N-centered eDFT, that we take in the regular N-electron ground-state DFT limit (*i.e.*, $\xi_+ = \xi_- = 0$), $\Delta^N_{\rm xc}$ is indeed a nonzero correction to the KS gap that can be expressed more explicitly as follows,

$$\Delta^N_{\rm xc} = \left.\frac{\partial E^{(\xi_-,0)}_{\rm xc}[n_{\Psi^N_0}]}{\partial \xi_-}\right|_{\xi_-=0} + \left.\frac{\partial E^{(0,\xi_+)}_{\rm xc}[n_{\Psi^N_0}]}{\partial \xi_+}\right|_{\xi_+=0}. \tag{5.87}$$

Note that we used in Eq. (5.87) the in-principle-exact decomposition

$$E^{(\xi_-,\xi_+)}_{\rm Hxc}[n] = E_{\rm H}[n] + E^{(\xi_-,\xi_+)}_{\rm xc}[n], \tag{5.88}$$

where the regular (weight-independent) Hartree functional is employed. The practical disadvantage of such a decomposition will be extensively discussed in Section 6.1. We focus here on the exact theory.

In the language of N-centered eDFT, $\Delta_{\rm xc}^N$ describes the variation in ensemble weights (while holding the ensemble density fixed and equal to the N-electron ground-state density $n_{\Psi_0^N}$) of the N-centered ensemble xc energy due to the infinitesimal removal/addition of an electron from/to the N-electron system. Evidently, standard (local or semi-local) DFAs do not incorporate such a weight dependence because they were not designed for N-centered eDFT calculations (we recall that the concept of N-centered ensemble has been proposed quite recently [91, 327, 103]). Therefore, when such DFAs are used, the physical gap is systematically approximated by the (also approximate) KS one. Note that the resulting underestimation of the fundamental gap is highly problematic, for example, when computing transport properties [340, 341]. The interpretation that is given in PPLB for $\Delta_{\rm xc}^N$ is completely different. The latter actually originates from the discontinuity that the xc potential (which is the functional derivative of the xc energy) exhibits when crossing an integer electron number, hence the name *derivative discontinuity*. In the language of PPLB, $\Delta_{\rm xc}^N$ is not described at all when (semi-) local xc functionals are employed, simply because the latter do not incorporate functional derivative discontinuities. The connection between these two very different interpretations will be made in Section 5.3.

5.3 Connection between PPLB and N-centered pictures

Crossing an integer electron number, which is a key concept in PPLB, can be described in the context of N-centered eDFT by considering so-called left and right N-centered ensembles [327]. These ensembles are recovered when $\xi_+ = 0$ (electron removal only) and $\xi_- = 0$ (electron addition only), respectively. In the following,

we will use the following shorthand notations,

$$\text{left } N\text{-centered ensemble: } (\xi_-, 0) \overset{notation}{\equiv} \xi_-, \tag{5.89}$$

$$\text{right } N\text{-centered ensemble: } (0, \xi_+) \overset{notation}{\equiv} \xi_+, \tag{5.90}$$

for convenience. For example, the right N-centered ensemble Hxc functional and KS orbital energies will be denoted as $E_{\text{Hxc}}^{\xi_+}[n] \equiv E_{\text{Hxc}}^{(0,\xi_+)}[n]$ and $\varepsilon_i^{\xi_+} \equiv \varepsilon_i^{(0,\xi_+)}$, respectively. The exact left and right N-centered ensemble densities read as [see Eq. (5.3)]

$$n^{\xi_-}(\mathbf{r}) \equiv \left(1 - \frac{(N-1)\xi_-}{N}\right) n_{\Psi_0^N}(\mathbf{r}) + \xi_- n_{\Psi_0^{N-1}}(\mathbf{r}), \tag{5.91}$$

and

$$n^{\xi_+}(\mathbf{r}) \equiv \left(1 - \frac{(N+1)\xi_+}{N}\right) n_{\Psi_0^N}(\mathbf{r}) + \xi_+ n_{\Psi_0^{N+1}}(\mathbf{r}), \tag{5.92}$$

respectively. Note that, with these notations, we have the following equivalence relation,

$$\xi_- = 0 \Leftrightarrow \xi_+ = 0, \tag{5.93}$$

as readily seen from Eqs. (5.91) and (5.92). When Eq. (5.93) is fulfilled, the system is in its pure N-electron ground state which means, in the language of PPLB, that it contains exactly the integer number N of electrons.

A clearer connection between the two theories can be established by comparing the two limits $\xi_+ \to 0^+$ (which describes the infinitesimal addition of an electron to the N-electron system) and $\xi_+ = 0$ (or, equivalently, $\xi_- = 0$). For that purpose, we first need to realize that, by analogy with PPLB (see Appendix E for the proof in the simpler 1D case), the exact IP/EA theorems of N-centered eDFT in Eqs. (5.30) and (5.31) can be alternatively written as follows [103],

$$A_0^N = I_0^{N+1} \overset{\xi_+ \geq 0}{=} -\varepsilon_{N+1}^{\xi_+} + v_{\text{xc}}^{\xi_+}(\infty) \tag{5.94}$$

and

$$I_0^N \overset{\xi_- \geq 0}{=} -\varepsilon_N^{\xi_-} + v_{\text{xc}}^{\xi_-}(\infty), \tag{5.95}$$

where we recall that $v_{\text{xc}}^{\xi_\pm}(\mathbf{r}) \equiv \delta E_{\text{xc}}^{\xi_\pm}[n]/\delta n(\mathbf{r})\big|_{n=n^{\xi_\pm}}$. Thus, from the explicit expression of the LZ shift [see the second term on the right-hand side of Eq. (5.25)], we

obtain the following exact expressions for the asymptotic values of the right and left N-centered ensemble xc potentials, respectively:

$$v_{\rm xc}^{\xi_+}(\infty) \overset{\xi_+ \geq 0}{=} \left(\frac{\xi_+}{N} - 1\right) \left.\frac{\partial E_{\rm xc}^{\xi_+}[n]}{\partial \xi_+}\right|_{n=n^{\xi_+}} - \frac{1}{N}\left(E_{\rm Hxc}^{\xi_+}[n^{\xi_+}] - \int d\mathbf{r}\, v_{\rm Hxc}^{\xi_+}(\mathbf{r}) n^{\xi_+}(\mathbf{r})\right) \tag{5.96}$$

and

$$v_{\rm xc}^{\xi_-}(\infty) \overset{\xi_- \geq 0}{=} \left(\frac{\xi_-}{N} + 1\right) \left.\frac{\partial E_{\rm xc}^{\xi_-}[n]}{\partial \xi_-}\right|_{n=n^{\xi_-}} - \frac{1}{N}\left(E_{\rm Hxc}^{\xi_-}[n^{\xi_-}] - \int d\mathbf{r}\, v_{\rm Hxc}^{\xi_-}(\mathbf{r}) n^{\xi_-}(\mathbf{r})\right). \tag{5.97}$$

We recall that the decomposition of Eq. (5.88) is employed for a direct comparison with PPLB. Let us now consider the $\xi_+ \to 0^+$ and $\xi_- = 0$ limits in Eqs. (5.96) and (5.97), respectively. Since

$$n^{\xi_+ \to 0^+}(\mathbf{r}) = n^{\xi_- = 0}(\mathbf{r}) = n_{\Psi_0^N}(\mathbf{r}), \tag{5.98}$$

$$v_{\rm H}^{\xi_+ \to 0^+}(\mathbf{r}) = v_{\rm H}^{\xi_- = 0}(\mathbf{r}), \tag{5.99}$$

$$E_{\rm Hxc}^{\xi_+}[n^{\xi_+}]\Big|_{\xi_+ \to 0^+} = E_{\rm Hxc}^{\xi_-}[n^{\xi_-}]\Big|_{\xi_- = 0} = E_{\rm Hxc}[n_{\Psi_0^N}], \tag{5.100}$$

it comes, by subtraction,

$$\int \frac{d\mathbf{r}}{N}\left(v_{\rm xc}^{\xi_+ \to 0^+}(\mathbf{r}) - v_{\rm xc}^{\xi_+ = 0}(\mathbf{r})\right) n_{\Psi_0^N}(\mathbf{r}) = v_{\rm xc}^{\xi_+ \to 0^+}(\infty) - v_{\rm xc}^{\xi_+ = 0}(\infty) + \Delta_{\rm xc}^N, \tag{5.101}$$

or, equivalently,

$$\Delta_{\rm xc}^N = \int \frac{d\mathbf{r}}{N}\Big[\left(v_{\rm xc}^{\xi_+ \to 0^+}(\mathbf{r}) - v_{\rm xc}^{\xi_+ \to 0^+}(\infty)\right) - \left(v_{\rm xc}^{\xi_+ = 0}(\mathbf{r}) - v_{\rm xc}^{\xi_+ = 0}(\infty)\right)\Big] n_{\Psi_0^N}(\mathbf{r}), \tag{5.102}$$

where we used Eq. (5.87) and the relation $v_{\rm xc}^{\xi_- = 0}(\mathbf{r}) = v_{\rm xc}^{\xi_+ = 0}(\mathbf{r})$, according to Eq. (5.93). Note that, as readily seen from Eq. (5.102), $\Delta_{\rm xc}^N$ is insensitive to constant shifts in the xc potential, as expected from Eq. (5.86).

The connection that is made explicit in Eq. (5.102) between the N-centered ensemble weight derivative $\Delta_{\rm xc}^N$ of the xc density-functional energy [see Eq. (5.87)] and the xc potential is an important result that was highlighted very recently in

Ref. [103]. It proves that weight derivatives and derivative discontinuities are equivalent, thus extending to charged excitations what was already known for neutral excitations [104]. Indeed, if we systematically *choose* (but we do not have to in the N-centered formalism, unlike in PPLB) the xc potential that asymptotically goes to zero, *i.e.*,

$$v_{\rm xc}^{\xi_\pm}(\infty)=0, \;\; \xi_\pm \geq 0, \tag{5.103}$$

then we recover what looks like a Janak's theorem [see Eqs. (5.94) and (5.95)] and, according to Eq. (5.101),

$$\int d\mathbf{r} \left(v_{\rm xc}^{\xi_+ \to 0^+}(\mathbf{r}) - v_{\rm xc}^{\xi_+ = 0}(\mathbf{r}) \right) n_{\Psi_0^N}(\mathbf{r}) = N \Delta_{\rm xc}^N \neq 0. \tag{5.104}$$

It then becomes clear that, in the region of the system under study (*i.e.*, where the density $n_{\Psi_0^N}(\mathbf{r})$ is nonzero), the xc potentials obtained in the $\xi_+ \to 0^+$ and $\xi_+ = 0$ limits, respectively, *cannot* match. In order to fulfill the arbitrary constraint of Eq. (5.103), while still reproducing for $\xi_+ > 0$ the correct density in all regions of space [which includes a proper description of the density's asymptotic behavior (see Appendix E)], the xc potential must be shifted in the region the system, thus ensuring that the ground-state density $n_{\Psi_0^N}(\mathbf{r})$ is also correctly reproduced in that region. This has been nicely illustrated in Ref. [103] for an atom in 1D. Thus, we recover a well-known result of PPLB: When an electron is infinitesimally added (*i.e.*, $\xi_+ \to 0^+$) to a system with an integer number of electrons ($\xi_+ = 0$ case), the xc potential exhibits a jump (in the region of the system) which, according to Eqs. (5.86) and (5.104), corresponds exactly to the deviation in fundamental gap of the true system from the KS one.

5.4 Suppression of the derivative discontinuity

The fundamental gap expression of Eq. (5.24), which has been derived within the N-centered eDFT formalism, may intrigue PPLB practitioners. Indeed, it makes it possible to describe charged excitations, in principle exactly, without invoking explicitly the concept of derivative discontinuity. Instead, all our attention should be focused on the weight dependence of the N-centered ensemble xc density functional. Note that, despite this major difference between N-centered eDFT

and PPLB, the xc potential exhibits derivative discontinuities in both theories, as we have seen in Section 5.3. One may argue that modeling weight dependencies in ensemble xc density functionals is actually easier than modeling functional derivative discontinuities. Nevertheless, as discussed in further detail in Secs. 6.1 and 6.2, designing weight-dependent exchange and correlation DFAs from first principles raises several fundamental questions to which, up to now, no definitive answers have been given.

From a conceptual point of view, the fact that we do not need anymore to put efforts into the explicit description of derivative discontinuities, once we have moved from the standard PPLB picture to the N-centered one, can be interpreted as follows. Unlike in PPLB, the constraint in Eq. (5.103) is arbitrary because the KS potential remains unique up to a constant when charged excitations occur in N-centered eDFT, by construction. If, for simplicity, we keep this constraint for $\xi_+ = 0$, *i.e.*, we set $\tilde{v}_{\rm xc}^{\xi_+=0}(\mathbf{r}) \equiv v_{\rm xc}^{\xi_+=0}(\mathbf{r})$ so that $\tilde{v}_{\rm xc}^{\xi_+=0}(\infty) = 0$, which is likely to be fulfilled in a practical N-electron DFT calculation, it can be relaxed as follows, when $\xi_+ \to 0^+$,

$$v_{\rm xc}^{\xi_+\to 0^+}(\mathbf{r}) \quad \to \quad \tilde{v}_{\rm xc}^{\xi_+\to 0^+}(\mathbf{r}) = v_{\rm xc}^{\xi_+\to 0^+}(\mathbf{r}) - \Delta_{\rm xc}^{N}, \tag{5.105}$$

thus leading to $\tilde{v}_{\rm xc}^{\xi_+\to 0^+}(\infty) = -\Delta_{\rm xc}^{N}$. We stress that $\tilde{v}_{\rm xc}^{\xi_+}$ is as exact as $v_{\rm xc}^{\xi_+}$. However, according to Eq. (5.102), which also holds for the new (shifted) potential $\tilde{v}_{\rm xc}^{\xi_+}(\mathbf{r})$, the relation in Eq. (5.104) now reads as

$$\int d\mathbf{r} \left(\tilde{v}_{\rm xc}^{\xi_+\to 0^+}(\mathbf{r}) - \tilde{v}_{\rm xc}^{\xi_+=0}(\mathbf{r}) \right) n_{\Psi_0^N}(\mathbf{r}) = 0. \tag{5.106}$$

In other words, *via* the shifting procedure of Eq. (5.105), we can simply move the derivative discontinuity away from the system, *i.e.*, in regions where the density is essentially equal to zero. Consequently, with this change of paradigm, the absence of derivative discontinuities in standard semi-local DFAs should not be considered as an issue anymore. The ability of the *local density approximation* (LDA) to reproduce relatively accurate LZ-shifted KS orbital energies, as shown in a 1D atomic model [103], is actually encouraging since the latter are central in the evaluation of both the IP and the EA [see Eqs. (5.32) and (5.33)]. On the other hand, the resulting charged excitation energies are rather poor because weight dependencies

are completely absent from standard LDA [103]. We hope that, in the near future, (much) more efforts will be put into the design of weight-dependent DFAs. Recent developments based on uniform electron gas models [109, 110] are a first and important step in this direction.

Chapter 6

Exchange and correlation energies in ensemble DFT

In Chapter 4 we introduced TGOK-DFT for describing neutral excitations, and two methods for charged excitations, *i.e.* the PPLB method, and N-centered eDFT. The latter as we have seen, places neutral and charged excitations in a unified eDFT framework with the use of weight-dependent functionals. This is advantageous since now we can benefit from developments of TGOK-DFT when designing weight-dependent functionals for N-centered eDFT, and vice-versa. However, in practice, we are currently still far away from knowing reliable and systematically improvable approximations. For example, unlike in regular ground-state DFT, there is no ensemble equivalent "Jacob's ladder" of DFAs, which would allow us to pick the most suitable functional for our computation. The present chapter focuses on the ensemble Hxc functional, which is treated as a sum of the ensemble Hartree-exchange and correlation functionals,

$$E_{\mathrm{Hxc}}^{\mathbf{w}}[n] \;\; = E_{\mathrm{Hx}}^{\mathbf{w}}[n] + E_{\mathrm{c}}^{\mathbf{w}}[n]. \tag{6.1}$$

In Section 6.1, the problem of designing weight dependent DFAs for the ensemble Hartee-exchange is briefly summarized. Then, in Section 6.2, we delve more deeply into discussions on the issue of correlation energy in eDFT. Numerical results are presented for the asymmetric Hubbard dimer. Section 6.3 closes this chapter with a brief summary and comments on future directions of ensemble DFT. The content of this chapter, including the numerical results, is mostly inspired by Sections 4 and

5 in the book chapter "Ensemble density functional theory of neutral and charged excitations".

6.1 The exact Hartree-exchange dilemma in eDFT

6.1.1 Overview

This short section summarizes the problematic in design of weight-dependent exchange DFAs. Despite several (scarce though) attempts [315, 342, 343, 110], it is still unclear how weight dependencies can be introduced into standard (semi-) local exchange functionals in a general and systematically improvable way. The use of orbital-dependent exchange functionals seems much more promising in this respect [108, 109, 344].

As mentioned before, in regular KS-DFT for ground-states, combining (a fraction of) exact exchange energy with (semi-)local density functionals gave rise to the well-known hybrid functionals such as B3LYP. As we will see in the following, its extension to ensembles is nontrivial, because different formulations with distinct pros and cons are possible. For simplicity, we will focus on TGOK ensembles, but the discussion applies to other eDFTs like, for example PPLB or N-centered eDFT (see Section 5.2).

6.1.2 Ensemble density matrix functional approach (eDMHF)

We start with a brief review of the procedure that is usually followed by DFT practitioners for extending HF to (TGOK in the present case) ensembles. In the regular scheme, the ensemble HF energy is evaluated variationally by inserting the *ensemble* (spin-summed one-electron reduced) *density matrix* (eDM) into the ground-state DM-functional HF energy. For that reason, we refer to the approach as eDMHF. The corresponding ensemble energy can be expressed as follows,

$$E^{\mathbf{w}}_{\mathrm{eDMHF}} \equiv \min_{\{\Phi_I\}} \left\{ \sum_I \mathtt{w}_I \langle \Phi_I | \hat{T} + \hat{V}_{\mathrm{ext}} | \Phi_I \rangle + W^{\mathrm{HF}} \left[\sum_I \mathtt{w}_I \boldsymbol{\gamma}_{\Phi_I} \right] \right\}, \tag{6.2}$$

where $\hat{V}_{\mathrm{ext}} = \int d\mathbf{r}\, v(\mathbf{r})_{\mathrm{ext}} \hat{n}(\mathbf{r})$ is an external (usually nuclear) potential operator. The eDM is evaluated from the trial orthonormal set $\{\Phi_I\}$ of *single-configuration*

wave functions (*i.e.*, Slater determinants or configuration state functions). The *ground-state* HF interaction functional reads as

$$W^{\mathrm{HF}}[\boldsymbol{\gamma}] = \frac{1}{2}\int d\mathbf{r}\int d\mathbf{r}'\frac{\gamma(\mathbf{r},\mathbf{r})\gamma(\mathbf{r}',\mathbf{r}') - \frac{1}{2}\gamma^2(\mathbf{r},\mathbf{r}')}{|\mathbf{r}-\mathbf{r}'|}, \tag{6.3}$$

where

$$\gamma_{\Phi_I}(\mathbf{r},\mathbf{r}') = \sum_{kl}\varphi_k(\mathbf{r})\varphi_l(\mathbf{r}')\sum_{\sigma\in\{\uparrow,\downarrow\}}\langle\Phi_I|\hat{c}^\dagger_{k\sigma}\hat{c}_{l\sigma}|\Phi_I\rangle \tag{6.4}$$

is the spin-summed one-electron reduced density matrix (spin-summed 1RDM) of the configuration Φ_I, and $\{\varphi_k\}$ is an orthonormal orbital basis. The most appealing feature of this approach is that we can show that the minimizing orbitals in Eq. (6.2) fulfill eigenvalue equations akin to that of the Fock operator (see Eqs. (1.31) - (1.35)), with the only difference being that some orbitals can be fractionally occupied. However, the eDMHF energy is unphysical in many ways. For example, by construction, it varies quadratically with the ensemble weights [see Eqs. (6.2) and (6.3)] while the true physical ensemble energy is expected to vary linearly. Another problem related to this discrepancy are the so-called *ghost-interactions* (GIs), which are unphysical couplings between individual states in the ensemble. This can be seen more explicitly,

$$\begin{aligned} W^{\mathrm{HF}}\left[\sum_I \mathtt{w}_I\boldsymbol{\gamma}_{\Phi_I}\right] = \frac{1}{2}\sum_{IJ}\mathtt{w}_I\mathtt{w}_J\int d\mathbf{r}\int d\mathbf{r}'\frac{1}{|\mathbf{r}-\mathbf{r}'|} \\ \times\left(\gamma_{\Phi_I}(\mathbf{r},\mathbf{r})\gamma_{\Phi_J}(\mathbf{r}',\mathbf{r}') - \frac{1}{2}\gamma_{\Phi_I}(\mathbf{r},\mathbf{r}')\gamma_{\Phi_J}(\mathbf{r},\mathbf{r}')\right), \end{aligned} \tag{6.5}$$

where, as readily seen, GI terms arise from all "$I \neq J$" pairs. Let us stress that, already in the original formulation of TGOK-DFT [89], the ensemble Hartree energy, which is evaluated from the standard (ground-state) Hartree functional [see Eq. (4.23)], includes GI errors [see the first term on the right-hand side of Eq. (6.5)]. In the exact theory, the latter are supposed to be removed by the *weight-dependent* ensemble exchange functional. It is not necessarily the case in practice when, for example, standard (weight-independent) local or semi-local DFAs are employed [345, 101]. For this reason, we present another approach, known as the *State-averaged Hartree-Fock* (SAHF) which is GI-free by construction.

6.1.3 State-averaged Hartree-Fock approach (SAHF)

If we inspect again Eq. (6.5), we can come up with a simple correction to the GI errors by transforming it into an ensemble-weighted sum of functionals of spin-summed 1RDMs of individual configurations. More precisely, if we make the following substitution into the eDMHF energy expression in Eq. (6.2),

$$W^{\mathrm{HF}}\left[\sum_I \mathtt{w}_I \boldsymbol{\gamma}_{\Phi_I}\right] \longrightarrow \sum_I \mathtt{w}_I W^{\mathrm{HF}}\left[\boldsymbol{\gamma}_{\Phi_I}\right], \tag{6.6}$$

we arive at a different energy expression, which will be referred to as *state-averaged HF* (SAHF) energy in the following. It reads as,

$$E^{\mathbf{w}}_{\mathrm{eSAHF}} \equiv \min_{\{\Phi_I\}} \left\{ \sum_I \mathtt{w}_I \left(\langle \Phi_I | \hat{T} + \hat{V}_{\mathrm{ext}} | \Phi_I \rangle + W^{\mathrm{HF}}\left[\boldsymbol{\gamma}_{\Phi_I}\right] \right) \right\}, \tag{6.7}$$

where we assume for simplicity that interaction energies can be evaluated from the individual (one-electron reduced) density matrices. Such a simplification is always valid for single Slater determinants. For more general multideterminant (single configuration though) wave functions, the simplification in Eq. (6.6) might be used as an (additional) approximation. As we can see, one clear advantage of the SAHF approach is that unlike eDMHF, it is explicitly GI-free. This point is probably the strongest argument for promoting SAHF over eDMHF. On the other hand, in SAHF, one cannot find a simple analogue to the Fock operator by minimizing Eq. (6.7) with respect to orbitals. Note that both schemes would be good starting points for turning the recently formulated ensemble reduced density matrix functional theory (w-RDMFT) [346] into a practical method for the computation of low-lying excited states.

6.2 Individual correlation energies in eDFT

While the previous section summarized the key approaches in description of orbital- and weight-dependent ensemble Hx energies, this section deals with correlation effects in many-body ensembles. For convenience, we continue focusing on TGOK ensembles but the discussion applies to other types of ensembles like, for example, N-centered [91] or thermal ones [93, 94, 95, 78]. We will work within the

original TGOK-DFT formalism [89], where a local multiplicative ensemble- density-functional Hxc potential is employed, but the discussion holds also when orbital-dependent exchange energies are employed (see Section 6.1).

6.2.1 State-of-the-art ensemble correlation DFAs and beyond

To the best of our knowledge, very few works have addressed the construction of weight-dependent ensemble correlation DFAs from first principles. We can essentially distinguish two different general strategies. In the first and most straightforward one, which we hereafter refer to as GS-ic, the (weight-independent) ground-state correlation functional is recycled as follows [108],

$$E_{\rm c}^{\mathbf{w}}[n^{\mathbf{w}}] \overset{\rm GS-ic}{\approx} \sum_I \mathtt{w}_I E_{\rm c}[n_{\Phi_I^{\mathbf{w}}}], \tag{6.8}$$

where, in the exact theory, the KS wave functions $\{\Phi_I^{\mathbf{w}}\}$ are expected to reproduce the true ensemble density $n^{\mathbf{w}}$.

More recently [109, 110], Loos and coworkers explored another path. They designed a first generation of weight-dependent ensemble LDA (eLDA) correlation functionals where the regular ground-state LDA functional $E_{\rm c}^{\rm LDA}[n] = \int d\mathbf{r}\, n(\mathbf{r})\epsilon_{\rm c}(n(\mathbf{r}))$, which is based on the *infinite* uniform electron gas (UEG) model, is combined with the density-functional correlation excitation energies of a *finite* UEG (hence the acronym fLDA used below) as follows,

$$E_{\rm c}^{\mathbf{w}}[n] \overset{\rm eLDA}{\approx} E_{\rm c}^{\rm LDA}[n] + \sum_{I>0} \mathtt{w}_I \left(\mathcal{E}_{{\rm c},I}^{f\rm LDA}[n] - \mathcal{E}_{{\rm c},I=0}^{f\rm LDA}[n] \right). \tag{6.9}$$

The individual correlation functional $\mathcal{E}_{{\rm c},I}^{f\rm LDA}[n] = \int d\mathbf{r}\, n(\mathbf{r})\epsilon_{{\rm c},I}^{f}(n(\mathbf{r}))$ is constructed from the Ith state of the finite UEG:

$$N_f\, \epsilon_{{\rm c},I}^{f}(n) \equiv \langle \Psi_I(n)|\hat{T} + \hat{W}_{\rm ee}|\Psi_I(n)\rangle - \langle \Phi_I(n)|\hat{T} + \hat{W}_{\rm ee}|\Phi_I(n)\rangle\,, \tag{6.10}$$

where N_f is the number of electrons in the finite gas. If N_f is fixed, a parameterization of the correlation energy per particle $\epsilon_{{\rm c},I}^{f}(n)$ as a function of the uniform density n is obtained by varying the volume of the gas [109]. Note that, in a uniform system, there is no need to introduce weight dependencies into the interacting and

non-interacting (ground- or excited-state) density-functional wave functions, unlike in the general definition of Eq. (4.28). Indeed, all the eigenstates of the (interacting or non-interacting) uniform gas have the same (uniform) density n, which then becomes the ensemble density of the gas, whatever the value of the ensemble weights:

$$\sum_I \mathtt{w}_I n_{\Psi_I(n)} = \sum_I \mathtt{w}_I n_{\Phi_I(n)} = n \sum_I \mathtt{w}_I = n. \tag{6.11}$$

Note also that, while the finite UEG allows for the incorporation of weight dependencies into the correlation functional, the use of a regular LDA correlation functional reduces finite-size errors. Refinements are possible, for example, by including a dependence in the Fermi hole curvature [347].

The strategies depicted in Eqs. (6.8) and (6.9) miss various correlation effects that we briefly review below. More insight will be given in the next subsections. Let us start with the GS-ic approximation. From the exact expression,

$$E_{\rm c}[n_{\Phi_I^{\mathbf{w}}}] = \left\langle \hat{T} + \hat{W}_{\rm ee} \right\rangle_{\Psi_0[n_{\Phi_I^{\mathbf{w}}}]} - \left\langle \hat{T} + \hat{W}_{\rm ee} \right\rangle_{\Phi_0[n_{\Phi_I^{\mathbf{w}}}]}, \tag{6.12}$$

where $\Psi_0[n]$ and $\Phi_0[n]$ are the interacting and KS non-interacting *ground-state* density-functional wave functions of regular KS-DFT, respectively, we immediately identify two sources of errors. The first one is related to the fact that, as already mentioned in Subsection 4.2.4, the individual KS density $n_{\Phi_I^{\mathbf{w}}}$ does not necessarily match the interacting individual one n_{Ψ_I}. This subtle point was recently highlighted by Gould and Pittalis [96, 348]. It induces what the authors referred to as *density-driven* (DD) correlation effects. Even if the true individual densities $\{n_{\Psi_I}\}$ (which can be extracted in principle exactly from the KS ensemble, as shown in Eq. (4.30) and Ref. [97]) were inserted into the expression of Eq. (6.12), we would still not recover the correct individual excited-state correlation energies simply because $\Psi_0[n_{\Psi_I}]$ will always be a ground-state wave function, even when n_{Ψ_I} is an excited-state density. The missing energy contribution is connected to the concept of *state-driven* (SD) correlation [96]. Interestingly, eLDA describes (approximately) SD correlations, as readily seen from Eq. (6.10). However, it completely misses DD ones, simply because KS and interacting (ground- or excited-state) wave functions have the same density in a uniform system.

Even though the physical meaning of DD and SD correlations is rather clear, it is less obvious how their contributions to the total exact ensemble correlation energy should be defined mathematically [96, 97, 348, 349]. Addressing this fundamental question is of primary importance for the design of more accurate and systematically improvable ensemble correlation DFAs, which is probably the most challenging task in TGOK-DFT. Up to now, we have discussed the concept of DD and SD correlations in the light of the GS-ic approximation [see Eqs. (6.8) and (6.12)]. We may actually wonder if a proper definition can be (or should be) given without referring explicitly to the GS correlation functional of KS-DFT. Indeed, the latter appears naturally in TGOK-DFT only in the limiting $\mathbf{w} = 0$ case. Gould and Pittalis [96], and then Fromager [97], recently addressed this SD/DD ensemble correlation energy decomposition issue from that perspective. A detailed and complemented review of the two approaches is presented in the following.

6.2.2 Weight dependence of the KS wave functions in TGOK-DFT

Before proceeding with the extraction of individual correlation energies from the TGOK-DFT ensemble energy, which is convenient for deriving in-principle-exact SD/DD decompositions [97], we would like to highlight the importance of weight dependencies in the KS wave functions. It might be surprising at first sight because the true ground and excited states of the system under study are of course weight-independent. We explain below, with a simple argument, why it cannot be the case in the KS ensemble.

Since the KS and true ensemble densities match for any set of weights $\mathbf{w}$, their derivatives with respect to the weights also match. Therefore, if we consider the ground-state $\mathbf{w} = 0$ limit of TGOK-DFT, it comes

$$\frac{\partial}{\partial \mathtt{w}_J}\left(\sum_I \mathtt{w}_I n_{\Psi_I}(\mathbf{r})\right)\Bigg|_{\mathbf{w}=0} \overset{J\geq 0}{=} \frac{\partial}{\partial \mathtt{w}_J}\left(\sum_I \mathtt{w}_I n_{\Phi_I^{\mathbf{w}}}(\mathbf{r})\right)\Bigg|_{\mathbf{w}=0}, \tag{6.13}$$

or, equivalently,

$$n_{\Psi_J}(\mathbf{r}) - n_{\Psi_0}(\mathbf{r}) = n_{\Phi_J}(\mathbf{r}) - n_{\Phi_0}(\mathbf{r}) + \left.\frac{\partial n_{\Phi_0^{\mathbf{w}}}(\mathbf{r})}{\partial \mathtt{w}_J}\right|_{\mathbf{w}=0}, \tag{6.14}$$

where $\{\Phi_I\}$ denote here the ground- and excited-state KS wave functions generated from a regular ground-state KS-DFT calculation. In KS-DFT, the density constraint applies to the ground state only, *i.e.*, $n_{\Phi_0}(\mathbf{r}) = n_{\Psi_0}(\mathbf{r})$, not to the excited states. Thus, we obtain the exact individual excited-state density expression, which can be recovered from Eq. (4.30) when $\mathbf{w} = 0$,

$$n_{\Psi_J}(\mathbf{r}) - n_{\Phi_J}(\mathbf{r}) \overset{J\geq 0}{=} \left.\frac{\partial n_{\Phi_0^{\mathbf{w}}}(\mathbf{r})}{\partial \mathtt{w}_J}\right|_{\mathbf{w}=0} \neq 0, \tag{6.15}$$

where we readily see that, in TGOK-DFT, the KS wave functions (the ground-state one in the present case) are necessarily *weight-dependent*. This feature is central in the design of DD correlation energies [97], as discussed further in the following. We refer to Eq. (6.57) for an illustrative example (based on the prototypical Hubbard dimer) of weight-dependent KS ground-state density.

6.2.3 Extraction of individual correlation energies

In this section we revisit the derivation of the individual energy levels in Eq. (4.39) in order to construct individual correlation energies within the ensemble under study. For that purpose, we start from the exact relation between individual and ensemble energies in Eq. (4.11), and the variational TGOK-DFT ensemble energy expression of Eq. (4.17), thus leading to, according to the Hellmann–Feynman theorem,

$$\begin{aligned} E_J = &\sum_{I\geq 0} \mathtt{w}_I \langle \Phi_I^{\mathbf{w}} | \hat{T} + \hat{V}_{\text{ext}} | \Phi_I^{\mathbf{w}} \rangle + E_{\text{Hxc}}^{\mathbf{w}}[n^{\mathbf{w}}] \\ &+ \sum_{I>0} (\delta_{IJ} - \mathtt{w}_I) \left[\langle \Phi_I^{\mathbf{w}} | \hat{T} + \hat{V}_{\text{ext}} | \Phi_I^{\mathbf{w}} \rangle - \langle \Phi_0^{\mathbf{w}} | \hat{T} + \hat{V}_{\text{ext}} | \Phi_0^{\mathbf{w}} \rangle \right] \\ &+ \sum_{I>0} (\delta_{IJ} - \mathtt{w}_I) \left[\frac{\partial E_{\text{Hxc}}^{\mathbf{w}}[n^{\mathbf{w}}]}{\partial \mathtt{w}_I} - \left.\frac{\partial E_{\text{Hxc}}^{\boldsymbol{\xi}}[n^{\boldsymbol{\xi},\mathbf{w}}]}{\partial \mathtt{w}_I}\right|_{\boldsymbol{\xi}=\mathbf{w}} \right], \end{aligned} \tag{6.16}$$

or, equivalently,

$$\begin{aligned} E_J = &\langle \Phi_J^{\mathbf{w}} | \hat{T} + \hat{V}_{\text{ext}} | \Phi_J^{\mathbf{w}} \rangle + E_{\text{Hxc}}^{\mathbf{w}}[n^{\mathbf{w}}] \\ &+ \sum_{I>0} (\delta_{IJ} - \mathtt{w}_I) \left[\frac{\partial E_{\text{Hxc}}^{\mathbf{w}}[n^{\mathbf{w}}]}{\partial \mathtt{w}_I} - \left.\frac{\partial E_{\text{Hxc}}^{\boldsymbol{\xi}}[n^{\boldsymbol{\xi},\mathbf{w}}]}{\partial \mathtt{w}_I}\right|_{\boldsymbol{\xi}=\mathbf{w}} \right], \end{aligned} \tag{6.17}$$

where the following double-weight ensemble KS density has been introduced:

$$n^{\boldsymbol{\xi},\mathbf{w}}(\mathbf{r}) = \sum_{I\geq 0} \xi_I n_{\Phi_I^{\mathbf{w}}}(\mathbf{r}). \tag{6.18}$$

The last contribution (that is subtracted) on the right-hand side of Eq. (6.17) originates from the Hellmann–Feynman theorem. In other words, derivatives of the KS wave functions (and, therefore, of their densities) do not contribute to the derivatives of the *total* ensemble energy, because the latter is variational.

As shown in Refs. [109, 97], the Hx contribution to the individual Jth energy level reduces to the expectation value of the two-electron repulsion operator evaluated for the Jth KS state, as one would guess. Indeed, once we have realized that, for given weight values $\boldsymbol{\xi}$, the ensemble KS potential that reproduces $n^{\boldsymbol{\xi},\mathbf{w}}$ is simply the one that reproduces the true ensemble density $n^{\mathbf{w}}$, we deduce from Eq. (4.27) that

$$E_{\mathrm{Hx}}^{\boldsymbol{\xi}}[n^{\boldsymbol{\xi},\mathbf{w}}] = \sum_{K\geq 0} \xi_K \left\langle \Phi_K^{\mathbf{w}} | \hat{W}_{\mathrm{ee}} | \Phi_K^{\mathbf{w}} \right\rangle, \tag{6.19}$$

and, consequently,

$$\left.\frac{\partial E_{\mathrm{Hx}}^{\boldsymbol{\xi}}[n^{\boldsymbol{\xi},\mathbf{w}}]}{\partial \mathtt{w}_I}\right|_{\boldsymbol{\xi}=\mathbf{w}} = \sum_{K\geq 0} \mathtt{w}_K \frac{\partial \left\langle \Phi_K^{\mathbf{w}} | \hat{W}_{\mathrm{ee}} | \Phi_K^{\mathbf{w}} \right\rangle}{\partial \mathtt{w}_I}. \tag{6.20}$$

As a result, since $E_{\mathrm{Hx}}^{\mathbf{w}}[n^{\mathbf{w}}] = E_{\mathrm{Hx}}^{\mathbf{w}}[n^{\mathbf{w},\mathbf{w}}]$, it comes

$$\frac{\partial E_{\mathrm{Hx}}^{\mathbf{w}}[n^{\mathbf{w}}]}{\partial \mathtt{w}_I} - \left.\frac{\partial E_{\mathrm{Hx}}^{\boldsymbol{\xi}}[n^{\boldsymbol{\xi},\mathbf{w}}]}{\partial \mathtt{w}_I}\right|_{\boldsymbol{\xi}=\mathbf{w}} = \left\langle \Phi_I^{\mathbf{w}} | \hat{W}_{\mathrm{ee}} | \Phi_I^{\mathbf{w}} \right\rangle - \left\langle \Phi_0^{\mathbf{w}} | \hat{W}_{\mathrm{ee}} | \Phi_0^{\mathbf{w}} \right\rangle, \tag{6.21}$$

thus leading to the expected result:

$$\begin{aligned} &E_{\mathrm{Hx}}^{\mathbf{w}}[n^{\mathbf{w}}] + \sum_{I>0} (\delta_{IJ} - \mathtt{w}_I) \left[\frac{\partial E_{\mathrm{Hx}}^{\mathbf{w}}[n^{\mathbf{w}}]}{\partial \mathtt{w}_I} - \left.\frac{\partial E_{\mathrm{Hx}}^{\boldsymbol{\xi}}[n^{\boldsymbol{\xi},\mathbf{w}}]}{\partial \mathtt{w}_I}\right|_{\boldsymbol{\xi}=\mathbf{w}} \right] \\ &= \left\langle \Phi_J^{\mathbf{w}} | \hat{W}_{\mathrm{ee}} | \Phi_J^{\mathbf{w}} \right\rangle. \end{aligned} \tag{6.22}$$

We conclude from Eq. (6.17) that the energy levels can be evaluated exactly within TGOK-DFT as follows,

$$E_J = \left\langle \Phi_J^{\mathbf{w}} | \hat{H} | \Phi_J^{\mathbf{w}} \right\rangle + E_{\mathrm{c},J}^{\mathbf{w}}[n^{\mathbf{w}}], \tag{6.23}$$

where the individual correlation energy of the Jth state is determined from the ensemble correlation density functional as follows,

$$E_{\mathrm{c},J}^{\mathbf{w}}[n^{\mathbf{w}}] = E_{\mathrm{c}}^{\mathbf{w}}[n^{\mathbf{w}}] + \sum_{I>0} (\delta_{IJ} - \mathtt{w}_I) \left[\frac{\partial E_{\mathrm{c}}^{\mathbf{w}}[n^{\mathbf{w}}]}{\partial \mathtt{w}_I} - \left.\frac{\partial E_{\mathrm{c}}^{\boldsymbol{\xi}}[n^{\boldsymbol{\xi},\mathbf{w}}]}{\partial \mathtt{w}_I}\right|_{\boldsymbol{\xi}=\mathbf{w}} \right]. \tag{6.24}$$

In the following section, we will see how the concept of DD correlation emerges from Eq. (6.24), once it has been rewritten more explicitly in terms of individual densities.

6.2.4 Individual correlations versus individual components

According to the definition of the ensemble correlation functional in GOK-DFT [see Eq. (4.28)], the exact ensemble correlation energy can be decomposed as follows,

$$E_{\rm c}^{\mathbf{w}}[n^{\mathbf{w}}] = \sum_{J\geq 0} \mathtt{w}_J \mathcal{E}_{{\rm c},J}^{\mathbf{w}}[n^{\mathbf{w}}], \tag{6.25}$$

$$\mathcal{E}_{{\rm c},J}^{\mathbf{w}}[n^{\mathbf{w}}] = \langle \Psi_J | \hat{T} + \hat{W}_{\rm ee} | \Psi_J \rangle - \langle \Phi_J^{\mathbf{w}} | \hat{T} + \hat{W}_{\rm ee} | \Phi_J^{\mathbf{w}} \rangle \, . \tag{6.26}$$

Let us stress that these components do *not* match the individual correlation energies of Eq. (6.24). Indeed, unlike the latter [see Eq. (6.23)], they do not give access to the exact individual energy levels,

$$\begin{aligned} \langle \Phi_J^{\mathbf{w}} | \hat{H} | \Phi_J^{\mathbf{w}} \rangle + \mathcal{E}_{{\rm c},J}^{\mathbf{w}}[n^{\mathbf{w}}] &= \langle \Psi_J | \hat{T} + \hat{W}_{\rm ee} | \Psi_J \rangle + \int d\mathbf{r}\, v_{\rm ext}(\mathbf{r}) n_{\Phi_J^{\mathbf{w}}}(\mathbf{r}) \\ &\neq E_J, \end{aligned} \tag{6.27}$$

simply because the KS density $n_{\Phi_J^{\mathbf{w}}}$ does not match, in general, the true physical density n_{Ψ_J}. The concept of DD correlation, which was introduced recently by Gould and Pittalis [96], originates from this observation. The important property that the true individual correlation energies share with the individual correlation components is that both of them can be used to construct the total ensemble correlation energy, *i.e.*,

$$E_{\rm c}^{\mathbf{w}}[n^{\mathbf{w}}] = \sum_{J\geq 0} \mathtt{w}_J E_{{\rm c},J}^{\mathbf{w}}[n^{\mathbf{w}}]. \tag{6.28}$$

The above expression can be deduced from Eq. (6.24) and the fact that, for any $\{\Delta_I\}_{I>0}$,

$$\begin{aligned} \sum_{J\geq 0} \mathtt{w}_J \left(\sum_{I>0} (\delta_{IJ} - \mathtt{w}_I) \Delta_I \right) &= \sum_{I>0} \sum_{J\geq 0} \delta_{IJ} \mathtt{w}_J \Delta_I - \left(\sum_{J\geq 0} \mathtt{w}_J \right) \sum_{I>0} \mathtt{w}_I \Delta_I \\ &= \sum_{I>0} \mathtt{w}_I \Delta_I - \sum_{I>0} \mathtt{w}_I \Delta_I \\ &= 0. \end{aligned} \tag{6.29}$$

From now on we will substitute the decomposition of Eq. (6.28) for the more conventional one of Eq. (6.25). As shown in the following, with this change of paradigm, DD-type correlation energy contributions will naturally emerge from the derivation of a more explicit expression. Unlike in Ref. [96], the approach of Ref. [97], which is reviewed in the next section, does not require additional (state-specific) KS systems, thus avoiding formal issues such as the non-uniqueness of KS potentials for individual excited states or v-representability issues [97].

6.2.5 Density-driven ensemble correlation energy expression

Let us now derive a more explicit expression for the ensemble correlation energy, on the basis of Eq. (6.28). We start with a simplification of the true individual correlation energy expression of Eq. (6.24), where the standard decomposition into components [see Eq. (6.25)] of the ensemble correlation energy will be employed. On the one hand, we will have

$$\frac{\partial E_{\mathrm{c}}^{\mathbf{w}}[n^{\mathbf{w}}]}{\partial \mathtt{w}_I} = \mathcal{E}_{\mathrm{c},I}^{\mathbf{w}}[n^{\mathbf{w}}] - \mathcal{E}_{\mathrm{c},0}^{\mathbf{w}}[n^{\mathbf{w}}] + \sum_{K>0} \mathtt{w}_K \frac{\partial \mathcal{E}_{\mathrm{c},K}^{\mathbf{w}}[n^{\mathbf{w}}]}{\partial \mathtt{w}_I}, \tag{6.30}$$

where, according to Eq. (6.26),

$$\begin{aligned} \frac{\partial \mathcal{E}_{\mathrm{c},K}^{\mathbf{w}}[n^{\mathbf{w}}]}{\partial \mathtt{w}_I} &= -\frac{\partial}{\partial \mathtt{w}_I} \left[\langle \Phi_K^{\mathbf{w}} | \hat{T} + \hat{W}_{\mathrm{ee}} | \Phi_K^{\mathbf{w}} \rangle \right] \\ &= -2 \left\langle \Phi_K^{\mathbf{w}} \middle| \hat{T} + \hat{W}_{\mathrm{ee}} \middle| \frac{\partial \Phi_K^{\mathbf{w}}}{\partial \mathtt{w}_I} \right\rangle . \end{aligned} \tag{6.31}$$

As readily seen from Eq. (6.31), the weight derivatives of the individual correlation components are evaluated solely from the KS wave functions and their (static) linear response to variations in the ensemble weights. The true interacting wave functions are not involved since, unlike the KS wave functions, they do not vary with the ensemble weights [see the comment that follows Eq. (4.28), and Eq. (6.26)]. Combining Eqs. (6.25), (6.30), and (6.31) leads to the following expression for the first two contributions in Eq. (6.24) to the true individual correlation energy:

$$\begin{aligned} &E_{\mathrm{c}}^{\mathbf{w}}[n^{\mathbf{w}}] + \sum_{I>0} (\delta_{IJ} - \mathtt{w}_I) \frac{\partial E_{\mathrm{c}}^{\mathbf{w}}[n^{\mathbf{w}}]}{\partial \mathtt{w}_I} \\ &= \mathcal{E}_{\mathrm{c},J}^{\mathbf{w}}[n^{\mathbf{w}}] - 2 \sum_{I>0} \sum_{K>0} (\delta_{IJ} - \mathtt{w}_I) \mathtt{w}_K \left\langle \Phi_K^{\mathbf{w}} \middle| \hat{T} + \hat{W}_{\mathrm{ee}} \middle| \frac{\partial \Phi_K^{\mathbf{w}}}{\partial \mathtt{w}_I} \right\rangle . \end{aligned} \tag{6.32}$$

On the other hand, according to Eq. (6.18),

$$\left.\frac{\partial E_{\rm c}^{\boldsymbol{\xi}}[n^{\boldsymbol{\xi},\mathbf{w}}]}{\partial \mathtt{w}_I}\right|_{\boldsymbol{\xi}=\mathbf{w}} = \int d\mathbf{r} \frac{\delta E_{\rm c}^{\mathbf{w}}[n^{\mathbf{w}}]}{\delta n(\mathbf{r})} \sum_{K\geq 0} \mathtt{w}_K \frac{\partial n_{\Phi_K^{\mathbf{w}}}(\mathbf{r})}{\partial \mathtt{w}_I}, \tag{6.33}$$

thus leading to [see Eq. (4.30)]

$$-\sum_{I>0} (\delta_{IJ} - \mathtt{w}_I) \left.\frac{\partial E_{\rm c}^{\boldsymbol{\xi}}[n^{\boldsymbol{\xi},\mathbf{w}}]}{\partial \mathtt{w}_I}\right|_{\boldsymbol{\xi}=\mathbf{w}} = \int d\mathbf{r} \frac{\delta E_{\rm c}^{\mathbf{w}}[n^{\mathbf{w}}]}{\delta n(\mathbf{r})} \left(n_{\Phi_J^{\mathbf{w}}}(\mathbf{r}) - n_{\Psi_J}(\mathbf{r})\right). \tag{6.34}$$

Finally, by combining Eqs. (6.24), (6.32), and (6.34), we recover the expression of Ref. [97] for the deviation of the true Jth individual correlation energy from the component $\mathcal{E}_{{\rm c},J}^{\mathbf{w}}[n^{\mathbf{w}}]$,

$$\begin{aligned} E_{{\rm c},J}^{\mathbf{w}}[n^{\mathbf{w}}] - \mathcal{E}_{{\rm c},J}^{\mathbf{w}}[n^{\mathbf{w}}] = -2 \sum_{I>0} \sum_{K\geq 0} (\delta_{IJ} - \mathtt{w}_I) \mathtt{w}_K \left\langle \Phi_K^{\mathbf{w}} \middle| \hat{T} + \hat{W}_{\rm ee} \middle| \frac{\partial \Phi_K^{\mathbf{w}}}{\partial \mathtt{w}_I} \right\rangle \\ + \int d\mathbf{r} \frac{\delta E_{\rm c}^{\mathbf{w}}[n^{\mathbf{w}}]}{\delta n(\mathbf{r})} \left(n_{\Phi_J^{\mathbf{w}}}(\mathbf{r}) - n_{\Psi_J}(\mathbf{r})\right), \end{aligned} \tag{6.35}$$

thus leading [see Eq. (6.26)] to the following exact expression for individual correlation energies:

$$\begin{aligned} E_{{\rm c},J}^{\mathbf{w}}[n^{\mathbf{w}}] = \; & \langle \Psi_J | \hat{T} + \hat{W}_{\rm ee} | \Psi_J \rangle - \langle \Phi_J^{\mathbf{w}} | \hat{T} + \hat{W}_{\rm ee} | \Phi_J^{\mathbf{w}} \rangle \\ & - 2 \sum_{I>0} \sum_{K\geq 0} (\delta_{IJ} - \mathtt{w}_I) \mathtt{w}_K \left\langle \Phi_K^{\mathbf{w}} \middle| \hat{T} + \hat{W}_{\rm ee} \middle| \frac{\partial \Phi_K^{\mathbf{w}}}{\partial \mathtt{w}_I} \right\rangle \\ & + \int d\mathbf{r} \frac{\delta E_{\rm c}^{\mathbf{w}}[n^{\mathbf{w}}]}{\delta n(\mathbf{r})} \left(n_{\Phi_J^{\mathbf{w}}}(\mathbf{r}) - n_{\Psi_J}(\mathbf{r})\right). \end{aligned} \tag{6.36}$$

The above expression is a key result of Ref. [97] which, as we will see, allows us to explore in-principle-exact SD/DD correlation energy decompositions.

Let us now analyze the different contributions on the right-hand side of Eq. (6.36). While, on the first line, the bare Jth correlation energy component is recovered, the additional terms on the second and third lines ensure that the external potential energy is evaluated with the correct true density (see Eqs. (6.23) and (6.27), and the supplementary material of Ref. [97]). Interestingly, in the summation (in K) over all the states that belong to the ensemble [see the second line of Eq. (6.36)], one may separate the contribution of the state under consideration (*i.e.*, the Jth state) from the others, thus defining an individual SD correlation energy:

$$\begin{aligned} E_{{\rm c},J}^{\mathbf{w},{\rm SD}}[n^{\mathbf{w}}] = \; & \langle \Psi_J | \hat{T} + \hat{W}_{\rm ee} | \Psi_J \rangle - \langle \Phi_J^{\mathbf{w}} | \hat{T} + \hat{W}_{\rm ee} | \Phi_J^{\mathbf{w}} \rangle \\ & - 2 \mathtt{w}_J \sum_{I>0} (\delta_{IJ} - \mathtt{w}_I) \left\langle \Phi_J^{\mathbf{w}} \middle| \hat{T} + \hat{W}_{\rm ee} \middle| \frac{\partial \Phi_J^{\mathbf{w}}}{\partial \mathtt{w}_I} \right\rangle. \end{aligned} \tag{6.37}$$

The above definition, which was denoted $\overline{\text{SD}}$ in Ref. [97] (the "overline" notation is dropped in the present work, for simplicity), differs substantially from the definition of Gould and Pittalis [96]. In the latter, an additional state-specific KS wave function, which is expected to reproduce the true individual density of the state under consideration, is introduced. In this case, the name "state-driven" means that the correlation energy is evaluated from interacting and non-interacting wave functions which share the *same* density. Here, no additional KS wave function is introduced, which is obviously appealing from a computational point of view. One possible criticism about the definition in Eq. (6.37) is its arbitrariness. Indeed, we may opt for a more density-based definition, in the spirit of what Gould and Pittalis proposed, by introducing, for example, the following auxiliary wave functions:

$$\overline{\Phi}_J^{\mathbf{w}} = \Phi_J^{\mathbf{w}} + \sum_{I>0} \sum_{K\geq 0} \sqrt{|\delta_{IJ} - \mathtt{w}_I|\mathtt{w}_K} \left(\text{sgn}(\delta_{IJ} - \mathtt{w}_I)\, \Phi_K^{\mathbf{w}} + \frac{\partial \Phi_K^{\mathbf{w}}}{\partial \mathtt{w}_I} \right) . \tag{6.38}$$

Note that, in the ground-state $\mathbf{w} = 0$ limit, $\overline{\Phi}_0^{\mathbf{w}}$ reduces to the conventional KS wave function $\Phi_0^{\mathbf{w}=0}$ of KS-DFT. What might be interesting in the (somehow artificial) construction of the above individual auxiliary KS states is the possibility it gives to recover, like in the Gould-Pittalis approach [96], all the KS contributions (to the individual correlation energy) that appear on the first two lines of Eq. (6.36) from a single expectation value, thus generating, on the other hand, (several) additional terms that should ultimately be removed:

$$\begin{aligned} &\big\langle \overline{\Phi}_J^{\mathbf{w}} \big| \hat{T} + \hat{W}_{\text{ee}} \big| \overline{\Phi}_J^{\mathbf{w}} \big\rangle \\ &= \langle \Phi_J^{\mathbf{w}} | \hat{T} + \hat{W}_{\text{ee}} | \Phi_J^{\mathbf{w}} \rangle + 2 \sum_{I>0} \sum_{K\geq 0} (\delta_{IJ} - \mathtt{w}_I)\mathtt{w}_K \left\langle \Phi_K^{\mathbf{w}} \middle| \hat{T} + \hat{W}_{\text{ee}} \middle| \frac{\partial \Phi_K^{\mathbf{w}}}{\partial \mathtt{w}_I} \right\rangle \\ &\quad + \ldots \end{aligned} \tag{6.39}$$

Moreover, according to Eq. (4.30), we recover (among other terms) the correct physical density:

$$\begin{aligned} \big\langle \overline{\Phi}_J^{\mathbf{w}} \big| \hat{n}(\mathbf{r}) \big| \overline{\Phi}_J^{\mathbf{w}} \big\rangle &= n_{\Phi_J^{\mathbf{w}}}(\mathbf{r}) + \sum_{I>0} \sum_{K\geq 0} (\delta_{IJ} - \mathtt{w}_I)\mathtt{w}_K \frac{\partial n_{\Phi_K^{\mathbf{w}}}(\mathbf{r})}{\partial \mathtt{w}_I} + \ldots \\ &= n_{\Psi_J}(\mathbf{r}) + \ldots \end{aligned} \tag{6.40}$$

On that basis, we could argue that the first two lines on the right-hand side of Eq. (6.36) should be interpreted as a SD correlation energy, while the third line

would correspond to the missing DD correlation energy. The issue with such a decomposition is that the individual DD correlation energies would then cancel out in the weighted sum:

$$\begin{aligned}&\sum_{J\geq 0} \mathtt{w}_J \int d\mathbf{r} \frac{\delta E_{\rm c}^{\mathbf{w}}[n^{\mathbf{w}}]}{\delta n(\mathbf{r})} \left(n_{\Phi_J^{\mathbf{w}}}(\mathbf{r}) - n_{\Psi_J}(\mathbf{r})\right) \\ &= \int d\mathbf{r} \frac{\delta E_{\rm c}^{\mathbf{w}}[n^{\mathbf{w}}]}{\delta n(\mathbf{r})} \left(n^{\mathbf{w}}(\mathbf{r}) - n^{\mathbf{w}}(\mathbf{r})\right) = 0,\end{aligned} \tag{6.41}$$

which means that the ensemble DD correlation energy would be zero. As a result, with such an interpretation, the concept of DD correlation would not be of any help in the development of correlation DFAs for ensembles. This is of course not what we want [96]. In this respect, the definition in Eq. (6.37) is much more appealing. We will stick to this definition from now on. Consequently, the complementary ensemble DD correlation energy will read as [see Eqs. (6.25), (6.26), and (6.37)]

$$E_{\rm c}^{\mathbf{w},\rm DD}[n^{\mathbf{w}}] = E_{\rm c}^{\mathbf{w}}[n^{\mathbf{w}}] - \sum_{J\geq 0} \mathtt{w}_J E_{{\rm c},J}^{\mathbf{w},\rm SD}[n^{\mathbf{w}}] \tag{6.42}$$

$$= 2 \sum_{J\geq 0} \mathtt{w}_J^2 \sum_{I>0} (\delta_{IJ} - \mathtt{w}_I) \left\langle \Phi_J^{\mathbf{w}} \middle| \hat{T} + \hat{W}_{\rm ee} \middle| \frac{\partial \Phi_J^{\mathbf{w}}}{\partial \mathtt{w}_I} \right\rangle . \tag{6.43}$$

Thus, we recover another key result of Ref. [97]. As readily seen from Eq. (6.43), the exact evaluation of the DD correlation energy only requires computing the static linear response of the KS wave functions that belong to the ensemble, which is computationally affordable.

Finally, at a more formal level, we note that the ensemble DD correlation energy expression of Eq. (6.43) is related to the individual components $f_J^{\mathbf{w}}[n] = \langle \Phi_J^{\mathbf{w}}[n] | \hat{T} + \hat{W}_{\rm ee} | \Phi_J^{\mathbf{w}}[n] \rangle$ of the Hx-only approximation to the universal TGOK functional [see Eqs. (4.14), (4.16), and (4.27)]

$$f^{\mathbf{w}}[n] := T_{\rm s}^{\mathbf{w}}[n] + E_{\rm Hx}^{\mathbf{w}}[n] = \sum_K \mathtt{w}_K \left\langle \Phi_K^{\mathbf{w}}[n] | \hat{T} + \hat{W}_{\rm ee} | \Phi_K^{\mathbf{w}}[n] \right\rangle , \tag{6.44}$$

as follows,

$$E_{\rm c}^{\mathbf{w},\rm DD}[n^{\mathbf{w}}] = \sum_{J\geq 0} \mathtt{w}_J^2 \sum_{I>0} (\delta_{IJ} - \mathtt{w}_I) \frac{\partial f_J^{\mathbf{w}}[n^{\mathbf{w}}]}{\partial \mathtt{w}_I}. \tag{6.45}$$

We can even establish a direct connection with the total ensemble functional $f^{\mathbf{w}}[n]$, by analogy with Eq. (6.19). Indeed, since

$$f^{\boldsymbol{\xi}}\left[n^{\boldsymbol{\xi},\mathbf{w}}\right] = \sum_K \xi_K \left\langle \Phi_K^{\mathbf{w}} | \hat{T} + \hat{W}_{\rm ee} | \Phi_K^{\mathbf{w}} \right\rangle , \tag{6.46}$$

it comes

$$f_J^{\mathbf{w}}\left[n^{\mathbf{w}}\right] = f^{\mathbf{w}}\left[n^{\mathbf{w}}\right] + \sum_{I>0}\left(\delta_{IJ} - \mathtt{w}_I\right)\left.\frac{\partial f^{\boldsymbol{\xi}}\left[n^{\boldsymbol{\xi},\mathbf{w}}\right]}{\partial \xi_I}\right|_{\boldsymbol{\xi}=\mathbf{w}}. \tag{6.47}$$

6.2.6 Application to the Hubbard dimer

The importance of DD correlations, which was revealed in Ref. [96], has been confirmed in Ref. [97], in the weakly asymmetric and stronly correlated regime of the two-electron Hubbard dimer. We propose in the following to complete the study of Ref. [97] by exploring all asymmetry and correlation regimes, and comparing exact results with that of standard approximations.

6.2.6.1 Exact theory and approximations

The key DFAs for correlation energies, and the concept SD/DD decomposition of correlation energies are investigated in the asymmetric Hubbard dimer model, which has been introduced in Chapter 2. In this simple model system, exact (two-electron and singlet) bi-ensemble density-functional correlation energies $E_{\mathrm{c}}^{\mathtt{w}}(n)$ can be evaluated through Lieb maximizations [98, 76] from the following analytical expressions for the exact potential-functional interacting energies [78, 99, 100]:

$$E_I(\Delta v) = \frac{2U}{3} + \frac{2r}{3}\cos\left(\theta + \frac{2\pi}{3}(I+1)\right), \quad I = 0, 1, \tag{6.48}$$

where

$$r = \sqrt{3(4t^2 + \Delta v^2) + U^2} \tag{6.49}$$

and

$$\theta = \frac{1}{3}\arccos\left[\frac{9U(\Delta v^2 - 2t^2) - U^3}{r^3}\right]. \tag{6.50}$$

Exact ground- and excited-state densities are then obtained from the Hellmann–Feynman theorem [see Eq. (2.7)],

$$n_{\Psi_I} = 1 - \frac{\partial E_I(\Delta v)}{\partial \Delta v}, \tag{6.51}$$

and the cubic polynomial equation that the energies fulfill (see the Appendix of Ref. [98]). The resulting bi-ensemble density reads as $n^{\mathtt{w}} = (1-\mathtt{w})n_{\Psi_0} + \mathtt{w}\, n_{\Psi_1}$. The Hx-only TGOK functional introduced in Eq. (6.44) can be expressed analytically as

follows [98],

$$\begin{aligned} f^{\xi}(n) &= T_{\rm s}^{\xi}(n) + E_{\rm Hx}^{\xi}(n) \\ &= -2t\sqrt{(1-\xi)^2-(1-n)^2} + \frac{U}{2}\left[1+\xi-\frac{(3\xi-1)(1-n)^2}{(1-\xi)^2}\right], \end{aligned} \tag{6.52}$$

so that, as shown in Appendix F, the exact DD ensemble correlation energy reads explicitly as

$$\begin{aligned} E_{\rm c}^{\mathtt{w},\rm DD}(n^{\mathtt{w}}) = &-\mathtt{w}(n^{\mathtt{w}}-1)(n_{\Psi_1}-1) \\ &\times\left[\frac{2t}{\sqrt{(1-\mathtt{w})^2-(1-n^{\mathtt{w}})^2}}+\frac{U(1+\mathtt{w})}{(1-\mathtt{w})^2}\right]. \end{aligned} \tag{6.53}$$

Since the KS excited-state density is always equal to 1 in this model [98], the prefactor $(n_{\Psi_1}-1)$ matches the deviation in density of the true physical excited state from the KS one:

$$n_{\Psi_1} - 1 = n_{\Psi_1} - n_{\Phi_1^{\mathtt{w}}}. \tag{6.54}$$

Then it becomes clear that $E_{\rm c}^{\mathtt{w},\rm DD}(n^{\mathtt{w}})$ is a DD correlation energy. We also see from the expression of Eq. (6.53) that, in the regular ground-state DFT limit ($\mathtt{w}=0$), this type of correlation disappears.

In the following we test two common DFAs: A (weight-independent) *ground-state* density-functional description of the *ensemble correlation* energy (GS-ec) [101, 98],

$$E_{\rm c}^{\mathtt{w}}(n^{\mathtt{w}}) \overset{\rm GS-ec}{\approx} E_{\rm c}(n^{\mathtt{w}}), \tag{6.55}$$

where $E_{\rm c}(n) = E_{\rm c}^{\mathtt{w}=0}(n)$, and the GS-ic approximation introduced in Subsection 6.2.1 which, in the present case, gives

$$\begin{aligned} E_{\rm c}^{\mathtt{w}}(n^{\mathtt{w}}) &\overset{\rm GS-ic}{\approx} (1-\mathtt{w})E_{\rm c}(n_{\Phi_0^{\mathtt{w}}}) + \mathtt{w}E_{\rm c}(n_{\Phi_1^{\mathtt{w}}}) \\ &= (1-\mathtt{w})E_{\rm c}(n_{\Phi_0^{\mathtt{w}}}) + \mathtt{w}E_{\rm c}(n=1). \end{aligned} \tag{6.56}$$

Note that the KS ground-state density $n_{\Phi_0^{\mathtt{w}}}$ fulfills the constraint $(1-\mathtt{w})n_{\Phi_0^{\mathtt{w}}} + \mathtt{w}n_{\Phi_1^{\mathtt{w}}} = n^{\mathtt{w}}$, thus leading to

$$n_{\Phi_0^{\mathtt{w}}} = \frac{n^{\mathtt{w}}-\mathtt{w}}{(1-\mathtt{w})} = n_{\Psi_0} + \frac{\mathtt{w}(n_{\Psi_1}-1)}{(1-\mathtt{w})}, \tag{6.57}$$

where we readily see that, in general, $n_{\Phi_0^{\mathtt{w}}} \neq n_{\Psi_0}$. In the following, the local potential will be fixed. It is then analogous to the external potential of *ab initio* calculations, hence the notation $\Delta v = \Delta v_{\rm ext}$.

6.2.6.2 Results and discussion

Let us first discuss the strictly symmetric ($\Delta v_{\text{ext}} = 0$) dimer in which simple analytical expressions can be derived for both exact and approximate ensemble correlation energies. In this special case, ground- and excited-state densities are equal to 1, in both KS and physical interacting systems. Consequently, the ensemble DD correlation energy vanishes [see Eq. (6.53)]. Total and SD ensemble correlation energies are equal and vary linearly with the ensemble weight [76] as

$$E_{\text{c}}^{\mathtt{w}}(n^{\mathtt{w}} = 1) = 2t(1 - \mathtt{w}) \left(1 - \sqrt{1 + \frac{U^2}{16t^2}} \right) = (1 - \mathtt{w}) E_{\text{c}}(n = 1), \tag{6.58}$$

with the positive slope $-E_{\text{c}}(n = 1)$. As readily seen, the excited state exhibits no correlation effects in this density regime. Turning to the approximations, GS-ic erroneously assigns a (ground-state) correlation energy to the excited state [see Eq. (6.56)], thus leading to a total ensemble correlation energy that is wrong and equal to $E_{\text{c}}(n = 1)$, like in GS-ec [see Eq. (6.55)]. In conclusion, in the symmetric case, both GS-ic and GS-ec approximations completely miss the weight dependence of the ensemble correlation energy.

We now discuss the performance of GS-ec and GS-ic in the asymmetric dimer. Results are shown in Fig. 6.1. The features described in the symmetric case are preserved in the weakly asymmetric regime (see the top left panel of Fig. 6.1). When the asymmetry is more pronounced, both exact and approximate ensemble correlation energies exhibit curvature. By construction, these energies all reduce to the same (ground-state) correlation energy when $\mathtt{w} = 0$. They differ substantially by their slope in the ground-state limit ($\mathtt{w} = 0$). Further insight into GS-ic, for example, is obtained from the following analytical expression,

$$\begin{aligned} \left. \frac{\partial E_{\text{c}}^{\mathtt{w}}(n^{\mathtt{w}})}{\partial \mathtt{w}} \right|_{\mathtt{w}=0} &\overset{\text{GS-ic}}{\approx} E_{\text{c}}(n = 1) - E_{\text{c}}(n = n_{\Psi_0}) \\ &\quad + (n_{\Psi_1} - 1) \left. \frac{\partial E_{\text{c}}(n)}{\partial n} \right|_{n = n_{\Psi_0}}, \end{aligned} \tag{6.59}$$

where $E_{\text{c}}(n = 1) - E_{\text{c}}(n = n_{\Psi_0}) \leq 0$, as readily seen from Fig. 4 of Ref. [76]. Interestingly, in the strongly asymmetric $\Delta v_{\text{ext}}/U \gg 1$ regime, the true ground- (n_{Ψ_0}) and excited-state (n_{Ψ_1}) densities tend to 2 and 1, respectively (see Fig. 1 of

Ref. [98]). This is the situation where the slope in weight expressed in Eq. (6.59) reaches its maximum (in absolute value), thus inducing a large deviation from the exact slope, as shown in the bottom left panel of Fig. 6.1. At the GS-ec level of approximation, the situation is less critical, at least for small weight values. As readily seen from the following expression [see Eq. (6.55)],

$$\left.\frac{\partial E_{\rm c}^{\mathtt{w}}(n^{\mathtt{w}})}{\partial \mathtt{w}}\right|_{\mathtt{w}=0} \overset{\rm GS-ec}{\approx} (n_{\Psi_1} - n_{\Psi_0}) \left.\frac{\partial E_{\rm c}(n)}{\partial n}\right|_{n=n_{\Psi_0}}, \tag{6.60}$$

when $\Delta v_{\rm ext} \sim U$, the slope (at $\mathtt{w} = 0$) is relatively small since $n_{\Psi_1} \sim n_{\Psi_0}$ (see Fig. 1 of Ref. [98]). This is in agreement with the right panels of Fig. 6.1. Note that, in this regime, GS-ic can exhibit positive slopes (see the top right panel of Fig. 6.1). In this case, the density derivative contribution [second line of Eq. (6.59)], which is positive [98, 76], is not negligible anymore and it (more than) compensates the negative correlation energy difference [first line of Eq. (6.59)]. When the asymmetry of the dimer is more pronounced (*i.e.*, $\Delta v_{\rm ext} \gg U$), the GS-ec slope (in weight) remains negligible, as shown in the bottom left panel of Fig. 6.1. Indeed, in this case, n_{Ψ_0} tends to 2. Moreover, since the ground-state correlation functional expands as follows in the weakly and strongly correlated regimes [76],

$$E_{\rm c}(n) = E_{\rm c}^{\mathtt{w}=0}(n) \overset{U/t \ll 1}{\approx} -\frac{U^2 \left(1 - (1-n)^2\right)^{5/2}}{16t}, \tag{6.61}$$

and

$$E_{\rm c}(n) \overset{U/t \gg 1}{\approx} U \left[|n-1| - \frac{1}{2}(1 + (n-1)^2) \right], \tag{6.62}$$

respectively, we immediately see that $\partial E_{\rm c}(n)/\partial n \approx 0$ when n approaches 2, whether U/t is large or small. Note finally that, as already mentioned, in regimes where the asymmetry is weaker than the correlation, *i.e.*, $\Delta v_{\rm ext}/t < t/U < 1$ (see the top left panel of Fig. 6.1), the slopes obtained at $\mathtt{w} = 0$ with GS-ec and GS-ic are identical and relatively weak. This can now be understood from the expressions in Eqs. (6.59) and (6.60), and the fact that $\partial E_{\rm c}(n)/\partial n|_{n=1} = 0$ [76], knowing that $n_{\Psi_0} \approx 1$ [98] in this case.

We see in Fig. 6.1 that the overall weight dependence of the exact ensemble correlation energy differs substantially from that of the GS-ec and GS-ic approximations. It is again instructive to look at the slope at $\mathtt{w} = 0$. It can be expressed

exactly as follows,

$$\left.\frac{\partial E_{\rm c}^{\mathtt{w}}(n^{\mathtt{w}})}{\partial \mathtt{w}}\right|_{\mathtt{w}=0} = (n_{\Psi_1} - n_{\Psi_0}) \left.\frac{\partial E_{\rm c}(n)}{\partial n}\right|_{n=n_{\Psi_0}} + \left.\frac{\partial E_{\rm c}^{\mathtt{w}}(n_{\Psi_0})}{\partial \mathtt{w}}\right|_{\mathtt{w}=0}, \tag{6.63}$$

where we readily see from Eq. (6.60) that GS-ec neglects the derivative in weight of the ensemble correlation density functional. As highlighted in Eq. (4.40) [see also Section 5.3 for a more detailed discussion in the context of charged excitations], the latter contribution is connected to the derivative discontinuity that the xc potential exhibits when an excited state is incorporated into the ensemble. Since, in the weakly correlated regime [76],

$$\begin{aligned} E_{\rm c}^{\mathtt{w}}(n) \overset{U/t\ll 1}{\approx} & -\frac{U^2\left((1-\mathtt{w})^2-(1-n)^2\right)^{3/2}}{16t(1-\mathtt{w})^2} \\ & \times\left[1+\frac{(1-n)^2}{(1-\mathtt{w})^2}\left(3-\frac{4(1-3\mathtt{w})^2}{(1-\mathtt{w})^2}\right)\right], \end{aligned} \tag{6.64}$$

it comes

$$\left.\frac{\partial E_{\rm c}^{\mathtt{w}}(n_{\Psi_0})}{\partial \mathtt{w}}\right|_{\mathtt{w}=0} \overset{U/t\ll 1}{\approx} \frac{U^2}{16t}\left(n_{\Psi_0}(2-n_{\Psi_0})\right)^{3/2}\left(1-12(n_{\Psi_0}-1)^2\right). \tag{6.65}$$

Therefore, as long as the ground state does not deviate too much from the symmetric $n_{\Psi_0}=1$ density profile, which is the case when $\Delta v_{\rm ext} \ll U$, the exact slope is not negligible, and it is positive. This is in agreement with the top left panel of Fig. 6.1. Interestingly, in this density regime, this feature is preserved when the strength of electron correlation increases (not shown). Indeed, in this case, the ensemble correlation functional reads as [76]

$$E_{\rm c}^{\mathtt{w}}(n) \overset{U/t\gg 1,\,|n-1|\leq \mathtt{w}}{\approx} -\frac{U}{2}\left[(1-\mathtt{w})-\frac{(3\mathtt{w}-1)(n-1)^2}{(1-\mathtt{w})^2}\right], \tag{6.66}$$

$$\overset{n=n_{\Psi_0}}{\approx} \frac{U}{2}(\mathtt{w}-1), \tag{6.67}$$

thus leading to $\partial E_{\rm c}^{\mathtt{w}}(n_{\Psi_0})/\partial \mathtt{w} \approx U/2$. When the dimer is strongly asymmetric, the ground-state density approaches 2 and, in this case [76],

$$\begin{aligned} E_{\rm c}^{\mathtt{w}}(n) \overset{U/t\gg 1,\,\mathtt{w}\leq|n-1|\leq 1-\mathtt{w}}{\approx} & U|n-1| \\ & -\frac{U}{2}\left[(1+\mathtt{w})-\frac{(3\mathtt{w}-1)(n-1)^2}{(1-\mathtt{w})^2}\right], \end{aligned} \tag{6.68}$$

so that

$$\left.\frac{\partial E_{\rm c}^{\mathtt{w}}(n_{\Psi_0})}{\partial \mathtt{w}}\right|_{\mathtt{w}=0} \overset{U/t\gg 1}{\approx} -\frac{U}{2}\left(1-(n_{\Psi_0}-1)^2\right), \tag{6.69}$$

thus leading to $\partial E_{\rm c}^{\mathtt{w}}(n_{\Psi_0})/\partial \mathtt{w}|_{\mathtt{w}=0} \approx 0$. As readily seen from Eq. (6.65), the same result is obtained in the weakly correlated regime. This is in complete agreement with the bottom left panel of Fig. 6.1. It also explains why the deviation of GS-ec from the exact result drastically reduces when $\Delta v_{\rm ext}$ increases for a fixed interaction strength U and relatively small weight values. Finally, in the particular case where $\Delta v_{\rm ext} = U$, the computed ground-state densities equal $n_{\Psi_0} \approx 1.30$ and $n_{\Psi_0} \approx 1.46$ in the moderately $U/t = 1$ and strongly $U/t = 5$ correlated regimes, respectively. As expected from Eqs. (6.65) and (6.69), the exact slope will be substantial and negative, which agrees with the right panels of Fig. 6.1.

We now focus on the exact SD/DD decomposition of the ensemble correlation energy. Results are shown in Fig. 6.2 for various correlation and asymmetry regimes. In the ground-state limit, the slope of the DD ensemble correlation energy reads as [see Eq. (6.53)]

$$\left.\frac{\partial E_{\rm c}^{\mathtt{w},\rm DD}(n^{\mathtt{w}})}{\partial \mathtt{w}}\right|_{\mathtt{w}=0} = -(n_{\Psi_0}-1)(n_{\Psi_1}-1)\left[\frac{2t}{\sqrt{1-(1-n_{\Psi_0})^2}}+U\right]. \tag{6.70}$$

Interestingly, when $\Delta v_{\rm ext} \approx U$ [$n_{\Psi_0} \approx n_{\Psi_1}$ in this case], the slope is nonzero (and negative), whether the dimer is strongly correlated or not, as seen from the top right and bottom left panels of Figs. 6.2. In the strongly correlated regime, the DD ensemble correlation energy essentially varies in $\mathtt{w}$ as [see Eq. (6.53)]

$$E_{\rm c}^{\mathtt{w},\rm DD}(n^{\mathtt{w}}) \overset{U/t\gg 1}{\approx} -U(n_{\Psi_1}-1)(n_{\Psi_0}-1+\mathtt{w}(n_{\Psi_1}-n_{\Psi_0}))\frac{\mathtt{w}(1+\mathtt{w})}{(1-\mathtt{w})^2}, \tag{6.71}$$

which means that, when approaching the equiensemble $\mathtt{w} = 1/2$ case, it systematically decreases with the ensemble weight (because of the term $(1-\mathtt{w})^2$ in the denominator), unlike the total ensemble correlation energy [see Eq. (6.66)]. As long as the dimer remains close to symmetric, which requires that $\Delta v_{\rm ext}$ reduces as U increases (see Fig. 1 of Ref. [98]), the numerator in Eq. (6.71) will be small enough such that DD correlations are at most equal to the total correlation energy. This feature is actually observed in the moderately correlated $U/t = 1$ regime (see the top left panel of Fig. 6.2). However, in asymmetric and strongly correlated regimes where $0 < \Delta v_{\rm ext} \ll U$ ($n_{\Psi_0} \approx 1$ and $n_{\Psi_1} > 1$ in this case) or $\Delta v_{\rm ext} \approx U$ (*i.e.*, $n_{\Psi_0} \approx n_{\Psi_1} \approx 1.5$) [98], the numerator is not negligible

anymore and, consequently, the DD ensemble correlation energy is significantly lower than the total one (see the bottom left panel of Fig. 6.2; see also Ref. [97]). In such cases, the complementary SD ensemble correlation energy can be large and positive. This may look unphysical at first sight but, if we return to the definition of Eq. (6.37), we see that the individual SD correlation energies are not guaranteed to be negative. The reason is that, unlike the total ensemble correlation energy, they are *not* evaluated variationally. Note finally that, when $\Delta v_{\text{ext}} > U \gg t$ ($n_{\Psi_0} \approx 2$ and $n_{\Psi_1} \approx 1$ in this case), the numerator in Eq. (6.71) will be relatively small, because of the $(n_{\Psi_1} - 1)$ prefactor, thus reducing the energy difference between total and DD correlations (see the bottom right panel of Fig. 6.2).

In summary, with the present SD/DD decomposition [see Eqs. (6.42) and (6.43)], both SD and DD correlation energies become relatively large (when compared to the total ensemble correlation energy), especially in the commonly used equiensemble case, and they mostly compensate when the Hubbard dimer has a pronounced asymmetry. This is clearly not a favorable situation for the development of DFAs, which was the initial motivation for introducing the SD/DD decomposition [96, 97]. The latter should definitely be implemented for atoms and diatomics, for example, in order to get further insight. In the case of stretched diatomics, the present study of the Hubbard dimer might be enlightening [350]. We should also stress that, in the asymmetric $\Delta v_{\text{ext}} = U$ case, standard GS-ic and GS-ec approximations give ensemble correlation energies that are of the same order of magnitude as the exact one, unlike the SD and DD correlation energies. As briefly mentioned in Subsection 6.2.1, exploring alternative SD/DD decompositions that rely explicitly on GS-ic, which is maybe a better starting point, would be relevant in this respect. Work is currently in progress in this direction.

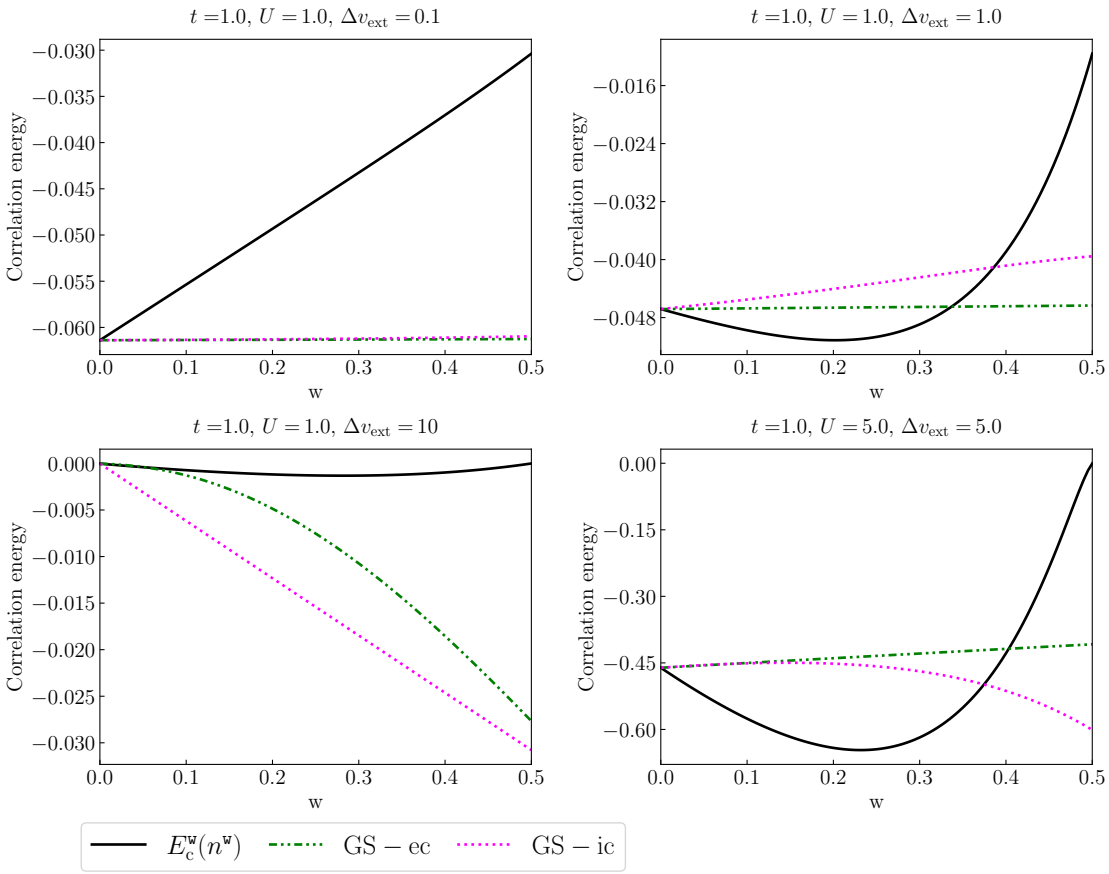

Figure 6.1: Exact (solid black lines) and approximate ensemble correlation energies plotted as functions of the bi-ensemble weight for the Hubbard dimer in various correlation and asymmetry regimes. See text for further details.

6.3 Conclusions and perspectives

In this chapter, recent progress in the design of weight-dependent xc DFAs has been reviewed. While the focus was exclusively on TGOK ensembles, the conclusions can be easily applied to N-centered or other types of ensembles. Firstly, the pros and cons of using an (orbital-dependent) ensemble density matrix functional exchange energy or state-averaging individual exact exchange energies have been discussed. Turning to the design of DFAs for ensemble correlation energies, state-of-the-art strategies have been discussed, in particular the combination of finite and infinite uniform electron gas models as well as the recycling of standard (ground-state) correlation DFAs through state-averaging. In the latter case, further improvements may emerge from the concept of density-driven correlation, which does not exist in

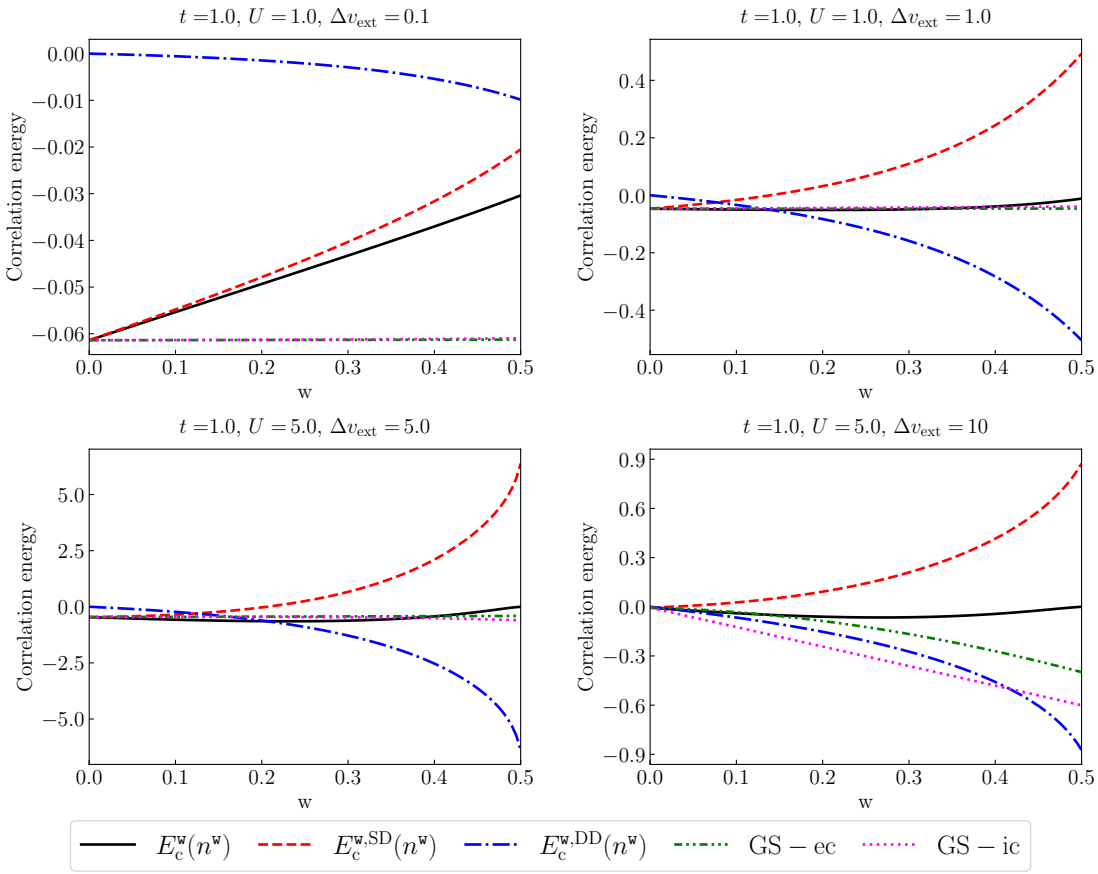

Figure 6.2: Exact SD/DD decomposition of the ensemble correlation energy plotted as a function of the bi-ensemble weight $\mathtt{w}$ in various asymmetry and correlation regimes. Comparison is made with the approximate GS-ec and GS-ic ensemble correlation energies, for analysis purposes. See text for further details.

ground-state KS-DFT. How to define mathematically the corresponding correlation energy is an open question to which we provided a tentative answer [see Eqs. (6.43) and (6.45)]. Test calculations on the Hubbard dimer reveal how difficult it is to have a definition that is both rigorous and useful for the development of approximations. Work is currently in progress in other (briefly discussed) directions. Even though it was not mentioned explicitly in the review, we would like to stress that current formulations of eDFT do not give a direct access to exact response properties such as oscillator strengths (see Eq. (3.32)), Dyson orbitals, or non-adiabatic couplings. Extending Görling–Levy perturbation theory [351, 352, 353] to ensembles might be enlightening in this respect. We recently became aware of such an extension [354]

for the computation of excitation energies within the DEC scheme [316, 77], which is an important first step. Nevertheless, a general quasi-degenerate density-functional perturbation theory based on ensembles, where individual energy levels and properties can be evaluated, is still highly desirable. Work is currently in progress in this direction. In this thesis, we also propose a strategy for development of implicit ensemble density functionals with the use of quantum embedding, which is the main topic of Chapter 8. In any case, the various formal (discused in Section 4.2) and practical aspects of the theory that we discussed in Section 4.2 and the present chapter should be investigated further in the near future in order to turn eDFT into a reliable and low-cost computational method for excited states.

Chapter 7

Derivative discontinuities in ensemble DFT for neutral electronic excitations: An N-centered perspective

The content of this chapter will be published in the forthcoming paper,

Cernatic, F.; Loos, P.-F.; Senjean, B. and Fromager, E. "Exact ensemble density functional theory of neutral electronic excitations revisited: An extended N-centered approach to exchange-correlation derivative discontinuities", in preparation (2023).

In Chapter 4, we introduced TGOK-DFT for neutral excitations, followed by the introduction of the N-centered eDFT in Chapter 5, which is an extension of TGOK-DFT for describing charged excitations with exactly the same mathematical language as the former, *i.e.,* through weight dependence of the appropriate ensemble version of the Hxc density functional. In this chapter, we present *extended* N-centered ensembles, a new formalism which combines the TGOK and (regular) N-centered ensembles into even more general ensembles that describe both neutral and charged excitations. The density-functional theory of the extended N-centered ensemble formalism describes excitation processes that are missing in TGOK and N-centered eDFT, and sheds another light on the concept of derivative discontinuity

for neutral excitations [104, 355], which is less discussed in the literature than the corresponding derivative discontinuity for charged excitations (for the latter, see Sections 5.2, 5.3 and 5.4).

This chapter is organized as follows. In Section 7.1, we discuss the problem of exactification of Kohn-Sham orbital energies in the context of neutral excitations. In Section 7.2, we briefly review some pertinent concepts of TGOK-DFT (which has already been introduced in Section 4.2). Following that, in Section 7.3, we introduce the extended N-centered ensemble formalism and provide the key equations for its density-functionalization. In Section 7.4, we demonstrate the procedure of exactifying KS orbital energies in the extended N-centered eDFT perspective by focusing on a particular ensemble of N-electron (ground and excited) states and the $(N-1)$-electron ground state. It is shown that in this perspective, exactification of the KS orbital energies for a given neutral excitation energy comes with the appearance of a derivative discontinuity in the xc potential, which matches the ensemble weight derivative of the xc energy. This key result, which was originally highlighted by Levy [104], is now generally applicable to any system, including finite models and lattice systems. As an illustrative example, we show this result in the Hubbard dimer for different asymmetry regimes.

7.1 On the exactification of Kohn–Sham orbital energies

In regular N-electron ground-state KS-DFT (see Subsection 1.2.4), the occupied and virtual orbital energies $\{\varepsilon_i\}_{i=1,2,\ldots}$ generated from a self-consistent KS calculation can be used to compute total ground- and excited-state N-electron KS energies,

$$\mathcal{E}_\nu^N = \sum_i n_\nu^i \varepsilon_i, \tag{7.1}$$

where $n_\nu^i \in \{0,1,2\}$ denotes the integer occupation of the ith KS orbital in the νth KS state ($\nu \geq 0$) and $\sum_i n_\nu^i = N$. It is well-known that, when it comes to describe neutral excitation processes, the bare KS excitation energies and the true interacting ones $\{\omega_\nu\}_{\nu>0}$ do not match:

$$\omega_\nu \equiv E_\nu^N - E_0^N \quad \neq \quad \mathcal{E}_\nu^N - \mathcal{E}_0^N. \tag{7.2}$$

In the context of linear response TD-DFT, these two quantities are connected through the Hxc kernel, *i.e.*, the density-functional derivative of the (time-dependent) Hxc potential (for example, see Eq. (3.35)). We focus in the following on in-principle-exact time-independent density-functional approaches to neutral electronic excitations and, more specifically, to ensemble ones. At this point we should stress that, unlike in charged processes, any constant shift in the Hxc potential and therefore in the orbital energies,

$$\varepsilon_i \to \varepsilon_i + c, \tag{7.3}$$

leaves neutral KS excitation energies unchanged:

$$\mathcal{E}_\nu^N - \mathcal{E}_0^N \to \left(\mathcal{E}_\nu^N + Nc\right) - \left(\mathcal{E}_0^N + Nc\right) = \mathcal{E}_\nu^N - \mathcal{E}_0^N. \tag{7.4}$$

From this standpoint, it seems impossible to exactify the KS orbital energies in the description of neutrally excited states. Nevertheless, as recalled in the next section, it is possible to describe exactly the deviation of the physical excitation energy from the KS one by means of an ensemble-weight-dependent Hxc density functional. We follow a slightly different (but connected) path in the present work by achieving such a description through an exactification of the KS orbital energies for specific

excitations. The key idea, which is based on the observation made in Eq. (7.4) and the seminal work of Levy [104], consists in evaluating a neutral excitation energy *via* two different *charged* processes, namely the ionization of the ground ($\nu = 0$) and the targeted excited ($\nu > 0$) N-electron states, *i.e.*,

$$E_\nu^N - E_0^N = I_0^N - I_\nu^N, \tag{7.5}$$

where

$$\left\{ I_\nu^N = E_0^{N-1} - E_\nu^N \right\}_{\nu \geq 0} \tag{7.6}$$

are the ground- and excited-state ionization potentials (IPs). Turning to the KS system, specific shifts can be applied to the Hxc potential (which is unique up to a constant as long as the number of electrons is fixed to the integer N) for each ionization process separately so that the true interacting IPs are reproduced:

$$\begin{aligned} \varepsilon_i &\to \varepsilon_i + c_1 = \overline{\varepsilon}_i, \\ \mathcal{E}_0^{N-1} - \mathcal{E}_0^N &\to \mathcal{E}_0^{N-1} - \mathcal{E}_0^N - c_1 \overset{!}{=} I_0^N, \end{aligned} \tag{7.7}$$

and

$$\begin{aligned} \varepsilon_i &\to \varepsilon_i + c_2 = \widetilde{\varepsilon}_i, \\ \mathcal{E}_0^{N-1} - \mathcal{E}_\nu^N &\to \mathcal{E}_0^{N-1} - \mathcal{E}_\nu^N - c_2 \overset{!}{=} I_\nu^N, \end{aligned} \tag{7.8}$$

where the two constant shifts c_1 and c_2 are not necessarily equal. If, for example, the excited state of interest ν is described by a single-electron excitation (one hole, one particle) from the highest occupied molecular orbital (HOMO) $i = N$ to a virtual one $i = \nu$, then we automatically obtain from Eqs. (7.5), (7.7), and (7.8) what we consider as the exactification of the KS orbital energies for neutral excitations, *i.e.*,

$$E_\nu^N - E_0^N = \widetilde{\varepsilon}_{N+\nu} - \overline{\varepsilon}_N. \tag{7.9}$$

The question that is addressed in the rest of this work is how such a construction can be derived, in principle exactly, from a unified ensemble density-functional formalism in which both charged and neutral excitation processes can be described simultaneously. At this point we should stress that the proposed formalism, which is referred to as extended N-centered ensemble DFT for reasons that will become clear later on, is general enough such that multiple-electron excitations, which are absent from standard (adiabatic) linear response TD-DFT spectra (see Subsection 3.1.3), can be described along the same lines. In the particular case of double excitations, for example, we would consider double ionization processes instead.

7.2 Brief review of regular TGOK ensemble DFT

TGOK ensemble DFT was already reviewed in Chapter 4. Here we put an emphasis on a subset of concepts in TGOK-DFT that are relevant in the context of extended N-centered ensemble DFT, which is introduced in Section 7.3. To reiterate what has been said before, TGOK-DFT is a time-independent extension of standard ground-state DFT to neutral excited states where the ground-state energy is replaced by the so-called ensemble energy, which is a convex combination of (N-electron) ground- and excited-state energies,

$$E^{\boldsymbol{\xi}} \overset{\text{TGOK}}{:=} \left(1 - \sum_{\nu>0} \xi_\nu^N\right) E_0^N + \sum_{\nu>0} \xi_\nu^N E_\nu^N, \tag{7.10}$$

where $\boldsymbol{\xi} \equiv \left\{\xi_\nu^N\right\}_{\nu>0}$[1] is the collection of positive and *independent* ensemble weight values that are assigned to the ordered-in-energy N-electron excited states $\left\{\Psi_\nu^N\right\}_{\nu>0}$, *i.e.*,

$$E_\nu^N = \left\langle \Psi_\nu^N \middle| \hat{H} \middle| \Psi_\nu^N \right\rangle < E_{\nu+1}^N. \tag{7.11}$$

Note that the weight ξ_0^N assigned to the ground-state energy E_0^N in Eq. (7.10) is such that the collection of weights (including the ground-state one) is normalized:

$$\xi_0^N + \sum_{\nu>0} \xi_\nu^N \overset{\text{TGOK}}{=} 1. \tag{7.12}$$

This constraint, where ξ_0^N is an affine function of the independent excited-state ensemble weights [310], ensures that the total number of electrons is preserved when deviating from the ground-state $\boldsymbol{\xi} = 0$ limit of the theory, *i.e.*,

$$\int d\mathbf{r}\, n^{\boldsymbol{\xi}}(\mathbf{r}) = N, \;\; \forall \boldsymbol{\xi}, \tag{7.13}$$

where

$$\begin{aligned} n^{\boldsymbol{\xi}}(\mathbf{r}) \overset{\text{TGOK}}{:=} & \left(1 - \sum_{\nu>0} \xi_\nu^N\right) n_{\Psi_0^N}(\mathbf{r}) \\ & + \sum_{\nu>0} \xi_\nu^N n_{\Psi_\nu^N}(\mathbf{r}), \end{aligned} \tag{7.14}$$

[1] The notation for TGOK ensemble weights in this chapter is completely equivalent to the notation $\mathbf{w} \equiv \{\mathtt{w}_I\}_{I>0}$ used in Chapters 4 and 6. The change from the latter to the former is made in anticipation of the extended N-centered ensembles (see Section 7.3).

is the ensemble density, $\left\{n_{\Psi_\nu^N}(\mathbf{r})\right\}_{\nu\geq 0}$ being the individual N-electron ground- and excited-state densities. In the following, we use the more compact notation,

$$n^{\boldsymbol{\xi}}(\mathbf{r}) = \mathrm{Tr}\left[\hat{\Gamma}^{\boldsymbol{\xi}}\hat{n}(\mathbf{r})\right], \tag{7.15}$$

where $\hat{\Gamma}^{\boldsymbol{\xi}}$ is the ensemble density matrix operator,

$$\begin{aligned}\hat{\Gamma}^{\boldsymbol{\xi}} \overset{\text{TGOK}}{=} &\left(1 - \sum_{\nu>0}\xi_\nu^N\right)|\Psi_0^N\rangle\langle\Psi_0^N| \\ &+ \sum_{\nu>0}\xi_\nu^N\,|\Psi_\nu^N\rangle\langle\Psi_\nu^N|\,,\end{aligned} \tag{7.16}$$

and Tr denotes the trace. Note that we have assumed, for simplicity, that both ground and excited states are not degenerate but the formalism can be extended straightforwardly to ensembles of multiplets [89].

The TGOK ensemble energy, as defined in Eqs. (7.10) and (7.11), can be determined variationally, *i.e.*,

$$E^{\boldsymbol{\xi}} = \min_{\hat{\gamma}^{\boldsymbol{\xi}}}\mathrm{Tr}\left[\hat{\gamma}^{\boldsymbol{\xi}}\hat{H}\right] = \mathrm{Tr}\left[\hat{\Gamma}^{\boldsymbol{\xi}}\hat{H}\right], \tag{7.17}$$

where $\hat{\gamma}^{\boldsymbol{\xi}} = \sum_\nu \xi_\nu^N|\tilde{\Psi}_\nu^N\rangle\langle\tilde{\Psi}_\nu^N|$ is a trial ensemble density matrix operator, provided that the ensemble weights are collected in decreasing order [88]:

$$\xi_\nu^N \geq \xi_{\nu+1}^N, \quad \nu \geq 0. \tag{7.18}$$

In the context of ensemble TGOK-DFT [89], the variational ensemble energy expression of Eq. (7.17) can be recast into a minimization over noninteracting ensemble density matrix operators,

$$E^{\boldsymbol{\xi}} = \min_{\hat{\gamma}^{\boldsymbol{\xi}}}\left\{\mathrm{Tr}\left[\hat{\gamma}^{\boldsymbol{\xi}}\left(\hat{T}+\hat{V}_{\text{ext}}\right)\right] + E_{\text{Hxc}}^{\boldsymbol{\xi}}[n_{\hat{\gamma}^{\boldsymbol{\xi}}}]\right\}, \tag{7.19}$$

where $E_{\text{Hxc}}^{\boldsymbol{\xi}}[n]$ is the ensemble Hxc density functional [see Eqs. (4.22) and (4.27)–(4.28)], and the (weight-dependent [92]) minimizing KS wave functions $\left\{\Phi_\nu^{\boldsymbol{\xi}}\right\}_{\nu\geq 0}$ fulfill the following self-consistent noninteracting Schrödinger equation,

$$\left(\hat{T}+\hat{V}_{\text{ext}} + \int d\mathbf{r}\, v_{\text{Hxc}}^{\boldsymbol{\xi}}(\mathbf{r})\hat{n}(\mathbf{r})\right)|\Phi_\nu^{\boldsymbol{\xi}}\rangle = \mathcal{E}_\nu^{\boldsymbol{\xi}}\,|\Phi_\nu^{\boldsymbol{\xi}}\rangle\,, \tag{7.20}$$

$v_{\text{Hxc}}^{\boldsymbol{\xi}}(\mathbf{r}) = \delta E_{\text{Hxc}}^{\boldsymbol{\xi}}[n]/\delta n(\mathbf{r})\Big|_{n=n^{\boldsymbol{\xi}}}$ being the weight-dependent Hxc potential. Equivalently, the orbitals from which the KS ensemble is constructed fulfill the following

ensemble KS equations,

$$\left(-\frac{\nabla_{\mathbf{r}}^2}{2} + v_{\text{ext}}(\mathbf{r}) + v_{\text{Hxc}}^{\boldsymbol{\xi}}(\mathbf{r})\right)\varphi_i^{\boldsymbol{\xi}}(\mathbf{r}) = \varepsilon_i^{\boldsymbol{\xi}}\varphi_i^{\boldsymbol{\xi}}(\mathbf{r}). \tag{7.21}$$

The latter differ from regular (ground-state) KS equations by *(i)* the weight dependence of the Hxc potential and *(ii)* the fact that the KS orbitals, which reproduce the exact ensemble density $n^{\boldsymbol{\xi}}(\mathbf{r})$, are fractionally occupied, *i.e.*,

$$n^{\boldsymbol{\xi}}(\mathbf{r}) = \sum_{\nu\geq 0}\xi_\nu n_{\Phi_\nu^{\boldsymbol{\xi}}}(\mathbf{r}) \tag{7.22}$$

$$= \sum_i\left(\sum_{\nu\geq 0}\xi_\nu n_\nu^i\right)\left|\varphi_i^{\boldsymbol{\xi}}(\mathbf{r})\right|^2, \tag{7.23}$$

where n_ν^i is the occupation of the KS orbital $\varphi_i^{\boldsymbol{\xi}}$ in the KS analog $\Phi_\nu^{\boldsymbol{\xi}}$ of the pure state ν. Note that the (weight-dependent) total KS energies simply read

$$\mathcal{E}_\nu^{\boldsymbol{\xi}} = \sum_i n_\nu^i\varepsilon_i^{\boldsymbol{\xi}}. \tag{7.24}$$

Turning to the problematic raised in Section 7.1, we should first recall that the exact deviation of the true interacting excitation energies from the KS ones is given by the derivative with respect to the ensemble weights (while holding the ensemble density constant) of the ensemble Hxc density functional energy [89, 310] (see also Eq. (4.33)):

$$E_\nu^N - E_0^N - \left(\mathcal{E}_\nu^{\boldsymbol{\xi}} - \mathcal{E}_0^{\boldsymbol{\xi}}\right) = \left.\frac{\partial E_{\text{Hxc}}^{\boldsymbol{\xi}}[n]}{\partial\xi_\nu^N}\right|_{n=n^{\boldsymbol{\xi}}}. \tag{7.25}$$

Therefore, within regular TGOK-DFT, the exactification of the (ensemble) KS orbital energies occurs only when the above ensemble weight derivative vanishes, which may happen for very specific (*a priori* unknown) weight values [355, 98]. In other words, such an exactification cannot, in general, be achieved, unless we introduce intermediate ionization processes, as suggested in Section 7.1. The main challenge in this case lies in the design of a unified ensemble density-functional formalism where both neutral and charged excitations can be described. A solution to this problem is proposed in the next section.

7.3 Extended N-centered ensemble DFT

Senjean and Fromager [91] have introduced some years ago the so-called N-centered ensemble DFT formalism where the fundamental gap of N-electron ground states

is described with the exact same mathematical language as in TGOK-DFT (see Chapter 5). The approach also allows for a separate description of ionization and affinity processes [91, 327, 103, 92], which is essential in the present context. The close resemblance of N-centered ensemble DFT with TGOK-DFT is exploited in the following in order to provide an in principle exact ensemble density-functional description of ionized excited states. The resulting ensemble formalism, where neutral excited states are incorporated into a regular (ground-state) N-centered ensemble, will be referred to as *extended* N-centered ensemble formalism.

7.3.1 Combining TGOK with N-centered ensembles

By analogy with regular N-centered ensemble DFT, where the ensemble weights assigned to the $(N-1)$- and $(N+1)$-electron ground states are allowed to vary independently [91], we propose to combine TGOK and N-centered (Nc) ensembles as follows,

$$\begin{aligned}\hat{\Gamma}^{\boldsymbol{\xi}} \overset{\text{TGOK}+N\text{c}}{=} &\left(1 - \sum_{\nu>0} \frac{N_\nu}{N} \xi_\nu\right) |\Psi_0\rangle\langle\Psi_0| \\ &+ \sum_{\nu>0} \xi_\nu \, |\Psi_\nu\rangle\langle\Psi_\nu| \,,\end{aligned} \tag{7.26}$$

where $\Psi_0 \equiv \Psi_0^N$ is the reference N-electron ground state to which all possible excitation processes (neutral and charged, including multiple-electron excitations) can be applied. In other words, the integer number of electrons $N_\nu = \int d\mathbf{r}\, n_{\Psi_\nu}(\mathbf{r})$ that is described by the excited-state wave function Ψ_ν ($\nu > 0$) is not necessarily equal to the number of electrons in the ground state,

$$N_0 = N, \tag{7.27}$$

that is referred to as the central (integer) number of electrons. However, by construction, the ensemble density still integrates to N, like in TGOK-DFT [see Eqs. (7.13) and (7.15)]. As further discussed in Section 7.4, the fact that the net number of electrons in the ensemble does *not* vary with the ensemble weights, unlike in DFT for fractional electron numbers, is absolutely central in the description of xc derivative discontinuities as ensemble weight derivatives [103, 92]. Note also that, just like in conventional ensembles (like TGOK ones), the ensemble weights assigned to the

ground and excited states are positive,

$$\xi_0 = 1 - \sum_{\nu>0} \frac{N_\nu}{N} \xi_\nu \geq 0, \tag{7.28a}$$

$$\xi_\nu \geq 0, \ \ \forall \nu > 0, \tag{7.28b}$$

but they do *not* necessarily sum up to 1 anymore:

$$\sum_{\nu\geq 0} \xi_\nu = 1 + \sum_{\nu>0} \frac{(N - N_\nu)}{N} \xi_\nu \neq 1. \tag{7.29}$$

In addition, within each subensemble containing all the states with the same number $N \pm p$ ($p = 0, 1, 2, \ldots, N$) of electrons, we impose the following weight ordering constraints [see Eq. (7.18)],

$$\xi_\nu \overset{N_\nu = N_{\nu+1} = N \pm p}{\geq} \xi_{\nu+1}, \tag{7.30}$$

in order to be able to exploit, if necessary, the TGOK variational principle within each $(N \pm p)$-electron sector of the Fock space. We assume, by construction, that a given sector is described by a single range of ν indices. Note that, in the present work, the constraint of Eq. (7.30) will be used only for N-electron states (*i.e.*, $p = 0$) while the $(N - 1)$ sector will boil down to ground states only. The $(N + 1)$ sector will not be used. These choices are motivated by the problematic raised in Section 7.1 and are by no means a limitation of the present ensemble formalism, which is very general.

Let us finally turn to the extended N-centered ensemble energy,

$$E^{\boldsymbol{\xi}} \overset{\text{TGOK+Nc}}{=} \left(1 - \sum_{\nu>0} \frac{N_\nu}{N} \xi_\nu\right) E_0 + \sum_{\nu>0} \xi_\nu E_\nu, \tag{7.31}$$

where $E_0 = E_0^N$ is the reference N-electron ground-state energy and E_ν is an N_ν-electron eigenvalue of the electronic Hamiltonian, *i.e.*,

$$\hat{H} \left|\Psi_\nu\right\rangle = E_\nu \left|\Psi_\nu\right\rangle, \ \ \nu \geq 0, \tag{7.32}$$

with $N_\nu \in \{N, N \pm 1, N \pm 2, \ldots\}$. Like in TGOK-DFT [310], the linearity of the ensemble energy in the ensemble weights

$$\boldsymbol{\xi} \overset{\text{TGOK+Nc}}{\equiv} \{\xi_\nu\}_{\nu>0}, \tag{7.33}$$

allows for a straightforward extraction of individual energy levels (and, therefore, of the excitation energies) through first-order differentiations. Indeed, since both ground- ($\nu = 0$) [see Eq. (7.27)] and excited-state ($\nu > 0$) energies can be expressed as follows,

$$E_\nu \underset{\nu\geq 0}{=} \frac{N_\nu}{N} E_0 + \sum_{\lambda>0} \delta_{\lambda\nu} \left(E_\lambda - \frac{N_\lambda}{N} E_0 \right), \tag{7.34}$$

where, according to Eq. (7.31),

$$\frac{\partial E^{\boldsymbol{\xi}}}{\partial \xi_\lambda} = E_\lambda - \frac{N_\lambda}{N} E_0 \tag{7.35}$$

and

$$E_0 = E^{\boldsymbol{\xi}} - \sum_{\lambda>0} \xi_\lambda \frac{\partial E^{\boldsymbol{\xi}}}{\partial \xi_\lambda}, \tag{7.36}$$

we immediately obtain the following compact expression in terms of the ensemble energy (and its first-order derivatives),

$$E_\nu \underset{\nu\geq 0}{=} \frac{N_\nu}{N} E^{\boldsymbol{\xi}} + \sum_{\lambda>0} \left(\delta_{\lambda\nu} - \frac{N_\nu}{N} \xi_\lambda \right) \frac{\partial E^{\boldsymbol{\xi}}}{\partial \xi_\lambda}. \tag{7.37}$$

Note that Eq. (7.37) generalizes expressions that have been derived previously and separately in regular TGOK [310] (for neutral excited states) and N-centered [91, 92] (for charged excited states) ensemble theories [see Eqs. (4.11), and (5.8)–(5.10)]. As shown in the following section, once a KS density-functional description of the extended N-centered ensemble energy $E^{\boldsymbol{\xi}}$ is established, it becomes possible to relate formally any charged or neutral KS excitation energy to the true physical one.

7.3.2 Density-functionalization of the approach

According to both regular (ground-state) Rayleigh–Ritz and TGOK variational principles, the extended N-centered ensemble energy of Eq. (7.31) can be determined variationally, thus allowing for its in-principle-exact ensemble density-functional description. The exact same formalism as in TGOK-DFT can actually be used [see Eqs. (7.19)–(7.24)]. The only difference is that we are now allowed to consider occupations in the KS wave functions [see Eq. (7.24)] that do not necessarily sum up

to N:

$$\sum_i n_\nu^i = N_\nu. \tag{7.38}$$

By rewriting the ensemble energy as follows [see Eqs. (7.19), (7.20), and (7.22)],

$$E^{\boldsymbol{\xi}} = \sum_{\nu\geq 0} \xi_\nu \mathcal{E}_\nu^{\boldsymbol{\xi}} + E_{\text{Hxc}}^{\boldsymbol{\xi}}[n^{\boldsymbol{\xi}}] - \int d\mathbf{r}\, v_{\text{Hxc}}^{\boldsymbol{\xi}}(\mathbf{r}) n^{\boldsymbol{\xi}}(\mathbf{r}), \tag{7.39}$$

and applying the Hellmann-Feynman theorem to its variational expression in Eq. (7.19), which leads to

$$\frac{\partial E^{\boldsymbol{\xi}}}{\partial \xi_\lambda} = \mathcal{E}_\lambda^{\boldsymbol{\xi}} - \frac{N_\lambda}{N}\mathcal{E}_0^{\boldsymbol{\xi}} + \left.\frac{\partial E_{\text{Hxc}}^{\boldsymbol{\xi}}[n]}{\partial \xi_\lambda}\right|_{n=n^{\boldsymbol{\xi}}}, \tag{7.40}$$

we deduce from Eq. (7.37) the following exact expression for any individual energy level included into the ensemble,

$$\begin{aligned} E_\nu \underset{\nu\geq 0}{=} \mathcal{E}_\nu^{\boldsymbol{\xi}} + \frac{N_\nu}{N}\left(E_{\text{Hxc}}^{\boldsymbol{\xi}}[n^{\boldsymbol{\xi}}] - \int d\mathbf{r}\, v_{\text{Hxc}}^{\boldsymbol{\xi}}(\mathbf{r}) n^{\boldsymbol{\xi}}(\mathbf{r})\right) \\ + \sum_{\lambda>0}\left(\delta_{\lambda\nu} - \frac{N_\nu}{N}\xi_\lambda\right)\left.\frac{\partial E_{\text{Hxc}}^{\boldsymbol{\xi}}[n]}{\partial \xi_\lambda}\right|_{n=n^{\boldsymbol{\xi}}}, \end{aligned} \tag{7.41}$$

where, in the second term on the right-hand side, we recognize the analog for ensembles of the Levy–Zahariev shift in potential [319, 310, 91] [cf. Eqs. (4.34) and (5.25)]. At this point we should make an important observation that will be exploited later on, namely that the above expression is invariant under constant shifts in the ensemble Hxc potential $v_{\text{Hxc}}^{\boldsymbol{\xi}}(\mathbf{r}) \to v_{\text{Hxc}}^{\boldsymbol{\xi}}(\mathbf{r}) + c$ since [see Eqs. (7.13), (7.24), and (7.38)]

$$\begin{aligned} &\mathcal{E}_\nu^{\boldsymbol{\xi}} - \frac{N_\nu}{N}\int d\mathbf{r}\, v_{\text{Hxc}}^{\boldsymbol{\xi}}(\mathbf{r}) n^{\boldsymbol{\xi}}(\mathbf{r}) \\ &= \left(\mathcal{E}_\nu^{\boldsymbol{\xi}} + N_\nu c\right) - \frac{N_\nu}{N}\int d\mathbf{r}\, \left(v_{\text{Hxc}}^{\boldsymbol{\xi}}(\mathbf{r}) + c\right) n^{\boldsymbol{\xi}}(\mathbf{r}), \end{aligned} \tag{7.42}$$

even though the ensemble may contain states that describe different numbers of electrons. This major difference between (extended or not) N-centered ensemble DFT and the conventional DFT for fractional electron numbers originates from the fact that, in the former theory, the number of electrons is artificially held constant and equal to the integer N [see Eq. (7.13)].

We finally conclude from Eq. (7.41) that the energy associated to any (charged or neutral) excitation $\nu \to \kappa$ can be expressed exactly in terms of its KS analog as

follows,

$$\begin{aligned} E_\kappa - E_\nu &= \mathcal{E}_\kappa^{\boldsymbol{\xi}} - \mathcal{E}_\nu^{\boldsymbol{\xi}} \\ &+ \frac{(N_\kappa - N_\nu)}{N} \left(E_{\text{Hxc}}^{\boldsymbol{\xi}}[n^{\boldsymbol{\xi}}] - \int d\mathbf{r}\, v_{\text{Hxc}}^{\boldsymbol{\xi}}(\mathbf{r}) n^{\boldsymbol{\xi}}(\mathbf{r}) \right) \\ &+ \sum_{\lambda>0} \left(\delta_{\lambda\kappa} - \delta_{\lambda\nu} - \frac{(N_\kappa - N_\nu)}{N} \xi_\lambda \right) \left. \frac{\partial E_{\text{Hxc}}^{\boldsymbol{\xi}}[n]}{\partial \xi_\lambda} \right|_{n=n^{\boldsymbol{\xi}}} . \end{aligned} \tag{7.43}$$

Eq. (7.43) is our first key result. It generalizes the neutral excitation energy expression of TGOK-DFT [89, 310] that was recalled in Eq. (7.25).

7.4 Revisiting density-functional derivative discontinuities induced by neutral excitations

In order to achieve an exactification of the KS orbital energies along the lines of Section 7.1, we apply the general formalism of Sec. 7.3 to a particular type of extended N-centered ensemble consisting of ground and excited N-electron states (with weights ξ_ν^N) *and* the $(N-1)$-electron ground state (with weight $\xi_- := \xi_0^{N-1}$), *i.e.*,

$$\boldsymbol{\xi} \equiv \left(\{\xi_\nu^N\}_{\nu>0}, \xi_- \right) . \tag{7.44}$$

According to Eqs. (7.5) and (7.43), where κ now refers to the ionized ground state, the exact ground- and excited-state ionization potentials read (we focus for simplicity, but without loss of generality, on single-electron excitations)

$$\begin{aligned} I_\nu^N \underset{\nu\geq 0}{=} & -\varepsilon_{N+\nu}^{\boldsymbol{\xi}} - \frac{1}{N} \left(E_{\text{Hxc}}^{\boldsymbol{\xi}}[n^{\boldsymbol{\xi}}] - \int d\mathbf{r}\, v_{\text{Hxc}}^{\boldsymbol{\xi}}(\mathbf{r}) n^{\boldsymbol{\xi}}(\mathbf{r}) \right) \\ & + \left(1 + \frac{\xi_-}{N} \right) \left. \frac{\partial E_{\text{Hxc}}^{\boldsymbol{\xi}}[n]}{\partial \xi_-} \right|_{n=n^{\boldsymbol{\xi}}} \\ & + \sum_{\lambda>0} \left(\frac{\xi_\lambda^N}{N} - \delta_{\lambda\nu} \right) \left. \frac{\partial E_{\text{Hxc}}^{\boldsymbol{\xi}}[n]}{\partial \xi_\lambda^N} \right|_{n=n^{\boldsymbol{\xi}}} . \end{aligned} \tag{7.45}$$

As pointed out previously [see Eq. (7.42)], the above expression is invariant under any constant shift in the ensemble Hxc potential. Therefore, we can always adjust the latter potential in order to exactify the Koopmans theorem for a given ground

or excited N-electron state ν and a given choice of ensemble weight values $\boldsymbol{\xi}$:

$$\begin{aligned} I_\nu^N &= -\varepsilon_{N+\nu}^{\boldsymbol{\xi}} \\ &\Updownarrow \\ \int d\mathbf{r}\, v_{\text{Hxc}}^{\boldsymbol{\xi}}(\mathbf{r}) n^{\boldsymbol{\xi}}(\mathbf{r}) &= E_{\text{Hxc}}^{\boldsymbol{\xi}}[n^{\boldsymbol{\xi}}] \\ &\quad - (N+\xi_-)\left.\frac{\partial E_{\text{Hxc}}^{\boldsymbol{\xi}}[n]}{\partial \xi_-}\right|_{n=n^{\boldsymbol{\xi}}} \\ &\quad + \sum_{\lambda>0}\left(N\delta_{\lambda\nu} - \xi_\lambda^N\right)\left.\frac{\partial E_{\text{Hxc}}^{\boldsymbol{\xi}}[n]}{\partial \xi_\lambda^N}\right|_{n=n^{\boldsymbol{\xi}}} . \end{aligned} \tag{7.46}$$

Eq. (7.46), which is the second key result of this work, uniquely defines (not up to a constant anymore) the Hxc potential. Interestingly, unlike in traditional DFT approaches to electronic excitations, this alternative and explicit adjustment procedure of the Hxc potential does *not* rely on the asymptotic behavior of the density (see Refs. [103, 92] for a comparison of the two formalisms in the ground state), which means that it is not only applicable to *ab initio* molecular systems but it should also be transferable to finite-size lattice models or extended systems, for example.

Let us finally have a closer look at the ionization of the ground (first scenario) and νth excited (second scenario) states separately. In order to reach variationally the latter state we only need to consider all the states that are lower in energy, which can be denoted as follows,

$$\boldsymbol{\xi} \equiv \left(\boldsymbol{\xi}_\nu^N, 0, 0, \ldots, 0, \xi_-\right), \tag{7.47}$$

where (note the bold font)

$$\boldsymbol{\xi}_\nu^N \equiv \left(\xi_1^N, \xi_2^N, \ldots, \xi_\nu^N\right) \tag{7.48}$$

is a shorthand notation for the ν non-zero and monotonically decreasing ensemble weights. In the first scenario, we adjust the Hxc potential such that the Koopmans theorem is fulfilled for the ground state ($\nu = 0$). As neutral excited states are not involved in this case, the ensemble can be reduced to a regular N-centered ensemble [91]:

$$\boldsymbol{\xi}_1 \equiv \left(\boldsymbol{\xi}_\nu^N = \mathbf{0}, 0, 0, \ldots, 0, \xi_- > 0\right). \tag{7.49}$$

On the other hand, in the second scenario (ionization of the νth excited state), assigning an infinitesimal weight to the ionized ground state is sufficient, *i.e.*,

$$\boldsymbol{\xi}_2 \equiv \left(\boldsymbol{\xi}_\nu^N > 0, 0, 0, \ldots, 0, \xi_- \to 0^+\right), \tag{7.50}$$

so that the ensemble weight derivative $\partial E_{\text{Hxc}}^{\boldsymbol{\xi}}[n]/\partial\xi_-$ in Eq. (7.46) can be evaluated. As a consequence of Eq. (7.46), we finally reach, without ever invoking fractional electron numbers nor referring to the asymptotic behavior of the ensemble density, the desired exactification of the KS orbital energies, with a clear and explicit construction of the corresponding Hxc potentials:

$$E_\nu^N - E_0^N = \varepsilon_{N+\nu}^{\boldsymbol{\xi}_2} - \varepsilon_N^{\boldsymbol{\xi}_1}. \tag{7.51}$$

Most importantly, the first and second scenarios have a connection point which is reached when $\xi_- \to 0^+$ and $\boldsymbol{\xi}_\nu^N \to \mathbf{0}^+$, respectively, and which corresponds to the regular N-electron ground-state formulation of DFT (the density equals $n_{\Psi_0^N}$ in this case). If we simply denote

$$\boldsymbol{\xi}_\nu^N \underset{notation}{\equiv} \left(\boldsymbol{\xi}_\nu^N, 0, 0, \ldots, 0, \xi_- \to 0^+\right), \tag{7.52}$$

then comparing from Eq. (7.46) the two scenarios in Hxc potential at this connection point leads to our third key result:

$$\begin{aligned} &\int \frac{d\mathbf{r}}{N} \left(v_{\text{Hxc}}^{\boldsymbol{\xi}_\nu^N \to \mathbf{0}^+}(\mathbf{r}) - v_{\text{Hxc}}^{\boldsymbol{\xi}_\nu^N = \mathbf{0}}(\mathbf{r})\right) n_{\Psi_0^N}(\mathbf{r}) \\ &= \left.\frac{\partial E_{\text{Hxc}}^{\boldsymbol{\xi}_\nu^N}[n_{\Psi_0^N}]}{\partial \xi_\nu^N}\right|_{\boldsymbol{\xi}_\nu^N = 0}. \end{aligned} \tag{7.53}$$

If we use the formally convenient decomposition of the ensemble Hxc energy in terms of the regular (weight-independent) Hartree functional and the weight-dependent xc functional,

$$E_{\text{Hxc}}^{\boldsymbol{\xi}}[n] = E_{\text{H}}[n] + E_{\text{xc}}^{\boldsymbol{\xi}}[n], \tag{7.54}$$

then all Hartree terms can be removed from Eq. (7.53). Thus we recover, in a rather different (N-centered) ensemble perspective, a feature that was originally highlighted by Levy [104], namely that the exactification of neutral KS excitation energies is conditioned by the appearance of a derivative discontinuity in the xc potential, once the excitation of interest has been included into the ensemble. Moreover, that derivative discontinuity matches the ensemble weight derivative of the xc energy, as readily seen from Eq. (7.53).

7.5 Application to the Hubbard dimer

The theory hitherto discussed is applied on the asymmetric Hubbard dimer (see Eq. (2.7) in Chapter 2). We illustrate the key result in Eq. (7.53), together with the two ionization scenarios of ground and excited states (Eq. (7.49) and Eq. (7.50), respectively) for the dimer in three different asymmetry regimes. The extended N-centered ensemble that we work with consists of the singlet ground states in the 2- and 1-electron Fock spaces (neutral and ionic ground state, respectively), while for the neutral excited state, we choose the lowest singlet excited state in the 2-electron Fock space. Therefore, the ensemble is characterized by two weights, $\boldsymbol{\xi} \equiv (\xi_1, \xi_-)$, where ξ_1 controls the fraction of the neutral excited state, and ξ_- controls the fraction of the 1-electron ground state. According to Eqs. (7.28) and (7.30), the ensemble weight constraints read as $0 \leq \xi_- \leq 2$, and $0 \leq \xi \leq 1/2 - \xi_-/4$. Moreover, for a given (fixed) set of ensemble weights, the ensemble under study is invariant with respect to arbitrary shifts in the external (or KS) potential (see Eq. (2.7)),

$$\frac{\Delta v}{2} \to \frac{\Delta v}{2} - \mu. \tag{7.55}$$

Here, we show that adjusting the constant shift μ in the KS potential in order to fulfill an exact Koopmans' theorem (Eq. (7.46)), brings about derivative discontinuities of the Hxc potential. The exact noninteracting kinetic energy and Hartree-exchange density functionals for our particular extended N-centered ensemble can be obtained by generalizing the analogous bi-ensemble density functionals in TGOK-DFT [98] and N-centered eDFT [91]:

$$T_{\rm s}^{\boldsymbol{\xi}}(n) = -2t\sqrt{(1-\xi)^2 - (1-n)^2}, \tag{7.56}$$

$$E_{\rm Hx}^{\boldsymbol{\xi}}(n) = \frac{U}{2}\left[1 + \xi - \frac{\xi_-}{2} + \left(1 - 3\xi - \frac{\xi_-}{2}\right)\frac{(1-n)^2}{(1-\xi)^2}\right], \tag{7.57}$$

while the correlation energy, $E_{\rm c}^{\boldsymbol{\xi}}(n) = F^{\boldsymbol{\xi}}(n) - T_{\rm s}^{\boldsymbol{\xi}}(n) - E_{\rm Hx}^{\boldsymbol{\xi}}(n)$, can be obtained by Lieb maximization for any density n [98, 91]. The Hxc potential for a given site i in the dimer is then determined as,

$$v_{{\rm Hxc},i}^{\boldsymbol{\xi}} = \left((-1)^{i-1}\Delta v_{\rm Hxc}^{\boldsymbol{\xi}}/2\right) - \mu_{\rm Hxc}^{\boldsymbol{\xi}}, \;\; i = 0, 1, \tag{7.58}$$

where $\Delta v_{\rm Hxc}^{\boldsymbol{\xi}} = \Delta v_{\rm KS}^{\boldsymbol{\xi}}(n^{\boldsymbol{\xi}}) - \Delta v_{\rm ext}$, and (see Ref. [98])

$$\Delta v_{\rm KS}^{\boldsymbol{\xi}}(n) = \frac{\partial T_{\rm s}^{\boldsymbol{\xi}}(n)}{\partial n} = \frac{2t(n-1)}{\sqrt{(1-\xi)^2 - (1-n)^2}}. \tag{7.59}$$

In Eq. (7.58), the constant shift $\mu_{\text{Hxc}}^{\boldsymbol{\xi}}$ is determined, for a given ionization process, from Eq. (7.46). Figure 7.1 displays the variation of $v_{\text{Hxc},1}^{\boldsymbol{\xi}}$ for the two ionization scenarios considered (*i.e.* red-colored curves for the ionization of the 2-electron ground state, and blue-colored curves for the ionization of the 2-electron first (singlet) excited state). In the first scenario (red curves), the Hxc potential plotted in Figure 7.1 is constrained to fulfill Eq. (7.46) for the 2-electron ground state ionization potential $I_0^N = E_0^{N-1} - E_0^N$, which, for the Hubbard dimer, reads as

$$\begin{aligned} I_0^N = &- \varepsilon_h^{\boldsymbol{\xi}}(n^{\boldsymbol{\xi}}) - \frac{1}{2}\left(E_{\text{Hxc}}^{\boldsymbol{\xi}}(n^{\boldsymbol{\xi}}) - \sum_{i=0}^{1} v_{\text{Hxc},i}^{\boldsymbol{\xi}} n_i^{\boldsymbol{\xi}}\right) \\ &+ \left(1 + \frac{\xi_-}{2}\right) \left.\frac{\partial E_{\text{Hxc}}^{\boldsymbol{\xi}}(n)}{\partial \xi_-}\right|_{n=n^{\boldsymbol{\xi}}}, \end{aligned} \tag{7.60}$$

where

$$\varepsilon_h^{\boldsymbol{\xi}}(n^{\boldsymbol{\xi}}) = -\sqrt{t^2 + \frac{[\Delta v_{\text{KS}}^{\boldsymbol{\xi}}(n^{\boldsymbol{\xi}})]^2}{4}} \tag{7.61}$$

is the highest occupied molecular orbital (HOMO) energy of the KS system for the unshifted ($\mu = 0$ in Eq. (7.58)) Hxc potential [98]. In the second scenario (blue curves in Figure 7.1), the Hxc potential is constrained to fulfill Eq. (7.46) for the ionization of the 2-electron excited state $I_1^N = E_0^{N-1} - E_1^N$, which reads as,

$$\begin{aligned} I_1^N = &- \varepsilon_l^{\boldsymbol{\xi}}(n^{\boldsymbol{\xi}}) - \frac{1}{2}\left(E_{\text{Hxc}}^{\boldsymbol{\xi}}(n^{\boldsymbol{\xi}}) - \sum_{i=0}^{1} v_{\text{Hxc},i}^{\boldsymbol{\xi}} n_i^{\boldsymbol{\xi}}\right) \\ &+ \left(1 + \frac{\xi_-}{2}\right) \left.\frac{\partial E_{\text{Hxc}}^{\boldsymbol{\xi}}(n)}{\partial \xi_-}\right|_{n=n^{\boldsymbol{\xi}}} \\ &+ \left(\frac{\xi}{2} - 1\right) \left.\frac{\partial E_{\text{Hxc}}^{\boldsymbol{\xi}}(n)}{\partial \xi}\right|_{n=n^{\boldsymbol{\xi}}}, \end{aligned} \tag{7.62}$$

where $\varepsilon_l^{\boldsymbol{\xi}}(n^{\boldsymbol{\xi}}) = -\varepsilon_h^{\boldsymbol{\xi}}(n^{\boldsymbol{\xi}})$. These considerations lead to the appearance of the derivative discontinuity, which is clearly observed for all asymmetry regimes when passing from the set of limiting weights ($\xi_1 = 0, \xi_- \to 0^+$) to ($\xi_1 \to 0^+, \xi_- \to 0^+$). For comparison, we also plot "exchange-only" results (dotted curves). The latter are obtained from Eqs. (7.60) and (7.62) by keeping only the Hartree-exchange (Hx) density functional $E_{\text{Hx}}^{\boldsymbol{\xi}}(n)$ (and its ensemble weight derivatives). For the sake of consistency, the exchange-only results are evaluated at the exact extended N-centered ensemble density $n^{\boldsymbol{\xi}}$, hence the exact Hxc potential difference $\Delta v_{\text{Hxc}}^{\boldsymbol{\xi}}$ is kept in Eqs. (7.60) and (7.62), even for calculating the exchange-only values.

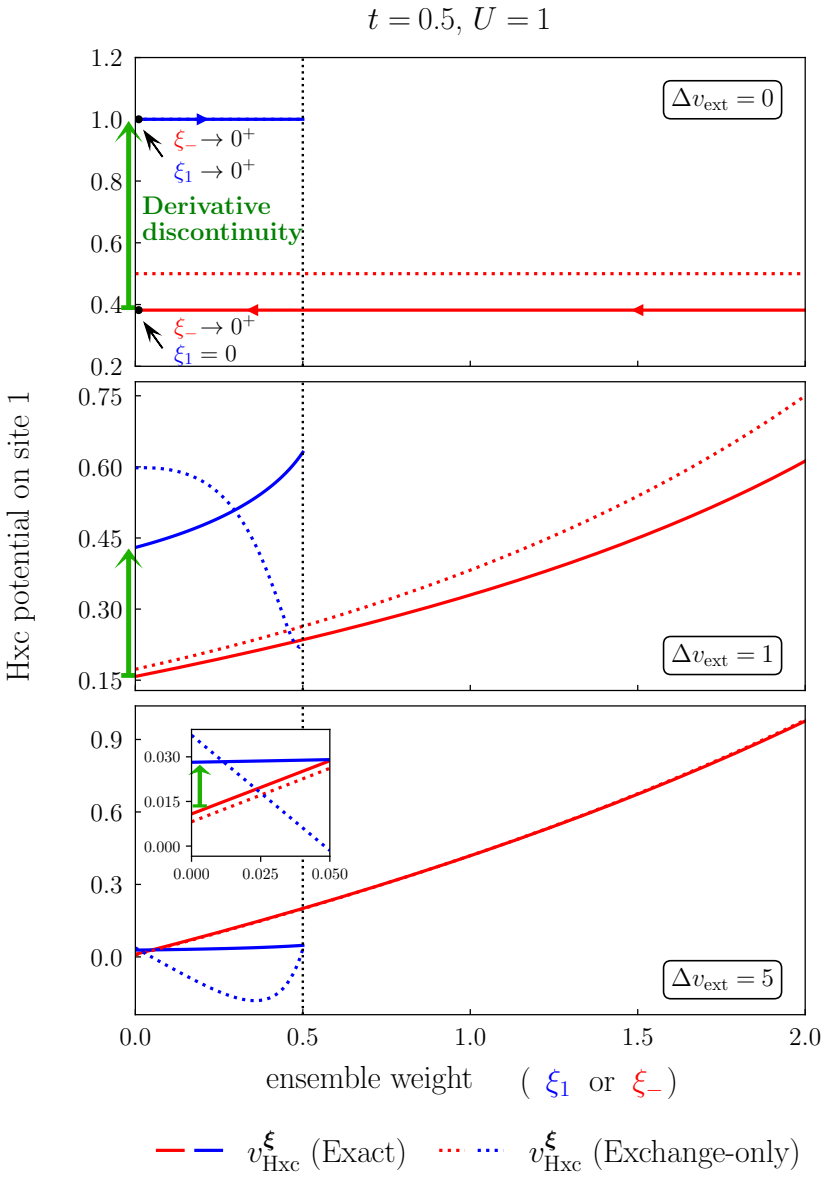

Figure 7.1: Variation of the exact Hxc potential of the extended N-centered ensemble, and its exhange-only approximation, with ensemble weights in the Hubbard dimer with different asymmetries (see main text for more pertinent details). For each case, the derivative discontinuity is highlighted with the green arrow at limiting ensemble weight values between the first scenario (Eq. (7.49)) and the second one (Eq. (7.50)). The vertical (dotted) black line at $\xi = 1/2$ indicates the TGOK equiensemble position.

Chapter 8

Quantum embedding strategy for ensembles of electronic states

In the last section of Chapter 1, we introduced density matrix embedding theory (DMET) for ground states. An idea that emerged in the course of my PhD was to consider the possibility of adapting the single-shot embedding strategy of DMET (or Ht-DMFET, see Subsection 1.3.2) for ensembles of ground and excited states. The material presented in this chapter will be published in the forthcoming papers,

Cernatic, F.; Yalouz, S. "Quantum embedding strategy for multiple electronic states", in preparation (2023).

Cernatic, F.; Lasorne, B.; Fromager, E. "Perspectives in ensemble DFT of electronic excited states", invited "Perspective" paper, to be submitted to JCP (2023).

Cernatic, F.; Yalouz, S.; and Fromager, E. "Self-consistent local potential functional embedding theory of many-electron ensembles", in preparation (2023).

In the aforementioned section on DMET in Chapter 1, we introduced the approach for constructing a quantum bath by means of unitary transformation in the single-electron picture, the simplicity of which is very appealing. This way, as we have seen, one can design embedding clusters that capture local correlations in a large system without the need for solving the full-size problem. One may wonder whether such a procedure can be extended to neutral or even charged excitations, where ideally, an embedding cluster would reflect the changes in the wavefunction upon

electronic excitation. The approach that we present here is intented for targeting neutral excitations of molecules, where the goal is not to calculate the whole spectrum but a small number of low-lying excitations. For this reason, we adopt the formalism of TGOK ensembles, which affords a systematic and balanced treatment of all individual states for excitations of interest. As will be shown in the following, it turns out that we are also able to design an embedding cluster that is suitable for multiple states, with the use of successive Householder transformations on the non-interacting TGOK ensemble (see Subsection 4.2.3) 1RDM.

The present chapter is organized as follows. Section 8.1 reintroduces DMET and quantum embedding in the context of excited states. Section 8.3 discusses about the problematic of clusterization of an ensemble 1RDM, which is non-idempotent due to fractional occupation numbers. Our solution by means of successive Householder transformations is proposed. In Section 8.3, a single-shot embedding strategy for ensembles is introduced, which can be seen as a multi-state extension of Ht-DMFET [105]. Example calculations on three toy models are presented. In the final section, we discuss various features and challenges of ensemble embedding theory, and of capturing particular excited states, and point out possible improvements and extensions of the present strategy.

8.1 Introduction

DMET has enjoyed great success in describing several regimes and systems of interest in quantum chemistry and condensed-matter physics. Some of the applications are stated in the review of DMET in Subsection 1.3.2. However, to our knowledge, there are not too many applications of DMET or related methods to excited states. For molecules, Tran *et al.* have combined DMET with SCF metadynamics for embedding specific excited states [106]. *Bootstrap embedding* (BE) has also been adapted for targeting excited states in a state-specific way [356]. Mitra *et al.* have studied excited states of crystalline point defects by means of combining multiconfigurational wavefunction-based methods and DMET [227]. For extended systems, DMET has been applied to a response wavefunction for obtaining spectral functions of Hubbard lattices [357, 358]. DMET has also been extended to finite temperatures in *finite*

temperature density matrix embedding theory (FT-DMET) by Sun *et al.* [216], which has been applied on the one and two-dimensional Hubbard models.

We would like to propose a strategy that is suitable for simultaneously describing multiple electronic states. This is inspired by the *Theophilou-Gross-Oliveira-Kohn* (TGOK) variational principle (see Eq. (7.17)). As a proof of concept, we stick to a simple two-state ensemble, consisting of ground and singlet first-excited state, and a single-impurity embedding. Just like in DMET for ground states, we can split our strategy in two steps. The first step is to design an embedding cluster that is in the mean-field (or noninteracting) limit exact for the aforementioned ensemble. Then, once an embedding cluster is produced at the mean-field level, the single-shot embedding calculation proceeds like in Ht-DMFET[1] - by adjusting a chemical potential so as to correct the number of electrons in the ground and excited state. After optimization, the ground and first-excited state solutions of the embedding cluster are used as approximations to true individual states.

8.2 Methodology

8.2.1 Step 1: Construction of the embedding cluster

8.2.1.1 The problematic of embedding excited states

The Householder transformation in introduced in 1.3.2.3 gives a closed embedding cluster for a reference full-size 1RDM that comes from a Slater determinant $|\Phi\rangle$. The key reason, as was stated there, is the idempotency of 1RDM, i.e., $\boldsymbol{\gamma}_\Phi^2 = \boldsymbol{\gamma}_\Phi$. This implies that not just mean-field ground states, but any excited state with only doubly occupied orbitals will be amenable to exact clusterization. However, there are several challenges associated with describing excited states of an interacting system with this approach. Firstly, when embedding excited states individually, it is difficult to decide *a priori* which solution of the embedding Hamiltonian should be chosen as a local approximation to the excited state of the full-size system. The problem of identifying individual states inside a cluster with states of the full-size system may to some extent be solved by combining quantum embedding theory with TGOK

[1] Or DMET. The two theories are equivalent in the conventional ground-state case (see Subsection 1.3.2, and Refs. [111, 214]).

ensembles, which is the purpose of this work. This will ensure that at the mean-field level, the ground and excited states within the embedding cluster correspond in ordering to the ground and excited states in the full-size system[2], provided that we can design a unitary matrix that transforms the average of 1RDMs of individual states, weighted by TGOK ensemble weights (i.e. the ensemble 1RDM), exactly into a block diagonal form for any set of weights. Secondly, 1RDMs of excited states are generally non-idempotent. For example, already at the mean-field level, the lowest (singlet) excited state (excluding possible symmetry constraints) is a singly excited state from the highest occupied molecular orbital (HOMO) to the lowest unoccupied molecular orbital (LUMO), which is described by the following configuration state function (CSF),

$$|^1\Phi_h^l\rangle \;= \frac{1}{\sqrt{2}}\left(\hat{a}^\dagger_{N/2+1,\uparrow}\hat{a}_{N/2,\uparrow} + \hat{a}^\dagger_{N/2+1,\downarrow}\hat{a}_{N/2,\downarrow}\right)|\Phi_0\rangle, \tag{8.1}$$

where $h = N/2$ (HOMO), $l = N/2+1$ (LUMO), $|\Phi_0\rangle$ is the (HF or KS) ground-state Slater determinant, $\{\hat{a}^\dagger_{\kappa,\sigma}\}_{1\leq\kappa\leq L}$ and $\{\hat{a}_{\kappa,\sigma}\}_{1\leq\kappa\leq L}$ are the creation and annihilation operators, respectively, in the molecular spin-orbital basis $\{|\varphi_{\kappa\sigma}\rangle = |\varphi_\kappa\rangle\,|\sigma\rangle = \hat{a}^\dagger_{\kappa\sigma}|vac\rangle\}_{1\leq\kappa\leq L,\,\sigma\in\{\uparrow,\downarrow\}}$. In that basis (which we hereafter refer to as the MO basis), the 1RDM of $|^1\Phi_h^l\rangle$, which we label as,

$$\gamma_{1\kappa,\kappa'} \equiv \langle{}^1\Phi_h^l|\hat{a}^\dagger_{\kappa\uparrow}\hat{a}_{\kappa'\uparrow}|^1\Phi_h^l\rangle = \langle{}^1\Phi_h^l|\hat{a}^\dagger_{\kappa\downarrow}\hat{a}_{\kappa'\downarrow}|^1\Phi_h^l\rangle \tag{8.2}$$

is diagonal. Consider the concrete example of a 6-site and 6-electron Hubbard chain (see Model 3 in Figure 8.4). In this case, γ_1 reads

$$\boldsymbol{\gamma}_1 \;=\; \begin{array}{c} \\ \langle\varphi_1| \\ \langle\varphi_2| \\ \langle\varphi_3| \\ \langle\varphi_4| \\ \langle\varphi_5| \\ \langle\varphi_6| \end{array} \begin{array}{c} \begin{array}{cccccc} |\varphi_1\rangle & |\varphi_2\rangle & |\varphi_3\rangle & |\varphi_4\rangle & |\varphi_5\rangle & |\varphi_6\rangle \end{array} \\ \begin{bmatrix} 1 & 0 & 0 & 0 & 0 & 0 \\ 0 & 1 & 0 & 0 & 0 & 0 \\ 0 & 0 & 0.5 & 0 & 0 & 0 \\ 0 & 0 & 0 & 0.5 & 0 & 0 \\ 0 & 0 & 0 & 0 & 0 & 0 \\ 0 & 0 & 0 & 0 & 0 & 0 \end{bmatrix} \end{array} \tag{8.3}$$

[2]Complications may arise, for example, if the double HOMO $\rightarrow$LUMO excitation is degenerate or higher in energy to the single HOMO $\rightarrow$ LUMO+1 excitation. In that case, if an embedding cluster contains the HOMO and LUMO orbitals (but not LUMO+1), it will not be able to (locally) match the singly-excited state with excitation into LUMO+1, and the TGOK variational principle for the full-size system will not be correctly reproduced inside such a cluster.

The two fractionally occupied spin-orbitals, $|\varphi_3\rangle$ (HOMO) and $|\varphi_4\rangle$ (LUMO) make the above matrix non-idempotent ($\boldsymbol{\gamma}_1^2 \neq \boldsymbol{\gamma}_1$), which means that a single Householder transformation will not give a two-orbital embedding cluster as in the ground-state case (see 1.3.2.3). Therefore, if we are to stick to embedding a singly-excited state (with correct spin symmetry), we have to find another strategy. A price to pay is that we may have to produce more bath orbitals for achieving a disentanglement, thereby increasing the cluster's size. In fact, in Ref. [105], there was already a hint that we could apply a string of successive Householder transformations on submatrices of the 1RDM to generate additional bath orbitals and further resolve the couplings of the impurity and impurity's environment. Such a technique is used in the tridiagonalization of matrices [359, 18], which is a preprocessing step for computing the eigenvalues of symmetric matrices [19]. The following subsection explains in more detail the mathematical intricacies of this technique.

8.2.1.2 Clusterization via successive Householder transformations

Let us begin by defining successive Householder transformations through a recurrence relation. Starting with a general matrix $\boldsymbol{\gamma}$, the $i+1$-th Householder-transformed matrix $\tilde{\boldsymbol{\gamma}}^{(i+1)}$ is obtained as [19]

$$\begin{aligned} \tilde{\boldsymbol{\gamma}}^{(1)} &= \boldsymbol{\gamma} \\ \tilde{\boldsymbol{\gamma}}^{(i+1)} &\underset{i\geq 1}{=} \mathbf{P}^{(i)} \tilde{\boldsymbol{\gamma}}^{(i)} \mathbf{P}^{(i)} \end{aligned} \tag{8.4}$$

where

$$\mathbf{P}^{(i)} = \begin{bmatrix} \mathbf{1}_{(i-1)\times(i-1)} & \mathbf{0}_{(i-1)\times(L-i+1)} \\ \mathbf{0}_{(L-i+1)\times(i-1)} & \mathbf{P}[\tilde{\boldsymbol{\gamma}}^{(i)}[i^-:, i^-:]] \end{bmatrix}. \tag{8.5}$$

$\mathbf{P}$ is the Householder transformation as defined in Eqs. (1.134), (1.135) and (1.136), and $\tilde{\boldsymbol{\gamma}}^{(i)}[i^-:, i^-:]$ is a submatrix of $\tilde{\boldsymbol{\gamma}}^{(i)}$ obtained by deletion of the first $i-1$ rows and columns. Defined this way, $\tilde{\boldsymbol{\gamma}}^{(2)} = \mathbf{P}^{(1)}\boldsymbol{\gamma}\mathbf{P}^{(1)}$ is the singly Householder-transformed matrix as in Eq. (1.137). The effect of further transformations $\{\mathbf{P}^{(i)}\}_{i\geq 2}$ is the conversion of $\boldsymbol{\gamma}$ to a tridiagonal form, which is displayed in Figure 8.1.

We can also define the i-th partial tridiagonalization as,

$$\mathbf{Q}^{(i)} = \mathbf{P}^{(1)}\mathbf{P}^{(2)}\ldots\mathbf{P}^{(i)}. \tag{8.6}$$

Unlike $\mathbf{P}^{(i)}$, which is unitary and Hermitian (as Householder transformations are), $\mathbf{Q}^{(i)}$ is unitary but not Hermitian, since the different $\mathbf{P}^{(i)}$ are not commutative. This can be easily seen by rewriting $\mathbf{P}^{(i)}$ as

$$\mathbf{P}^{(i)} = \mathbf{1}_{L\times L} - 2\mathbf{v}^{(i)}\mathbf{v}^{\dagger(i)}, \tag{8.7}$$

where $\mathbf{1}_{L\times L}$ is the identity matrix and $\mathbf{v}^{(i)}$ is the i-th Householder vector. Then, for $i \neq j$,

$$\mathbf{P}^{(i)}\mathbf{P}^{(j)} = \mathbf{1}_{L\times L} - 2(\mathbf{v}^{(i)}\mathbf{v}^{\dagger(i)} + \mathbf{v}^{(j)}\mathbf{v}^{\dagger(j)}) + 4(\mathbf{v}^{\dagger(i)}\mathbf{v}^{(j)})\mathbf{v}^{(i)}\mathbf{v}^{\dagger(j)}. \tag{8.8}$$

Now, since $\mathbf{v}^{(i)}\mathbf{v}^{\dagger(j)} \neq \mathbf{v}^{(j)}\mathbf{v}^{\dagger(i)}$, it follows that $\mathbf{P}^{(i)}\mathbf{P}^{(j)} \neq \mathbf{P}^{(j)}\mathbf{P}^{(i)}$, unless $\mathbf{v}^{\dagger(i)}\mathbf{v}^{(j)} = 0$ (which is the case if $\boldsymbol{\gamma}$ is already tridiagonal). Thus, $\mathbf{Q}^{\dagger(i)} = \mathbf{P}^{(i)}\mathbf{P}^{(i-1)}\ldots\mathbf{P}^{(1)} \neq \mathbf{Q}^{(i)}$.

As a consequence, care must be taken when defining transformations between bases. This point will be raised later again when we construct an embedding cluster for a two-state ensemble, based on successive Householder transformations as defined above.

For the moment, let us label the initial localized spin-orbital (sites in the Hubbard model) basis of $\boldsymbol{\gamma}$ as $\{|\chi_k\rangle\}_{1\leq k\leq L}$, and the basis of $\tilde{\boldsymbol{\gamma}}^{(i)}$ as $\{|\chi_k^{(i)}\rangle\}_{1\leq k\leq L}$.

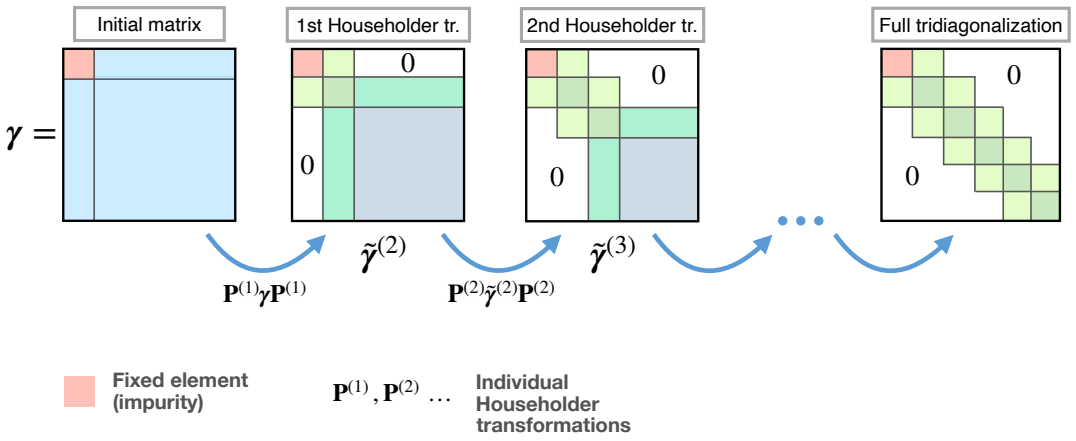

Figure 8.1: Schematic representation of applying successive Householder transformations to $\boldsymbol{\gamma}$.

8.2.2 Step 2: Two-state ensemble embedding strategy

8.2.2.1 Transformation from local to embedding basis

We are interested in describing the lowest singlet excitation for a given system. As a starting point, we chose a mean-field (or non-interacting) description of the full system, where the idea is to find a suitable basis of spin-orbitals that affords an embedding cluster for the TGOK ensemble of ground and singly excited states,

$$\hat{\Gamma}^{\xi} = (1-\xi)\,|\Phi_0\rangle\langle\Phi_0| + \xi\,\left|{}^1\Phi_h^l\right\rangle\!\left\langle{}^1\Phi_h^l\right|, \tag{8.9}$$

where $0 \leq \xi \leq 1/2$ such that the TGOK variational principle is fulfilled. Adopting the clusterization procedure in Ht-DMFET (see 1.3.2.3), we work with ensemble 1RDM. In the local basis, it is defined as,

$$\gamma^{\xi}_{ij\sigma} = \mathrm{Tr}\left[\hat{\Gamma}^{\xi}\hat{c}^{\dagger}_{i\sigma}\hat{c}_{j\sigma}\right] = (1-\xi)\gamma^{\Phi_0}_{ij\sigma} + \xi\gamma^{{}^1\Phi_h^l}_{ij\sigma}. \tag{8.10}$$

We define $\gamma^{\xi}_{ij} \equiv \gamma^{\xi}_{ij\uparrow} = \gamma^{\xi}_{ij\downarrow}$ (since we work with singlet states). In the MO basis of our 6-site/6-electron Hubbard chain, such a matrix looks like,

$$\boldsymbol{\gamma}^{\xi} = \begin{array}{c} \\ \langle\varphi_1| \\ \langle\varphi_2| \\ \langle\varphi_3| \\ \langle\varphi_4| \\ \langle\varphi_5| \\ \langle\varphi_6| \end{array} \begin{array}{c} \begin{array}{cccccc} |\varphi_1\rangle & |\varphi_2\rangle & |\varphi_3\rangle & |\varphi_4\rangle & |\varphi_5\rangle & |\varphi_6\rangle \end{array} \\ \begin{bmatrix} 1 & 0 & 0 & 0 & 0 & 0 \\ 0 & 1 & 0 & 0 & 0 & 0 \\ 0 & 0 & \frac{1-\xi}{2} & 0 & 0 & 0 \\ 0 & 0 & 0 & \frac{\xi}{2} & 0 & 0 \\ 0 & 0 & 0 & 0 & 0 & 0 \\ 0 & 0 & 0 & 0 & 0 & 0 \end{bmatrix} \end{array}. \tag{8.11}$$

The fractional occupations of the HOMO and LUMO are now controlled by ξ, a single variable which directly indicates the presence of the excited state. In order to capture the excitation, we would like to include both HOMO and LUMO inside the embedding cluster. Therefore, we can expect the sought-after cluster to have at least two bath spin-orbitals. Again, this is best illustrated with the Hubbard chain example. We start with the equi-ensemble ($\xi = 1/2$ in Eq. (8.9)), and construct the ensemble 1RDM in the localized basis,

$$\boldsymbol{\gamma} := \boldsymbol{\gamma}^{\boldsymbol{\xi}} = \begin{array}{c} \\ \langle\chi_1| \\ \langle\chi_2| \\ \langle\chi_3| \\ \langle\chi_4| \\ \langle\chi_5| \\ \langle\chi_6| \end{array} \begin{array}{c} \begin{array}{cccccc} |\chi_1\rangle & |\chi_2\rangle & |\chi_3\rangle & |\chi_4\rangle & |\chi_5\rangle & |\chi_6\rangle \end{array} \\ \begin{bmatrix} 0.5 & 0.3751 & 0 & -0.085 & 0 & 0.0149 \\ 0.3751 & 0.5 & 0.2902 & 0 & -0.07 & 0 \\ 0 & 0.2902 & 0.5 & 0.3051 & 0 & -0.085 \\ -0.085 & 0 & 0.3051 & 0.5 & 0.2902 & 0 \\ 0 & -0.07 & 0 & 0.2902 & 0.5 & 0.3751 \\ 0.0149 & 0 & -0.085 & 0 & 0.3751 & 0.5 \end{bmatrix} \end{array}, \tag{8.12}$$

where the goal is to embed the first site, $|\chi_1\rangle$. After applying the first Householder transformation (the weight-dependence dropped for simplicity), $\tilde{\boldsymbol{\gamma}}^{(2)} = \mathbf{P}\boldsymbol{\gamma}\mathbf{P}$, we get the expected result where the top left 2×2 subblock is still coupled to the rest of the matrix:

$$\tilde{\boldsymbol{\gamma}}^{(2)} = \begin{array}{c} \\ \langle\chi_1| \\ \langle\chi_2^{(2)}| \\ \langle\chi_3^{(2)}| \\ \langle\chi_4^{(2)}| \\ \langle\chi_5^{(2)}| \\ \langle\chi_6^{(2)}| \end{array} \begin{array}{c} \begin{array}{cccccc} |\chi_1\rangle & |\chi_2^{(2)}\rangle & |\chi_3^{(2)}\rangle & |\chi_4^{(2)}\rangle & |\chi_5^{(2)}\rangle & |\chi_6^{(2)}\rangle \end{array} \\ \begin{bmatrix} 0.5 & -0.3849 & 0 & 0 & 0 & 0 \\ -0.3849 & 0.5 & -0.2122 & 0 & 0.1177 & 0 \\ 0 & -0.2122 & 0.5 & 0.3613 & 0 & -0.0948 \\ 0 & 0 & 0.3613 & 0.5 & 0.2692 & 0 \\ 0 & 0.1177 & 0 & 0.2692 & 0.5 & 0.3788 \\ 0 & 0 & -0.0948 & 0 & 0.3788 & 0.5 \end{bmatrix} \end{array}. \tag{8.13}$$

It turns out that, after applying three successive Householder transformations, $\tilde{\boldsymbol{\gamma}}^{(4)} = \mathbf{P}^{(3)\dagger}\tilde{\boldsymbol{\gamma}}^{(3)}\mathbf{P}^{(3)}$, we obtain the representation of the ensemble 1RDM with a block-diagonalized structure (note the first three spin-orbitals in the matrix below come from previous 1RDMs in succession, $\{\tilde{\boldsymbol{\gamma}}^{(i)}\}_{1\leq i\leq 3}$, due to the recurrence in Eq. (8.4)).

$$\tilde{\boldsymbol{\gamma}}^{(4)} = \begin{array}{c} \\ \langle\chi_1| \\ \langle\chi_2^{(2)}| \\ \langle\chi_3^{(3)}| \\ \langle\chi_4^{(4)}| \\ \langle\chi_5^{(4)}| \\ \langle\chi_6^{(4)}| \end{array} \begin{array}{c} \begin{array}{cccccc} |\chi_1\rangle & |\chi_2^{(2)}\rangle & |\chi_3^{(3)}\rangle & |\chi_4^{(4)}\rangle & |\chi_5^{(4)}\rangle & |\chi_6^{(4)}\rangle \end{array} \\ \begin{bmatrix} 0.5 & -0.3849 & 0 & 0 & 0 & 0 \\ -0.3849 & 0.5 & 0.2426 & 0 & 0 & 0 \\ 0 & 0.2426 & 0.5 & 0.3247 & 0 & 0 \\ 0 & 0 & 0.3247 & 0.5 & 0 & 0 \\ 0 & 0 & 0 & 0 & 0.5 & 0.5 \\ 0 & 0 & 0 & 0 & 0.5 & 0.5 \end{bmatrix} \end{array}. \tag{8.14}$$

This is a very favourable result. Already from the traces of sub-blocks, we can see that in the top-left 4×4 subblock, we have 2 electrons per spin, and in the bottom-right 2×2 subblock, we have 1 electron per spin. If we diagonalize each subblock

separately, we find the following sets of eigenvalues (displayed as functions of the ensemble weight ξ),

$$\boldsymbol{\gamma} = \begin{array}{c} \\ \langle\mu_1| \\ \langle\mu_2| \\ \langle\mu_3| \\ \langle\mu_4| \\ \langle\nu_1| \\ \langle\nu_2| \end{array} \begin{array}{c} \begin{array}{cccccc} |\mu_1\rangle & |\mu_2\rangle & |\mu_3\rangle & |\mu_4\rangle & |\nu_1\rangle & |\nu_2\rangle \end{array} \\ \begin{bmatrix} 1 & 0 & 0 & 0 & 0 & 0 \\ 0 & \frac{1-\xi}{2} & 0 & 0 & 0 & 0 \\ 0 & 0 & \frac{\xi}{2} & 0 & 0 & 0 \\ 0 & 0 & 0 & 0 & 0 & 0 \\ 0 & 0 & 0 & 0 & 1 & 0 \\ 0 & 0 & 0 & 0 & 0 & 0 \end{bmatrix} \end{array}, \tag{8.15}$$

where the two fractionally occupied orbitals can be identified with the HOMO and LUMO in Eq. (8.11), i.e., $|\mu_2\rangle = |\varphi_3\rangle$ (HOMO), and $|\mu_3\rangle = |\varphi_4\rangle$ (LUMO). Furthermore, $|\mu_1\rangle$ is the only fully occupied MO that has a nonzero overlap with the impurity $|\chi_1\rangle$, in analogy with the single-impurity embedding cluster in regular DMET (see Eq. (37) in Ref. [105]). Evidently, with three successive Householder transformations, $\mathbf{Q}^{(3)} = \mathbf{P}^{(1)}\mathbf{P}^{(2)}\mathbf{P}^{(3)}$, we managed to completely capture the excitation inside a 4×4 cluster. Based on this result, we can use the spin-orbital subspace,

$$|\chi_1\rangle \oplus |\chi_2^{(2)}\rangle \oplus |\chi_3^{(3)}\rangle \oplus |\chi_4^{(4)}\rangle \tag{8.16}$$

to form the *ensemble embedding cluster* that is suitable for both ground $|\Phi_0\rangle$ and singly-excited state $\left|{}^1\Phi_h^l\right\rangle$. As shown in Figure 8.2, compared to the single-state embedding cluster in DMET, the ensemble embedding cluster is enlarged with three bath spin-orbitals instead of one, where two of the latter are the HOMO and LUMO, and another bath spin-orbital comes from the "inactive" orbitals of the ensemble (fully occupied in both $|\Phi_0\rangle$ and $\left|{}^1\Phi_h^l\right\rangle$). The transformation matrix $\mathbf{Q}^{(3)}$ is also easily expressed in second quantization. If we write $\mathbf{Q}^{(3)}$ as $\mathbf{Q}$ for simplicity, the change of basis reads,

$$\hat{d}_{i\sigma}^\dagger = \sum_{j=1}^{L} Q_{ji}\hat{c}_{j\sigma}^\dagger \qquad \hat{d}_{i\sigma} = \sum_{j=1}^{L} Q_{ji}\hat{c}_{j\sigma}. \tag{8.17}$$

Then, the subset of operators $\{\hat{c}_{1\sigma}^\dagger = \hat{d}_{1\sigma}^\dagger, \hat{c}_{1\sigma} = \hat{d}_{1\sigma}, \hat{d}_{2\sigma}^\dagger, \hat{d}_{2\sigma}, \hat{d}_{3\sigma}^\dagger, \hat{d}_{3\sigma}, \hat{d}_{4\sigma}^\dagger, \hat{d}_{4\sigma}\}$ act on the ensemble embedding cluster. The bath spin-orbital subspace is then given as,

$$\{|\chi_{i\sigma}^{(i)}\rangle = \hat{d}_{i\sigma}^\dagger |vac\rangle\}_{2\leq i\leq 4, \sigma\in\{\uparrow,\downarrow\}}. \tag{8.18}$$

The bath spin-orbitals are delocalized over the impurity's environment, as shown for the Hubbard chain in Figure 8.3 (see the next section for further discussion on this model).

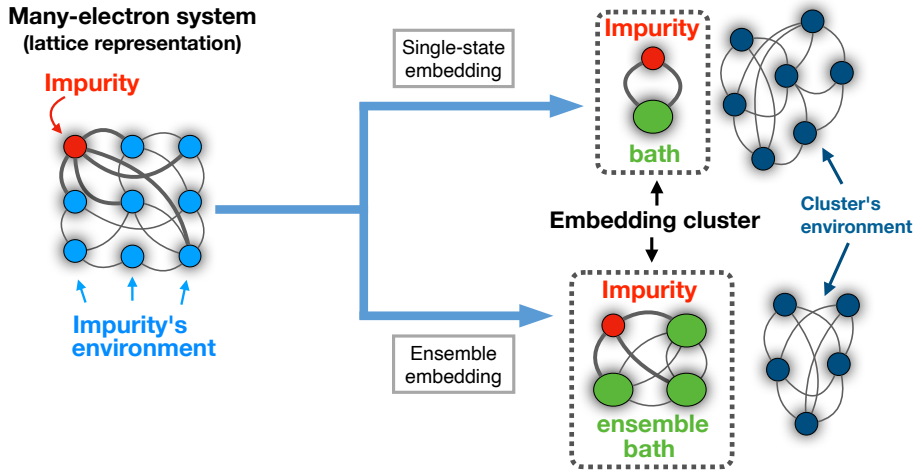

Figure 8.2: Comparison of embedding clusters for single states, and two-state ensembles.

8.2.2.2 Single-shot two-state ensemble embedding calculation

Once the transformation $\mathbf{Q}$ for the two-state ensemble has been determined, the computation step proceeds much the same way as in regular DMET. Firstly, we construct the (ensemble) embedding Hamiltonian,

$$\hat{\mathcal{H}}^{\text{ens}-\text{emb.}} = \hat{\mathcal{Q}}\hat{H}\hat{\mathcal{Q}} - \mu_1\hat{n}_1, \tag{8.19}$$

where the many-body projector $\hat{\mathcal{Q}}$ spans the Fock space constructed from the impurity+bath spin-orbitals in Eq. (8.16). The goal is to extract the ground and the lowest singlet excited state from the embedding Hamiltonian. Just like in regular DMET (see Subsection 1.3.2), we perform the embedding over all localized spin-orbitals (or lattice sites). The strategy that we choose in the following, is to add a chemical potential on each localized spin-orbital. This time, chemical potentials are

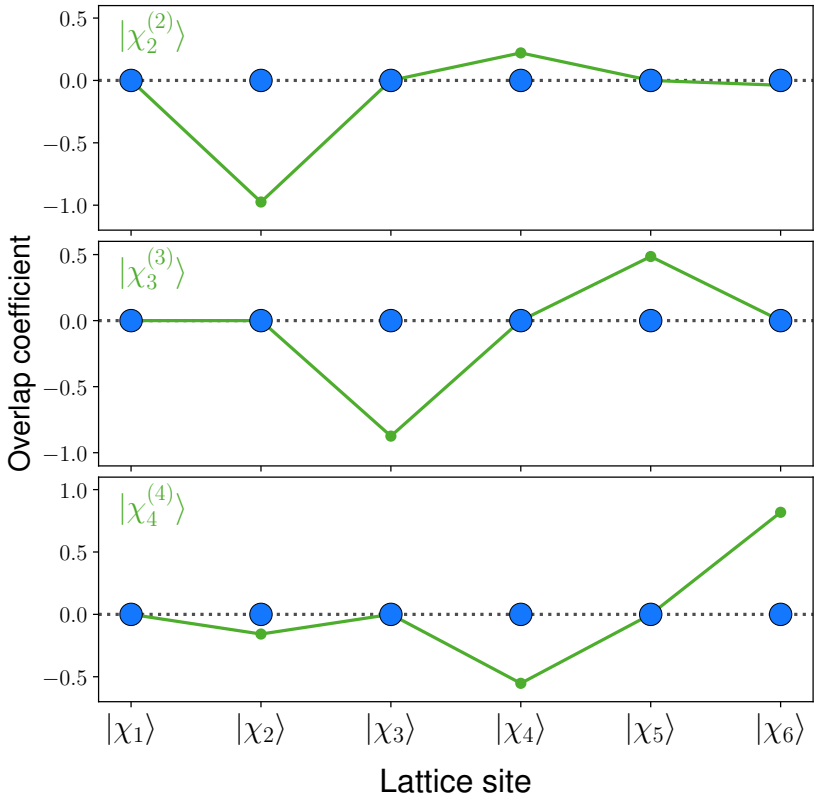

Figure 8.3: Bath spin-orbital coefficients in lattice site basis for the 6-site Hubbard chain.

set to be different for each spin-orbital, i.e. $\{\mu_i\}_{1\leq i\leq L}$, and are tuned to optimize the number of electrons in both ground and first excited state, for which we consider the following cost function,

$$\mathrm{CF}(\{\mu_i\}) = \sum_{I=0,1} \left(\sum_{i=1}^{L} \langle \Psi_I^{\mathcal{C}_i}(\mu_i) | \hat{n}_i | \Psi_I^{\mathcal{C}_i}(\mu_i) \rangle - N \right)^2 . \tag{8.20}$$

Although the above cost function does not fulfill any exact TGOK ensemble constraint (for example, ensemble local occupations, or density-driven correlations that we discussed in Section 6.2 are not guaranteed at all to be obtained correctly using the cost function in Eq. (8.20)), we expect it to produce reasonable results if the system of interest is homogeneous (e.g. homoatomic molecules, see Section 8.3).

After optimization, the ground and first excited states of the embedding cluster are used as approximations to the ground and first excited states of the true system, which in practice means that 1RDM and 2RDM elements are evaluated locally from embedding clusters. Then, the reconstruction of individual energy levels is done

with democratic partitioning, as in Eqs. (1.158) and (1.159),

$$\begin{aligned}\gamma_{ij}^{\Psi_I} &\approx \frac{1}{2}\sum_{t\in\{i,j\}} \langle \Psi_I^{\mathcal{C}_t}|\hat{c}_{i\sigma}^\dagger \hat{c}_{j\sigma}|\Psi_I^{\mathcal{C}_t}\rangle, \\ \Gamma_{ijkl}^{\Psi_I} &\approx \frac{1}{4}\sum_{t\in\{i,j,k,l\}}\sum_{\sigma,\sigma'\in\{\uparrow,\downarrow\}^2} \langle \Psi_I^{\mathcal{C}_t}|\hat{c}_{i\sigma}^\dagger \hat{c}_{j\sigma'}^\dagger \hat{c}_{l\sigma'}\hat{c}_{k\sigma}|\Psi_I^{\mathcal{C}_t}\rangle,\end{aligned} \tag{8.21}$$

where $\Gamma = \Gamma^{(2)}$ is the 2RDM, Ψ_I is the wavefunction of the I-th stationary state ($|\Psi_0\rangle$ being the ground state, and $|\Psi_1\rangle$ the first excited state) of the true system, and $\Psi_I^{\mathcal{C}_t}$ is the wavefunction of the I-th stationary state of cluster $\mathcal{C}_t$ localized on impurity $|\chi_t\rangle$.

8.3 Illustrative examples

The two-state embedding strategy presented in the previous section is applied to three simple systems (shown in Figure 8.4), one being an *ab-initio* system, and the other two model systems. All calculations at the FCI and embedding levels were carried out using QuantNBody - an open-source Python package with inbuilt functions for easy construction and manipulation of many-body fermionic/bosonic operators [107]. For analysis purposes, we also plot for each system overlap coefficients of individual FCI states with the mean-field states $|\Phi_0\rangle$ and $\left|{}^1\Phi_h^l\right\rangle$. In addition, we also plot FCI state overlaps with the HOMO $\rightarrow$LUMO doubly excited state, which is given by the following Slater determinant

$$\left|\Phi_{2h}^{2l}\right\rangle = \hat{a}_{N/2+1,\uparrow}^\dagger \hat{a}_{N/2,\uparrow} \hat{a}_{N/2+1,\downarrow}^\dagger \hat{a}_{N/2,\downarrow} \left|\Phi_0\right\rangle . \tag{8.22}$$

The latter choice is motivated by the observation that the double HOMO $\rightarrow$LUMO excitation can also be mapped into a cluster like the one in Eq. (8.14), since the HOMO and LUMO are fully contained inside the cluster (see Eq. (8.15) and the subsequent discussion). For this reason, the embedding cluster may also recover some double excitation character in individual states.

8.3.1 *Ab-initio* system consisting of Hydrogen dimers

The first system we chose for the application of our embedding strategy consists of an arrangement of six hydrogen atoms, which was first studied by Tran *et al.* in

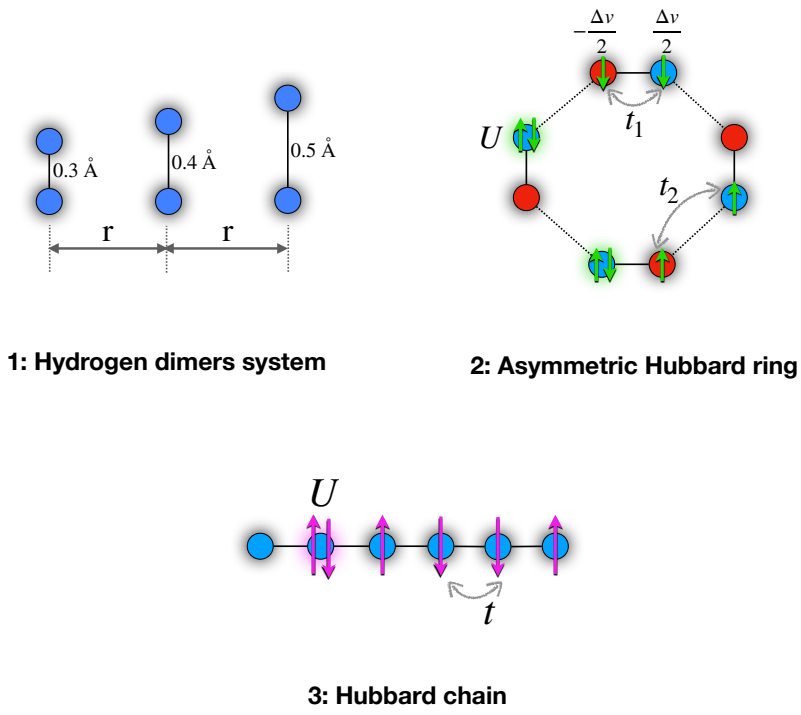

Figure 8.4: Schematic depiction of the three models used in our ensemble embedding calculations.

their work on extending DMET to excited states [106]. One- and two-electron integrals were calculated with the Psi4 Python package [360], using the STO-3G basis set. Since the original atomic orbitals are not necessarily orthogonal, an additional preprocessing was carried out with Löwdin's orthogonalization scheme to produce *orthogonal atomic orbitals* (OAOs) [210, 211, 212], which were used as a starting point for the construction of the embedding cluster and subsequent embedding calculations. For obtaining a reference mean-field description of the full system, we run a RHF calculation with Psi4. After extracting RHF molecular orbitals, we build the ensemble 1RDM of the reference. We work in the equiensemble case ($\xi = 1/2$). We observe that the chemical potential adjustment is almost negligible, probably because the system is homoatomic (see Figure 8.5). Just like the state-specific approach of Tran *et al.* (see Figure 2 in Ref. [106]), our embedding calculations show very good agreement with FCI results for the ground and first-excited state, even in the region of avoided crossing close to $r \approx 0.65$Å. One reason why embedding was successful can be seen by inspecting the overlap values between the FCI states and their mean-field approximations. As seen on Figure 8.6, the dominant contributing

states are $|\Phi_0\rangle$ in the ground state, and $\left|{}^1\Phi_h^l\right\rangle$ in the first excited state, which are precisely those mean-field states that were used as the starting point for constructing the embedding cluster (see Eq. (8.9)).

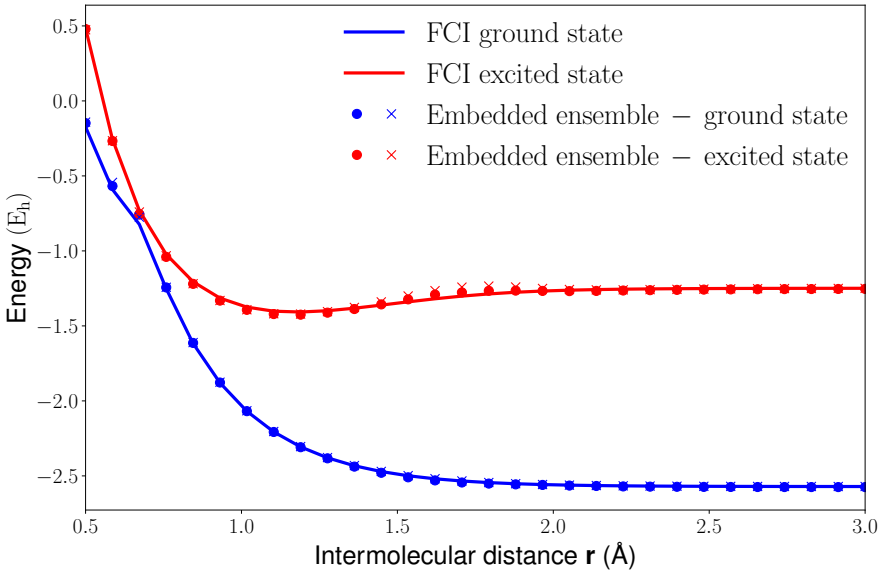

Figure 8.5: Dissociation curves of the FCI ground and first excited singlet states (blue and red lines, respectively), and embedding results for the ground and first excited state (blue and red markers, respectively) for the model of Hydrogen atoms by Tran *et al.* [106]. Embedding results are plotted with and without chemical potential tuning (dot (•) and cross (×) markers, respectively).

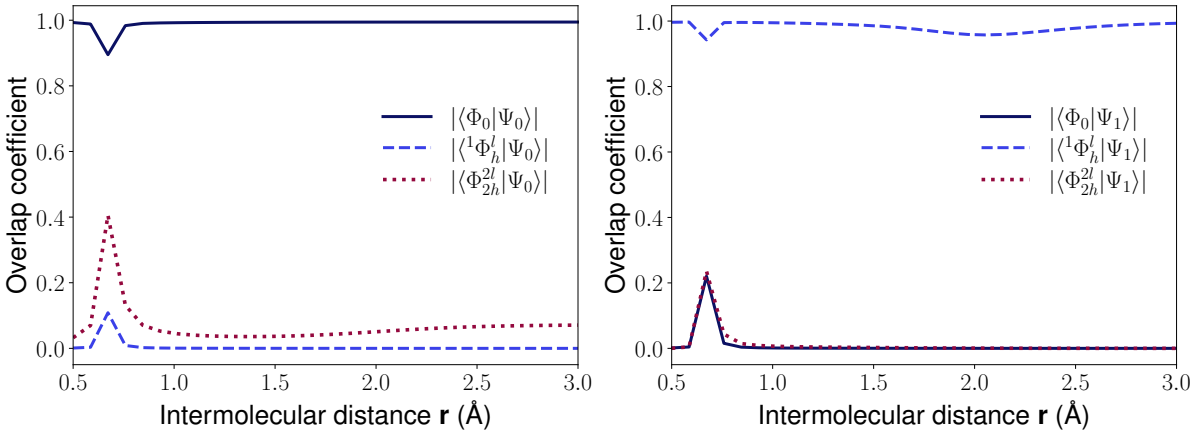

Figure 8.6: Absolute overlap coefficients of the FCI ground and first excited singlet states (left and right panel, respectively) with different mean-field states (see main text) for the model of Hydrogen atoms by Tran *et al.* [106].

8.3.2 Asymmetric Hubbard ring

We now apply our ensemble embedding strategy to a model Hamiltonian that we call the "asymmetric Hubbard ring". The model Hamiltonian of the ring reads,

$$\hat{H} = -\sum_{i=1}^{8} t_i \sum_{\sigma\in\{\uparrow,\downarrow\}} (\hat{c}^\dagger_{i\sigma}\hat{c}_{i+1\sigma} + \hat{c}^\dagger_{i+1\sigma}\hat{c}_{i\sigma}) + U\sum_{i=1}^{8}\hat{n}_{i\uparrow}\hat{n}_{i\downarrow} + \frac{\Delta v}{2}\sum_{i=1}^{8}(-1)^i\hat{n}_i, \quad (8.23)$$

where

$$t_i = \begin{cases} t_1 & \text{if } i \text{ is odd.} \\ t_2 & \text{if } i \text{ is even.,} \end{cases} \quad (8.24)$$

where periodic ($\hat{c}^\dagger_9 = \hat{c}^\dagger_1$) boundary conditions have been used. The ring is an 8-site and 8-electron lattice system with alternating bond length, tuned by the ratio t_2/t_1, and asymmetry imposed on pairs of nearest neighbouring sites by the potential Δv. The ratio t_2/t_2 plays a very similar role to intermolecular distance r in the previous model. The $t_2/t_1 \ll 1$ regime represents the bond breaking scenario, when the molecule turns into four separate dimers, and $t_2/t_1 \gg 1$ represents a molecule with strong overlap between dimers. The peculiar feature of this model is the energy crossing between the ground and first excited states at $t_2/t_1 = 1$, $U = 2$ and $\Delta v = 1$, which is a conical intersection (see Figure 8.7). It is probably an accidental conical intersection, since by changing the ratio $\Delta v/U$ we observe that the degeneracy at $t_2/t_1 = 1$ is lifted. In this model, the ensemble 1RDM and the embedding cluster are built from orbitals of the tight-binding ($U = 0$) system. We observe that embedding results are in very good agreement with FCI values for ground and excited states, especially in the region of the conical intersection. Surprisingly, in this model (and in the next model), we find that there is no chemical potential tuning necessary to optimize the global number of electrons as long as two-electron interactions with *unentangled occupied orbitals* in the cluster's environment $\left|\Phi^{\mathcal{E}_i}\right\rangle$ are properly included in the embedding Hamiltonian (interestingly, the same observation was reported by Marécat *et al.* in the application of their self-consistent embedding scheme on the 1D Hubbard model [361]). As in the previous model, we also plot overlap coefficients of true (FCI) states with $|\Phi_0\rangle$, $\left|{}^1\Phi^l_h\right\rangle$ and $\left|\Phi^{2l}_{2h}\right\rangle$. Again, we find that the ground and singly-excited configurations contribute the most to FCI wavefunctions.

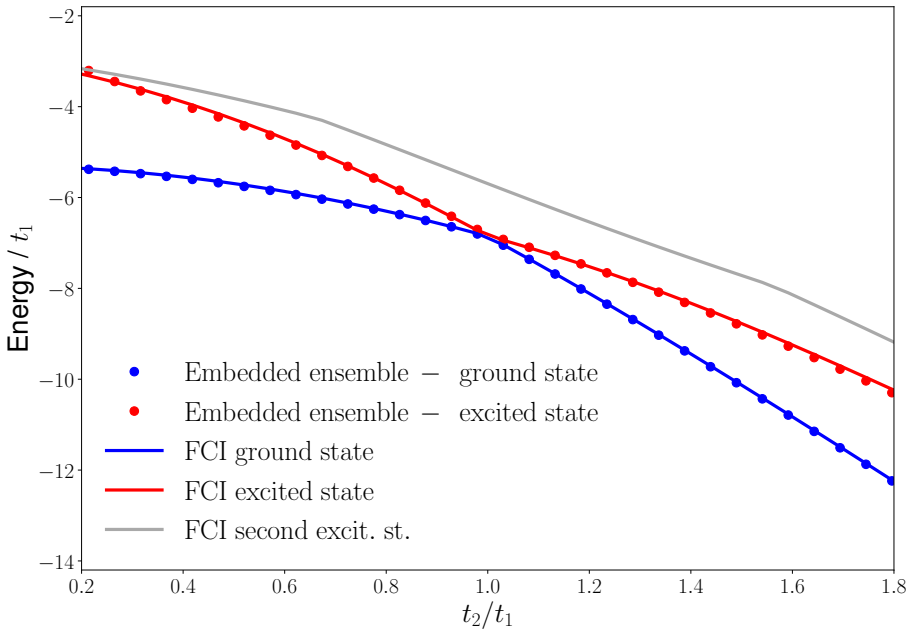

Figure 8.7: The FCI ground, first and second excited singlet states (blue, red and grey lines, respectively), and embedding results for the ground and first excited state (blue and red markers, respectively) for the asymmetric Hubbard ring model at $U = 2$, $\Delta v = 1$ and different ratios of t_2/t_1.

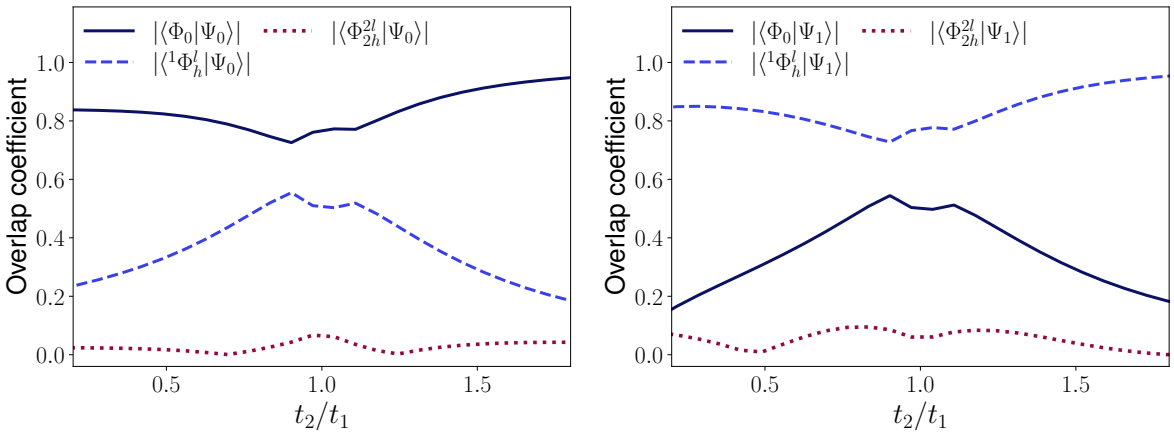

Figure 8.8: Absolute overlap coefficients of the FCI ground and first excited singlet states (left and right panel, respectively) with different mean-field states (see main text) for the asymmetric Hubbard ring model at $U = 2$, $\Delta v = 1$ and different ratios of t_2/t_1.

8.3.3 Hubbard chain

As a final model, we chose a Hubbard chain of 6 sites and 6 electrons, which is a finite 1D Hubbard model with open boundary conditions. This choice of boundary

conditions is a sort of tradeoff. While chosing periodic boundary conditions would make the model translationally invariant, the drawback is the degeneracy of HOMO and LUMO levels in the tight-binding limit. On the contrary, "cutting" the ring into a chain removes translational invariance, but it makes the HOMO and LUMO levels in the tight-binding limit nondegenerate, with the following energies,

$$\varepsilon_m \underset{1\leq m\leq L}{=} -2t\cos\left(\frac{\pi m}{L+1}\right). \tag{8.25}$$

Hence this is why we chose this model for our embedding study. As in the second model, we build the equiensemble 1RDM from the system in the tight-binding limit. We then proceed with the embedding calculations for $t = 1$ and U values in the range $0 < U < 10$, where $U = 10$ corresponds to a (very) strongly correlated regime. The challenge in this model is that near $U' \approx 1.79$, there is a crossing between the lowest two excited states of different symmetry. Overall, the chain has C_2 point group symmetry, which can gauged by the reflection plane operator (see Eqs. (8) - (9) in Ref. [362]),

$$\hat{\sigma} = \prod_{\sigma=\uparrow,\downarrow}\prod_{k=L/2}^{L}\left[1-(\hat{c}^{\dagger}_{k,\sigma}-\hat{c}^{\dagger}_{-k,-\sigma})(\hat{c}_{k,\sigma}-\hat{c}_{-k,-\sigma})\right]. \tag{8.26}$$

Firstly, the ground state (1^1A) is totally symmetric with $\langle\hat{\sigma}\rangle_{\Psi_0} = 1$. Turning to lowest excited states, to the left of crossing point ($U < U'$), the first excited state belongs to a different symmetry (1^1B) with $\langle\hat{\sigma}\rangle_{\Psi_1(U<U')} = -1$, than to the right side (2^1A), where $\langle\hat{\sigma}\rangle_{\Psi_1(U>U')} = 1$. As seen in Figure 8.9, our embedding strategy was able to successfully reproduce both ground and first excited state energy for $U < U'$. Perhaps this is unsurprising, as up to that point, the most important configurations to the true ground and excited states are $|\Phi_0\rangle$ and $\left|{}^1\Phi^l_h\right\rangle$, respectively. On the contrary, for $U > U'$, the model was unable to converge to the correct first excited state. One of the reasons, which can be immediately observed from the overlap coefficients in Figure 8.10 is that, in this regime, there is an abrupt switch in the dominant configuration of the first excited state from the HOMO $\rightarrow$LUMO singly-excited configuration $\left|{}^1\Phi^l_h\right\rangle$ to the HOMO $\rightarrow$LUMO doubly-excited one $\left|\Phi^{2l}_{2h}\right\rangle$, due to symmetry reasons. Moreover, in that regime, the true excited state becomes highly multiconfigurational, with other mean-field excitations, such as HOMO-1 $\rightarrow$ LUMO, and HOMO $\rightarrow$ LUMO+1, which are nearly degenerate to $\left|\Phi^{2l}_{2h}\right\rangle$, having non-negligible contributions in the FCI expansion. For comparison, we also plot overlap

coefficients with the following two states in Figure 8.10,

$$|^1\Phi^l_{h^-}\rangle = \frac{1}{\sqrt{2}}\left(\hat{a}^\dagger_{N/2+1,\uparrow}\hat{a}_{N/2-1,\uparrow} + \hat{a}^\dagger_{N/2+1,\downarrow}\hat{a}_{N/2-1,\downarrow}\right)|\Phi_0\rangle, \tag{8.27}$$

$$|^1\Phi^{l^+}_{h}\rangle = \frac{1}{\sqrt{2}}\left(\hat{a}^\dagger_{N/2+2,\uparrow}\hat{a}_{N/2,\uparrow} + \hat{a}^\dagger_{N/2+2,\downarrow}\hat{a}_{N/2,\downarrow}\right)|\Phi_0\rangle, \tag{8.28}$$

where $h^- = N/2 - 1$ (HOMO−1) and $l^+ = N/2 + 2$ (LUMO+1). Spin-orbitals that are involved in the latter excitations are currently not included in our ensemble. Including them would most likely improve the results, with a possible tradeoff being the requirement for more bath spin-orbitals.

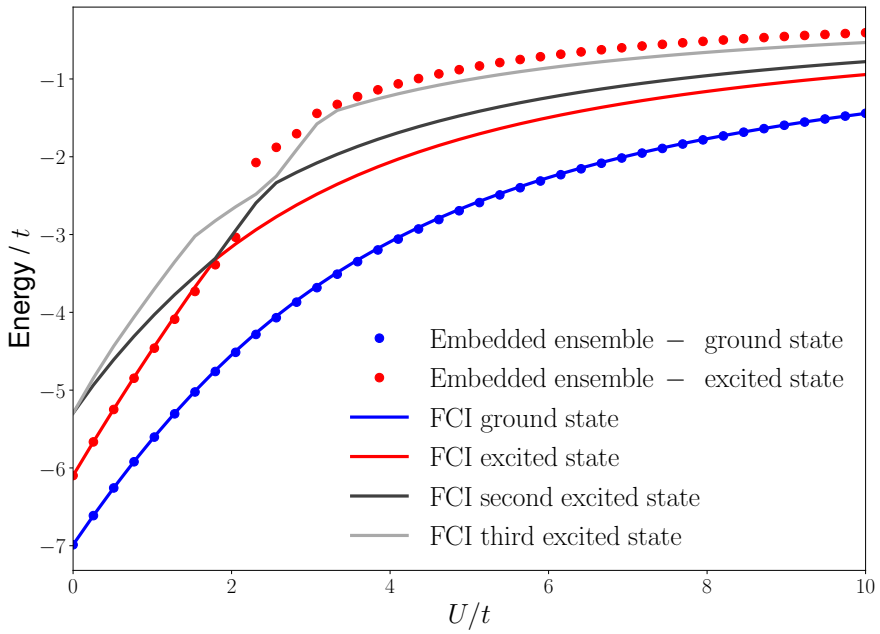

Figure 8.9: The FCI ground, first, second and third excited singlet states (blue, red, dark grey and light grey lines, respectively), and embedding results for the ground and first excited state (blue and red markers, respectively) for the Hubbard chain model at $t = 1$ and different U values.

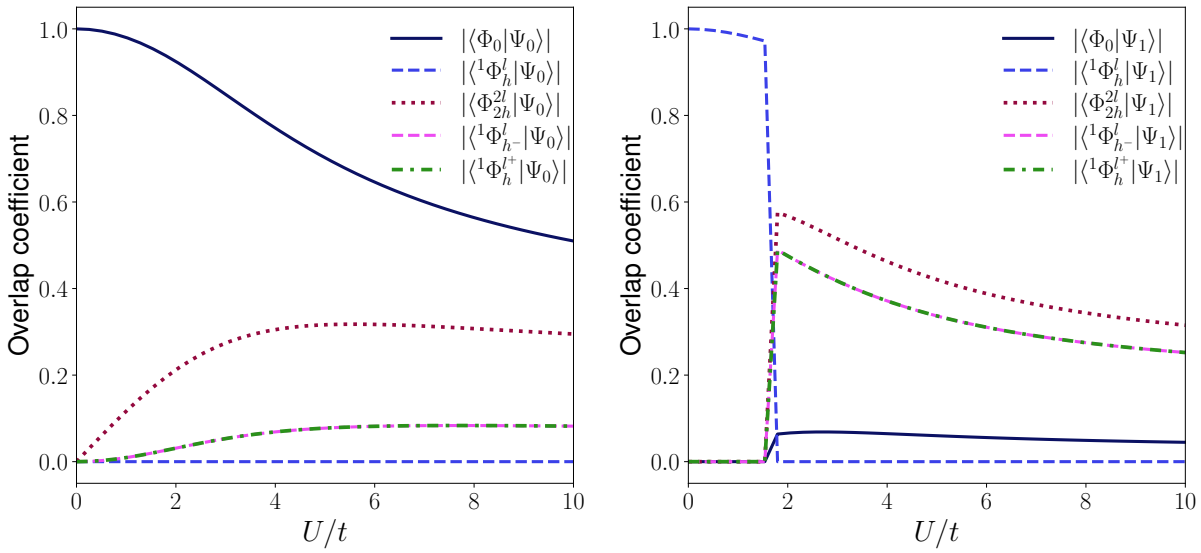

Figure 8.10: Absolute overlap coefficients of the FCI ground and first excited singlet states (left and right panel, respectively) with different mean-field states (see main text) for the Hubbard chain model at $t = 1$ and different U values.

8.4 Conclusion

In this chapter, we developed and implemented an embedding strategy for two-state TGOK ensembles of ground and singlet excited states. Firstly, we found that, by means of a partial tridiagonalization based on Householder transformations of the (mean-field or noninteracting) ensemble 1RDM, we were able to produce an embedding cluster with an impurity coupled to the bath subspace consisting of three delocalized spin-orbitals (instead of one, as obtained in the ground-state theory), which are completely decoupled from the rest of the system. This is a generalization of the clusterization of idempotent 1RDMs in DMET. Secondly, we exploited that result to construct an embedding Hamiltonian for simultaneously describing locally the ground and excited states of correlated systems. The strategy was applied to three simple toy systems which have shown promising results, and also new challenges when it comes to targeting excited states. We observe that in the cases where ground and first excited state levels are well-separated from higher excited states, and overlap well with mean-field states used in the construction of the embedding cluster, embedding results are in good agreement with the FCI results. On the contrary, as was observed in the case of the Hubbard chain, when there is a change in ordering of the excited states (for symmetry reasons or upon geometry variations, for example), the ensemble embedding based on a mean-field starting point with the single HOMO $\rightarrow$LUMO excitation does not describe the correct excited state of the interacting system. One possible solution to such problems would be to consider ensembles with excitations beyond HOMO and LUMO levels, for which we would need to further enlarge the embedding cluster. Another possible improvement, more in the spirit in LPFET [204, 111] (see Section 1.3.2), would be to make the embedding self-consistent with a local, or even nonlocal potential added to the mean-field Hamiltonian so as to enforce matching of the densities or 1RDMs of interacting and mean-field (or noninteracting) ensembles. Concretely, instead of the electron number constraint of the cost function in Eq. (8.20), we may consider the following two-state ensemble constraint,

$$\begin{aligned}&(1-\xi)\langle\Psi_0^{\mathcal{C}_i}(\mu_i)|\hat{n}_i|\Psi_0^{\mathcal{C}_i}(\mu_i)\rangle + \xi\langle\Psi_1^{\mathcal{C}_i}(\mu_i)|\hat{n}_i|\Psi_1^{\mathcal{C}_i}(\mu_i)\rangle \\ &= (1-\xi)\langle\Phi_0(\mu_i)|\hat{n}_i|\Phi_0(\mu_i)\rangle + \xi\langle{}^1\Phi_h^l(\mu_i)|\hat{n}_i|{}^1\Phi_h^l(\mu_i)\rangle,\end{aligned} \tag{8.29}$$

to be fulfilled for each embedding cluster, separately. This would turn the present single-shot ensemble embedding into a self-consistent strategy for developing DFAs for TGOK-DFT that depend implicitly on the density (or the occupation of localized spin-orbitals in the context of DMET), which is the main idea in LPFET that was originally developed for ground-state DFT of Hubbard lattices [204]. In addition, it would be of great benefit to find a way to model density-driven correlations within such an approach, as the individual densities (or occupations) will have no reason be the same for the interacting and mean-field systems (see Section 6.2). This will also be the case for the occupations, evaluated from the correlated embedding clusters, which will (in general) not individually match the mean-field ones in Eq. (8.29). Work is in progress in these directions.

Thesis conclusions

In this manuscript, we discussed extensively about electronic excitations, and presented different standard methods that are used for describing neutral and charged excitations. The central work of this thesis was further development of the ensemble density-functional formalism, which is an alternative to other well-established formalisms in quantum chemistry and condensed-matter physics. We discussed about various formal and practical aspects that are particular to ensemble density-functional theory, and made new theoretical developments. We have also made the first step toward a practical approach of embedding excited states by combining TGOK ensemble density functional theory and quantum embedding. In the following, we briefly overview the main findings and original contributions, presented in this thesis.

In Chapter 6, we reviewed recent progress in the design of weight-dependent xc DFAs, focusing separately on the issues inherent to ensemble exchange and correlation functionals. While the discussion was exclusively about TGOK ensembles, the conclusions can be easily applied to N-centered or other types of ensembles. In Section 6.1, we briefly overviewed two possible formulations for extending the exact exchange energy from KS-DFT to ensembles, namely the *ensemble density matrix Hartree-Fock* (eDMHF) approach, and the *state-averaged Hartree-Fock* (SAHF) approach. While the eDMHF suffers from ghost interactions, the SAHF approach, although being free from the latter, is not amenable to standard SCF routines. In Section 6.2 of that chapter, we discussed state-of-the-art strategies for the design of DFAs for ensemble correlation energies, including the combination of finite and infinite uniform electron gas models as well as the recycling of standard (ground-state) correlation DFAs through state-averaging. In the latter case, further improvements may emerge from the concept of density-driven correlation, which is a feature that

is peculiar to ensemble correlation energy functional. How to define mathematically the corresponding correlation energy is an open question to which we provided a tentative answer [see Eqs. (6.43) and (6.45)]. We have shown, with test calculations on the Hubbard dimer, that it is difficult to have a definition that is both rigorous and useful for the development of approximations. For example, the state- and density-driven correlations can become large and of opposite signs, and mostly compensating when the Hubbard dimer has a pronounced asymmetry, which is clearly an obstacle for the development of correlation DFAs for ensembles. We suggested that the standard Gs-ic and GS-ec approximations may be a better starting point in this respect. We concluded the chapter by pointing out possible directions for the development of ensemble DFT.

In Chapter 7, we presented the extended N-centered ensemble formalism, which combines the TGOK-DFT and the N-centered eDFT into an even more general ensemble density-functional theory that describes both neutral and charged excitations. This extended ensemble formalism now allows for extraction of ionization potentials not only for the N-electron ground state (which is already accessible in N-centered eDFT), but also for any (neutral or ionic) ground or excited state of our choice. A key result of this chapter is the exactification of KS orbital energies in the perspective of N-centered eDFT, which is achieved by imposing specific constraints on the Hxc potential in order to fulfill the Koopmans' theorem for a given ground or excited N-electron state. We have then shown that for a given neutral excitation of interest, the aforementioned constraints induce the discontinuity of the xc potential, which is related to the ensemble weight derivative of the xc functional. This result was originally derived by Levy [104] based on arguments about asymptotic behaviour of ensemble density. The key difference is that our derivation within the context of extended N-centered eDFT does not rely on asymptotic behaviour of electron density, and as such is not only applicable to finite *ab initio* systems, but also to extended systems and lattice models. This was one of the key results of this chapter, which was applied on the Hubbard dimer in different asymmetry regimes.

In Chapter 8, we presented a single-impurity embedding strategy for two-state TGOK ensembles of ground and singlet excited states. We have shown that, by means of a partial tridiagonalization based on Householder transformations of the

(mean-field or noninteracting) ensemble 1RDM, we can obtain a representation with a strictly decoupled block-diagonal structure consisting of the embedding cluster and its environment, similarly to the regular DMET. The main difference from the latter, where the (single-impurity) embedding cluster contained a single bath spin-orbital, is that in the present case, the embedding cluster has an enlarged bath subspace of three delocalized spin-orbitals, i.e. a single core spin-orbital that overlaps with the impurity, and the two "active" spin-orbitals which are involved in the HOMO-LUMO excitation and are fractionally occupied in the ensemble. Based on this result on the mean-field ensembles, we constructed an embedding Hamiltonian for simultaneously describing locally the ground and excited states of correlated systems. We applied our single-shot embedding strategy to three simple toy systems. We observed that when the ground and first excited state levels of the true (interacting) system are well-separated from higher excited states, and overlap well with mean-field states used in the construction of the embedding cluster, the embedding results of our strategy are in good agreement with the FCI results, even in strongly correlated regimes. On the other hand, when there are crossings among excited-state energy levels, the present strategy may not recover the correct excited state. We closed that chapter with some suggestions for improvement of the method, such as enlarging the ensemble by including excitations beyond the HOMO-LUMO levels, and making the embedding strategy self-consistent by imposing the TGOK ensemble density constraint on localized spin-orbitals. The latter would open a connection of the embedding strategy with TGOK-DFT, which would enable development of implicit density-functional approximations for ensembles in an approach similar to that of LPFET for ground states of Hubbard lattices. Work is in progress in these directions.

As a closing remark, while ensemble DFT shows great potential in describing diverse types of excitations, and has the ability to overcome certain limitations of other more standard approaches, such as linear response methods, there are still many exciting challenges that lie ahead before the ensemble formalism will beget practical methods that are widely used in quantum chemistry and condensed-matter physics.

Appendices

A Second quantization

Electrons are by nature fermions, and as such they obey Pauli's principle if more than one are present in the system. Considering the single-particle Hilbert space $\mathcal{H}_1$ with basis vectors $\{\phi_i(\mathbf{x})\}$, the basis of two-electron Hilbert space $\{\Phi_{ij}(\mathbf{x}_1, \mathbf{x}_2)\}$ should belong to the antisymmetrized tensor product (also known as wedge product) of $\mathcal{H}_1$ with itself,

$$|\Phi_{ij}\rangle = |\phi_i\rangle \wedge |\phi_j\rangle = \frac{1}{\sqrt{2}} \left(|\phi_i\rangle \otimes |\phi_j\rangle - |\phi_j\rangle \otimes |\phi_i\rangle \right) \in \mathcal{H}_1 \, \Lambda \, \mathcal{H}_1. \tag{A.1}$$

In this space, basis vectors where two electrons have the same state are properly set to zero, $|\phi_i\rangle \wedge |\phi_i\rangle = 0$. This can be extended to N-electron systems, where the basis vectors are elements of N-order antisymmetrized tensor product over $\mathcal{H}_1$,

$$|\Phi_{i_1 i_2 \ldots i_N}\rangle = |\phi_{i_1}\rangle \wedge |\phi_{i_2}\rangle \wedge \cdots \wedge |\phi_{i_N}\rangle \in \Lambda^N \mathcal{H}_1. \tag{A.2}$$

Projecting into position-spin basis $\langle \mathbf{x}_1, \mathbf{x}_2, \ldots, \mathbf{x}_N|$ gives the familiar Slater determinants,

$$\begin{aligned} \Phi_{i_1 i_2 \ldots i_N}(\mathbf{x}_1, \mathbf{x}_2, \ldots, \mathbf{x}_N) &= \langle \mathbf{x}_1, \mathbf{x}_2, \ldots, \mathbf{x}_N | \Phi_{i_1 i_2 \ldots i_N} \rangle \\ &= \frac{1}{\sqrt{N!}} \det \left[\{\phi_{i_\alpha}(\mathbf{x}_\beta)\}_{1 \leq \alpha, \beta \leq N} \right]. \end{aligned} \tag{A.3}$$

As we can see, the antisymmetrization procedure quickly becomes very tedious to handle, especially when we are describing systems with large numbers of electrons, or processes with changing numbers of electrons. These problems become easier to handle, if we ask the question: "In a given state, which orbital is occupied, and which is empty?". For this purpose, the idea of second quantization is introduced. Starting from a vacuum state $|vac\rangle$, which is a state with no electrons, addition of a new electron is represented by a quantum operator that "creates" an electron occupying an orbital ϕ_i,

$$|\phi_i\rangle = \hat{c}_i^\dagger \, |vac\rangle \, . \tag{A.4}$$

Adding another electron into another orbital ϕ_j simply means taking product of two creation operators, the end result being an antisymmetrized state,

$$\hat{c}_i^\dagger \hat{c}_j^\dagger \, |vac\rangle = \frac{1}{\sqrt{2}} \left(|\phi_i\rangle \otimes |\phi_j\rangle - |\phi_j\rangle \otimes |\phi_i\rangle \right). \tag{A.5}$$

Continuing this procedure, an N-electron Slater determinant is produced by a string of creation operators,

$$|\Phi_{i_1 i_2 \ldots i_N}\rangle = \hat{c}^\dagger_{i_1} \hat{c}^\dagger_{i_2} \ldots \hat{c}^\dagger_{i_N} |vac\rangle \,. \tag{A.6}$$

In this formalism, removing electrons is done by annihilation operators. Importantly, you cannot destroy an electron if there are none. That means, $\hat{c}_i |vac\rangle = 0$. These operators fulfill the anticommutation relations,

$$\begin{aligned} \left\{ \hat{c}^\dagger_i, \hat{c}^\dagger_j \right\} &= 0, \\ \left\{ \hat{c}_i, \hat{c}_j \right\} &= 0, \\ \left\{ \hat{c}^\dagger_i, \hat{c}_j \right\} &= \delta_{ij}. \end{aligned} \tag{A.7}$$

A similar role is fulfilled by the so-called field operators, which act in real space. Creating (or destroying) an electron with a specified position and spin $|\mathbf{x}\rangle = |\mathbf{r}, \sigma\rangle$ is done by the field operator $\hat{\Psi}^\dagger(\mathbf{x})$ (respectively $\hat{\Psi}(\mathbf{x})$),

$$|\mathbf{x}\rangle = \hat{\Psi}^\dagger(\mathbf{x}) |vac\rangle \,. \tag{A.8}$$

The field operators also obey a set of anticommutation relations,

$$\begin{aligned} \left\{ \hat{\Psi}^\dagger(\mathbf{x}), \hat{\Psi}^\dagger(\mathbf{x}') \right\} &= 0, \\ \left\{ \hat{\Psi}(\mathbf{x}), \hat{\Psi}(\mathbf{x}') \right\} &= 0, \\ \left\{ \hat{\Psi}^\dagger(\mathbf{x}), \hat{\Psi}(\mathbf{x}') \right\} &= \delta(\mathbf{x} - \mathbf{x}'). \end{aligned} \tag{A.9}$$

Conversions between creation/annihilation operators and field operators are easily obtained using completeness relation in orbital and position-spin representation,

$$\begin{aligned} |\phi_i\rangle = \int d\mathbf{x} \, |\mathbf{x}\rangle \, \langle \mathbf{x}|\phi_i\rangle = \int d\mathbf{x} \; |\mathbf{x}\rangle \, \phi_i(\mathbf{x}) = \int d\mathbf{x} \, \phi_i(\mathbf{x}) \, |vac\rangle \\ \iff \boxed{\hat{c}^\dagger_i = \int d\mathbf{x} \phi_i(\mathbf{x}) \hat{\Psi}^\dagger(\mathbf{x})}, \end{aligned} \tag{A.10}$$

$$\begin{aligned} |\mathbf{x}\rangle = \sum_i |\phi_i\rangle \, \langle \phi_i|\mathbf{x}\rangle = \sum_i |\phi_i\rangle \, \phi^*_i(\mathbf{x}) = \sum_i \phi^*_i(\mathbf{x}) \hat{c}^\dagger_i \, |vac\rangle \\ \iff \boxed{\hat{\Psi}^\dagger(\mathbf{x}) = \sum_i \phi^*_i(\mathbf{x}) \hat{c}^\dagger_i}. \end{aligned} \tag{A.11}$$

B Proofs of Hohenberg-Kohn theorems I and II

B.1 Proof of HK1

Proof of HK1, part 1: Suppose that Ψ_0 is simultaneously a ground state for two potentials that differ by more than a constant, $v'_{\rm ext}(\mathbf{r}) - v_{\rm ext}(\mathbf{r}) \neq const.$ If that is true, Ψ_0 is a solution of two different Schrödinger equations,

$$\begin{aligned} \hat{H}[v_{\rm ext}]\,|\Psi_0[v_{\rm ext}]\rangle &= E_0[v_{\rm ext}]\,|\Psi_0[v_{\rm ext}]\rangle\,, \\ \hat{H}[v'_{\rm ext}]\,|\Psi_0[v'_{\rm ext}]\rangle &= E_0[v'_{\rm ext}]\,|\Psi_0[v'_{\rm ext}]\rangle\,. \end{aligned} \tag{B.1}$$

Subtracting the two equations, with our assumption $\Psi_0[v'_{\rm ext}] = \Psi_0[v_{\rm ext}]$ leads to,

$$\left(\hat{H}[v_{\rm ext}] - \hat{H}[v'_{\rm ext}]\right)|\Psi_0[v_{\rm ext}]\rangle = \left(E_0[v_{\rm ext}] - E_0[v'_{\rm ext}]\right)|\Psi_0[v_{\rm ext}]\rangle\,. \tag{B.2}$$

Projecting into the position-spin basis, and subtracting $\hat{T}$ and $\hat{W}_{\rm ee}$ operators gives,

$$\left(\sum_{i=1}^{N}(v_{\rm ext}(\mathbf{r}_i) - v'_{\rm ext}(\mathbf{r}_i)\,) - \left(E_0[v_{\rm ext}] - E_0[v'_{\rm ext}]\right)\right)\Psi_0[v_{\rm ext}](\mathbf{x}_1, \mathbf{x}_2, \ldots, \mathbf{x}_N) = 0. \tag{B.3}$$

For a physical system, $\Psi_0 \neq 0$[3]. Therefore, the quantity inside parentheses has to vanish,

$$\sum_{i=1}^{N}\left(v_{\rm ext}(\mathbf{r}_i) - v'_{\rm ext}(\mathbf{r}_i) - \frac{E_0[v_{\rm ext}] - E_0[v'_{\rm ext}]}{N}\right) = 0, \tag{B.4}$$

which implies,

$$v_{\rm ext}(\mathbf{r}) - v'_{\rm ext}(\mathbf{r}) = \frac{E_0[v_{\rm ext}] - E_0[v'_{\rm ext}]}{N} = const. \tag{B.5}$$

Since this result contradicts our initial assumption, it must follow that $v'_{\rm ext}(\mathbf{r}) \neq v_{\rm ext}(\mathbf{r}) + const.$ implies $\Psi_0[v'_{\rm ext}] \neq \Psi_0[v_{\rm ext}]$.

Proof of HKI, part 2: Assume that the two different ground states, $\Psi_0[v_{\rm ext}]$ and $\Psi_0[v'_{\rm ext}]$ integrate to the same density, $n_{\Psi_0[v_{\rm ext}]} = n_{\Psi_0[v'_{\rm ext}]}$. Then, according to the variational principle,

$$E_0[v_{\rm ext}] = \langle\Psi_0[v_{\rm ext}]|\hat{H}|\Psi_0[v_{\rm ext}]\rangle < \langle\Psi_0[v'_{\rm ext}]|\hat{H}|\Psi_0[v'_{\rm ext}]\rangle. \tag{B.6}$$

[3]Except possibly on a set of measure zero. This includes all coordinates with coinciding electrons $\mathbf{x}_i = \mathbf{x}_j$, which is still vanishingly small compared to all possible position-spin coordinates. This assertion becomes problematic in a finite basis, or in lattice systems, where we can find two potentials that differ by more than a constant, but still giving the same ground state, thereby violating the HKI theorem [363].

The right-hand side can be developed further as,

$$\begin{aligned}\langle\Psi_0[v'_{\rm ext}]|\hat{H}|\Psi_0[v'_{\rm ext}]\rangle &= \langle\Psi_0[v'_{\rm ext}]|\hat{H}'|\Psi_0[v'_{\rm ext}]\rangle + \langle\Psi_0[v'_{\rm ext}]|\hat{V}_{\rm ext} - \hat{V}'_{\rm ext}|\Psi_0[v'_{\rm ext}]\rangle \\ &= E_0[v'_{\rm ext}] + \int d\mathbf{r}\, n_{\Psi_0[v_{\rm ext}]}(\mathbf{r})\left(v_{\rm ext}(\mathbf{r}) - v'_{\rm ext}(\mathbf{r})\right).\end{aligned} \tag{B.7}$$

Combining Eqs. (B.6) and (B.7) gives

$$E_0[v_{\rm ext}] < E_0[v'_{\rm ext}] + \int d\mathbf{r}\, n_{\Psi_0[v_{\rm ext}]}(\mathbf{r})\left(v_{\rm ext}(\mathbf{r}) - v'_{\rm ext}(\mathbf{r})\right). \tag{B.8}$$

Given our assumptions, the above inequality should be valid if we interchange primed (') and unprimed quantities. Adding the two versions together leads to the contradiction,

$$E_0[v_{\rm ext}] + E_0[v'_{\rm ext}] < E_0[v'_{\rm ext}] + E_0[v_{\rm ext}]. \tag{B.9}$$

Hence, we are left with the conclusion that if $v'_{\rm ext}(\mathbf{r}) \neq v_{\rm ext}(\mathbf{r}) + const.$, the ground-state densities of the two Hamiltonians are different, $n_{\Psi_0[v_{\rm ext}]} \neq n_{\Psi_0[v'_{\rm ext}]}$.

B.2 Proof of HKII

According to HKI part 2, for any *ground-state density* $n(\mathbf{r})$, the ground state $\Psi[n]$ is uniquely defined. Then, for any external potential $v_{\rm ext}(\mathbf{r})$, the HK energy functional (Eq. (1.91)) satisfies the variational principle,

$$\begin{aligned}E_{\rm HK}[v_{\rm ext}, n] &= F_{\rm HK}[n] + \int d\mathbf{r}\, v_{\rm ext}(\mathbf{r}) n(\mathbf{r}) \\ &= \langle\Psi[n]|\hat{T} + \hat{W}_{\rm ee}|\Psi[n]\rangle + \int d\mathbf{r}\, v_{\rm ext}(\mathbf{r}) n(\mathbf{r}) \\ &= \langle\Psi[n]|\hat{H}[v_{\rm ext}]|\Psi[n]\rangle \\ &\geq \langle\Psi_0[v_{\rm ext}]|\hat{H}[v_{\rm ext}]|\Psi_0[v_{\rm ext}]\rangle = E_0[v_{\rm ext}].\end{aligned} \tag{B.10}$$

When $n = n_{\Psi_0[v_{\rm ext}]}$, $\Psi[n] = \Psi_0[v_{\rm ext}]$, and

$$E_{\rm HK}[v_{\rm ext}, n_{\Psi_0[v_{\rm ext}]}] = E_0[v_{\rm ext}]. \tag{B.11}$$

C Functions, Functionals and calculus of variations

This appendix is to some extent influenced by Appendix A in the book *Density Functional Theory: An Advanced Course* by E. Engel and R. Dreizler [159].

C.1 From functions to functionals

To build the intuition on functionals, it is best to look at functions first. A multivariable function $f(\mathbf{r}) = f(x_1, x_2, \ldots, x_N)$ is a mapping $f : \mathcal{D}_f \in \mathbb{R}^N \to \mathbb{R}$ that takes as argument a discrete set of variables $\{x_i\}_{1\leq i\leq n}$ and outputs a number. The behaviour of a function around some point $\mathbf{r}_0$ in the direction of $\mathbf{v}$ can be assessed by the Taylor expansion,

$$f(\mathbf{r}_0 + \varepsilon\mathbf{v}) = f(\mathbf{r}_0) \; + \; \varepsilon \left.\frac{df(\mathbf{r}_0+\varepsilon\mathbf{v})}{d\varepsilon}\right|_{\varepsilon=0} \; + \; \frac{1}{2}\varepsilon^2 \left.\frac{d^2 f(\mathbf{r}_0+\varepsilon\mathbf{v})}{d\varepsilon^2}\right|_{\varepsilon=0} + \mathcal{O}(\varepsilon^3), \quad \text{(C.1)}$$

where

$$\left.\frac{df(\mathbf{r}_0+\varepsilon\mathbf{v})}{d\varepsilon}\right|_{\varepsilon=0} = \sum_{i=1}^{N} v_i \left.\frac{\partial f(\mathbf{r})}{\partial x_i}\right|_{\mathbf{r}=\mathbf{r}_0} = \mathbf{v}^{\mathrm{T}}\,\nabla f(\mathbf{r}_0) \quad \text{(C.2)}$$

and

$$\left.\frac{d^2 f(\mathbf{r}_0+\varepsilon\mathbf{v})}{d\varepsilon^2}\right|_{\varepsilon=0} = \sum_{i=1}^{N}\sum_{j=1}^{N} v_i v_j \left.\frac{\partial^2 f(\mathbf{r})}{\partial x_i \partial x_j}\right|_{\mathbf{r}=\mathbf{r}_0} = \mathbf{v}^{\mathrm{T}}\,\mathbf{H}_f(\mathbf{r}_0)\,\mathbf{v} \quad \text{(C.3)}$$

$\nabla f(\mathbf{r})$ and $\mathbf{H}_f(\mathbf{r})$ are the gradient and Hessian of f.

C.1.1 Practical example: Energy optimization in Hartree-Fock theory

In the section on HF theory, we have seen that the HF energy can be obtained variationally by orbital rotation. In practice, this may be done by the Newton method (see, for example, Ref. [28]). Starting with a trial set of orbital rotation parameters, $\boldsymbol{\kappa} = \{\kappa_{ij}\}_{i>j}$, the energy is expanded up to second order as,

$$E^{\mathrm{HF}}(\boldsymbol{\kappa}) = E^{\mathrm{HF}}(\boldsymbol{\kappa}=0) + \boldsymbol{\kappa}^{\mathrm{T}}\,E^{[1]} + \frac{1}{2}\boldsymbol{\kappa}^{\mathrm{T}} E^{[2]}\boldsymbol{\kappa}, \quad \text{(C.4)}$$

where $E^{[1]} = \nabla E^{\mathrm{HF}}(\boldsymbol{\kappa}=0)$ and $E^{[2]} = \mathbf{H}_{E^{\mathrm{HF}}}(\boldsymbol{\kappa}=0)$. Approximate stationary points $\boldsymbol{\kappa}^{+}$ may be obtained by finding the roots of first derivative of Eq. (C.4) with respect to $\boldsymbol{\kappa}$, which amounts to solving a system of linear equations,

$$E^{[2]}\boldsymbol{\kappa}^{+} = -E^{[1]}. \quad \text{(C.5)}$$

One can then solve the above system repeatedly to obtain new steps $\boldsymbol{\kappa}^+$ until convergence when $E^{[1]} = 0$.

C.2 Functional and functional derivative

Similarly to multivariable functions which map vectors to numbers, *functionals* map functions to numbers. Consider now a function $f : [a, b] \in \mathbb{R} \to \mathbb{R}$. We define a functional $F[f]$, which takes as input the values of f on its whole domain, and outputs a number. We can also do calculus with functionals. By taking a small variation η around f, subject to certain boundary conditions[4], the functional F at $f + \varepsilon\eta$ can be Taylor-expanded about $\varepsilon = 0$ as,

$$F[f + \varepsilon\eta] = F[f] + \varepsilon \left.\frac{dF[f + \varepsilon\eta]}{d\varepsilon}\right|_{\varepsilon=0} + \frac{1}{2}\varepsilon^2 \left.\frac{d^2F[f + \varepsilon\eta]}{d\varepsilon^2}\right|_{\varepsilon=0} + \mathcal{O}(\varepsilon^3). \tag{C.6}$$

The second term is then defined as functional derivative of F,

$$\left.\frac{dF[f + \varepsilon\eta]}{d\varepsilon}\right|_{\varepsilon=0} = \lim_{\varepsilon\to 0} \frac{F[f + \varepsilon\eta] - F[f]}{\varepsilon} = \int_a^b dx\, \eta(x) \frac{\delta F[f]}{\delta f(x)}. \tag{C.7}$$

Leaving out precise mathematical details regarding this definition[5], the sought after quantity is the linear operator $\delta F/\delta f$, which is what is usually called "functional derivative" in physical applications. Similarly, the second-order functional derivative is defined as,

$$\left.\frac{d^2F[f + \varepsilon\eta]}{d\varepsilon^2}\right|_{\varepsilon=0} = \int_a^b dx \int_a^b dx'\, \eta(x)\eta(x') \frac{\delta^2 F[f]}{\delta f(x)\delta f(x')}. \tag{C.8}$$

Eqs. (C.7) and (C.8) can be seen as continuous analogues of Eqs. (C.2) and (C.3), respectively, with $\delta F/\delta f$ looking like continuous version of gradient, and $\delta^2 F/\delta f \delta f$ the "continuous Hessian".

C.2.1 Some identities of functional differentiation

1. Chain rule: If F is a functional of G, which in turn is a functional of f, then the functional derivative of F with respect to f is obtained by,

$$\frac{\delta F[G[f]]}{\delta f(x)} = \int dx' \left.\frac{\delta F[G]}{\delta G(x')}\right|_{G=G[f]} \frac{\delta G[f]}{\delta f(x)}. \tag{C.9}$$

[4]Usually, boundary conditions for the "direction" η, such as fixed endpoints $\eta(a) = \eta(b)$ are required, so that a stationarity condition for $F[f]$ can be found. This is in contrast to differentiating a regular function $f(\mathbf{r})$, where any direction $\mathbf{v}$ may be taken.

[5]The definition in Eq. (C.7) as also known as *Gateaux derivative* in calculus of variations.

2. Regular function: If F is just a function of x, i.e. $F = f(x)$, the functional derivative becomes Dirac delta function

$$f(x) = \int dx \delta(x' - x) f(x'), \tag{C.10}$$

$$\frac{\delta F}{\delta f(x')} = \frac{\delta f(x)}{\delta f(x')} = \delta(x' - x). \tag{C.11}$$

C.2.2 Example: Hartree functional

Consider the Hartee functional (Eq. (1.105)) from DFT. Plugging in a density with small variation $n + \varepsilon\eta$ gives

$$\begin{aligned} E_{\mathrm{H}}[n + \varepsilon\eta] &= \frac{1}{2} \int d\mathbf{r} \int d\mathbf{r}' \, \frac{[n(\mathbf{r}) + \varepsilon\eta(\mathbf{r})][n(\mathbf{r}') + \varepsilon\eta(\mathbf{r}')]}{|\mathbf{r} - \mathbf{r}'|} \\ &= E_{\mathrm{H}}[n] \\ &+ \varepsilon \int d\mathbf{r} \, \eta(\mathbf{r}) \left(\int d\mathbf{r}' \, \frac{n(\mathbf{r}')}{|\mathbf{r} - \mathbf{r}'|} \right) \\ &+ \frac{1}{2} \varepsilon^2 \int d\mathbf{r} \int d\mathbf{r}' \, \eta(\mathbf{r}) \eta(\mathbf{r}') \frac{1}{|\mathbf{r} - \mathbf{r}'|}. \end{aligned} \tag{C.12}$$

From the different terms in ε, we can easily identify the first and second-order derivative of $E_{\mathrm{H}}[n]$, which in DFT are known as Hartree potential and kernel, respectively,

$$v_{\mathrm{H}}[n](\mathbf{r}) \equiv \frac{\delta E_{\mathrm{H}}[n]}{\delta n(\mathbf{r})} = \int d\mathbf{r}' \, \frac{n(\mathbf{r}')}{|\mathbf{r} - \mathbf{r}'|}, \tag{C.13}$$

$$f_{\mathrm{H}}[n](\mathbf{r}, \mathbf{r}') \equiv \frac{\delta E_{\mathrm{H}}[n]}{\delta n(\mathbf{r}) \delta n(\mathbf{r}')} = \frac{1}{|\mathbf{r} - \mathbf{r}'|}. \tag{C.14}$$

D Fourier transform

In Chapter 3, we use on several occasions the following Fourier transforms to switch between the time and frequency domains,

$$f(\omega) = \int_{-\infty}^{\infty} d\tau f(\tau) e^{i\omega\tau} \qquad f(\tau) = \frac{1}{2\pi} \int_{-\infty}^{\infty} d\tau f(\omega) e^{-i\omega\tau}. \tag{D.1}$$

For example, in TF-DFT (Section 3.1), in order to transition from the linear response function in the time domain, $\chi(\mathbf{r}, \mathbf{r}', \tau)$, to the same function in the frequency domain, $\chi(\mathbf{r}, \mathbf{r}', \omega)$, we need to evaluate integrals like,

$$-i \int_{-\infty}^{\infty} d\tau \theta(\tau) e^{i(\omega-\omega_I)\tau}. \tag{D.2}$$

Unfortunately, the above integral does not converge if we try to evaluate it directly. A popular trick in physics is to replace $\theta(\tau)$ with an η-dependent sequence of functions $\theta_\eta(\tau)$ that limit to $\theta(\tau)$ as $\eta \to 0^+$,

$$\theta_\eta(\tau) = \begin{cases} e^{-\eta\tau} & \tau \geq 0 \\ \\ 0 & \tau < 0 \end{cases}, \tag{D.3}$$

which does the job of converging the integral in Eq. (D.2),

$$\begin{aligned} &\lim_{\eta\to 0^+} -i \int_{-\infty}^{\infty} d\tau \theta_\eta(\tau) e^{i(\omega-\omega_I)\tau} \\ &= -i \lim_{\eta\to 0^+} \int_{0}^{\infty} d\tau e^{i(\omega-\omega_I+i\eta)\tau} \\ &= -i \frac{-1}{i(\omega-\omega_I+i0^+)} = \frac{1}{\omega-\omega_I+i0^+}. \end{aligned} \tag{D.4}$$

E Asymptotic behavior of the xc potential

This appendix is equivalent to Appendix A in the book chapter "Ensemble density functional theory of neutral and charged excitations" [92].

Let us consider the simpler one-dimensional (1D) case in which the KS-PPLB equations read as

$$-\frac{1}{2}\frac{d^2\varphi_i^\alpha(x)}{dx^2} + \left(v_{\text{ext}}(x) + v_{\text{Hxc}}^\alpha(x)\right)\varphi_i^\alpha(x) = \varepsilon_i^\alpha \varphi_i^\alpha(x), \tag{E.1}$$

thus leading to

$$\frac{d^2\varphi_i^\alpha(x)}{dx^2} \underset{|x|\to+\infty}{=} -2\left(\varepsilon_i^\alpha - v_{\text{xc}}^\alpha(\infty)\right)\varphi_i^\alpha(x), \tag{E.2}$$

where we used the limits $v_{\text{ext}}(\infty) = v_{\text{H}}^\alpha(\infty) = 0$. Note that $|\varphi_i^\alpha(x)|$ is expected to decay as $|x| \to +\infty$, which implies $-2\left(\varepsilon_i^\alpha - v_{\text{xc}}^\alpha(\infty)\right) > 0$. Therefore,

$$\varphi_i^\alpha(x) \underset{|x|\to+\infty}{\sim} e^{-\sqrt{-2(\varepsilon_i^\alpha - v_{\text{xc}}^\alpha(\infty))}|x|}, \tag{E.3}$$

and

$$n_{\hat{\gamma}_{\text{KS}}^\alpha}(x) \underset{|x|\to+\infty}{\sim} \alpha|\varphi_N^\alpha(x)|^2 \sim \alpha\, e^{-2\sqrt{-2(\varepsilon_N^\alpha - v_{\text{xc}}^\alpha(\infty))}|x|}. \tag{E.4}$$

In the true interacting system, the N-electron ground-state wave function Ψ_0^N fulfills

$$\begin{aligned}&\left[\sum_{i=1}^N\left(-\frac{1}{2}\frac{\partial^2}{\partial x_i^2} + v_{\text{ext}}(x_i)\right) + \sum_{1\le i<j}^N w_{\text{ee}}(|x_i - x_j|)\right]\Psi_0^N(x_1,\ldots,x_N)\\ &= E_0^N\Psi_0^N(x_1,\ldots,x_N),\end{aligned} \tag{E.5}$$

where $w_{\text{ee}}(|x_i - x_j|)$ is a well-behaved two-electron repulsion energy in 1D. Let us consider the situation where $|x_1| \to +\infty$ while $x_2,\ldots,x_N$ remain in the region of the system, which corresponds to an ionization process in the ground state. Since $w_{\text{ee}}(|x_1 - x_j|) \to 0$, the (to-be-antisymmetrized) wave function and its density can be rewritten as

$$\Psi_0^N(x_1,\ldots,x_N) \underset{|x_1|\to+\infty}{\sim} \varphi^{[N]}(x_1)\,\Psi_0^{N-1}(x_2,\ldots,x_N) \tag{E.6}$$

and

$$n_{\Psi_0^N}(x_1) \underset{|x_1|\to+\infty}{\sim} \left|\varphi^{[N]}(x_1)\right|^2, \tag{E.7}$$

respectively, where

$$\frac{d^2\varphi^{[N]}(x_1)}{dx_1^2} \underset{|x_1|\to+\infty}{\sim} -2\left(E_0^N - E_0^{N-1}\right)\varphi^{[N]}(x_1) = 2I_0^N\varphi^{[N]}(x_1), \tag{E.8}$$

thus leading to the explicit expression

$$\varphi^{[N]}(x) \underset{|x|\to+\infty}{\sim} e^{-\sqrt{2I_0^N}|x|}. \tag{E.9}$$

From the exact mapping of the ensemble PPLB density onto the KS system, we deduce from Eqs. (E.7) and (E.9) that

$$n_{\hat{\gamma}^\alpha_{\rm KS}}(x) \underset{|x|\to+\infty}{\sim} (1-\alpha)e^{-2\sqrt{2I_0^{N-1}}|x|} + \alpha\, e^{-2\sqrt{2I_0^N}|x|} \sim \alpha\, e^{-2\sqrt{2I_0^N}|x|}, \tag{E.10}$$

where we assumed that $E_g^{N-1} = I_0^{N-1} - I_0^N > 0$. Thus, we conlude from Eq. (E.4) that

$$I_0^N = -(\varepsilon_N^\alpha - v_{\rm xc}^\alpha(\infty)). \tag{E.11}$$

Any constant shift in the xc potential $v_{\rm xc}^\alpha(\mathbf{r})$ does not affect the above expression. Since, according to Janak's theorem, $I_0^N = -\varepsilon_N^\alpha$, the constant is imposed in PPLB and

$$v_{\rm xc}^\alpha(\infty) = 0. \tag{E.12}$$

We now turn to the left and right formulations of N-centered eDFT. We recall the shorthand notations $(\xi_-, 0) \overset{notation}{\equiv} \xi_-$ and $(0, \xi_+) \overset{notation}{\equiv} \xi_+$. When $\xi_+ > 0$, the right N-centered ensemble density, which is mapped onto a non-interacting KS ensemble, has the following asymptotic behavior [we just need to substitute $N+1$ for N in Eqs. (E.4), (E.7), and (E.9)],

$$n^{\xi_+}(x) \underset{|x|\to+\infty}{\sim} \xi_+\, e^{-2\sqrt{2I_0^{N+1}}|x|} \tag{E.13}$$

$$\sim \xi_+\, e^{-2\sqrt{-2(\varepsilon_{N+1}^{\xi_+} - v_{\rm xc}^{\xi_+}(\infty))}|x|}. \tag{E.14}$$

Similarly, for $\xi_- \geq 0$, we have

$$n^{\xi_-}(x) \underset{|x|\to+\infty}{\sim} \left(1 - \frac{(N-1)\xi_-}{N}\right) e^{-2\sqrt{2I_0^N}|x|} \tag{E.15}$$

$$\sim \left(1 - \frac{(N-1)\xi_-}{N}\right) e^{-2\sqrt{-2(\varepsilon_N^{\xi_-} - v_{\rm xc}^{\xi_-}(\infty))}|x|}. \tag{E.16}$$

Thus, we conclude that

$$A_0^N = I_0^{N+1} \overset{\xi_+ > 0}{=} -\varepsilon_{N+1}^{\xi_+} + v_{\mathrm{xc}}^{\xi_+}(\infty) \tag{E.17}$$

and

$$I_0^N \overset{\xi_- \geq 0}{=} -\varepsilon_N^{\xi_-} + v_{\mathrm{xc}}^{\xi_-}(\infty). \tag{E.18}$$

F Exact DD ensemble correlation energy in the Hubbard dimer

This appendix is equivalent to Appendix D in the book chapter "Ensemble density functional theory of neutral and charged excitations" [92].

For convenience, we will use the following exact expression for the ensemble DD correlation energy:

$$E_{\rm c}^{\mathtt{w},\rm DD}(n^{\mathtt{w}}) = -(1-\mathtt{w})^2\mathtt{w}\frac{\partial f_0^{\mathtt{w}}(n^{\mathtt{w}})}{\partial \mathtt{w}} + \mathtt{w}^2(1-\mathtt{w})\frac{\partial f_1^{\mathtt{w}}(n^{\mathtt{w}})}{\partial \mathtt{w}}. \tag{F.1}$$

The individual Hx-only GOK energies are extracted from the ensemble one,

$$f^{\xi}(n) = \; -2t\sqrt{(1-\xi)^2-(1-n)^2} + \frac{U}{2}\left[1+\xi-\frac{(3\xi-1)(1-n)^2}{(1-\xi)^2}\right], \tag{F.2}$$

as follows,

$$f_0^{\mathtt{w}}\left(n^{\mathtt{w}}\right) \;=\; f^{\mathtt{w}}\left(n^{\mathtt{w}}\right) - \mathtt{w}\left.\frac{\partial f^{\xi}\left(n^{\xi,\mathtt{w}}\right)}{\partial \xi}\right|_{\xi=\mathtt{w}}, \tag{F.3}$$

and

$$f_1^{\mathtt{w}}\left(n^{\mathtt{w}}\right) \;=\; f^{\mathtt{w}}\left(n^{\mathtt{w}}\right) + (1-\mathtt{w})\left.\frac{\partial f^{\xi}\left(n^{\xi,\mathtt{w}}\right)}{\partial \xi}\right|_{\xi=\mathtt{w}}, \tag{F.4}$$

where

$$n^{\xi,\mathtt{w}} = (1-\xi)n_{\Phi_0^{\mathtt{w}}} + \xi n_{\Phi_1^{\mathtt{w}}}. \tag{F.5}$$

Since $n_{\Phi_1^{\mathtt{w}}} = 1$ and

$$(1-\mathtt{w})n_{\Phi_0^{\mathtt{w}}} + \mathtt{w}n_{\Phi_1^{\mathtt{w}}} = n^{\mathtt{w}}, \tag{F.6}$$

or, equivalently,

$$n_{\Phi_0^{\mathtt{w}}} = \frac{n^{\mathtt{w}}-\mathtt{w}}{(1-\mathtt{w})}, \tag{F.7}$$

it comes

$$n^{\xi,\mathtt{w}} = (1-\xi)\frac{(n^{\mathtt{w}}-\mathtt{w})}{1-\mathtt{w}} + \xi \tag{F.8}$$

and

$$\left.\frac{\partial n^{\xi,\mathtt{w}}}{\partial \xi}\right|_{\xi=\mathtt{w}} = 1 - \frac{(n^{\mathtt{w}}-\mathtt{w})}{1-\mathtt{w}} = \frac{1-n^{\mathtt{w}}}{1-\mathtt{w}}. \tag{F.9}$$

From the weight derivative expression

$$\left.\frac{\partial f^{\xi}\left(n^{\xi,\mathtt{w}}\right)}{\partial \xi}\right|_{\xi=\mathtt{w}} = \left.\frac{\partial f^{\xi}(n^{\mathtt{w}})}{\partial \xi}\right|_{\xi=\mathtt{w}} + \left.\frac{\partial n^{\xi,\mathtt{w}}}{\partial \xi}\right|_{\xi=\mathtt{w}} \times \left.\frac{\partial f^{\mathtt{w}}(n)}{\partial n}\right|_{n=n^{\mathtt{w}}}, \tag{F.10}$$

where

$$\frac{\partial f^{\xi}(n)}{\partial \xi} = \frac{2t(1-\xi)}{\sqrt{(1-\xi)^2-(1-n)^2}} + \frac{U}{2}\left[1 - \frac{(n-1)^2(1+3\xi)}{(1-\xi)^3}\right] \tag{F.11}$$

and

$$\frac{\partial f^{\mathtt{w}}(n)}{\partial n} = \frac{2t(n-1)}{\sqrt{(1-\mathtt{w})^2-(1-n)^2}} + U\frac{(3\mathtt{w}-1)(1-n)}{(1-\mathtt{w})^2}, \tag{F.12}$$

thus leading to

$$\begin{aligned}\left.\frac{\partial f^{\xi}\left(n^{\xi,\mathtt{w}}\right)}{\partial \xi}\right|_{\xi=\mathtt{w}} = &\frac{2t(1-\mathtt{w})}{\sqrt{(1-\mathtt{w})^2-(1-n^{\mathtt{w}})^2}} \\ &- \frac{2t(1-n^{\mathtt{w}})^2}{(1-\mathtt{w})\sqrt{(1-\mathtt{w})^2-(1-n^{\mathtt{w}})^2}} \\ &+ \frac{U}{2}\left[1 - \frac{(n^{\mathtt{w}}-1)^2(1+3\mathtt{w})}{(1-\mathtt{w})^3}\right] \\ &+ U\frac{(3\mathtt{w}-1)(1-n^{\mathtt{w}})^2}{(1-\mathtt{w})^3},\end{aligned} \tag{F.13}$$

or, equivalently,

$$\left.\frac{\partial f^{\xi}\left(n^{\xi,\mathtt{w}}\right)}{\partial \xi}\right|_{\xi=\mathtt{w}} = \frac{2t\sqrt{(1-\mathtt{w})^2-(1-n^{\mathtt{w}})^2}}{(1-\mathtt{w})} + \frac{U}{2}\left[1 - \frac{3(1-n^{\mathtt{w}})^2}{(1-\mathtt{w})^2}\right], \tag{F.14}$$

it comes

$$f_0^{\mathtt{w}}\left(n^{\mathtt{w}}\right) = -\frac{2t\sqrt{(1-\mathtt{w})^2-(1-n^{\mathtt{w}})^2}}{(1-\mathtt{w})} + \frac{U}{2}\left[1 + \frac{(1-n^{\mathtt{w}})^2}{(1-\mathtt{w})^2}\right] \tag{F.15}$$

and

$$f_1^{\mathtt{w}}\left(n^{\mathtt{w}}\right) = U\left[1 - \frac{(1-n^{\mathtt{w}})^2}{(1-\mathtt{w})^2}\right]. \tag{F.16}$$

As a result,

$$\frac{\partial f_0^{\mathtt{w}}(n^{\mathtt{w}})}{\partial \mathtt{w}} = \frac{2t(n^{\mathtt{w}}-1)(n_{\Psi_1}-1)}{(1-\mathtt{w})^2\sqrt{(1-\mathtt{w})^2-(1-n^{\mathtt{w}})^2}} + U\frac{(n^{\mathtt{w}}-1)(n_{\Psi_1}-1)}{(1-\mathtt{w})^3} \tag{F.17}$$

and

$$\frac{\partial f_1^{\mathtt{w}}(n^{\mathtt{w}})}{\partial \mathtt{w}} = -\frac{2U(n^{\mathtt{w}}-1)(n_{\Psi_1}-1)}{(1-\mathtt{w})^3}, \tag{F.18}$$

which leads, according to Eq. (F.1), to the final compact expression

$$\begin{aligned}E_{\mathrm{c}}^{\mathtt{w},\mathrm{DD}}(n^{\mathtt{w}}) = &-\mathtt{w}(n^{\mathtt{w}}-1)(n_{\Psi_1}-1) \\ &\times\left[\frac{2t}{\sqrt{(1-\mathtt{w})^2-(1-n^{\mathtt{w}})^2}} + \frac{U(1+\mathtt{w})}{(1-\mathtt{w})^2}\right].\end{aligned} \tag{F.19}$$

Bibliography

[1] Runge, E.; Gross, E. K. U. Density-Functional Theory for Time-Dependent Systems. *Phys. Rev. Lett.* **1984**, *52*, 997–1000.

[2] Casida, M.; Huix-Rotllant, M. Progress in Time-Dependent Density-Functional Theory. *Annu. Rev. Phys. Chem.* **2012**, *63*, 287–323, PMID: 22242728.

[3] Hedin, L. New Method for Calculating the One-Particle Green's Function with Application to the Electron-Gas Problem. *Phys. Rev.* **1965**, *139*, A796–A823.

[4] Aryasetiawan, F.; Gunnarsson, O. The GW method. *Rep. Prog. Phys.* **1998**, *61*, 237.

[5] Holm, B.; von Barth, U. Fully self-consistent GW self-energy of the electron gas. *Phys. Rev. B* **1998**, *57*, 2108–2117.

[6] García-González, P.; Godby, R. W. Self-consistent calculation of total energies of the electron gas using many-body perturbation theory. *Phys. Rev. B* **2001**, *63*, 075112.

[7] Salpeter, E. E.; Bethe, H. A. A Relativistic Equation for Bound-State Problems. *Phys. Rev.* **1951**, *84*, 1232–1242.

[8] Strinati, G. Application of the Green's functions method to the study of the optical properties of semiconductors. *Riv. del Nuovo Cim.* **1988**, *11*, 1–86.

[9] Martin, R. M.; Reining, L.; Ceperley, D. M. *Interacting Electrons: Theory and Computational Approaches*; Cambridge University Press, 2016.

[10] Casida, M. E. In *Recent Advances in Density Functional Methods*; Chong, D. P., Ed.; World Scientific, 1995; Vol. 1; pp 155–192.

[11] Kohn, W.; Sham, L. J. Self-Consistent Equations Including Exchange and Correlation Effects. *Phys. Rev.* **1965**, *140*, A1133–A1138.

[12] Blase, X.; Duchemin, I.; Jacquemin, D.; Loos, P.-F. The Bethe–Salpeter Equation Formalism: From Physics to Chemistry. *J. Phys. Chem. Lett.* **2020**, *11*, 7371–7382, PMID: 32787315.

[13] Roos, B. O.; Taylor, P. R.; Sigbahn, P. E. A complete active space SCF method (CASSCF) using a density matrix formulated super-CI approach. *Chem. Phys.* **1980**, *48*, 157–173.

[14] Werner, H.; Meyer, W. A quadratically convergent MCSCF method for the simultaneous optimization of several states. *J. Chem. Phys.* **1981**, *74*, 5794–5801.

[15] Knizia, G.; Chan, G. K.-L. Density Matrix Embedding: A Simple Alternative to Dynamical Mean-Field Theory. *Phys. Rev. Lett.* **2012**, *109*, 186404.

[16] Knizia, G.; Chan, G. K.-L. Density Matrix Embedding: A Strong-Coupling Quantum Embedding Theory. *J. Chem. Theory Comput.* **2013**, *9*, 1428–1432, PMID: 26587604.

[17] Wouters, S.; Jiménez-Hoyos, C. A.; Sun, Q.; Chan, G. K.-L. A Practical Guide to Density Matrix Embedding Theory in Quantum Chemistry. *J. Chem. Theory Comput.* **2016**, *12*, 2706–2719, PMID: 27159268.

[18] Householder, A. S. Unitary Triangularization of a Nonsymmetric Matrix. *J. ACM* **1958**, *5*, 339–342.

[19] Burden, R.; Faires, J. *Numerical Analysis. 9th Edition*; Brookscole: Boston, 2011; pp 593–597.

[20] Born, M.; Oppenheimer, R. Zur Quantentheorie der Molekeln. *Annalen der Physik* **1927**, *389*, 457–484.

[21] Pauli, W. In *Writings on Physics and Philosophy*; Enz, C. P., von Meyenn, K., Eds.; Springer Berlin Heidelberg, 1994; pp 165–181.

[22] Slater, J. C. Note on Hartree's Method. *Phys. Rev.* **1930**, *35*, 210–211.

[23] Fock, V. *Z. Phys.* **1930**, *61*, 126–148.

[24] Roothaan, C. C. J. New developments in molecular orbital theory. *Rev. Mod. Phys.* **1951**, *23*, 69.

[25] Hall, G. The molecular orbital theory of chemical valency VIII. A method of calculating ionization potentials. *Proceedings of the Royal Society of London. Series A. Mathematical and Physical Sciences* **1951**, *205*, 541–552.

[26] Löwdin, P.-O. Quantum Theory of Many-Particle Systems. III. Extension of the Hartree-Fock Scheme to Include Degenerate Systems and Correlation Effects. *Phys. Rev.* **1955**, *97*, 1509–1520.

[27] Azadi, S.; Singh, R.; Kühne, T. D. Resonating valence bond quantum Monte Carlo: Application to the ozone molecule. *Int. J. Quantum Chem.* **2015**, *115*, 1673–1677.

[28] Helgaker, T.; Jørgensen, P.; Olsen, J. *Molecular Electronic-Structure Theory*; John Wiley Sons, 2014.

[29] Olsen, J.; Roos, B. O.; Jo/rgensen, P.; Jensen, H. J. A. Determinant based configuration interaction algorithms for complete and restricted configuration interaction spaces. *J. Chem. Phys.* **1988**, *89*, 2185–2192.

[30] Jensen, H. J. A.; Jørgensen, P.; Helgaker, T.; Olsen, J. Accurate calculations of the dynamic dipole polarizability of N2. A multiconfigurational linear response study using restricted active space (RAS) wavefunctions. *Chem. Phys. Lett.* **1989**, *162*, 355–360.

[31] Malmqvist, P. A.; Rendell, A.; Roos, B. O. The restricted active space self-consistent-field method, implemented with a split graph unitary group approach. *J. Phys. Chem.* **1990**, *94*, 5477–5482.

[32] Andersson, K.; Malmqvist, P.; Roos, B. O. Second-order perturbation theory with a complete active space self-consistent field reference function. *J. Chem. Phys.* **1992**, *96*, 1218–1226.

[33] Angeli, C.; Cimiraglia, R.; Evangelisti, S.; Leininger, T.; Malrieu, J.-P. Introduction of n-electron valence states for multireference perturbation theory. *J. Chem. Phys.* **2001**, *114*, 10252–10264.

[34] Angeli, C.; Cimiraglia, R.; Malrieu, J.-P. N-electron valence state perturbation theory: a fast implementation of the strongly contracted variant. *Chem. Phys. Lett.* **2001**, *350*, 297–305.

[35] Angeli, C.; Cimiraglia, R.; Malrieu, J.-P. n-electron valence state perturbation theory: A spinless formulation and an efficient implementation of the strongly contracted and of the partially contracted variants. *J. Chem. Phys.* **2002**, *117*, 9138–9153.

[36] Buenker, R. J.; Peyerimhoff, S. D. Individualized configuration selection in CI calculations with subsequent energy extrapolation. *Theor. Chim. Acta* **1974**, *35*, 33–58.

[37] Buenker, R. J.; Peyerimhoff, S. D.; Butscher, W. Applicability of the multi-reference double-excitation CI (MRD-CI) method to the calculation of electronic wavefunctions and comparison with related techniques. *Mol. Phys.* **1978**, *35*, 771–791.

[38] Werner, H.; Knowles, P. J. An efficient internally contracted multiconfiguration–reference configuration interaction method. *J. Chem. Phys.* **1988**, *89*, 5803–5814.

[39] Jeziorski, B.; Monkhorst, H. J. Coupled-cluster method for multideterminantal reference states. *Phys. Rev. A* **1981**, *24*, 1668–1681.

[40] MAHAPATRA, U. S.; DATTA, B.; MUKHERJEE, D. A state-specific multi-reference coupled cluster formalism with molecular applications. *Mol. Phys.* **1998**, *94*, 157–171.

[41] Mahapatra, U. S.; Datta, B.; Mukherjee, D. A size-consistent state-specific multireference coupled cluster theory: Formal developments and molecular applications. *J. Chem. Phys.* **1999**, *110*, 6171–6188.

[42] Lyakh, D. I.; Musiał, M.; Lotrich, V. F.; Bartlett, R. J. Multireference Nature of Chemistry: The Coupled-Cluster View. *Chem. Rev.* **2012**, *112*, 182–243, PMID: 22220988.

[43] Köhn, A.; Hanauer, M.; Mück, L. A.; Jagau, T.-C.; Gauss, J. State-specific multireference coupled-cluster theory. *WIREs Comput. Mol. Sci.* **2013**, *3*, 176–197.

[44] Thomas, L. H. The calculation of atomic fields. *Mathematical Proceedings of the Cambridge Philosophical Society* **1927**, *23*, 542–548.

[45] Fermi, E. Un Metodo Statistico per la Determinazione di alcune Prioprietà dell'Atomo. *Rend. Accad. Naz. Lincei* **1927**, *6*.

[46] Hohenberg, P.; Kohn, W. Inhomogeneous Electron Gas. *Phys. Rev.* **1964**, *136*, B864–B871.

[47] Levy, M. Universal variational functionals of electron densities, first-order density matrices, and natural spin-orbitals and solution of the v-representability problem. *Proc. Natl. Acad. Sci.* **1979**, *76*, 6062–6065.

[48] Levy, M. Electron densities in search of Hamiltonians. *Phys. Rev. A* **1982**, *26*, 1200–1208.

[49] Lieb, E. H. Density functionals for coulomb systems. *Int. J. Quantum Chem. 24*, 243–277.

[50] Wesolowski, T. A.; Warshel, A. Frozen density functional approach for ab initio calculations of solvated molecules. *J. Phys. Chem.* **1993**, *97*, 8050–8053.

[51] Gomes, A. S. P.; Jacob, C. R. Quantum-chemical embedding methods for treating local electronic excitations in complex chemical systems. *Annu. Rep. Prog. Chem., Sect. C: Phys. Chem.* **2012**, *108*, 222–277.

[52] Senatore, G.; Subbaswamy, K. Density dependence of the dielectric constant of rare-gas crystals. *Phys. Rev. B* **1986**, *34*, 5754.

[53] Jacob, C. R.; Neugebauer, J. Subsystem density-functional theory. *Wiley Interdiscip. Rev. Comput. Mol. Sci.* **2014**, *4*, 325–362.

[54] Govind, N.; Wang, Y.; Da Silva, A.; Carter, E. Accurate ab initio energetics of extended systems via explicit correlation embedded in a density functional environment. *Chem. Phys. Lett.* **1998**, *295*, 129–134.

[55] Govind, N.; Wang, Y. A.; Carter, E. A. Electronic-structure calculations by first-principles density-based embedding of explicitly correlated systems. *J. Chem. Phys.* **1999**, *110*, 7677–7688.

[56] Klüner, T.; Govind, N.; Wang, Y. A.; Carter, E. A. Prediction of electronic excited states of adsorbates on metal surfaces from first principles. *Phys. Rev. Lett.* **2001**, *86*, 5954.

[57] Klüner, T.; Govind, N.; Wang, Y. A.; Carter, E. A. Periodic density functional embedding theory for complete active space self-consistent field and configuration interaction calculations: Ground and excited states. *J. Chem. Phys.* **2002**, *116*, 42–54.

[58] Höfener, S.; Severo Pereira Gomes, A.; Visscher, L. Molecular properties via a subsystem density functional theory formulation: A common framework for electronic embedding. *J. Chem. Phys.* **2012**, *136*, 044104.

[59] Georges, A.; Kotliar, G. Hubbard model in infinite dimensions. *Phys. Rev. B* **1992**, *45*, 6479–6483.

[60] Georges, A.; Kotliar, G.; Krauth, W.; Rozenberg, M. J. Dynamical mean-field theory of strongly correlated fermion systems and the limit of infinite dimensions. *Rev. Mod. Phys.* **1996**, *68*, 13–125.

[61] Kotliar, G.; Vollhardt, D. Strongly Correlated Materials: Insights From Dynamical Mean-Field Theory. *Phys. Today* **2004**, *57*, 53–59.

[62] Kotliar, G.; Savrasov, S. Y.; Haule, K.; Oudovenko, V. S.; Parcollet, O.; Marianetti, C. A. Electronic structure calculations with dynamical mean-field theory. *Rev. Mod. Phys.* **2006**, *78*, 865–951.

[63] Held, K. Electronic structure calculations using dynamical mean field theory. *Adv. Phys.* **2007**, *56*, 829–926.

[64] Vollhardt, D.; Byczuk, K.; Kollar, M. In *Strongly Correlated Systems: Theoretical Methods*; Avella, A., Mancini, F., Eds.; Springer Berlin Heidelberg: Berlin, Heidelberg, 2012; pp 203–236.

[65] Martin, R. M.; Reining, L.; Ceperley, D. M. *Interacting Electrons: Theory and Computational Approaches*; Cambridge University Press, 2016.

[66] Werner, P.; Casula, M. Dynamical screening in correlated electron systems—from lattice models to realistic materials. *J. Phys. Condens. Matter* **2016**, *28*, 383001.

[67] Georges, A. The beauty of impurities: Two revivals of Friedel's virtual bound-state concept. *C. R. Phys.* **2016**, *17*, 430–446.

[68] Wouters, S.; A. Jiménez-Hoyos, C.; K.L. Chan, G. *Fragmentation*; John Wiley Sons, Ltd, 2017; Chapter 8, pp 227–243.

[69] Hubbard, J. Electron correlations in narrow energy bands. *Proc. R. Soc. London A* **1963**, *276*, 238–257.

[70] Hubbard, J. Electron correlations in narrow energy bands. II. The degenerate band case. *Proc. R. Soc. London A* **1964**, *277*, 237–259.

[71] Hubbard, J. Electron correlations in narrow energy bands III. An improved solution. *Proc. R. Soc. London A* **1964**, *281*, 401–419.

[72] Hubbard, J. Electron correlations in narrow energy bands - IV. The atomic representation. *Proc. R. Soc. London A* **1965**, *285*, 542–560.

[73] Senjean, B.; Tsuchiizu, M.; Robert, V.; Fromager, E. Local density approximation in site-occupation embedding theory. *Mol. Phys.* **2017**, *115*, 48–62.

[74] Li, C.; Requist, R.; Gross, E. K. U. Density functional theory of electron transfer beyond the Born-Oppenheimer approximation: Case study of LiF. **2018**, *148*, 084110.

[75] Carrascal, D. J.; Ferrer, J.; Maitra, N.; Burke, K. Linear response time-dependent density functional theory of the Hubbard dimer. *Eur. Phys. J. B* **2018**, *91*, 142.

[76] Deur, K.; Mazouin, L.; Senjean, B.; Fromager, E. Exploring weight-dependent density-functional approximations for ensembles in the Hubbard dimer. *Eur. Phys. J. B* **2018**, *91*, 162.

[77] Sagredo, F.; Burke, K. Accurate double excitations from ensemble density functional calculations. **2018**, *149*, 134103.

[78] Smith, J. C.; Pribram-Jones, A.; Burke, K. Exact thermal density functional theory for a model system: Correlation components and accuracy of the zero-temperature exchange-correlation approximation. *Phys. Rev. B* **2016**, *93*, 245131.

[79] Maitra, N. T. Double and Charge-Transfer Excitations in Time-Dependent Density Functional Theory. *Annu. Rev. Phys. Chem.* **2022**, *73*, 117–140, PMID: 34910562.

[80] Lacombe, L.; Maitra, N. T. Non-adiabatic approximations in time-dependent density functional theory: progress and prospects. *Npj Comput. Mater.* **2023**, *9*.

[81] Dreuw, A.; Head-Gordon, M. Failure of Time-Dependent Density Functional Theory for Long-Range Charge-Transfer Excited States: The ZincbacteriochlorinBacteriochlorin and BacteriochlorophyllSpheroidene Complexes. *J. Am. Chem. Soc.* **2004**, *126*, 4007–4016, PMID: 15038755.

[82] Hieringer, W.; Görling, A. Failure of time-dependent density functional methods for excitations in spatially separated systems. *Chem. Phys. Lett.* **2006**, *419*, 557–562.

[83] Autschbach, J. Charge-Transfer Excitations and Time-Dependent Density Functional Theory: Problems and Some Proposed Solutions. *ChemPhysChem* **2009**, *10*, 1757–1760.

[84] Levine, B. G.; Ko, C.; Quenneville, J.; MartÍnez, T. J. Conical intersections and double excitations in time-dependent density functional theory. *Mol. Phys.* **2006**, *104*, 1039–1051.

[85] Tapavicza, E.; Tavernelli, I.; Rothlisberger, U.; Filippi, C.; Casida, M. E. Mixed time-dependent density-functional theory/classical trajectory surface hopping study of oxirane photochemistry. *J. Chem. Phys.* **2008**, *129*, 124108.

[86] Theophilou, A. K. The energy density functional formalism for excited states. *J. Phys. C: Solid State Phys.* **1979**, *12*, 5419.

[87] Theophilou, A. K. In *The single particle density in physics and chemistry*; March, N. H., Deb, B. M., Eds.; Academic Press, 1987; pp 210–212.

[88] Gross, E. K. U.; Oliveira, L. N.; Kohn, W. Rayleigh-Ritz variational principle for ensembles of fractionally occupied states. *Phys. Rev. A* **1988**, *37*, 2805.

[89] Gross, E. K. U.; Oliveira, L. N.; Kohn, W. Density-functional theory for ensembles of fractionally occupied states. I. Basic formalism. *Phys. Rev. A* **1988**, *37*, 2809.

[90] Oliveira, L. N.; Gross, E. K. U.; Kohn, W. Density-functional theory for ensembles of fractionally occupied states. II. Application to the He atom. *Phys. Rev. A* **1988**, *37*, 2821.

[91] Senjean, B.; Fromager, E. Unified formulation of fundamental and optical gap problems in density-functional theory for ensembles. *Phys. Rev. A* **2018**, *98*, 022513.

[92] Cernatic, F.; Senjean, B.; Robert, V.; Fromager, E. In *New Horizons in Computational Chemistry Software*; Filatov, M., Choi, C. H., Olivucci, M., Eds.; Springer International Publishing: Cham, 2022; pp 237–316.

[93] Pastorczak, E.; Gidopoulos, N. I.; Pernal, K. Calculation of electronic excited states of molecules using the Helmholtz free-energy minimum principle. **2013**, *87*, 062501.

[94] Pittalis, S.; Proetto, C. R.; Floris, A.; Sanna, A.; Bersier, C.; Burke, K.; Gross, E. K. U. Exact Conditions in Finite-Temperature Density-Functional Theory. *Phys. Rev. Lett.* **2011**, *107*, 163001.

[95] Pribram-Jones, A.; Burke, K. Connection formulas for thermal density functional theory. *Phys. Rev. B* **2016**, *93*, 205140.

[96] Gould, T.; Pittalis, S. Density-driven correlations in many-electron ensembles: theory and application for excited states. **2019**, *123*, 016401.

[97] Fromager, E. Individual Correlations in Ensemble Density Functional Theory: State-and Density-Driven Decompositions without Additional Kohn-Sham Systems. **2020**, *124*, 243001.

[98] Deur, K.; Mazouin, L.; Fromager, E. Exact ensemble density functional theory for excited states in a model system: Investigating the weight dependence of the correlation energy. *Phys. Rev. B* **2017**, *95*, 035120.

[99] Carrascal, D. J.; Ferrer, J.; Smith, J. C.; Burke, K. The Hubbard dimer: a density functional case study of a many-body problem. *J. Phys. Condens. Matter* **2015**, *27*, 393001.

[100] Carrascal, D.; Ferrer, J.; Smith, J.; Burke, K. Corrigendum: The Hubbard dimer: a density functional case study of a many-body problem (2015 J. Phys.: Condens. Matter 27 393001). *J. Phys. Condens. Matter* **2016**, *29*, 019501.

[101] Senjean, B.; Knecht, S.; Jensen, H. J. .; Fromager, E. Linear interpolation method in ensemble Kohn-Sham and range-separated density-functional approximations for excited states. *Phys. Rev. A* **2015**, *92*, 012518.

[102] Perdew, J. P.; Parr, R. G.; Levy, M.; Balduz Jr, J. L. Density-functional theory for fractional particle number: derivative discontinuities of the energy. *Phys. Rev. Lett.* **1982**, *49*, 1691.

[103] Hodgson, M. J. P.; Wetherell, J.; Fromager, E. Exact exchange-correlation potentials for calculating the fundamental gap with a fixed number of electrons. **2021**, *103*, 012806.

[104] Levy, M. Excitation energies from density-functional orbital energies. *Phys. Rev. A* **1995**, *52*, R4313.

[105] Sekaran, S.; Tsuchiizu, M.; Saubanère, M.; Fromager, E. Householder-transformed density matrix functional embedding theory. *Phys. Rev. B* **2021**, *104*, 035121.

[106] Tran, H. K.; Van Voorhis, T.; Thom, A. J. W. Using SCF metadynamics to extend density matrix embedding theory to excited states. *J. Chem. Phys.* **2019**, *151*, 034112.

[107] Yalouz, S.; Gullin, M. R.; Sekaran, S. QuantNBody: a Python package for quantum chemistry and physics to build and manipulate many-body operators and wave functions. *J. Open Source Softw.* **2022**, *7*, 4759.

[108] Filatov, M. Spin-restricted ensemble-referenced Kohn–Sham method: basic principles and application to strongly correlated ground and excited states of molecules. *WIREs Comput. Mol. Sci.* **2015**, *5*, 146.

[109] Loos, P.-F.; Fromager, E. A weight-dependent local correlation density-functional approximation for ensembles. **2020**, *152*, 214101.

[110] Marut, C.; Senjean, B.; Fromager, E.; Loos, P.-F. Weight dependence of local exchange–correlation functionals in ensemble density-functional theory: double excitations in two-electron systems. *Faraday Discuss.* **2020**, *224*, 402–423.

[111] Yalouz, S.; Sekaran, S.; Fromager, E.; Saubanère, M. Quantum embedding of multi-orbital fragments using the block-Householder transformation. *J. Chem. Phys.* **2022**, *157*, 214112.

[112] Jensen, F. *Introduction to computational chemistry*, 3rd ed.; John Wiley & Sons: Nashville, TN, 2017.

[113] Gilbert, T. L. Hohenberg-Kohn theorem for nonlocal external potentials. *Phys. Rev. B* **1975**, *12*, 2111–2120.

[114] Sun, Q.; Chan, G. K.-L. Quantum Embedding Theories. *Acc. Chem. Res.* **2016**, *49*, 2705–2712, PMID: 27993005.

[115] Schrödinger, E. An Undulatory Theory of the Mechanics of Atoms and Molecules. *Phys. Rev.* **1926**, *28*, 1049–1070.

[116] Piela, L. *Ideas of quantum chemistry*, 3rd ed.; Elsevier Science: London, England, 2020; p 315.

[117] "Born, M.; Huang, K. *"Dynamical Theory of Crystal Lattices"*; "Oxford University Press": "Oxford, UK", 1954.

[118] Abedi, A.; Maitra, N. T.; Gross, E. K. U. Exact Factorization of the Time-Dependent Electron-Nuclear Wave Function. *Phys. Rev. Lett.* **2010**, *105*, 123002.

[119] Abedi, A.; Maitra, N. T.; Gross, E. K. U. Correlated electron-nuclear dynamics: Exact factorization of the molecular wavefunction. *J. Chem. Phys.* **2012**, *137*, 22A530.

[120] Gidopoulos, N. I.; Gross, E. K. U. Electronic non-adiabatic states: towards a density functional theory beyond the Born–Oppenheimer approximation. *Philos. Trans. R. Soc. Lond. A: Math., Phys. Eng. Sci.* **2014**, *372*, 20130059.

[121] Hunter, G. Conditional probability amplitudes in wave mechanics. *Int. J. Quantum Chem.* **1975**, *9*, 237–242.

[122] Slater, J. C. The Theory of Complex Spectra. *Phys. Rev.* **1929**, *34*, 1293–1322.

[123] Hartree, D. R. The Wave Mechanics of an Atom with a Non-Coulomb Central Field. Part I. Theory and Methods. *Math. Proc. Camb. Philos. Soc.* **1928**, *24*, 89–110.

[124] Hartree, D. R. The Wave Mechanics of an Atom with a Non-Coulomb Central Field. Part II. Some Results and Discussion. *Math. Proc. Camb. Philos. Soc.* **1928**, *24*, 111–132.

[125] Condon, E. U. The Theory of Complex Spectra. *Phys. Rev.* **1930**, *36*, 1121–1133.

[126] Szabo, A.; Ostlund, N. *Modern Quantum Chemistry: Introduction to Advanced Electronic Structure Theory*; Dover Books on Chemistry; Dover Publications, 1996.

[127] Bartlett, R. J. Many-Body Perturbation Theory and Coupled Cluster Theory for Electron Correlation in Molecules. *Annu. Rev. Phys. Chem.* **1981**, *32*, 359–401.

[128] Čížek, J. On the Correlation Problem in Atomic and Molecular Systems. Calculation of Wavefunction Components in Ursell-Type Expansion Using Quantum-Field Theoretical Methods. *J. Chem. Phys.* **1966**, *45*, 4256–4266.

[129] Paldus, J.; Čížek, J.; Shavitt, I. Correlation Problems in Atomic and Molecular Systems. IV. Extended Coupled-Pair Many-Electron Theory and Its Application to the BH_3 Molecule. *Phys. Rev. A* **1972**, *5*, 50–67.

[130] Purvis, I., George D.; Bartlett, R. J. A full coupled-cluster singles and doubles model: The inclusion of disconnected triples. *J. Chem. Phys.* **1982**, *76*, 1910–1918.

[131] Raghavachari, K.; Trucks, G. W.; Pople, J. A.; Head-Gordon, M. A fifth-order perturbation comparison of electron correlation theories. *Chem. Phys. Lett.* **1989**, *157*, 479–483.

[132] Dutta, A.; Sherrill, C. D. Full configuration interaction potential energy curves for breaking bonds to hydrogen: An assessment of single-reference correlation methods. *J. Chem. Phys.* **2003**, *118*, 1610–1619.

[133] Xu, E.; Shen, J.; Kou, Z.; Li, S. Coupled cluster with singles, doubles, and partial higher-order excitations based on the corresponding orbitals: The formulation and test applications for bond breaking processes. *J. Chem. Phys.* **2010**, *132*, 134110.

[134] Bulik, I. W.; Henderson, T. M.; Scuseria, G. E. Can Single-Reference Coupled Cluster Theory Describe Static Correlation? *J. Chem. Theory Comput.* **2015**, *11*, 3171–3179, PMID: 26575754.

[135] Stein, C. J.; Reiher, M. Automated Selection of Active Orbital Spaces. *J. Chem. Theory Comput.* **2016**, *12*, 1760–1771, PMID: 26959891.

[136] Aquilante, F. *et al.* Molcas 8: New capabilities for multiconfigurational quantum chemical calculations across the periodic table. *J. Comput. Chem.* **2016**, *37*, 506–541.

[137] Dyall, K. G. The choice of a zeroth-order Hamiltonian for second-order perturbation theory with a complete active space self-consistent-field reference function. *J. Chem. Phys.* **1995**, *102*, 4909–4918.

[138] Angeli, C.; Pastore, M.; Cimiraglia, R. New perspectives in multireference perturbation theory: the n-electron valence state approach. *Theor. Chem. Acc.* **2006**, *117*, 743–754.

[139] Battaglia, S.; Fdez. Galván, I.; Lindh, R. In *Theoretical and Computational Photochemistry*; García-Iriepa, C., Marazzi, M., Eds.; Elsevier, 2023; pp 135–162.

[140] Serrano-Andrés, L.; Merchán, M.; Nebot-Gil, I.; Lindh, R.; Roos, B. O. Towards an accurate molecular orbital theory for excited states: Ethene, butadiene, and hexatriene. *J. Chem. Phys.* **1993**, *98*, 3151–3162.

[141] Roos, B. O.; Andersson, K.; Fülscher, M. P.; Serrano-Andrés, L.; Pierloot, K.; Merchán, M.; Molina, V. Applications of level shift corrected perturbation theory in electronic spectroscopy. *J. Mol. Struct. THEOCHEM* **1996**, *388*, 257–276.

[142] Serrano-Andrés, L.; Merchán, M.; Lindh, R. Computation of conical intersections by using perturbation techniques. *J. Chem. Phys.* **2005**, *122*, 104107.

[143] Bernales, V.; League, A. B.; Li, Z.; Schweitzer, N. M.; Peters, A. W.; Carlson, R. K.; Hupp, J. T.; Cramer, C. J.; Farha, O. K.; Gagliardi, L. Computationally Guided Discovery of a Catalytic Cobalt-Decorated Metal–Organic Framework for Ethylene Dimerization. *J. Phys. Chem. C* **2016**, *120*, 23576–23583.

[144] Gagliardi, L.; Roos, B. O. Multiconfigurational quantum chemical methods for molecular systems containing actinides. *Chem. Soc. Rev.* **2007**, *36*, 893–903.

[145] Levine, D. S.; Hait, D.; Tubman, N. M.; Lehtola, S.; Whaley, K. B.; Head-Gordon, M. CASSCF with Extremely Large Active Spaces Using the Adaptive Sampling Configuration Interaction Method. *J. Chem. Theory Comput.* **2020**, *16*, 2340–2354, PMID: 32109055.

[146] Marti, K. H.; Ondík, I. M.; Moritz, G.; Reiher, M. Density matrix renormalization group calculations on relative energies of transition metal complexes and clusters. *J. Chem. Phys.* **2008**, *128*, 014104.

[147] Hohenstein, E. G.; Luehr, N.; Ufimtsev, I. S.; Martínez, T. J. An atomic orbital-based formulation of the complete active space self-consistent field method on graphical processing units. *J. Chem. Phys.* **2015**, *142*, 224103.

[148] White, S. R. Density matrix formulation for quantum renormalization groups. *Phys. Rev. Lett.* **1992**, *69*, 2863–2866.

[149] White, S. R. Density-matrix algorithms for quantum renormalization groups. *Phys. Rev. B* **1993**, *48*, 10345–10356.

[150] Mazziotti, D. A. Pure-N-representability conditions of two-fermion reduced density matrices. *Phys. Rev. A* **2016**, *94*, 032516.

[151] Donnelly, R. A.; Parr, R. G. Elementary properties of an energy functional of the first-order reduced density matrix. *J. Chem. Phys.* **1978**, *69*, 4431–4439.

[152] Donnelly, R. A. On a fundamental difference between energy functionals based on first- and on second-order density matrices. *J. Chem. Phys.* **1979**, *71*, 2874–2879.

[153] Dumaz, M.; Boucher, R.; Marques, M. A. L.; Romero, A. H. Authorship and citation cultural nature in Density Functional Theory from solid state computational packages. *Scientometrics* **2021**, *126*, 6681–6695.

[154] Teller, E. On the Stability of Molecules in the Thomas-Fermi Theory. *Rev. Mod. Phys.* **1962**, *34*, 627–631.

[155] Dirac, P. A. M. Note on Exchange Phenomena in the Thomas Atom. *Mathematical Proceedings of the Cambridge Philosophical Society* **1930**, *26*, 376–385.

[156] v. Weizsäcker, C. F. Zur Theorie der Kernmassen. *Z. Phys.* **1935**, *96*, 431–458.

[157] García-González, P.; Alvarellos, J. E.; Chacón, E. Kinetic-energy density functional: Atoms and shell structure. *Phys. Rev. A* **1996**, *54*, 1897–1905.

[158] Witt, W. C.; del Rio, B. G.; Dieterich, J. M.; Carter, E. A. Orbital-free density functional theory for materials research. *J. Mater. Res.* **2018**, *33*, 777–795.

[159] "Engel, E.; Dreizler, R. M. *"Density Functional Theory: An Advanced Course"*, 2011th ed.; "Theoretical and mathematical physics"; "Springer": "Berlin, Germany", 2011.

[160] Valone, S. M. Consequences of extending 1-matrix energy functionals from pure–state representable to all ensemble representable 1 matrices. *J. Chem. Phys.* **1980**, *73*, 1344–1349.

[161] Toulouse, J. Review of approximations for the exchange-correlation energy in density-functional theory. 2022.

[162] Perdew, J. P.; Schmidt, K. Jacob's ladder of density functional approximations for the exchange-correlation energy. *AIP Conf. Proc.* **2001**, *577*, 1–20.

[163] Loos, P.-F.; Gill, P. M. W. The uniform electron gas. *Wiley Interdiscip. Rev. Comput. Mol. Sci.* **2016**, *6*, 410–429.

[164] Vosko, S. H.; Wilk, L.; Nusair, M. Accurate spin-dependent electron liquid correlation energies for local spin density calculations: a critical analysis. *Can. J. Phys.* **1980**, *58*, 1200–1211.

[165] Perdew, J. P.; Wang, Y. Accurate and simple analytic representation of the electron-gas correlation energy. *Phys. Rev. B* **1992**, *45*, 13244–13249.

[166] Perdew, J. P.; Yue, W. Accurate and simple density functional for the electronic exchange energy: Generalized gradient approximation. *Phys. Rev. B* **1986**, *33*, 8800–8802.

[167] Becke, A. D. Density-functional exchange-energy approximation with correct asymptotic behavior. *Phys. Rev. A* **1988**, *38*, 3098–3100.

[168] Lee, C.; Yang, W.; Parr, R. G. Development of the Colle-Salvetti correlation-energy formula into a functional of the electron density. *Phys. Rev. B* **1988**, *37*, 785–789.

[169] Perdew, J. P. Unified theory of exchange and correlation beyond the local density approximation. Electronic Structure of Solids '91. Berlin, 1991; pp 11–20.

[170] Perdew, J. P.; Chevary, J. A.; Vosko, S. H.; Jackson, K. A.; Pederson, M. R.; Singh, D. J.; Fiolhais, C. Atoms, molecules, solids, and surfaces: Applications of the generalized gradient approximation for exchange and correlation. *Phys. Rev. B* **1992**, *46*, 6671–6687.

[171] Burke, K.; Perdew, J. P.; Wang, Y. In *Electronic Density Functional Theory: Recent Progress and New Directions*; Dobson, J. F., Vignale, G., Das, M. P., Eds.; Springer US: Boston, MA, 1998; pp 81–111.

[172] Perdew, J. P.; Burke, K.; Ernzerhof, M. Generalized Gradient Approximation Made Simple. *Phys. Rev. Lett.* **1996**, *77*, 3865–3868.

[173] Tao, J.; Perdew, J. P.; Staroverov, V. N.; Scuseria, G. E. Climbing the Density Functional Ladder: Nonempirical Meta–Generalized Gradient Approximation Designed for Molecules and Solids. *Phys. Rev. Lett.* **2003**, *91*, 146401.

[174] Sun, J.; Ruzsinszky, A.; Perdew, J. P. Strongly Constrained and Appropriately Normed Semilocal Density Functional. *Phys. Rev. Lett.* **2015**, *115*, 036402.

[175] Gräfenstein, J.; Kraka, E.; Cremer, D. The impact of the self-interaction error on the density functional theory description of dissociating radical cations: Ionic and covalent dissociation limits. *J. Chem. Phys.* **2004**, *120*, 524–539.

[176] Mori-Sánchez, P.; Cohen, A. J.; Yang, W. Many-electron self-interaction error in approximate density functionals. *J. Chem. Phys.* **2006**, *125*.

[177] Cohen, A. J.; Mori-Sánchez, P.; Yang, W. Fractional charge perspective on the band gap in density-functional theory. *Phys. Rev. B* **2008**, *77*, 115123.

[178] Mori-Sánchez, P.; Cohen, A. J.; Yang, W. Localization and Delocalization Errors in Density Functional Theory and Implications for Band-Gap Prediction. *Phys. Rev. Lett.* **2008**, *100*, 146401.

[179] Becke, A. D. Density-functional thermochemistry. III. The role of exact exchange. *J. Chem. Phys.* **1993**, *98*, 5648–5652.

[180] Becke, A. D. A new mixing of Hartree–Fock and local density-functional theories. *J. Chem. Phys.* **1993**, *98*, 1372–1377.

[181] Savin, A. In *Recent Developments and Applications of Modern Density Functional Theory*; Seminario, J., Ed.; Theoretical and Computational Chemistry; Elsevier, 1996; Vol. 4; pp 327–357.

[182] Iikura, H.; Tsuneda, T.; Yanai, T.; Hirao, K. A long-range correction scheme for generalized-gradient-approximation exchange functionals. *J. Chem. Phys.* **2001**, *115*, 3540–3544.

[183] Yanai, T.; Tew, D. P.; Handy, N. C. A new hybrid exchange–correlation functional using the Coulomb-attenuating method (CAM-B3LYP). *Chem. Phys. Lett.* **2004**, *393*, 51–57.

[184] Cornaton, Y.; Fromager, E. Double hybrid density-functional theory using the coulomb-attenuating method. *Int. J. Quantum Chem.* **2014**, *114*, 1199–1211.

[185] Seidl, A.; Görling, A.; Vogl, P.; Majewski, J. A.; Levy, M. Generalized Kohn-Sham schemes and the band-gap problem. *Phys. Rev. B* **1996**, *53*, 3764–3774.

[186] Talman, J. D.; Shadwick, W. F. Optimized effective atomic central potential. *Phys. Rev. A* **1976**, *14*, 36–40.

[187] Ivanov, S.; Hirata, S.; Bartlett, R. J. Exact Exchange Treatment for Molecules in Finite-Basis-Set Kohn-Sham Theory. *Phys. Rev. Lett.* **1999**, *83*, 5455–5458.

[188] Görling, A. New KS Method for Molecules Based on an Exchange Charge Density Generating the Exact Local KS Exchange Potential. *Phys. Rev. Lett.* **1999**, *83*, 5459–5462.

[189] Cramer, C. J.; Truhlar, D. G. Density functional theory for transition metals and transition metal chemistry. *Phys. Chem. Chem. Phys.* **2009**, *11*, 10757–10816.

[190] Grimme, S. Accurate description of van der Waals complexes by density functional theory including empirical corrections. *J. Comput. Chem.* **2004**, *25*, 1463–1473.

[191] Dion, M.; Rydberg, H.; Schröder, E.; Langreth, D. C.; Lundqvist, B. I. Van der Waals Density Functional for General Geometries. *Phys. Rev. Lett.* **2004**, *92*, 246401.

[192] Lee, K.; Murray, E. D.; Kong, L.; Lundqvist, B. I.; Langreth, D. C. Higher-accuracy van der Waals density functional. *Phys. Rev. B* **2010**, *82*, 081101.

[193] Vydrov, O. A.; Van Voorhis, T. Improving the accuracy of the nonlocal van der Waals density functional with minimal empiricism. *J. Chem. Phys.* **2009**, *130*.

[194] Vydrov, O. A.; Van Voorhis, T. Nonlocal van der Waals Density Functional Made Simple. *Phys. Rev. Lett.* **2009**, *103*, 063004.

[195] Vydrov, O. A.; Van Voorhis, T. Nonlocal van der Waals density functional: The simpler the better. *J. Chem. Phys.* **2010**, *133*.

[196] Grimme, S. Semiempirical hybrid density functional with perturbative second-order correlation. *J. Chem. Phys.* **2006**, *124*, 034108.

[197] Sharkas, K.; Toulouse, J.; Savin, A. Double-hybrid density-functional theory made rigorous. *J. Chem. Phys.* **2011**, *134*, 064113.

[198] Fromager, E. Rigorous formulation of two-parameter double-hybrid density-functionals. *J. Chem Phys.* **2011**, *135*, 244106.

[199] Ángyán, J. G.; Gerber, I. C.; Savin, A.; Toulouse, J. van der Waals forces in density functional theory: Perturbational long-range electron-interaction corrections. *Phys. Rev. A* **2005**, *72*, 012510.

[200] Anisimov, V. I.; Zaanen, J.; Andersen, O. K. Band theory and Mott insulators: Hubbard U instead of Stoner I. *Phys. Rev. B* **1991**, *44*, 943–954.

[201] Liechtenstein, A. I.; Anisimov, V. I.; Zaanen, J. Density-functional theory and strong interactions: Orbital ordering in Mott-Hubbard insulators. *Phys. Rev. B* **1995**, *52*, R5467–R5470.

[202] Cococcioni, M.; de Gironcoli, S. Linear response approach to the calculation of the effective interaction parameters in the LDA + U method. *Phys. Rev. B* **2005**, *71*, 035105.

[203] Paul, A.; Birol, T. Applications of DFT + DMFT in Materials Science. *Annu. Rev. Mater. Res.* **2019**, *49*, 31–52.

[204] Sekaran, S.; Saubanère, M.; Fromager, E. Local Potential Functional Embedding Theory: A Self-Consistent Flavor of Density Functional Theory for Lattices without Density Functionals. *Computation* **2022**, *10*.

[205] Bulik, I. W.; Scuseria, G. E.; Dukelsky, J. Density matrix embedding from broken symmetry lattice mean fields. *Phys. Rev. B* **2014**, *89*, 035140.

[206] Bulik, I. W.; Chen, W.; Scuseria, G. E. Electron correlation in solids via density embedding theory. *J. Chem. Phys.* **2014**, *141*, 054113.

[207] Mordovina, U.; Reinhard, T. E.; Theophilou, I.; Appel, H.; Rubio, A. Self-Consistent Density-Functional Embedding: A Novel Approach for Density-Functional Approximations. *J. Chem. Theory Comput.* **2019**, *15*, 5209–5220, PMID: 31490684.

[208] Gunnarsson, O.; Schönhammer, K. Density-Functional Treatment of an Exactly Solvable Semiconductor Model. *Phys. Rev. Lett.* **1986**, *56*, 1968–1971.

[209] Schönhammer, K.; Gunnarsson, O.; Noack, R. M. Density-functional theory on a lattice: Comparison with exact numerical results for a model with strongly correlated electrons. *Phys. Rev. B* **1995**, *52*, 2504–2510.

[210] Löwdin, P.-O. On the non-orthogonality problem connected with the use of atomic wave functions in the theory of molecules and crystals. *J. Chem. Phys.* **1950**, *18*, 365–375.

[211] Carlson, B.; Keller, J. M. Orthogonalization procedures and the localization of Wannier functions. *Phys. Rev.* **1957**, *105*, 102.

[212] Mayer, I. On Löwdin's method of symmetric orthogonalization. *Int. J. Quantum Chem.* **2002**, *90*, 63–65.

[213] Nielsen, M. A.; Chuang, I. Quantum computation and quantum information. 2002.

[214] Sekaran, S.; Bindech, O.; Fromager, E. A unified density matrix functional construction of quantum baths in density matrix embedding theory beyond the mean-field approximation. *J. Chem. Phys.* **2023**, *159*, 034107.

[215] Zheng, B.-X. Density Matrix Embedding Theory and Strongly Correlated Lattice Systems. 2018.

[216] Sun, C.; Ray, U.; Cui, Z.-H.; Stoudenmire, M.; Ferrero, M.; Chan, G. K.-L. Finite-temperature density matrix embedding theory. *Phys. Rev. B* **2020**, *101*, 075131.

[217] Rotella, F.; Zambettakis, I. Block Householder transformation for parallel QR factorization. *Appl. Math. Lett.* **1999**, *12*, 29–34.

[218] Nusspickel, M.; Ibrahim, B.; Booth, G. H. Effective Reconstruction of Expectation Values from Ab Initio Quantum Embedding. *J. Chem. Theory Comput.* **2023**, *19*, 2769–2791, PMID: 37155201.

[219] Welborn, M.; Tsuchimochi, T.; Van Voorhis, T. Bootstrap embedding: An internally consistent fragment-based method. *J. Chem. Phys.* **2016**, *145*, 074102.

[220] Ricke, N.; Welborn, M.; Ye, H.-Z.; Voorhis, T. V. Performance of Bootstrap Embedding for long-range interactions and 2D systems. *Mol. Phys.* **2017**, *115*, 2242–2253.

[221] Ye, H.-Z.; Ricke, N. D.; Tran, H. K.; Van Voorhis, T. Bootstrap Embedding for Molecules. *J. Chem. Theory Comput.* **2019**, *15*, 4497–4506, PMID: 31343878.

[222] Fan, Z.; Jie, Q.-l. Cluster density matrix embedding theory for quantum spin systems. *Phys. Rev. B* **2015**, *91*, 195118.

[223] Gunst, K.; Wouters, S.; De Baerdemacker, S.; Van Neck, D. Block product density matrix embedding theory for strongly correlated spin systems. *Phys. Rev. B* **2017**, *95*, 195127.

[224] Qiao, J.; Jie, Q. Density matrix embedding theory of excited states for spin systems. *Comput. Phys. Commun.* **2021**, *261*, 107712.

[225] Ai, Y.; Sun, Q.; Jiang, H. Efficient Multiconfigurational Quantum Chemistry Approach to Single-Ion Magnets Based on Density Matrix Embedding Theory. *J. Phys. Chem. Lett.* **2022**, *13*, 10627–10634, PMID: 36350106.

[226] Kretchmer, J. S.; Chan, G. K.-L. A real-time extension of density matrix embedding theory for non-equilibrium electron dynamics. *J. Chem. Phys.* **2018**, *148*, 054108.

[227] Mitra, A.; Pham, H. Q.; Pandharkar, R.; Hermes, M. R.; Gagliardi, L. Excited States of Crystalline Point Defects with Multireference Density Matrix Embedding Theory. *J. Phys. Chem. Lett.* **2021**, *12*, 11688–11694, PMID: 34843250.

[228] Faulstich, F. M.; Kim, R.; Cui, Z.-H.; Wen, Z.; Kin-Lic Chan, G.; Lin, L. Pure State v-Representability of Density Matrix Embedding Theory. *J. Chem. Theory Comput.* **2022**, *18*, 851–864, PMID: 35084855.

[229] Cancès, E.; Faulstich, F.; Kirsch, A.; Letournel, E.; Levitt, A. Some mathematical insights on Density Matrix Embedding Theory. 2023.

[230] Lacombe, L.; Maitra, N. T. Embedding via the Exact Factorization Approach. *Phys. Rev. Lett.* **2020**, *124*, 206401.

[231] Requist, R.; Gross, E. K. U. Fock-Space Embedding Theory: Application to Strongly Correlated Topological Phases. *Phys. Rev. Lett.* **2021**, *127*, 116401.

[232] Stephan, D. W.; Erker, G. Frustrated Lewis Pairs: Metal-free Hydrogen Activation and More. *Angew. Chem. Int. Ed.* **2010**, *49*, 46–76.

[233] Stephan, D. W.; Erker, G. Frustrated Lewis Pair Chemistry: Development and Perspectives. *Angew. Chem. Int. Ed.* **2015**, *54*, 6400–6441.

[234] Liu, L.; Lukose, B.; Jaque, P.; Ensing, B. Reaction mechanism of hydrogen activation by frustrated Lewis pairs. *Green Energy Environ.* **2019**, *4*, 20–28.

[235] Lieb, E. H.; Wu, F. Y. Absence of Mott Transition in an Exact Solution of the Short-Range, One-Band Model in One Dimension. *Phys. Rev. Lett.* **1968**, *20*, 1445–1448.

[236] Vollhardt, K.; Schore, E. *Organic Chemistry: Structure and Function*; W. H. Freeman and Company: New York, 2014; pp 620–624.

[237] Sarkar, R.; Heitz, M.-C.; Royal, G.; Boggio-Pasqua, M. Electronic Excited States and UV–Vis Absorption Spectra of the Dihydropyrene/Cyclophanediene Photochromic Couple: a Theoretical Investigation. *J. Phys. Chem. A* **2020**, *124*, 1567–1579, PMID: 32017559.

[238] Hüfner, S. *Photoelectron Spectroscopy*; Springer Berlin Heidelberg, 2003.

[239] Cardona, M., Ley, L., Eds. *Photoemission in Solids I*; Springer Berlin Heidelberg, 1978.

[240] Shankar, R. *Principles of Quantum Mechanics, second edition*; Springer US, 1994; p 417.

[241] Frenkel, J. *Wave Mechanics: Advanced General Theory*; Oxford: Clarendon, 1934.

[242] van Leeuwen, R. Causality and Symmetry in Time-Dependent Density-Functional Theory. *Phys. Rev. Lett.* **1998**, *80*, 1280–1283.

[243] van Leeuwen, R. Key concepts in time-dependent density-functional theory. *Int. J. Mod. Phys. B* **2001**, *15*, 1969–2023.

[244] Rajagopal, A. K. Time-dependent variational principle and the effective action in density-functional theory and Berry's phase. *Phys. Rev. A* **1996**, *54*, 3916–3922.

[245] Sundahl, B. E. Time Dependent Density-Functional Theory - Linear Response. Master's thesis, University of Tennessee, 2013.

[246] Toulouse, J. Introduction to many-body Green-function theory. 2019; `http://www.lct.jussieu.fr/pagesperso/toulouse/enseignement/introduction_green.pdf`, Lecture notes for the courses given at: 1st (2015) and 2nd (2017) editions of the International summer School in electronic structure Theory: electron correlation in Physics and Chemistry (ISTPC), Aussois, France.

[247] Elliott, P.; Goldson, S.; Canahui, C.; Maitra, N. T. Perspectives on double-excitations in TDDFT. *Chem. Phys.* **2011**, *391*, 110–119, Open problems and new solutions in time dependent density functional theory.

[248] Maitra, N. T.; Zhang, F.; Cave, R. J.; Burke, K. Double excitations within time-dependent density functional theory linear response. *J. Chem. Phys.* **2004**, *120*, 5932–5937.

[249] Ullrich, C. A.; Gossmann, U. J.; Gross, E. K. U. Time-Dependent Optimized Effective Potential. *Phys. Rev. Lett.* **1995**, *74*, 872–875.

[250] van Leeuwen, R. The Sham-Schlüter Equation in Time-Dependent Density-Functional Theory. *Phys. Rev. Lett.* **1996**, *76*, 3610–3613.

[251] Gritsenko, O. V.; Jan Baerends, E. Double excitation effect in non-adiabatic time-dependent density functional theory with an analytic construction of the exchange–correlation kernel in the common energy denominator approximation. *Phys. Chem. Chem. Phys.* **2009**, *11*, 4640–4646.

[252] Romaniello, P.; Sangalli, D.; Berger, J. A.; Sottile, F.; Molinari, L. G.; Reining, L.; Onida, G. Double excitations in finite systems. *J. Chem. Phys.* **2009**, *130*, 044108.

[253] Bruneval, F.; Sottile, F.; Olevano, V.; Del Sole, R.; Reining, L. Many-Body Perturbation Theory Using the Density-Functional Concept: Beyond the *GW* Approximation. *Phys. Rev. Lett.* **2005**, *94*, 186402.

[254] Sangalli, D.; Romaniello, P.; Onida, G.; Marini, A. Double excitations in correlated systems: A many–body approach. *J. Chem. Phys.* **2011**, *134*, 034115.

[255] Säkkinen, N.; Manninen, M.; van Leeuwen, R. The Kadanoff–Baym approach to double excitations in finite systems. *New J. Phys.* **2012**, *14*, 013032.

[256] Shao, Y.; Head-Gordon, M.; Krylov, A. I. The spin–flip approach within time-dependent density functional theory: Theory and applications to diradicals. *J. Chem. Phys.* **2003**, *118*, 4807–4818.

[257] Wang, F.; Ziegler, T. Time-dependent density functional theory based on a noncollinear formulation of the exchange-correlation potential. *J. Chem. Phys.* **2004**, *121*, 12191–12196.

[258] Minezawa, N.; Gordon, M. S. Optimizing Conical Intersections by SpinFlip Density Functional Theory: Application to Ethylene. *J. Phys. Chem. A* **2009**, *113*, 12749–12753, PMID: 19905013.

[259] Ullrich, C. A.; hui Yang, Z. A Brief Compendium of Time-Dependent Density Functional Theory. *Braz. J. Phys.* **2013**, *44*, 154–188.

[260] Tawada, Y.; Tsuneda, T.; Yanagisawa, S.; Yanai, T.; Hirao, K. A long-range-corrected time-dependent density functional theory. *J. Chem. Phys.* **2004**, *120*, 8425–8433.

[261] Stein, T.; Kronik, L.; Baer, R. Reliable Prediction of Charge Transfer Excitations in Molecular Complexes Using Time-Dependent Density Functional Theory. *J. Am. Chem. Soc.* **2009**, *131*, 2818–2820, PMID: 19239266.

[262] Kronik, L.; Stein, T.; Refaely-Abramson, S.; Baer, R. Excitation Gaps of Finite-Sized Systems from Optimally Tuned Range-Separated Hybrid Functionals. *J. Chem. Theory Comput.* **2012**, *8*, 1515–1531, PMID: 26593646.

[263] Maitra, N. T. Charge transfer in time-dependent density functional theory. *J. Phys. Condens. Matter* **2017**, *29*, 423001.

[264] Li, S. L.; Truhlar, D. G. Improving Rydberg Excitations within Time-Dependent Density Functional Theory with Generalized Gradient Approximations: The Exchange-Enhancement-for-Large-Gradient Scheme. *J. Chem. Theory Comput.* **2015**, *11*, 3123–3130, PMID: 26575749.

[265] Ullrich, C. A.; Yang, Z.-h. In *Density-Functional Methods for Excited States*; Ferré, N., Filatov, M., Huix-Rotllant, M., Eds.; Springer International Publishing: Cham, 2016; pp 185–217.

[266] Ghosh, S. K.; Dhara, A. K. Density-functional theory of many-electron systems subjected to time-dependent electric and magnetic fields. *Phys. Rev. A* **1988**, *38*, 1149–1158.

[267] Vignale, G. Mapping from current densities to vector potentials in time-dependent current density functional theory. *Phys. Rev. B* **2004**, *70*, 201102.

[268] Vignale, G.; Kohn, W. Current-Dependent Exchange-Correlation Potential for Dynamical Linear Response Theory. *Phys. Rev. Lett.* **1996**, *77*, 2037–2040.

[269] Vignale, G.; Ullrich, C. A.; Conti, S. Time-Dependent Density Functional Theory Beyond the Adiabatic Local Density Approximation. *Phys. Rev. Lett.* **1997**, *79*, 4878–4881.

[270] Sternheimer, R. M. Electronic Polarizabilities of Ions from the Hartree-Fock Wave Functions. *Phys. Rev.* **1954**, *96*, 951–968.

[271] Andrade, X.; Botti, S.; Marques, M. A. L.; Rubio, A. Time-dependent density functional theory scheme for efficient calculations of dynamic (hyper)polarizabilities. *J. Chem. Phys.* **2007**, *126*, 184106.

[272] Hofmann, F. The Sternheimer Approach to Linear Response Time-Dependent Density Functional Theory. Ph.D. thesis, 2020.

[273] Sottile, F. Fonctions de réponse des semi-conducteurs et des isolants : de l'équation de Bethe-Salpeter à la théorie de la fonctionnelle de la densité dépendante du temps. Ph.D. thesis, 2003; Thèse de doctorat dirigée par Reinina, Lucia et Tolédano, Jean-Claude Physique Palaiseau, Ecole polytechnique 2003.

[274] Bruneval, F. Echange et corrélation pour la structure électronique des solides, du silicium à l'oxyde cuivreaux : approximation GW et au-delà. Ph.D. thesis, 2005; Thèse de doctorat dirigée par Reining, Lucia Physique. Science des matériaux Palaiseau, Ecole polytechnique 2005.

[275] Hybertsen, M. S.; Louie, S. G. First-Principles Theory of Quasiparticles: Calculation of Band Gaps in Semiconductors and Insulators. *Phys. Rev. Lett.* **1985**, *55*, 1418–1421.

[276] Hybertsen, M. S.; Louie, S. G. Electron correlation in semiconductors and insulators: Band gaps and quasiparticle energies. *Phys. Rev. B* **1986**, *34*, 5390–5413.

[277] Strinati, G.; Mattausch, H. J.; Hanke, W. Dynamical Correlation Effects on the Quasiparticle Bloch States of a Covalent Crystal. *Phys. Rev. Lett.* **1980**, *45*, 290–294.

[278] Godby, R. W.; Schlüter, M.; Sham, L. J. Self-energy operators and exchange-correlation potentials in semiconductors. *Phys. Rev. B* **1988**, *37*, 10159–10175.

[279] von der Linden, W.; Horsch, P. Precise quasiparticle energies and Hartree-Fock bands of semiconductors and insulators. *Phys. Rev. B* **1988**, *37*, 8351–8362.

[280] Hybertsen, M. S.; Louie, S. G. Many-body calculation of surface states: As on Ge(111). *Phys. Rev. Lett.* **1987**, *58*, 1551–1554.

[281] Blase, X.; Zhu, X.; Louie, S. G. Self-energy effects on the surface-state energies of H-Si(111)1×1. *Phys. Rev. B* **1994**, *49*, 4973–4980.

[282] Rohlfing, M.; Krüger, P.; Pollmann, J. Efficient scheme for GW quasiparticle band-structure calculations with applications to bulk Si and to the Si(001)-(2×1) surface. *Phys. Rev. B* **1995**, *52*, 1905–1917.

[283] Hüser, F.; Olsen, T.; Thygesen, K. S. Quasiparticle GW calculations for solids, molecules, and two-dimensional materials. *Phys. Rev. B* **2013**, *87*, 235132.

[284] Reining, L. The GW approximation: content, successes and limitations. *Wiley Interdiscip. Rev. Comput. Mol. Sci.* **2018**, *8*, e1344.

[285] Golze, D.; Dvorak, M.; Rinke, P. The GW Compendium: A Practical Guide to Theoretical Photoemission Spectroscopy. *Frontiers in Chemistry* **2019**, *7*.

[286] Onida, G.; Reining, L.; Rubio, A. Electronic excitations: density-functional versus many-body Green's-function approaches. *Rev. Mod. Phys.* **2002**, *74*, 601–659.

[287] Blase, X.; Attaccalite, C. Charge-transfer excitations in molecular donor-acceptor complexes within the many-body Bethe-Salpeter approach. *Appl. Phys. Lett.* **2011**, *99*, 171909.

[288] Duchemin, I.; Deutsch, T.; Blase, X. Short-Range to Long-Range Charge-Transfer Excitations in the Zincbacteriochlorin-Bacteriochlorin Complex: A Bethe-Salpeter Study. *Phys. Rev. Lett.* **2012**, *109*, 167801.

[289] Blase, X.; Duchemin, I.; Jacquemin, D. The Bethe–Salpeter equation in chemistry: relations with TD-DFT, applications and challenges. *Chem. Soc. Rev.* **2018**, *47*, 1022–1043.

[290] Monino, E.; Loos, P.-F. Connections and performances of Green's function methods for charged and neutral excitations. *J. Chem. Phys.* **2023**, *159*, 034105.

[291] Loos, P.-F.; Blase, X. Dynamical correction to the Bethe–Salpeter equation beyond the plasmon-pole approximation. *J. Chem. Phys.* **2020**, *153*, 114120.

[292] Neese, F. The ORCA program system. *WIREs Comput. Mol. Sci.* **2012**, *2*, 73–78.

[293] Neese, F. Software update: the ORCA program system, version 4.0. *WIREs Comput. Mol. Sci.* **2018**, *8*, e1327.

[294] Neese, F.; Wennmohs, F.; Becker, U.; Riplinger, C. The ORCA quantum chemistry program package. *J. Chem. Phys.* **2020**, *152*, 224108.

[295] Neese, F. Software update: The ORCA program system—Version 5.0. *WIREs Comput. Mol. Sci.* **2022**, *12*, e1606.

[296] Jones, R. O.; Gunnarsson, O. The density functional formalism, its applications and prospects. *Rev. Mod. Phys.* **1989**, *61*, 689–746.

[297] Hellman, A.; Razaznejad, B.; Lundqvist, B. I. Potential-energy surfaces for excited states in extended systems. *J. Chem. Phys.* **2004**, *120*, 4593–4602.

[298] Stanton, J. F.; Bartlett, R. J. The equation of motion coupled-cluster method. A systematic biorthogonal approach to molecular excitation energies, transition probabilities, and excited state properties. *J. Chem. Phys.* **1993**, *98*, 7029–7039.

[299] Krylov, A. I. Equation-of-Motion Coupled-Cluster Methods for Open-Shell and Electronically Excited Species: The Hitchhiker's Guide to Fock Space. *Annu. Rev. Phys. Chem.* **2008**, *59*, 433–462, PMID: 18173379.

[300] Foresman, J. B.; Head-Gordon, M.; Pople, J. A.; Frisch, M. J. Toward a systematic molecular orbital theory for excited states. *J. Phys. Chem.* **1992**, *96*, 135–149.

[301] Gavnholt, J.; Olsen, T.; Engelund, M.; Schiøtz, J. Δ self-consistent field method to obtain potential energy surfaces of excited molecules on surfaces. *Phys. Rev. B* **2008**, *78*, 075441.

[302] Gilbert, A. T. B.; Besley, N. A.; Gill, P. M. W. Self-Consistent Field Calculations of Excited States Using the Maximum Overlap Method (MOM). *J. Phys. Chem. A* **2008**, *112*, 13164–13171, PMID: 18729344.

[303] Ye, H.-Z.; Welborn, M.; Ricke, N. D.; Van Voorhis, T. σ-SCF: A direct energy-targeting method to mean-field excited states. *J. Chem. Phys.* **2017**, *147*, 214104.

[304] Ye, H.-Z.; Van Voorhis, T. Half-Projected σ Self-Consistent Field For Electronic Excited States. *J. Chem. Theory Comput.* **2019**, *15*, 2954–2965, PMID: 30995060.

[305] Laio, A.; Parrinello, M. Escaping free-energy minima. *Proc. Natl. Acad. Sci.* **2002**, *99*, 12562–12566.

[306] Thom, A. J. W.; Head-Gordon, M. Locating Multiple Self-Consistent Field Solutions: An Approach Inspired by Metadynamics. *Phys. Rev. Lett.* **2008**, *101*, 193001.

[307] Finley, J.; Åke Malmqvist, P.; Roos, B. O.; Serrano-Andrés, L. The multi-state CASPT2 method. *Chem. Phys. Lett.* **1998**, *288*, 299–306.

[308] Angeli, C.; Borini, S.; Cestari, M.; Cimiraglia, R. A quasidegenerate formulation of the second order n-electron valence state perturbation theory approach. *J. Chem. Phys.* **2004**, *121*, 4043–4049.

[309] Gould, T.; Kronik, L.; Pittalis, S. Double excitations in molecules from ensemble density functionals: Theory and approximations. *Phys. Rev. A* **2021**, *104*, 022803.

[310] Deur, K.; Fromager, E. Ground and excited energy levels can be extracted exactly from a single ensemble density-functional theory calculation. **2019**, *150*, 094106.

[311] Gould, T.; Pittalis, S. Hartree and Exchange in Ensemble Density Functional Theory: Avoiding the Nonuniqueness Disaster. *Phys. Rev. Lett.* **2017**, *119*, 243001.

[312] Gould, T.; Stefanucci, G.; Pittalis, S. Ensemble density functional theory: Insight from the fluctuation-dissipation theorem. **2020**, *125*, 233001.

[313] Franck, O.; Fromager, E. Generalised adiabatic connection in ensemble density-functional theory for excited states: example of the H2 molecule. *Mol. Phys.* **2014**, *112*, 1684.

[314] Gould, T.; Kronik, L.; Pittalis, S. Charge transfer excitations from exact and approximate ensemble Kohn-Sham theory. *J. Chem. Phys.* **2018**, *148*, 174101.

[315] Nagy, A. Local ensemble exchange potential. *J. Phys. B: At. Mol. Opt. Phys.* **1996**, *29*, 389.

[316] Yang, Z.-h.; Pribram-Jones, A.; Burke, K.; Ullrich, C. A. Direct extraction of excitation energies from ensemble density-functional theory. *Phys. Rev. Lett.* **2017**, *119*, 033003.

[317] Senjean, B.; Hedegård, E. D.; Alam, M. M.; Knecht, S.; Fromager, E. Combining linear interpolation with extrapolation methods in range-separated ensemble density functional theory. *Mol. Phys.* **2016**, *114*, 968.

[318] Filatov, M.; Liu, F.; Martínez, T. J. Analytical derivatives of the individual state energies in ensemble density functional theory method. I. General formalism. **2017**, *147*, 034113.

[319] Levy, M.; Zahariev, F. Ground-State Energy as a Simple Sum of Orbital Energies in Kohn-Sham Theory: A Shift in Perspective through a Shift in Potential. *Phys. Rev. Lett.* **2014**, *113*, 113002.

[320] Perdew, J. P.; Levy, M. Physical content of the exact Kohn-Sham orbital energies: band gaps and derivative discontinuities. *Phys. Rev. Lett.* **1983**, *51*, 1884.

[321] Sottile, F.; Marsili, M.; Olevano, V.; Reining, L. Efficient ab initio calculations of bound and continuum excitons in the absorption spectra of semiconductors and insulators. *Phys. Rev. B* **2007**, *76*, 161103.

[322] Bruneval, F. Ionization energy of atoms obtained from GW self-energy or from random phase approximation total energies. **2012**, *136*, 194107.

[323] Bruneval, F.; Marques, M. A. Benchmarking the starting points of the GW approximation for molecules. **2012**, *9*, 324–329.

[324] Jiang, H. First-principles approaches for strongly correlated materials: A theoretical chemistry perspective. *Int. J. Quantum Chem.* **2015**, *115*, 722–730.

[325] Pacchioni, G. First principles calculations on oxide-based heterogeneous catalysts and photocatalysts: problems and advances. *Catal. Lett.* **2015**, *145*, 80–94.

[326] Ou, Q.; Subotnik, J. E. Comparison between GW and Wave-Function-Based Approaches: Calculating the Ionization Potential and Electron Affinity for 1D Hubbard Chains. **2016**, *120*, 4514–4525.

[327] Senjean, B.; Fromager, E. N-centered ensemble density-functional theory for open systems. **2020**, *120*, e26190.

[328] Kraisler, E.; Kronik, L. Piecewise linearity of approximate density functionals revisited: implications for frontier orbital energies. *Phys. Rev. Lett.* **2013**, *110*, 126403.

[329] Kraisler, E.; Kronik, L. Fundamental gaps with approximate density functionals: The derivative discontinuity revealed from ensemble considerations. *J. Chem. Phys.* **2014**, *140*, 18A540.

[330] Baerends, E. J. From the Kohn–Sham band gap to the fundamental gap in solids. An integer electron approach. **2017**, *19*, 15639–15656.

[331] Hodgson, M. J.; Kraisler, E.; Schild, A.; Gross, E. K. How interatomic steps in the exact Kohn–Sham potential relate to derivative discontinuities of the energy. **2017**, *8*, 5974–5980.

[332] Guandalini, A.; Rozzi, C. A.; Räsänen, E.; Pittalis, S. Fundamental gaps of quantum dots on the cheap. *Phys. Rev. B* **2019**, *99*, 125140.

[333] Guandalini, A.; Ruini, A.; Räsänen, E.; Rozzi, C. A.; Pittalis, S. Density functional approach to the band gaps of finite and periodic two-dimensional systems. *Phys. Rev. B* **2021**, *104*, 085110.

[334] Rauch, T. c. v.; Marques, M. A. L.; Botti, S. Accurate electronic band gaps of two-dimensional materials from the local modified Becke-Johnson potential. *Phys. Rev. B* **2020**, *101*, 245163.

[335] Rauch, T. c. v.; Marques, M. A. L.; Botti, S. Erratum: Accurate electronic band gaps of two-dimensional materials from the local modified Becke-Johnson potential [Phys. Rev. B 101, 245163 (2020)]. *Phys. Rev. B* **2020**, *102*, 119902.

[336] Baerends, E. J. On derivatives of the energy with respect to total electron number and orbital occupation numbers. A critique of Janak's theorem. *Mol. Phys.* **2020**, *118*, e1612955.

[337] Janak, J. F. Proof that $\frac{\partial E}{\partial n_i} = \epsilon$ in density-functional theory. *Phys. Rev. B* **1978**, *18*, 7165–7168.

[338] Levy, M.; Perdew, J. P.; Sahni, V. Exact differential equation for the density and ionization energy of a many-particle system. *Phys. Rev. A* **1984**, *30*, 2745–2748.

[339] Perdew, J. P.; Yang, W.; Burke, K.; Yang, Z.; Gross, E. K. U.; Scheffler, M.; Scuseria, G. E.; Henderson, T. M.; Zhang, I. Y.; Ruzsinszky, A., *et al.* Understanding band gaps of solids in generalized Kohn–Sham theory. *Proc. Natl. Acad. Sci.* **2017**, *114*, 2801–2806.

[340] Hofmann, D.; Kümmel, S. Integer particle preference during charge transfer in Kohn-Sham theory. *Phys. Rev. B* **2012**, *86*, 201109.

[341] Koentopp, M.; Burke, K.; Evers, F. Zero-bias molecular electronics: Exchange-correlation corrections to Landauer's formula. *Phys. Rev. B* **2006**, *73*, 121403.

[342] Paragi, G.; Gyémánt, I.; Van Doren, V. E. Investigation of exchange potentials for excited states by parameter fitting. *Chem. Phys. Lett.* **2000**, *324*, 440–446.

[343] Paragi, G.; Gyémánt, I.; VanDoren, V. E. Investigation of exchange-correlation potentials in ensemble density functional theory: parameter fitting and excitation energy. *J. Mol. Struct. (Theochem)* **2001**, *571*, 153–161.

[344] Gould, T.; Kronik, L. Ensemble generalized Kohn–Sham theory: The good, the bad, and the ugly. **2021**, *154*, 094125.

[345] Pastorczak, E.; Pernal, K. Ensemble density variational methods with self-and ghost-interaction-corrected functionals. *J. Chem. Phys.* **2014**, *140*, 18A514.

[346] Schilling, C.; Pittalis, S. Ensemble Reduced Density Matrix Functional Theory for Excited States and Hierarchical Generalization of Pauli's Exclusion Principle. *Phys. Rev. Lett.* **2021**, *127*, 023001.

[347] Loos, P.-F. Exchange functionals based on finite uniform electron gases. **2017**, *146*, 114108.

[348] Gould, T.; Pittalis, S. Density-driven correlations in ensemble density functional theory: Insights from simple excitations in atoms. *Aust. J. Chem.* **2020**, *73*, 714–723.

[349] Gould, T. Approximately self-consistent ensemble density functional theory: toward inclusion of all correlations. *J. Phys. Chem. Lett.* **2020**, *11*, 9907–9912.

[350] Fromager, E. On the exact formulation of multi-configuration density-functional theory: electron density versus orbitals occupation. *Mol. Phys.* **2015**, *113*, 419.

[351] Görling, A.; Levy, M. Exact Kohn-Sham scheme based on perturbation theory. *Phys. Rev. A* **1994**, *50*, 196.

[352] Görling, A.; Levy, M. DFT ionization formulas and a DFT perturbation theory for exchange and correlation, through adiabatic connection. **1995**, *56*, 93–108.

[353] Ivanov, S.; Levy, M. Accurate correlation potentials from integral formulation of density functional perturbation theory. **2002**, *116*, 6924–6929.

[354] Yang, Z.-h. Second-order perturbative correlation energy functional in the ensemble density-functional theory. *Phys. Rev. A* **2021**, *104*, 052806.

[355] Yang, Z.-h.; Trail, J. R.; Pribram-Jones, A.; Burke, K.; Needs, R. J.; Ullrich, C. A. Exact and approximate Kohn-Sham potentials in ensemble density-functional theory. *Phys. Rev. A* **2014**, *90*, 042501.

[356] Ye, H.-Z.; Tran, H. K.; Van Voorhis, T. Accurate Electronic Excitation Energies in Full-Valence Active Space via Bootstrap Embedding. *J. Chem. Theory Comput.* **2021**, *17*, 3335–3347, PMID: 33957050.

[357] Chen, Q.; Booth, G. H.; Sharma, S.; Knizia, G.; Chan, G. K.-L. Intermediate and spin-liquid phase of the half-filled honeycomb Hubbard model. *Phys. Rev. B* **2014**, *89*, 165134.

[358] Booth, G. H.; Chan, G. K.-L. Spectral functions of strongly correlated extended systems via an exact quantum embedding. *Phys. Rev. B* **2015**, *91*, 155107.

[359] Householder, A. S. Generated Error in Rotational Tridiagonalization. *J. ACM* **1958**, *5*, 335–338.

[360] Smith, D. G. A. *et al.* PSI4 1.4: Open-source software for high-throughput quantum chemistry. *J. Chem. Phys.* **2020**, *152*, 184108.

[361] Marécat, Q.; Lasorne, B.; Fromager, E.; Saubanère, M. Unitary transformations within density matrix embedding approaches: A perspective on the self-consistent scheme for electronic structure calculation. *Phys. Rev. B* **2023**, *108*, 155119.

[362] Heilmann, O. J.; Lieb, E. H. VIOLATION OF THE NONCROSSING RULE: THE HUBBARD HAMILTONIAN FOR BENZENE*. *Ann. N. Y. Acad. Sci.* **1971**, *172*, 584–617.

[363] Harriman, J. E. Geometry of density matrices. IV. The relationship between density matrices and densities. *Phys. Rev. A* **1983**, *27*, 632–645.

Université de Strasbourg

Filip Cernatic

EDSC École Doctorale des Sciences Chimiques

Ensemble density functional approach to electronic excitations: Exact theory and approximations using quantum embedding.

Résumé

Cette thèse se concentre sur les nouveaux développements dans la théorie de la fonctionnelle de la densité d'ensemble (eDFT), qui est une méthode indépendante du temps pour décrire des ensembles d'états électroniques fondamentaux et excités. Les aspects formels et pratiques de la méthode sont discutés en détail. Différentes approches sont introduites pour le développement d'approximations de la fonctionelle de la densité (DFA), appuyés par des calculs test sur le dimère asymétrique de Hubbard. Un nouveau formalisme dit "*N-centré étendu*" est introduit pour combiner excitations neutres et chargées en un seul ensemble. Cette approche permet notamment d'appréhender d'une nouvelle façon le concept de *dérivée discontinue* pour les excitations neutres. Enfin, une stratégie d'*embedding* quantique d'ensemble est proposée pour décrire plusieurs états électroniques. Cette derniere est basée sur le formalisme de la matrice à densité réduite à un électron (1RDM).

Mots-clés: Excitations électroniques, théorie de la fonctionnelle de la densité, formalisme d'ensemble, approximations de la fonctionnelle de la densité, dérivée discontinue, embedding quantique

Abstract

The thesis focuses on new developments in ensemble density-functional theory (eDFT), which is a time-independent method for describing ensembles of ground and excited electronic states. Formal and practical aspects of the method are discussed in detail. Different approaches for developing density-functional approximations (DFAs) are suggested, with test calculations presented for the asymmetric Hubbard dimer. A new formalism of "*extended N-centered*" ensembles is proposed, which combines neutral and charged excitations into a single ensemble. This approach elucidates in a new way the concept of derivative discontinuity for neutral excitations. Lastly, a quantum embedding strategy for describing multiple electronic states is proposed, based on the one-electron reduced density matrix (1RDM) formalism.

Keywords: Electronic excitations, density-functional theory, ensemble formalism, density-functional approximations, derivative discontinuity, quantum embedding